STUDIES ON SILICIDES AND OXIDES OF SOME TRANSITION METALS BY AUGER ELECTRON SPECTROSCOPY AND ELECTRON ENERGY LOSS SPECTROSCOPY

Thesis
Submitted in partial fulfilment
of the requirements for the degree of
DOCTOR OF PHILOSOPHY

by
SANTANU BERA

Under the Supervision of
Prof. J.K.N. Sharma

BIRLA INSTITUTE OF TECHNOLOGY & SCIENCE
PILANI (RAJASTHAN) INDIA

1994

BIRLA INSTITUTE OF TECHNOLOGY & SCIENCE
PILANI RAJASTHAN

CERTIFICATE

This is to certify that the thesis entitled "Studies on Silicides and Oxides of Some Transition Metals By Auger Electron Spectroscopy and Electron Energy Loss Spectroscopy" submitted by Santanu Bera (**ID. NO. 90 PZYF006**) *for award of Ph.D. Degree of the Institute, embodies original work done by him under my supervision.*

Signature in full ...JKNSharma...........

Name : Prof. J.K.N. Sharma, D. Phil (Oxon)

Date : 4th June 1994.

Designation : Ex-Scientist 'G' & Deputy Director
National Physical Laboratory, New Delhi.

ABSTRACT :

The increase of the surface to volume ratio in fine geometry microelectronic devices is the motivation to undertake research on thin silicide and oxide films of transition metals. For probing them with very high spatial and depth resolutions, surface analytical techniques have been employed. In the present work, model systems of transition metals with different number of d electrons, Ti (d^2), Ta (d^3), Mo (d^5) and Cu (d^{10}) are chosen and their respective oxides and silicides are prepared in UHV by evaporation using electron beam and effusion cells. The importance of having clean surfaces suitable for surface science studies has been highlighted, by finding the effects of ion beam bombardment on the lineshapes of different electronic transitions, and some angle dependent XPS studies in case of Si.

The electronic transitions in Auger electron spectroscopy (AES), electron energy loss spectroscopy (EELS), autoionization and X-ray photoelectron spectroscopy (XPS) that involve d band, are probed to understand the d band occupancy and the general, density of states (DOS) around the Fermi level. Empty DOS available in the d band of transition metals show some special features in EELS as interband transitions and quasiatomic p-d transition losses, or autoionization transitions in low energy AES. Such loss transitions at 39 and 49 eV in Ta, 47 eV in Mo and 45 eV in Ti show changes due to oxidation and silicidation. These features enhance in oxides but decrease in silicides indicating a redistribution of the DOS due to the formation of these compounds. The decrease or increase of the autoionization features at 44.5 eV in Ta, 34 eV in Mo or 41 eV in Ti due to silicidation or oxidation of the respective metals complements the information obtained by EELS. The multiplet splitting in AES structure and their change due to oxidation and silicidation is explained for the different charge transfer process in these two compunds.

The multiplet splitting originating from the interaction of the p-holes created in the Auger process and unpaired d electrons is found to decrease in the oxides, and increase in the silicides. Cu, with ten electrons occupy the d orbital, does not show the p-d quasiatomic transition and hence no autoionization. XPS valence band picture is added to these results to complement the information obtained by AES, ELS or autoionization process. Simultaneously, Si LVV Auger lineshape changes are observed. The decrease of the pp contribution out of the three (pp, sp and ss) in the Si LVV line is attributed to either the formation of some interface states with the p surface states or the change in the localization of the Si 3s orbitals. O KVV results indicate the charge transfer in the oxidation which reduces the multiplet splitting of metal Auger lines. Finally the data for each material by all the above techniques has been consolidated and trends of the behaviour of electronic transitions on the number of d electrons in the metal, have been drawn.

This study has shown the sensitivity and complementarity of all the techniques used to probe the silicides and oxides. The work has demonstrated that using conventional electron spectroscopic techniques, by observing electronic transitions involving d electrons, the DOS highly proximal to the Fermi level can be monitored. The present studies not only indicate this approach as a tool to evaluate charge transfer in silicides and oxides but also, through the data on dependence on transitions on d electron population, can help tailoring new materials for microelectronic devices.

To
My Parents

ACKNOWLEDGEMENTS

I wish to acknowledge, with a deep sense of gratitude, the guidance given by Dr. J.K.N. Sharma, the pioneer of the Surface Physics Activity at the National Physical Laboratory, India, under whose supervision this work has been done. His knowledge, experience, constant encouragement and support have helped me tremendously in completing this work .

I specially thank Dr. S.M. Shivaprasad, my friend-guide, who made me enjoy my work at NPL. My days at NPL, probably will remain vivid with the light of sweet memory of my association with him. Without him, this work could never get the present form.

I would like to sincerely thank Dr. B.R. Chakraborty for initiating me in this work. His help in performing experiments and understanding some results is deeply acknowledged. His role in obtaining my M.S. degree was very crucial. Thanks are due to Dr. P.K. Ashwini Kumar also, who introduced me to thin film technology and helped me in preparing the silicide and oxide films.

Mr. A.C. Gupta, Dr. K.K. Jain, Dr. N.Sen, Dr. P. Mohan, Dr. D.R. Sharma, Dr. A.K. Bandopadhaya, Mr. A. VijayKumar, Dr C. Anandan have all been helpful in terms of scientific discussions and encouragement to complete this thesis. I specially thank Mr. Sanjay Raizada of our Central Computer Facility whose help goes beyond helping with use of computers, but also in other aspects of daily lab-life.

Two of my friends Sandip Dhara and Subir Saha, are being acknowledged deeply. In my beginning days at NPL, they gave me confidence to get into instrumentation and computers. I am thankuful to

all research scholars of NPL, specially, S. Chatterjee (S.R.F.), Sanjit Das (S.R.F.) , R.N.Sharma (S.R.F.). P. Asthana(S.R.F.) , P.K. Basu (S.R.F.) and V.H.S. Murty (S.R.F.), who gave their valuable suggestions to understand and complete the work.

My gratitude is due to my teachers, Prof. S.K. Joshi, Dr. B.K. Das, Dr. S.T. Laxmikumar, Dr. V.C. Jain, Dr. S.N. Singh, Dr. P.K. Gupta and other scientists of NPL, for their efforts in helping me complete my M.S. course succesfully. The help of Mr. Khullar throughout the work is acknowledged.

I would like to thank Prof. E.S.R. Gopal, the Director of NPL, for encouraging us to do such contemporary work in this field.

The close association of Mr. V. Karmarkar helped me in understanding some aspects of electronics, S.S. Hiremath regarding computers and Mr. L. D. Kukreja for help in administrative matters.

I deeply acknowledge the financial assistance sponsored by Director NPL fellowship and C.S.I.R. for my Junior and Senior Research Fellowships.

(Santanu Bera)

Date : 4th June 1994

National Physical Laboratory

New Delhi. India.

Contents

	Title page	i
	Certificate	ii
	Abstract	iii
	Dedication	v
	Acknowledgement	vi

Chapter I Introduction

1.1	Silicides as device materials	1
1.2	Metallization	2
1.3	Oxides	4
1.4	Transition metal silicides and oxides	5
1.5	Materials	9
1.6	Deposit materials	9

Chapter II Overview of studies of silicides and oxides of transition metals

2	Introduction	13
2.1	Properties of silicides and oxides	13
2.1.1	Silicides	14
2.1.2	Oxides	16
2.2	Kinetics of silicidation and oxidation	17
2.2.1	Silicidation	18
2.2.2	Oxidation	20
2.3	Surface analytical studies of M/Si and M/O systems	22
2.3.1	Surface analysis on model metal monolayer on Si	24
2.3.2	Surface analysis of oxygen on metals	29
2.4	Concepts of surface analytical probes used	32
2.4.1	Auger Electron Spectroscopy	33
2.4.2	Reflected electron energy loss spectroscopy	37
2.4.3	X-ray photoelectron spectroscopy	39
2.4.4	Autoionization process	41
2.5	Conclusions	44

Chapter III Experimental

3	Introduction	51
3.1	Need for an UHV environment	51
3.2	Sample preparation	53
3.2.1	Silicides preparation	53
3.2.2	Oxide preparation	55
3.3	Analysis	56
3.3.1	Apparatus for AES, ELS and autoionization	56
3.3.1.a	System standardization	60
3.3.1.b	Parameters for AES	62
3.3.1.c	Parameters for EELS	62
3.3.2	XPS study	63

Chapter IV Results and discussions

Section 4A Ion beam effect

4a.	Sample cleaning and ion beam effect	66
4a.1	Modification of carbon by ion beam bombardment	67
4a.2	Ion beam effect on contaminated Ta	70
4a.3	Ion beam effect on contaminated Mo	71
4a.4	Ion beam effect on contaminated Si(111) surface	73
4a.5	Conclusion	78

Section 4B Valence band related electron spectroscopies

4b.	Introduction	81
4b.1	Electron enery loss spectroscopy	81
4b.1.1	ELS in Ta, Ta_2O_5 and $TaSi_2$	82
4b.1.2	ELS in Mo, MoO_3 and $MoSi_2$	85
4b.1.3	ELS in Ti, TiO_2 and $TiSi_2$	87
4b.1.4	ELS in Cu, CuO and $CuSi_2$	89
4b.2	Auger electron spectroscopy	90
4b.2.1	AES in Ta, Ta_2O_5 and $TaSi_2$	91
4b.2.2	AES in Mo, MoO_3 and $MoSi_2$	93
4b.2.3	AES in Ti, TiO_2 and $TiSi_2$	95

4b.2.4 AES in Cu, CuO and $CuSi_2$ 97
4b.2.5 Si LVV Auger analysis 99
4b.2.6 O KVV Auger lineshape 100
4b.3 Electron impact autoionization process 102
4b.3.1 Autoionization in Ta, Ta_2O_5 and $TaSi_2$ 103
4b.3.2 Autoionization in Mo, MoO_3 and $MoSi_2$ 105
4b.3.3 Autoionization in Ti, TiO_2 and $TiSi_2$ 107
4b.3.4 Autoionization in Cu, CuO and $CuSi_2$ 108

Section 4C Discussions and Trends

4C.1 Consolidation for each metal 113
4C.2 Trends 120

Chapter V Conclusion

5.1 Conclusions 127
5.2 Limitations 131

Appendix I 133
List of publications 135

Chapter I
Introduction

1.1 Silicides as device materials :

Since the discovery of the semiconductors in the late thirties, Si has been the most important electronic material. Application of Si in solid state semiconductor devices has resulted in numerous applications including defence, space, communication, amusement media, etc. The demand for high speed and compact size instruments has driven the miniaturization of the devices. The driving force has been not only to look at the interesting new properties of Si, but also to diminish the semiconductor device dimensions. It has finally led to the idea of Integrated Circuit (IC) technology[1]. As a result the technology has advanced from small scale integration to very large scale integration, that arranges more than 10^5 components (resistors, capacitors, diodes, transistors) on a single chip (50 mil x 50 mil). These changes in this technology have taken place very rapidly since 1960. This exponential growth of the number of components per chip is represented by Moore et al[2], as shown in FIG.1.1.

The primary thrust in IC technology is to make devices that are smaller in dimension, faster in operation and consume lesser power. In lieu of the larger packing density, and need for stability and reliability of the devices, there is a renewed interest in the metallization scheme for low resistive gate interconnections and ohmic contacts. A prime requirement of such application is that the structure should be stable

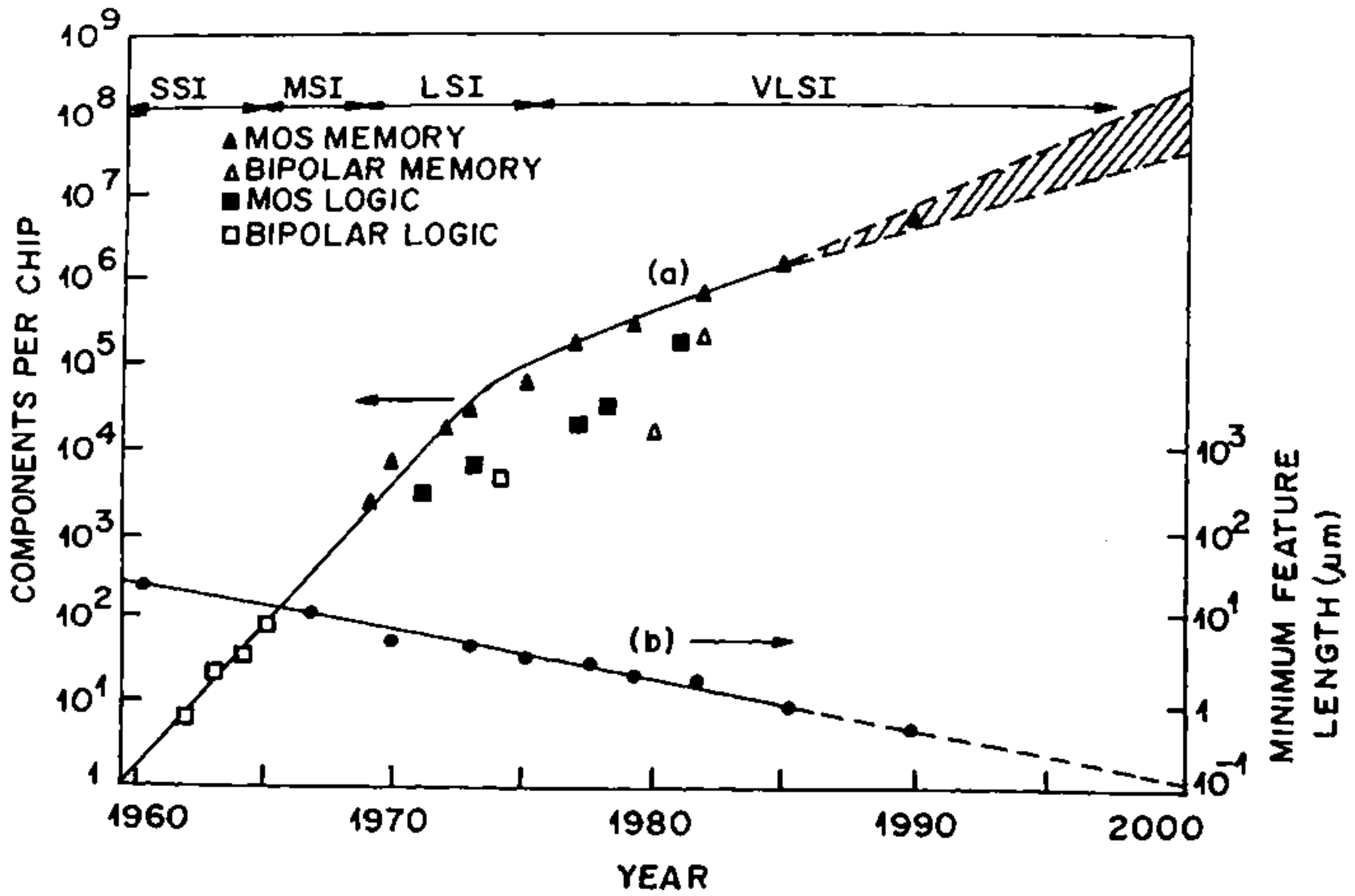

Fig.1. 1 : a) The number of components per IC chip and b) decrease of minimum device dimensions (Ref.2).

during device processing (oxidation, diffusion annealing, phosphorus-glass deposition etc.) following the silicide formation. The stability of silicide during oxidation is of special interest. In device processing a good dielectric oxide formed on the silicide is highly desirable . All these fundamental problems in the technology depend on the design and fabrication engineering with simultaneous research in tailoring new materials. It is not only a technological or scientific challenge to make high speed and reliable devices, but it should also render it economically viable. Due to the compactness, low cost of production and fantastic capabilities, ICs have played a leading role in the development of agricultural, industrial and information technology.

1.2 Metallization :

One of the important aspects of device fabrication is good metallization, to provide contacts on devices, interconnection between devices and with the outside world. Also metallization forms components of an active device (e.g. gates of Field Effect Transistor etc.). There has been enormous effort to find out properties of materials, modify them and to tailor-make suitable materials for metallization purposes. Some of the basic properties required for a good candidate[1] as metallization material are as follows :

i) ease of fabrication

ii) low resistivity ,

iii) oxidizability,

iv) mechanical stability,

v) no reaction with the final metal (metal for external connection)

vi) non-contamination of the devices,

vii) good device characteristics and carrier life times ,

viii) thermal and electrical stability,

ix) low contact resistance and minimal junction.

No metal can fulfill all these desired properties. Initially Al was thought to be ideal because of its good adheshion, good conductivity and corrosion resistance[3]. But, with the shrinkage of the device dimension laterally and vertically, it is found that it is difficult to use Al because of its diffusive penetration at high processing temperatures used in IC fabrication[3]. So since, metal silicides are considered as better alternatives. Silicides show metal like resistivity and are capable of forming protective layers required in integrated circuits. Moreover, making the metal react with the Si substrate itself forms a metal silicide which can give an in-situ control of barrier heights and other properties. Thus the possibility of forming silicides directly on polycrystalline Si (poly Si) preserves the basic poly Si MOS (Metal oxide semiconductor) gates, while decreasing the resistance. Even with this, it was found that the final contact metal, Al, reacts with silicides and penetrates into the Si device in the fabrication of FET (field effect transistor). So a metal layer, as a diffusion barrier to Al, was introduced in between Al and the silicide[4] (FIG. 1.2).

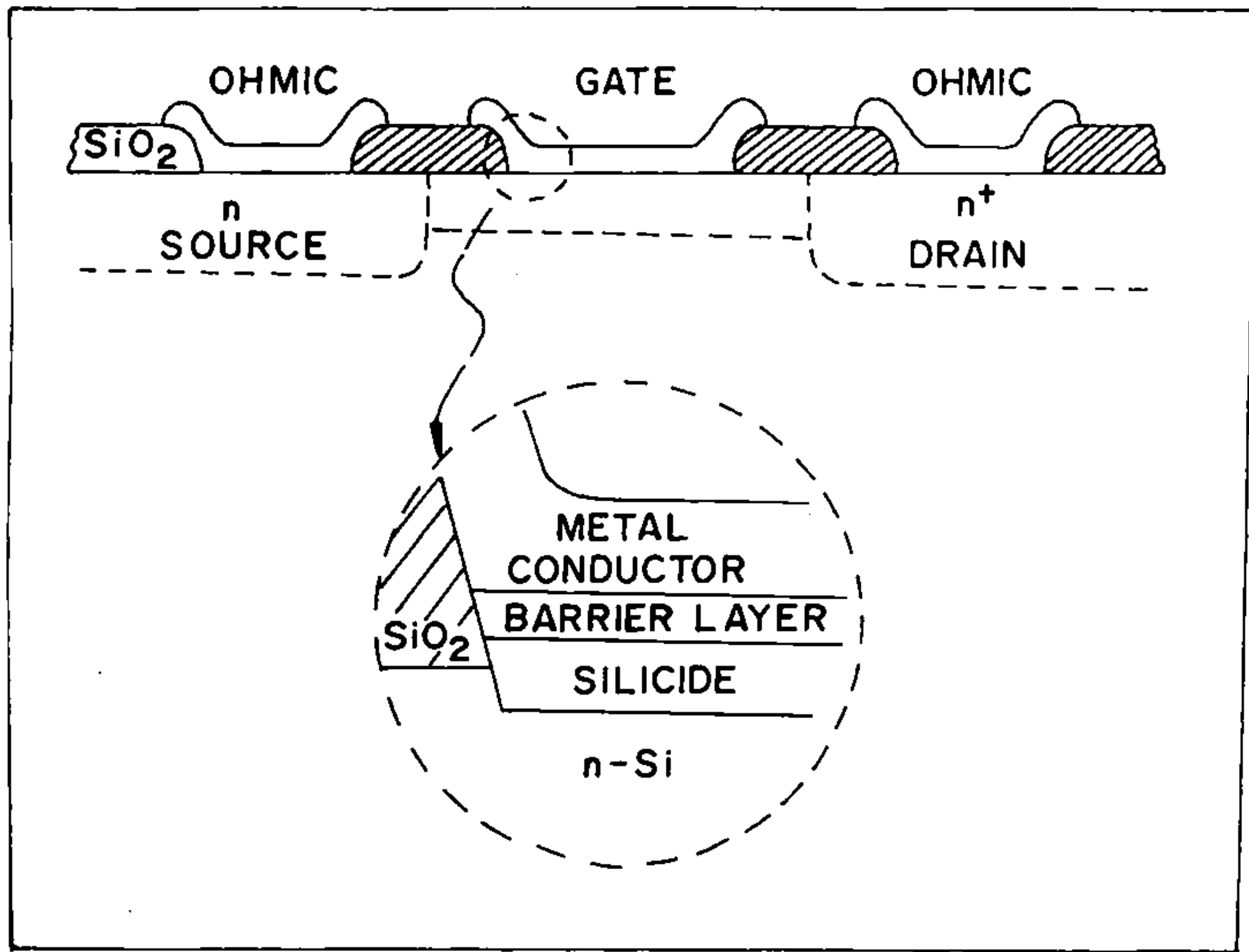

Fig.1. 2. : Schematic FET (Field Effect Transistor) showing the position of silicide and barrier layer.

1.3 Oxides :

Like silicides, metal oxides have a vast field of applications and scientific interest[5]. Particularly in microelectronics oxides are important for forming insulating or electrically isolating layers. Also in applications to corrosion , catalysis or in electrode reactions, oxides are the central material. The importance of oxides in device processing is based on two fundamental aspects : (i) The behaviour of the metal films on Si-O system and the kinetics of growth of metal silicide on Si-O system and ii) stability of the silicide towards oxygen. These two aspects are important in selecting the metal for metallization. The following properties of metal oxides are interesting to get an idea about the stability and stress accomodating capability during oxidation[4],

i) oxide to metal volume ratio,
ii) oxide melting point,
iii) oxygen solubility in metals,
iv) heat of formation of oxides.

Keeping in view all these reqirements for silicides and oxides, an optimization in choosing the material is necessary. Therefore a good understanding of both silicides and oxides from different angles is thus important in microelectronics and other industries.

1.4 Transition metal silicides and oxides :

The interest in transition metal silicides is due particularly to two properties that led to their applications in microelectronic industry,

i) the electrical resistivity generally exhibits a metallic behaviour , with typical specific resistivity values at room temperature between 15 to 150 μΩ cm.

ii) they exhibit good high temperature stability and useful oxidation resistance.

Another interesting property in transition metal silicides is their relatively low value of temperature coefficient of electrical resistivity. However for some of the transition metal silicides in the middle of the periodic table (e.g. Cr) this low temperature coefficient is combined with a high specific resistivity due to semiconducting nature of those silicides (suitable for fabrication of resistors)[6].

In the first application to the Si technology, to replace poly Si, the material had to be able to withstand high processing temperature, (1000 ^{o}C) oxidizing ambients and have low resistivity. These requirements cause focussing of attention on the refractory metal silicides, which combine good high temperature stability with specific thin film resistivity around 50 μΩcm. This value is more than one order of magnitude lower than highly doped poly-Si . The Schottky Barrier heights in the refractory metal silicides are quiet controllable ranging from 0.53 --0.65 eV (0.65--0.95 eV for near noble metals)[7]. In Si technology generally Si rich silicide, that is MSi_2 (metal disilicide) composition of the silicide is required, which is the most stable phase and is capable of withstanding high processing

temperature. In case of refractory metals there is a tendency of not forming any intermediate phase. The disilicide is formed directly because of the large negative value of the heat of formation, than in other phases.

Of all the silicides, platinum has been very commonly used as a contact material. In the gate and interconnection level, poly Si and refractory metal silicide bilayers have been used to replace the poly Si and providing a lower resistance. Refractory metal silicides are found to give the highest compatibility with other device components. The disilicides of molybdenum ($MoSi_2$), tantalum ($TaSi_2$) and tungsten (WSi_2) have been developed and are found to be successful in achieving good-quality high-speed microprocessors and Random Access Memories[4]. More recently $TiSi_2$ has replaced the above silicides due to its better conductivity. $CoSi_2$ is also found to be interesting in these applications. In case of oxidation the metallic Cr, Mo, W may pile up in the silicide exposed to oxidizing conditions. Group IVA and VA elements can reduce SiO_2[4]. Thus these silicides formed a mixed phase of oxides of both metal and Si. WSi_2 and $MoSi_2$ are found stable towards oxidation . Whereas Ti, Zr, Hf disilicides are decomposed to form metal oxides preference to Si-oxides, in an oxygen atmosphere. Several kinds of oxides are formed by most of the elements. The heat of formation is found to decrease with oxygen content in the oxide. But in VLSI only dioxides (oxygen rich) are generally formed because of the high processing temperature requirement.

About the stability of silicides in the oxidizing ambients, Murarka[4] has given several properties of metal-oxygen system like oxide to metal volume ratio, oxide melting point, heat of formation of oxides and oxygen solubility, which suggest that IVA and VA disilicides are more stable than

group VIA silicides in oxidizing conditions. The heat of formation of the oxides of Cr, W, Mo, Nb, V, Co, Pt, Pd are nearly same as or lower than the heat of formation of SiO_2. But in case of Hf, Zr, Ti whose oxides have considerably higher heat of formation compared to that for SiO_2, they are expected to oxidize differently. Murarka and Chang[8] have shown that on oxidation of $HfSi_2$, Hf is oxidised but Si remains unoxidised.

The refractory metal silicide and oxides are already being utilised in large scale industrial production. However, there have been many un-understood aspects of silicide formation and interfaces. This is the motivation for undertaking R and D in model silicide and oxide systems. Further research in this field can, not only answer some of the limitations that silicides and oxides encounters at present, but can also lead to new materials that can enhance device performance, reliability, stability and the ability for larger scale integration at lower costs. To understand the relation between the electronic structure and the formation of silicides and oxides on model systems and the mechanisms involved, it is important to use suitable characterization techniques. Along with the electrical and optical characterization studies, the use of surface analytical techniques play a very important role in finding the electronic structure and interface behaviour. Use of surface analytical techniques like AES (Auger electron spectroscopy) , XPS (X-ray photoelectron spectroscopy), ELS (energy loss spectroscopy) and SIMS (secondary ion mass spectroscopy) etc. are benificial in these small dimension devices (increased surface to volume ratio) where submicron resolution is needed. These techniques help in separating the behaviour of local regions with shallow information depths, which is crucial in knowing the effects of different parameters

ambient during the device formation, or in failure analysis. In the mechanism of formation bonding and non-bonding states below the Fermi level are studied by PES (photoelectron spectroscopy) and anti-bonding states above the Fermi level are studied by IPS (inverse photoelectron spectroscopy) or BIS (Bremsstrahlung isochromat spectroscopy).

Oxidation and silicidation of transition metals can be probed by AES, and ELS to understand the subtle differences in the electronic spectral features, in these covalent and ionic compounds, respectively. Due to chemical reaction the valence band redistribution takes place. In case of oxidation more vacant states are created where as in silicides the covalent bonding effectively fills up the vacant states in the metal valence band. Due to the different valence redistribution in oxides and silicides, the valence band related transitions show differences in the various surface excitation features. The valence band DOS manifests itself in the related transitions as variations in lineshapes of the observed spectra. Fingerprinting of spectral lineshapes can also be employed to find the behaviour of silicides when exposed to oxygen at different temperatures. For refractory metals, particularly, the autoionization process may be one of the best probes in understanding the DOS (density of states) above Fermi level in silicidation and oxidation. Autoionization process depends on the empty states available in the d band, so the p-d antibonding states in silicidation and charge transfer from metal in oxidation can be understood in details.

1.5 Materials :

Si(111) : The geometric and the electronic structure of Si is well characterized and undersood. The valence band of Si, $3s^1 3p^3$ forms two distinct band of 3s and 3p of binding energies 8 and 3 eV respectively. It has a diamond like crystal structure and according to the specific feature of such crystals, the atoms are bonded covalently with the neighbouring atoms, which are formed by well known sp^3 hybrids. At the ideal (111) face, one bond of the sp^3 hybrids is broken at every surface atom resulting in dangling bonds which are perpendicular to the surface. These dangling bonds are primarily p type electrons[9] and the backbonds of the surface Si atoms are primarily sp^2 like. In the band diagram these narrow half filled dangling bonds are present around the Fermi level and are called as 'surface states'. The interaction of metal with Si is always driven by its interaction with the surface states available on the plane.

1.6 Deposit materials : Ti, Ta, Mo and Cu :

Ti ($3p^6 3d^2$), Ta ($5p^6 5d^3$) , Mo ($4p^6 3d^5$) and Cu ($3p^6 3d^{10}$) are the deposit materials used in this work on Si (111) surface. Molecular oxygen is used for the oxidizing the metal film or sheet for forming oxides.

In the present work we have undertaken the formation of the silicides and oxides of some transition metals and probed their electronic structure and stoichiometry by surface analytical techniques like AES, EELS and XPS. AES and energy loss spectroscopy are used to monitor the silicidation as well as oxidation process of refractory transition metals like

Ti, Ta, Mo and noble metal Cu with 2,3,5 and 10 d electrons. Different Auger transitions, the multiplet splitting and the autoionization process depending of the d band occupancy are good areas for understanding the chemistry of these reaction. Different trends for multiplet splitting, autoionization energy plasmon losses as a function of d electrons are studied. This approach using conventional core level spectroscopic techniques prove to be very useful to probe the changes in the DOS, that are crucial in understanding the silicide and oxide formation and properties.

In this thesis an attempt has been made to consolidate the results of the experiments and interpretation of the results in five chapters :

The PRESENT CHAPTER is an introduction and deals with the choice of materials and motivation for the present work .

The SECOND CHAPTER is an overview of the studies and gives a brief literature survey of the work done on different transition metal silicides and oxides for understanding of the geometrical and electronic aspects of the mechanisms of growth and their dependence on the metal overlayer coverages. The chapter also discusses the concepts of the methods of investigations employed during these studies.

CHAPTER 3 describes the experimental set-up used to form the material and to characterize their electronic structure. In this section the details of standarizing the instrument is discussed.

The CHAPTER 4 describes the results and discussions and consists of three sections. The first section deals with the in-situ cleaning for surface analysis. It highlights the ion beam effects on the chemical state of

the sample during sputter cleaning. In the second section, based on the techniques utilised, the results are classified technique-wise for electron energy loss spectroscopy, Auger analysis and autoionization study. XPS results are included to complement the AES data. The third section consolidates the results and discussions and highlights the dependence of the electronic transitions on the nature of the transition metals (d electrons) as different trends.

CHAPTER 5 is the conclusion chapter which also indicates about the possible future extension of work and the limitations encountered in the present studies.

References:

1] S.M. Sze, " VLSI Technology (2nd. Ed.) " Mc-Graw-Hill International Ed. (1988).

2] G. Moore, "VLSI, What Does The Future Hold" Electron. Aust. 42, (1980) 14.

3] J.M. Poate, K.N. Tu and J.W. Mayer, " Thin film interdiffusion and reactions " A Wiely Interscience Publications (1979).

4] S.P. Murarka, " Silicides for VLSI Applications" Academic Press. NY (1983).

5] K. Wandelt, Surf. Sci. Rep. 2 (1987) 1.

6] A.H. Reader, A.H. van Ommen, P.J.W. Weijs, R.A.M. Wolters and D.J. Oostra, Rep. Prog. Phys. , 56 (1992) 1397.

7] E.H. Rhoderick and R.H. Williams, " Metal- semiconductor contacts" 2nd Ed. Oxford : Clarendon (1988).

8] S.P. Murarka and C. Chang, App. Phys. Lett. 37 (1980) 639.

9] S. Pick, Surf. Sci. Rep. 12 (1990) 99.

Chapter II
Overview

CHAPTER II :

OVERVIEW OF STUDIES OF SILICIDES AND OXIDES OF TRANSITION METALS

Introduction:

This chapter provides a background for the studies carried out, in terms of the properties of the silicides and oxides, kinetics of their formation and a brief literature survey to facilitate smooth reading and understanding of the results and discussions. The chapter also provides a brief conceptual background to the techniques used in this work.

2 . 1. Properties of silicides and oxides :

In microelectronics silicides are useful because of their metallic conductivity but oxides are useful for insulation or protection. Due to different atomic size and different electronegativity values of Si, metal and oxygen, the geometric and electronic structures are completely different in the compounds (silicides are covalent compound and oxides are ionic in nature). So properties dependent on the geometry and electronic structure of materials show a wide range of differences. Some of these properties that are of importance for microelectronics are discussed in brief, namely, i) resistivity, ii) stress behaviour, iii) crystal structure and iv) chemical reactivity.

2.1.1 Silicides

a. Resistivity : The resistivity of any material is fundamentally the result of the scattering processes of the flowing electrons in the material. In transition metal silicides the scattering is affected by a large number of factors like the number of d electrons of the metal, crystalline structure, size of the atom or metal-silicon and silicon-silicon bond lengths. An increase in resistivity in a given period may be due to the change in the crystalline sturcture. But in some cases the effect of the size of the atoms becomes dominating , specially in case of larger atoms. The relatively low resistivity of the group VIII metal silicides is due to the short metal-silicon bond length than Si-Si or metal-metal bond length[1]. Though many inter-dependencies affect the scattering process in a complicated way, some systematic trends have been observed. Generally, the resistivity of metals decreases with the increase in the number of d electrons (except Mn in the 3d series). But in silicides the resistivity shows a reverse behaviour in going from group IV A metal disilicides to group VI A metal disilicides. The change in resistivity along any group or period may also be due to change in atomic size. Thus resistivity of metal disilicides has been used as a good measure to confirm the silicidation.

b. Stress behaviour : In the process of silicide formation, the metal silicon interaction leads to a large volume decrease, which may be responsible for the stress observed in silicides. Understanding the stress behaviour in silicides is important because of the necessity of mechanical stability of the silicide for processing of the integrated circuits. The stress

behaviour of silicides varies from metal to metal. But in all metals the stress increases with the increase in the formation temperature and after a certain temperature it does not change. In Ti and Ta it is found to be true, but in case of Co at very high temperature (>800°C) again the stress is found to decrease sharply[2]. This has been interpreted as being due to epitaxial growth aspects on poly Si at high temperatures.

c. Crystalline structure : Silicides structures vary in complexity. Usually the number of atoms per unit cell is large. It is found that silicides of the same composition and group have the same crystalline structure. Several crystalline structures such as hexagonal ($CrSi_2$, VSi_2, $NbSi_2$, $TaSi_2$, $TiSi_2$), orthorhombic (PtSi), cubic ($CoSi_2$), tetragonal ($MoSi_2$, WSi_2, FeSi) have been observed in different silicides[3,4].

d. Reactivity : The reactivity of the silicides with chemicals like alkali solutions, HF solutions or aqua-regia is important to understand because of their utility in the etching processes in VLSI technology. Silicides are found soluble in fused alkali solution but hard in aqueous alkali solution. But fine line etching (Reactive Ion Etching) in VLSI technology demands the requirement to understand its reactivity towards different gases like CF_4, CF_4-O_2 mixture, SF_6, CCl_4 etc. used for dry gas etching. The reactivity of silicides with oxygen and the growth kinetics of oxides on silicides is of special importance for developing protective and insulating oxide layer on it.

2.1.2 Oxides :

Oxides of transition metals form a special class of materials due to their interesting properties. Transition metal mono-oxides which are isostructural, are sometimes metallic, as in TiO and VO and in the other extreme case are insulating as in MnO. Similarly TiO_2 is an insulator and CrO_2 is metallic and VO_2 undergoes a metallic to insulator transition at certain temperatures[5]. In microelectronics, transition metal oxide properties like oxide to metal volume ratio, oxide melting points, oxygen solubility in metals and heat of formation of the oxide are found to be important because of the higher stability of oxides than the respective metals. So many oxide layers in the device not only behave as an insulation but forms a protective layer that slows subsequent conversion of the metal to its oxides. For convenient processing, the subject of low temperature oxidation is important.

The melting point of oxides decrease as the group number increases and increases with the atomic weight in a given group (FIG.2.1). Heat of formation determines the ability of the metal to form an oxide in an oxidizing ambient. The heat of formation per oxygen atom of various oxides as compared with the heat per oxygen atom of SiO_2 is shown by Murarka (FIG2.2)[2]. Similarly, the solubility of oxygen in transition metals was observed to decrease rapidly with increasing group number (at 1000^oC) . Group IV A elements (refractory metals) have an oxygen solubility that increases with the atomic weight of metals[2]. In an oxygen environment gr. IVA and VA metals can dissolve considerable amount of oxygen prior to the formation of oxide. Gr. VI A , VII A and VIII have

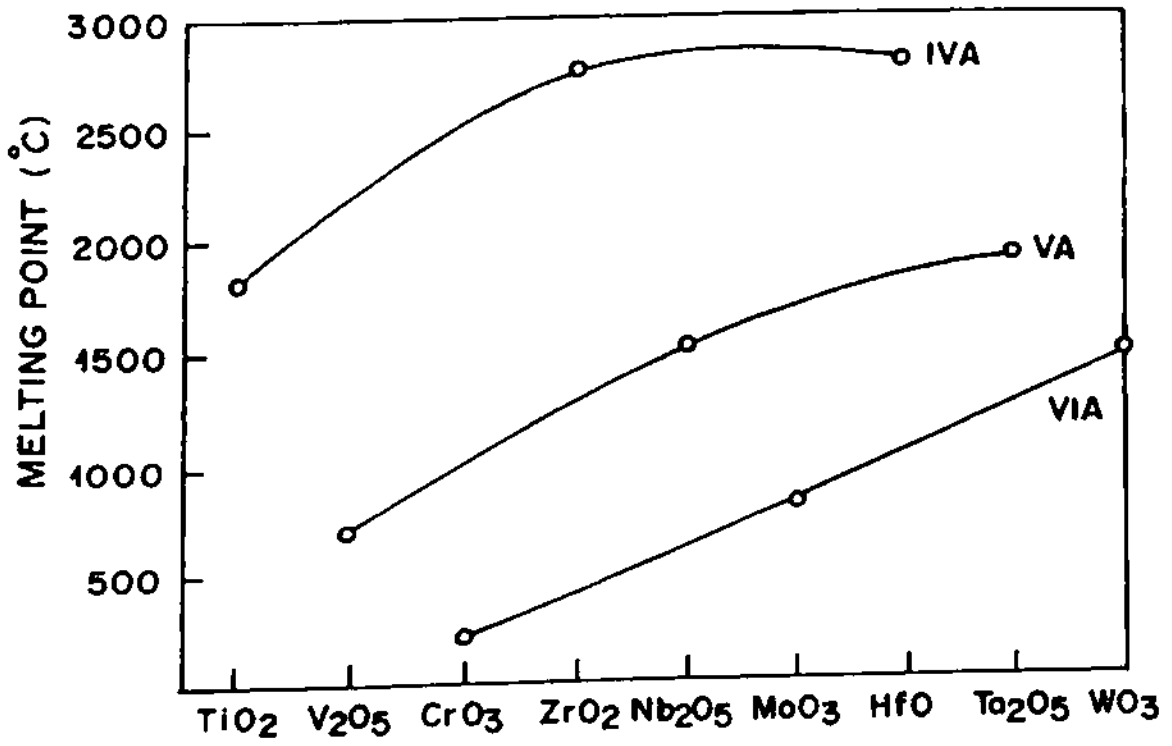

Fig. 2.1 : A plot of melting points of oxides of groups of elements(Ref.2).

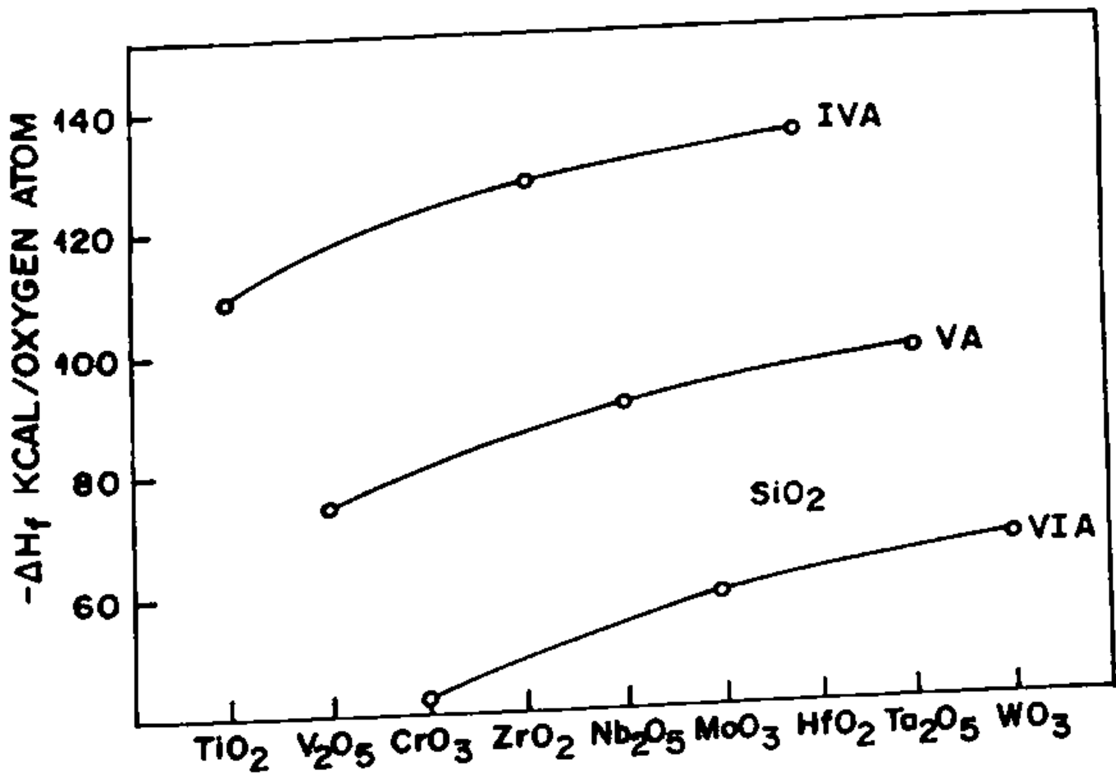

Fig.2.2 : Heats of formation (ΔH_f) /Oxygen atom for oxides (Ref.2).

almost negligible oxygen solubility. The oxide to metal volume ratio in an oxygen -metal system is important in studying the oxidation behaviour of the silicides during oxidation.

2 . 2. Kinetics of silicidation and oxidation :

To create controlled thin film structure for both oxides and silicides, the kinetics of growth or the mechanism of formation is important. Fundamentally silicidation is a solid-solid interaction and oxidation is a gas-solid interaction. Oxygen is highly electronegative with a large affinity for electrons, which is greater than the work function of metals, and there are vacant energy levels below the Fermi level of the metal. As a result, electrons may transfer partially to oxygen even at room temperature. So its growth mechanism can be explained from this point of view. But Si is covalently bonded and the bond breaking mechanism for chemical interaction is yet to be understood properly. Some evidence for room temperature silicidation observed at a critical thickness of metal film, leads to the thinking that other parameters play crucial roles in the initial stages of growth of silicides. So in the following discussion some typical models for silicidation and oxidation, proposed by different groups are presented.

2.2.1. Silicidation :

Typically, silicidation is a solid-solid reaction. Usually, the substrate is the covalently bonded Si on which a thin film that is metallic and fine grained is deposited. Upon heating the Si-metal system starts to form a distinct phase at 200°C and then the monosilicide at around 400°C and the respective disilicide at approximately 600°C. A general picture of Ni-Si interaction with temperature is given in FIG.2.3. However these formation temperatures are widely lower than either the Si or the metal melting points. The formation temperature is not high enough (even for refractory metals) such that bulk diffusion would be the dominating mass transport process. But as the metallic films are usually fine grained, the mass transport of the metal atoms can occur at their grain boundaries.

In the process of silicidation two phenomena are important, i) How the Si-Si covalent bonds break and ii) how the Si supply to the metal is maintained to form a silicide film. Bond breaking is explained in refractory metal disilicides formation, where high temperature is required. It is suggested that bond breaking takes place at the weak spots of the wafer like at kinks and ledges[6]. A high reaction temperature thus produces high frequency phonons, which free the surface Si atoms. Thus the silicide thickness is limited by the supply of Si atoms. Si atom is thought to be the dominating diffusing species as observed by the marker studies[7]. A model for Pd_2Si on Si (111) shown in FIG.2.4 is given by Buckley and Moss[6]. They showed that Pd atoms drop into the three positions around A and force the central atom out of the way moving it up

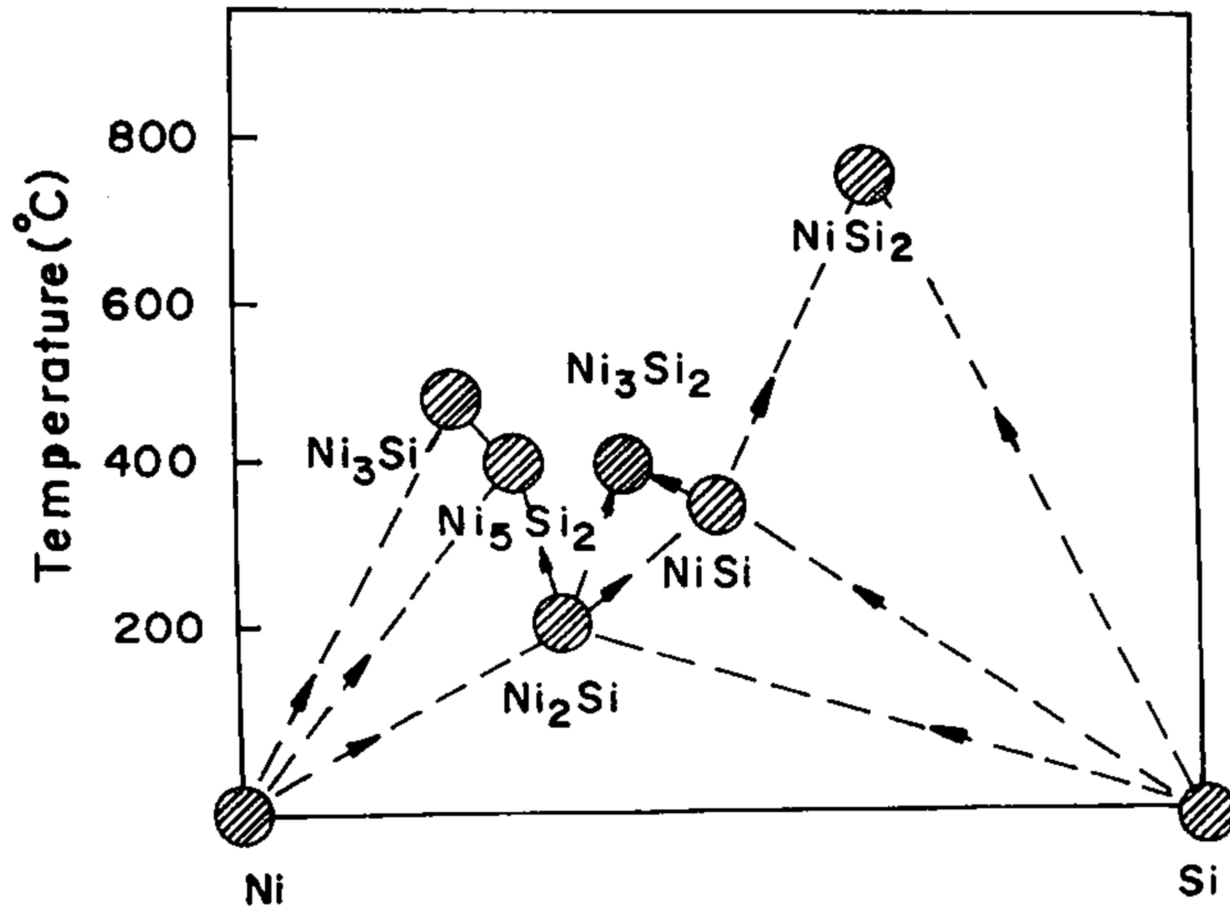

Fig.2.3 : Formation of various stoichiometric Ni-silicides at different temperatures.

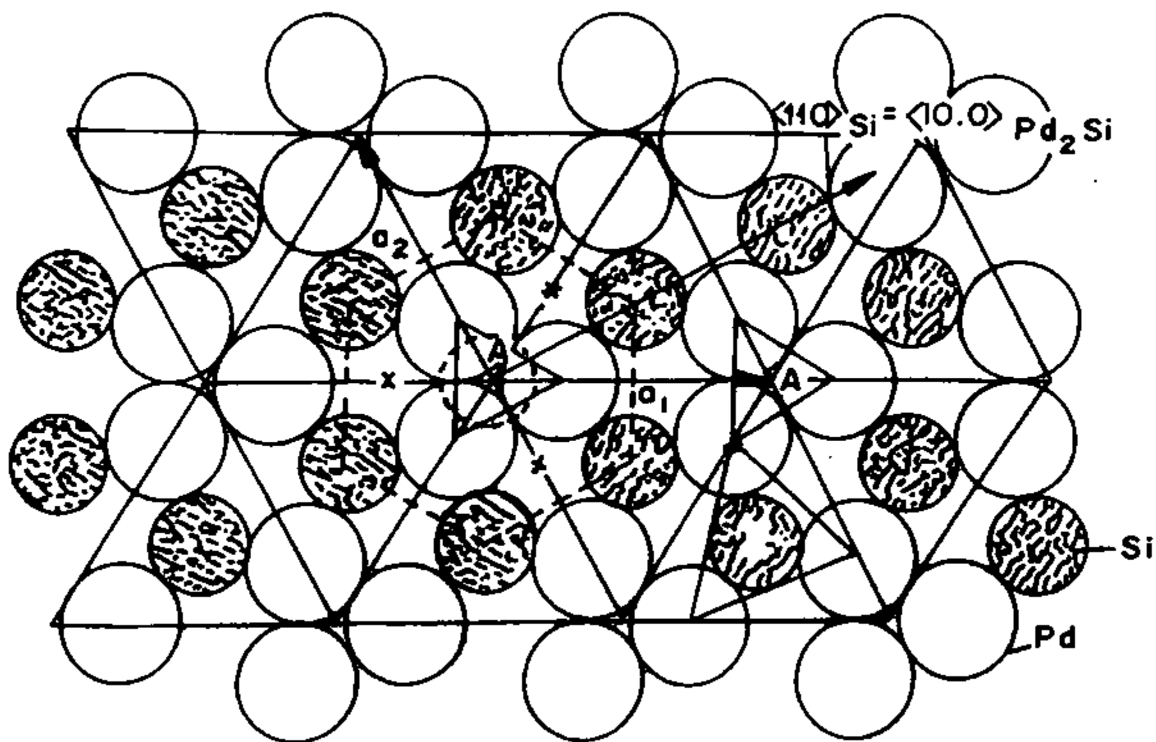

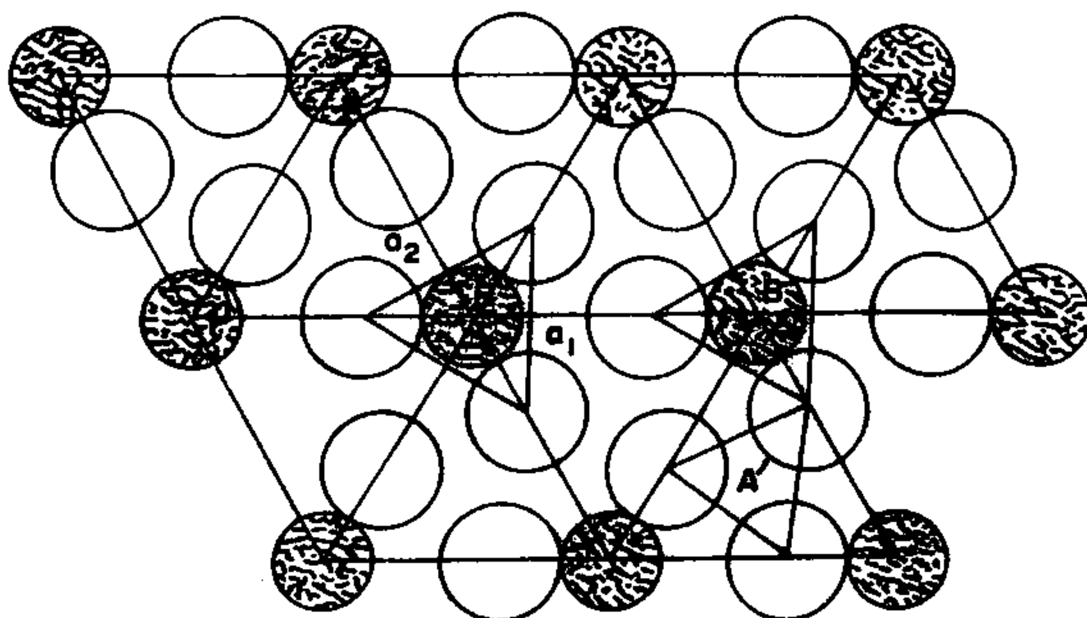

Fig.2.4 : Model for Pd and Si interdiffusion mechanism. Clear circles are Pd and black circles are Si. a) is the base plane of the hexagonal unit cell b) is a plane half way along C-axis (Ref. 6).

between them so that it nests on top of them to form the second plane of the silicide.

It is accepted that the growth mechanism of silicidation is a complicated and a not-well-understood process. Two mechanism are so far thought for the growth of silicide i) mass transport and ii) atomic motion across the metal /silicide and Si/silicide interface. If the thickening of the silicide film is linear with the square root of time, the formation of silicide is diffussion controlled i.e. rate determining step is the mass transport of atoms through the film. If however, the silicide growth is directly proportional to the annealing time then the growth is dominantly reaction controlled or interface controlled. In isothermal conditions the ultrathin film growth of silicide may be nucleation controlled. Thus to simplify the growth science of silicides, two distinct categories of silicide are made in the whole transition metals series. (i) Near noble metal (NNM) silicides and ii) refractory metal silicides (RM). NNM silicides are formed by the diffusion of predominantly the metal atoms into the Si. And the thickness growth is a function of square root of time t. In refractory metal silicidation, Si atoms are the dominantly moving species. And the growth kinetics show both the $t^{1/2}$ and t behaviour, suggesting the reaction steps influenced both by interface and diffusion mechanisms[8].

In metal rich silicidation , the reaction temperature is very low. In near-noble metals, where the formation temperature is not sufficient to break the Si-Si bonds at the surface, the interstitial mechanism of silicidation is proposed[9]. Here the metal atoms diffuse into the interstitial site of Si, as a result of which number of atoms increase in the Si co-ordination and an atomic hole is created at the initial metal atom

position. These effects weaken the Si-bonds. In the band picture, charge transfer from a covalent bond means creation of a hole in the valence band. But holes are not localised at a bond, thus, to free a Si atom several interstitial effects near the interface are required. Thus without the free metal atoms, to form the interstitial, the growth will be stopped. It is proposed that in metal rich silicides the metal atoms are the dominating diffusing species[9]. But $CrSi_2$ is formed at a very low temperature where as Co_2Si is formed above 350^oC. In these cases the bond breaking mechanism is still not clear.

The monosilicide phase is followed by the metal rich silicide. But when monosilicide itself is the first phase, then the explanation becomes complicated because of lack of sufficient data. However the different temperatures of monosilicidation is explained as being due to different diffusivity of metal atoms through metal rich silicides.

2.2.2 Oxidation :

The oxidation process of metal is a simple ionic type of chemical reaction,

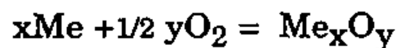

$$xMe + 1/2\, yO_2 = Me_xO_y$$

The driving force of oxidation is associated with the free energy change of the reactants to the oxide itself. The formation depends on other parameters, like the ambient oxygen pressure being greater than the

dissociation pressure p of the oxide in equilibrium with the metal, where

,

$$p = Exp(\Delta G/RT)$$

Where ΔG is the free energy of formation[10] of the oxide per mole of oxygen consumed. Surface oxidation is mostly determined by phase boundary reactions and diffusion processes. It is proposed that[10], initially, the adsorption of oxygen on the clean surface produces a partial ionization of oxygen atoms. Thus the strong electrical field set between metal and oxygen ion becomes the driving force for diffusion. The chemical potential gradient across the thick film also causes the diffusion.

The change in the work function during oxygen adsorption on metal surface indicates a surface rearrangement. LEED[11,12], HEED[13] and angle resolved photoemission[14] data are available providing the structural aspect of the oxidation process. In the reconstruction model, the chemisorption layer is pictured as the coexistence of metal and oxygen ions. The possibilities are given in FIG.2.5, Thus, it is suggested that the reconstruction is the necessary step for the development of 3D oxides. Disordered and amorphous structures have been reported in Al, Si, Cr etc. In order to explain uptake of the second monolayer of oxygen, Lanyon[15] suggested the mechanism of interchange of adsorbed oxygen atoms with the underlying metal atoms which is since known as place exchange. According to the suggestion by May[16], a part of the heat of chemisorption is used to form excited oxide molecules with high kinetic energy parallel to the surface. This can provide transport of the metal atoms over the surface

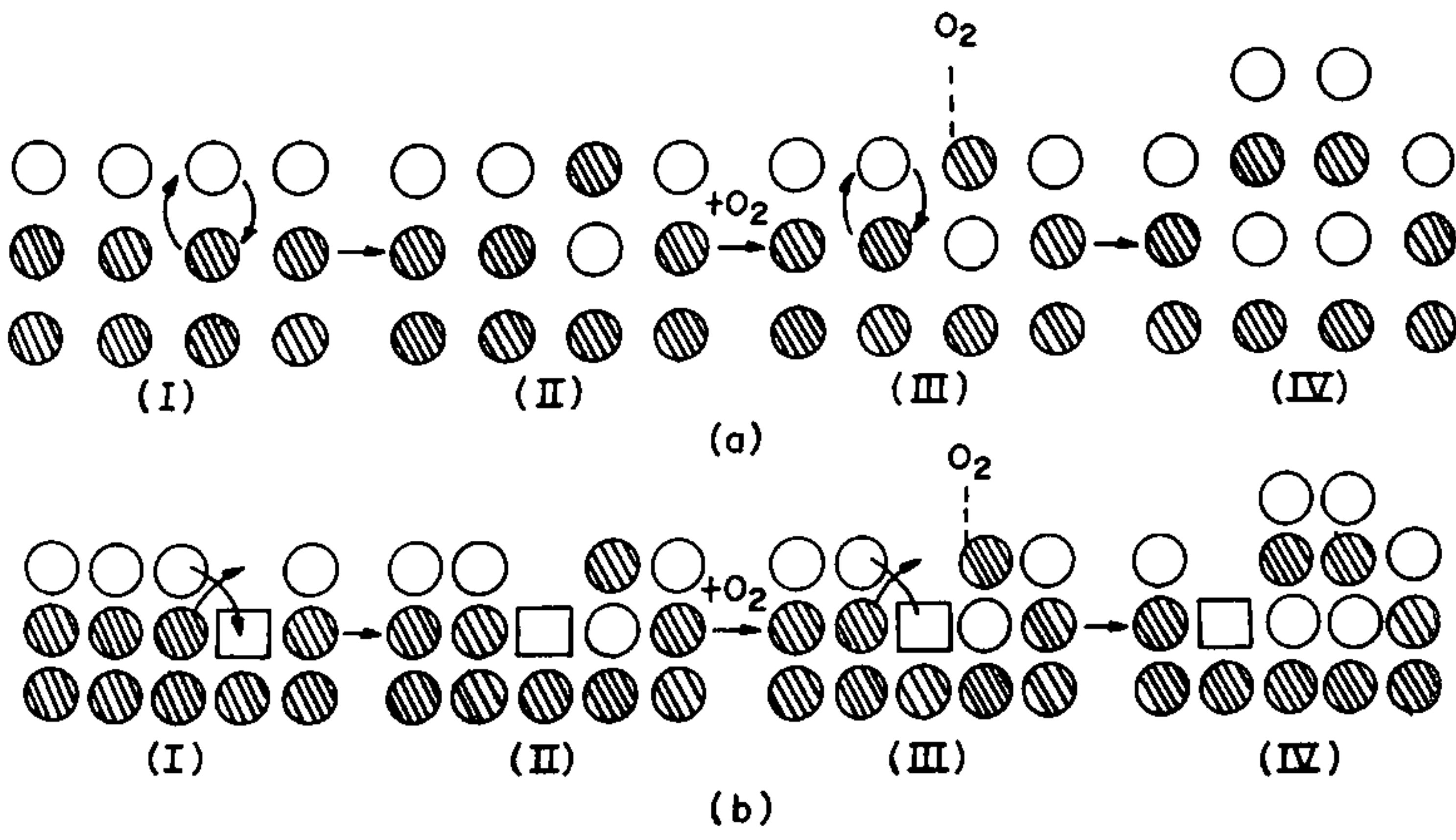

Fig.2.5 : Schematic representation of oxidation by place-exchange process in the presence of gaseous oxygen, a) surface free of defects and b) surface contains vacancies (Ref.10).

(FIG.2.5). The initial fast oxidation is also explained in terms of place exchange mechanism. The rate of the place exchange depends on the number of dipoles formed per unit time. All the available oxygen are expected to pick up electrons readily since electron tunneling is very easy in the initial stages of thin film growth on the surface. For elevated temperatures of oxidation, it is proposed that oxygen starts dissolving into the metal leaving a virtually clean surface. It has been reported that for Ni, upto 20 ML of O_2 will diffuse into the interior at 500K with a very high rate and has been attributed to quenching of vacancies[10].

2.3. Surface analytical studies of M/Si and M/O systems :

Several processes are developed to make shallow contacts, which is one of the fundamental goals of microelectronics. In the preparation of $MoSi_2$ films phosgene gas was used for doping the substrate by phosphorous[17] using snowplowing technique. But metals like Ta, Mo demand high processing temperatures for silicidation that may cause deep diffusion of the impurity, thus driving out the shallow contact facility. In case of codeposition technique the shallow junction is formed by controlling the deposition of a metal rich Si alloy on Si. Thus Pd_2Si-Si junction was formed by forming an alloy of $Pd_{80}Si_{20}$ on Si, which forms a silicide layer on successively annealing the deposit. The consumption of Si is 80 Å approximately[18]. The technique of epitaxial growth of metal films has revolutionized the silicide technology. In the device fabrication process, Arsenic is doped[19] on the metal (Pd, where Pd_2Si is to be the transport medium) and the amorphous Si is deposited. It was found that

in the solid phase epitaxial process below the silicide, a p-n junction was created by the transportation of As through the silicide. Selecting different parameters like deposition rate and substrate temperature, the silicides of Mo, Cr, Ni, Ir are formed succesfully[20,21].

Decrease in the device size poses complications in the measurement of various properties, since, i) the form of the material changes from the bulk to the film to the surface, ii) the physical size decreases and iii) the element concentration decreases from the major components. So analysis is required for characterization x-y spatial resolution in the 10-100Å range and depth resolution in the 20-30 Å range. Thus the material, characterization or the development of new material or the understanding of kinetics of silicidation and electronic mechanism of silicidation, require surface sensitive techniques. This has evolved a new field of work. It is found that the film thickness has a significant role in the compound formation. Even at room temperature $CoSi_2$ and $NiSi_2$ were found to form with one monolayer of metal deposition in UHV. Generally these model systems are characterized by surface sensitive techniques like AES (Auger electron spectroscopy), XPS (X-ray photoelectron spectroscopy), EELS (electron energy loss spectroscopy), LEED (low energy electron diffraction), ISS (ion scattering spectroscopy) etc. The specific role of each technique , its strength and its limitations are important to be understood.

2.3.1. Surface analysis of model metal monolayer on Si :

In principle, the cohesive energy between the metal atoms (for the bulk silicidation) is due to the d band formation. When Si atom enters into the metal lattice the d band narrows and weakens, thus loosing the cohesive energy. This loss actually creates the metal-Si bonding states which are stronger than either of the states from which they originate. In the photoelectric spectroscopic studies like XPS, UPS (ultraviolet photoelectron spectroscopy) or using synchrotron radiation, the different chemical states formed by metal d and Si p electrons at different temperatures are observed. The main interest of these studies is to understand common mechanisms for the metal silicidation. It is proposed[9] by Tu that in most cases the metal atoms initially enters into the Si interstitial positions and there by weakens the Si-Si covalent bond, which initiates an on-set of the reaction. However, Hiraki[23] proposed that the screening mechanism created by the free electrons of the metal overlayers, weakens the covalent bonding in Si. According to this theory a critical thickness of the metal overlayer is required to start the interaction. But in Ag/Si, where interface states are not found, the conception of critical thickness becomes difficult. So screening is not the only factor controlling the interaction. Thus an unified mechanism of silicidation still does not exist, and more efforts on finding the trends are in progress.

Different d metals like Ti, Ni, Pd, Pt, Ag have been extensively studied. LEED studies show that Si single crystal surface undergoes reconstruction in different patterns when monolayer (ML) level critical

thickness of film is deposited on it at different conditions of temperatures. After the same critical thickness of the metal film deposition, the chemical interaction also starts. In case of Ni, the chemical interaction happens even at room temperature. At 77K the 3d peak of Ni broadens at 1.5 ML thickness[24]. In case of Ti, the room temperature silicidation is a matter of controversy. Bultz et. al[25] concluded that there is no intermixing of Ti with Si at room temperature. But Loemen et al[26] showed some intermixing of Ti/Si even at room temperature. But the onset of distinct reaction is at 250°C for a 100Å film. 500°C thermal treatment results in a monosilicide phase and the disilicide phase is found at approximately 650°C. Of course the room temperature silicidation has also found evidence in ion scattering experiments and the critical film thickness is seen to be below $2.8X10^{15}$ Ti atoms/cm^2 (few ML).

In case of Pd, the interstitial diffusion of Pd is explained as the initiation of the interaction and the critical thickness for the interaction is observed to be 1ML. Initially Pd_2Si phase is found to form. The synchrotron radiation (PES) studies show the s-p contribution to the chemical bonding. The binding nature has been observed to be dependent on the coverage of the Pd on Si[27]. In case of Pt, at 300K and at 77K, chemical reactions with Si are observed. By studies using synchrotron radiation, different 5d nonbonding as well as p-d bonding states are observed, indicating room temperature growth of Pt on Si[28]. In the model proposed by the growth of Pt on Si, the coexistence of the metal and the reacted material is suggested to be present at the interface.

In Co-Si interaction, distinct phases are observed at different temperatures. But even at room temperature, UPS showed some

intermixed phase of Co-Si. By angle resolved XPS (AR-XPS) the presence of unreacted Co, for coverages greater than 4ML[29] was observed. And XPS shows the segregation of Si in the Co-overlayer. In V on Si chemisorption at room temperature, some interface states have been found but have been attributed to being simple chemisorption states. Stable states are available at around 200°C. The VSi_2 phase was observed[30] at around 500-550°C. This temperature is a bit lower than the normal temperature of disilicidation. Even $CrSi_2$ was found to form at lower temperatures at about 450°C and it is observed that the activation energy is lowest in case of $CrSi_2$ formation. Synchrotron radiation studies show some intermixing of Cr with Si at room temperature[31]. The room temperature intermixing of Si with refractory metals is not easily percieved, as they need higher temperatures for the disilicidation than the other transition metals.

Ag/Si interface is probably the most studied system because of the abrupt interface it forms. Si undergoes reconstruction in various structures during the deposition of Ag on it. It is found by ISS that there is some mixing at high temperature deposition. Accordingly, the R_3 layer consists of 2/3 ML of Ag atoms covering the whole surface uniformly and being embeded in the first double layer of the Si substrate. The embeded Ag atoms are found in the three fold hollows, approximately 0.7Å below Si surface. However, enough data does not exist to confirm the chemical interaction of Ag with Si at different temperatures[32,33]. But it is found that at very low coverages, (<1ML) significant redistribution of Si s-p electrons takes place similar to most d metal interfaces.

The silicidation of Au is not yet clear. It is predicted that Au-Si system forms some intermixing at the interface. However from Si LVV lineshape analysis it is assumed that Au-Si alloys with Si<30% is attributed to the formation of p-d bonding and antibonding structures[34]. In the work by Hiraki, the thickness dependent chemical interaction is suggested[35]. The chemical shift of Si (2p) and Au ($4f_{7/2}$) for higher amount of deposition (>3ML) indicates the onset of room temperature intermixing, thus forming a metal -Si metallic bonding state. However it is clear that gold does not form any stable silicide , which can act as an interface barrier for diffusion. UPS[36] shows that Au-d band structures move to higher binding energy and decrease in intensity as a function of annealing temperature upto 350°C. This suggests some intermixing between Si and Au, but there is not enough proof that a stable compound is formed. Recently, spatially resolved AES has shown that Au-Si reacted at the skin of the Au island formed due to ML deposition on it. From the core level study of Au 4f and Si 2p by photoelectron spectroscopy, the Au-Si chemical interaction at low coverages is observed[37]. But unlike Ag or Au, Cu forms distinct phases of silicides. The Cu-Si interface shows silicide like behaviour with intermixing and formation of Cu rich Cu-Si compounds. In fact Cu-Si compounds are regarded as electron phases with electron to atom ratio around 1.75 for the Cu_3Si polymorphs and are not exactly silicides[38]. Mechanism of ternary silicide formation in Ti-W-Si system is given by Umezawa et al.[39]. Electronic structure for Sn/Si interface is studied by Anyele et al[40]. Recent studies on rare earth silicides include Gd, Er mostly[41,42].

Thus by the photoelectron spectroscopic studies, different interactions like metal-metal, metal-Si and Si-Si, are interpreted from the hybridization state formation of metal d and Si s or p (in 4d and 5d metals). In disilicides or Si rich silicides metal d -Si p hybridization state dominates to form the bonding and antibonding states.

Si LVV Auger transition being a valence band related transition, is associated with the two hole final states in s or p bands. Thus in the final LVV Auger transition the main peak is due to the two hole final state in the p band. Other transitions of the s-p type represents only 10% of the intensity and the s-s is vanishingly small. Due to silicidation the s and p orbitals are strongly modified, as discussed in XPS and UPS report[31], hence some modification in the LVV line of Si is expected, along with the Auger chemical shift. Significant modifications in Si LVV lineshapes[43] are found in nickel silicide at different percentage of Ni. Most significant changes were observed in Pd_4Si[44] where the main transition is found to split giving a complete redistribution of DOS . In case of $ZrSi_2$, $NbSi_2$ and other silicides the p-p related peak is decreased with respect to the peak contributed by s-p or s-s. However the proper reason for this is still not clear[45]. Of course some explanation is available in terms of p type surface states which is converted into p-d chemical state (interface state). The behaviour of s band in Si is thought to be different from that in silicide which may also cause some change in the overall LVV peak shape.

It is important to observe electron energy loss spectra during the initial stages of growth and to some extent the chemical interaction between the substrate and the deposit. Different surface related structures like surface plasmon, surface states etc. show their changes when ML

deposition is done on Si-substrate. The EELS structure of Ag on Si is studied at different coverages at different temperatures of the substrate[33]. At room temperature the spectra are identical at low coverages, but different above 1 ML. The Ag bulk like spectrum is obtained at 2.5 ML. This is the consequence of the 2D growth of Ag on the first monolayer (Stranski-Krastanov growth mode). In case of gold, in the high temperature deposition, the main features in EELS narrow, and do not change their location. This suggests that the system formed after 1 ML is a stable one. For transition metals with unfilled d band, the interband transitions are interesting. Because metal-Si interaction basically depletes the empty states available for the electron energy loss transitions. Thus with the silicidation along with change of the plasmon loss features, interband transitions and their changes are observed for different metals like Fe, Ti[46,47] etc. APS (appearence potential spectroscopy) data are available for low coverages of Ti on Si[48].

2.3.2. Surface analysis of oxygen on metals :

The study related to oxides or oxidation of transition metals are mostly associated with understanding the mechanisms of oxidation. The initial step of the oxidation process involves chemisorption, followed by dissociation and finally ionization. It is found that most of the transition metals form oxides on the surface and the density of the oxide nucleii on the surface depends on the oxidation temperature and oxygen pressure.

Oxygen-metal reaction is of special interest in surface science to obtain information of surface chemistry and kinetics of oxidation both

qualitatively or quantitatively. Particularly, the electronic properties of the adsorbed surface and the local oxygen bonding geometry is of crucial importance and interest. Various oxygen states of adsorption have been distinguished such as molecular, atomic, chemisorbed and incorporated oxygen, depending on the reaction parameters e.g. temperature, pressure, etc. Structural changes with the adsorbed layer e.g. order-disorder transitions, with respect to the substrate can result in electronic charge redistribution, and hence in altered reactivity. Also, even low coverages can induce substitutional reconstruction of the metal surface. Many metals can have more than one stoichiometric oxide, and this has been confirmed by all the surface analytical techniques used. The complex interaction of oxygen with transition metals are best understood by photoelectron spectroscopy. The most immediate quantity obtained from photoelectron spectroscopy is the chemical shift. A detailed chemical shift of around 60 elements due to oxidation is given by Storp and Holm[49]. It is concluded that the chemical shifts in the oxides are a function of the atomic number and heats of formation (particularly for Ti, Nb , Ta).

In terms of kinetic information of oxidation, Ni is the most studied metal because of its utility in catalysis. The oxidation is described in three stages. The first stage is dissociative adsorption and in this chemisorption stage the oxygen atoms reside above fovourable high co-ordination sites. The second stage is incipient oxidation to a depth of 2-3 atomic layers. A nucleation and growth model is proposed by Holloway and Hudson[50-52] for Ni (100) and (111) surfaces. The nucleation growth is temperature dependent. The third stage finally is a slow thickening process. Different rate laws have been reported for different reaction temperatures[50-52]. The

best case of molecular oxygen adsorption on Pt (111) system as given by HREELS (high resolution EELS)[53]. The oxidation of Pt by molecular oxygen at different temperatures is studied mostly by HREELS and results the mixing of the M-O and O-O stretching vibration modes. The molecularly adsorbed oxygen is also reported[54] to exist on polycrystalline Cu and Cu clusters embeded in oxygen matrices, at very low temperatures.

The redistribution of the valence band in the third series transition metal oxides is monitored by Auger electron spectroscopy and the chemical shift, spin orbit splitting and exchange splitting have been monitored by Rao et al[5]. All the surface analytical techniques rely on the exclusive investigation of the chemical state of different oxides produced in different techniques, electronic structure, bonding mechanism, the local geometric site configuration etc. The O KLL Auger spectrum is also deriving interest where different peak to peak ratios in O KLL Auger transition is utilised to monitor the amount of charge transfer in the oxidation and the changes are also explained in terms of the nature of the d band[55,56].

Oxidation of silicides : The surface analytical techniques like UPS and XPS are employed by Nguyen et al[57] to understand the kinetics of oxidation of WSi_2 where they showed the oxidation of Si, but no W-O phase formation. The oxidation of $TaSi_2$ thin film on Si shows formation of different suboxides of Ta and Si even at room temperature[58]. Core level photoemission azimuthal anisotropy is employed to measure adsorption site of oxygen on metal system. Fadley[59] and coworkers have used high energy photoelectrons which create electron-atom single forward scattering to measure O adsorbed on Cu, which provide direct

information about the adsorption site. It is very important to understand the oxidation behaviour of silicides to be recommended as gate electrodes, specially on SiO_2. The silicides that are not candidates are those that do not dissolve oxygen and form oxides with a heat of formation (ΔH_f) lesser than that of SiO_2 to maintain the stability of VLSI fabrication during process. The silicides on metals e.g. Ti, Ta which dissolve oxygen form oxides, with ΔH_f slightly higher than that of SiO_2[60], have a tendency to reduce SiO_2 and thus form a good bonding layer.

Thus, it is important to get an idea of metal oxides and silicides and their effect on the Auger lineshapes or ELS features simultaneously, so that the kinetics of the mechanism of oxidation of silicides can be understood clearly. Oxides are mostly ionic and silicides are dominantly covalent in nature, so they leave distinct signature on the **Auger lineshape, autoionization or ELS** features. So in oxidation of silicides the behaviour of metal fingerprint help in characterization of the different phases of oxides and suboxides formed in the oxidation process and in the kinetics of oxidation mechanism of silicides. Following is a brief conceptual (physical basis) introduction of the surface analytical techniques which have been adapted for our work :

2.4. Concepts of surface analytical probes used :

Generally more than one technique are coupled together to evaluate any model in surface science . The techniques may couple geometric information to electronic information, or isolatedly geometric and electronic information by several complementary techniques. Auger

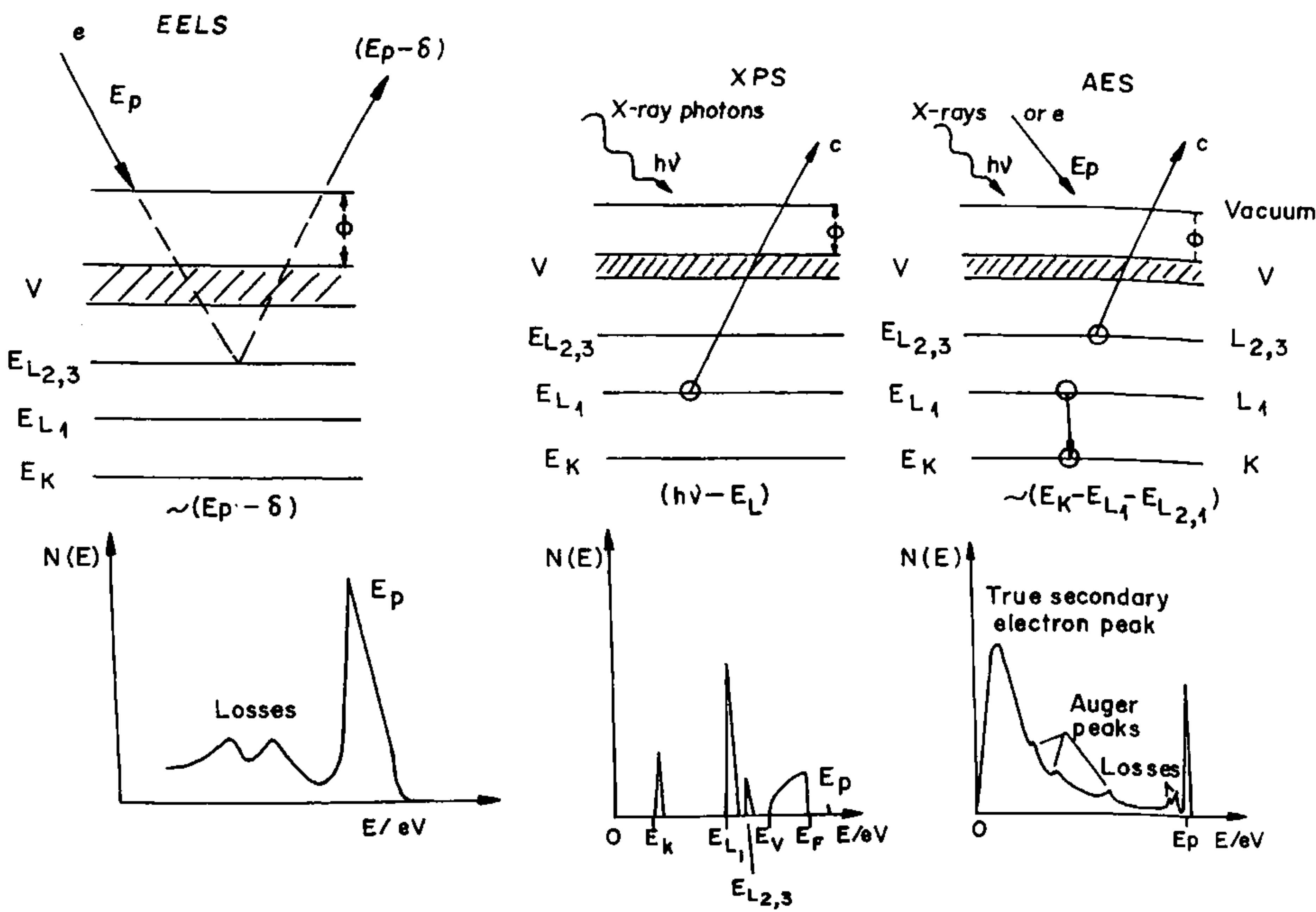

Fig. 2.6 : Schematic representation of AES, EELS and XPS. The one electron energy diagram at the top are for an ideal free atom. The graphs at the bottom show the electron energy distribution leaving the solid.(Ref.74).

electron spectroscopy coupled with ELS is useful in obtaining a complete understanding of electronic properties of materials. AES with transitions in the valence band gives the local DOS information while ELS gives the features above the Fermi level along with the characteristic plasmon losses. So for the present study AES and ELS are the complementary techniques. Electron impact autoionization transition is a special spectral feature in transition metals and may be considered as a part of Auger electron spectroscopy. A brief introduction of these techniques is given below, as a preview to the spectral interpretations made for the results and relavant discussion. An explanation of XPS is also presented for some of the interpretations based on our XPS results. Basic principles[61,62] of these techniques are shown in FIG.2.6.

2.4.1. Auger electron spectroscopy

For surface analysis Auger electron spectroscopy is widely used because of its short mean free path and information depth. It is a three level electronic transition process that occurs when an atom is excited by an external source. Out of the three levels, if the final two holes are created in the same orbital, due to the Auger process then it is called Coster Kronig transition. If all the three levels participating in the Auger process are in the same orbital, the process is called Super Coster Kronig (SCK) process. Their detection therefore provides a surface sensitive probe of chemical composition both qualitatively and quantitatively. In Auger peaks, three parameters are important for the characterization of

the materials, the energy value of the transition, the peak intensity and the peak lineshape .

The kinetic energy of the Auger electron $E_{kvv'}$ for three levels , k, v and v' is given by[61],

$$E_{kvv'} = E_k - E_v - E_{v'} - U_{vv'}$$

where $U_{vv'}$ is the hole-hole interaction energy between the final state holes. The Auger energy thus depends on the binding energies of the three levels associated in the Auger process and hence it is characteristic of the element. Any shift of energy levels, due to charge transfer in a reaction, creates a different energy value for Auger transition and is observed as an Auger chemical shift. The magnitude of Auger chemical shift is, in general, significantly greater than the photoelectron chemical shift since three energy levels are involved. The kinetic energy change between chemical states is given by,

$$\Delta E(KLL) = 3\Delta R(K^+) - \Delta\varepsilon(K),$$

where $\Delta\varepsilon(K)$ is 1s energy change and $\Delta R(K^+)$ is the change in the relaxation energy due to chemical interaction in the final singly ionized state[62].Thus chemical interaction to some extent can be identified from the Auger energy shift, though it is complicated by the final states of transitions. For quantitative analysis the intensity of Auger transition is important. A comprehensive discussion on quantification is given by several authors which show its complicacy and limitations[63-67].

Particularly valence band related Auger transition is strongly influenced by the chemical interaction involved in any electron transfer process. The lineshape analysis or the Auger finger printing study of materials these days finds lot of interest both in experimental and

theoretical research. In the lineshape, the DOS and the localization of the final state is reflected. Hence all lineshape analyses start with the determination of one electron DOS. So it is important to carefully observe[45] the intensity of deconvoluted peaks, width of peaks and satellites. The lineshape derives contributions from the DOS, different dynamic losses of electrons and other correlation effects. With the development of instrumentation, computer software and theoretical explanation and variation effects like localization behaviour, charge transfer, polarization etc., Auger lineshapes are now possible to be understood quite well. In the lineshape analysis, multiplet splitting is one of the most important parameters in explaining the fine structure. It can be explined in terms of L-S coupling of two hole final state left in an atom near the surface after the emission of an Auger electron. Particularly in case of transition metals the multiplet splitting is the result of the incomplete d shell which induces some Coulomb interaction. It is observed that in case of compounds the amplitude of splitting is a direct function of the ionicity of any compound and the number of unpaired electrons in the d shell[68] Thus it is possible to get information on electronic phenomena and this motivates the interpretation of Auger lineshapes.

Related to the lineshape analysis, Si LVV lineshape is of one of the special interest for the present study. The Si LVV lineshape is associated with three types of of final state valence band Auger transition : two p holes , one s hole and one p hole or two s holes known as the pp, sp and ss types, respectively. These three contributions are not equal owing to the surface effects or delocalization of 3s orbitals in the presence of core holes. So an irregular lineshape convoluted with these three contributions is

observed in general. Jennison[69] indicated, about the dissimilar transition intensity of the three transitions as that, the bonding charge must be excluded from the total charge because Auger process samples the charge local to the atom with the core hole. This reduces, the ss and sp contributions because s orbitals are very diffuse in nature. Sometimes it is thought that the surface effect is the cause for the dominating pp contribution. As Si surface contains mostly p dangling bonds, the surface states of p electrons contribute more than the s related transitons. On the other hand, arguments are made suggesting the dynamic screening effect that arises from the orthogonality of the initial and final state orbitals that result due to the initial core hole and final no core hole state. The non orthogonality introduces the shake-up satellites. The final state shake-off has effect of redistribution on the Auger intensity over a wide range which reduces some of the components in the overall distribution. Of course the diffusion of 3s orbitals in the ground state Si, contract in the presence of a core hole, which causes the reduction in the ss and sp Auger transitions.

A theoretical expession for generating KVV term is generally given by[70],

$$I_{KVV}(E) = B \sum_{ll'} [p_{kll'} R_l R_{l'} A(E + \delta\lambda\lambda', \Delta U_{\lambda\lambda'}, \rho_l, \rho_{l'})]$$

here A is Cini-Sawatzky function[71-73]. B is the normalization factor, and ρ's and $p_{kll'}$'s are core hole screening factors, and atomic Auger matrix element respectively. ΔU is the correlation parameter. In the equation, the different components in A make the total theoretical KVV lineshape as the sum of components with each ll' component (e.g. ss, sp and pp)

having an energy shift, $\delta_{\lambda\lambda'}$ and a hole -hole correlation parameter ΔU and with each component derived from a fold of the ρ_l and $\rho_{l'}$ DOS (e.g. s or p). These parameters are chosen to give the optimal agreement with the experimental results.

2.4.2. Reflected electron energy loss spectroscopy : (also called slow electron energy loss spectroscopy):

In the electronic excitation spectrum of solids, inelastic electron scattering experiments are very useful because of the range of accessible energies. Inelastic neutron scattering is powerful in the low energy range while inelastic x-ray scattering is useful for high energy transfer. In the intermediate range, the inelastic scattering of electrons is the most useful technique for electronic structure study of the metal surfaces. In the process of inelastic scattering the primary electron can lose energy in various processes. The smallest energy loss is due to the excitation of the latice vibration or creation of phonon, called phonon-losses.The order of this loss is in the meV range. High- resolution EELS is used to observe phonon losses to get information about lattice vibrations which is characteristic of the materials . The electron may excite the cloud of free electrons causing its oscillation either in the bulk or in the surface. The loss due to this inelastic scattering is called plasmon loss. The loss due to two dimensional excitation of the electron group is called surface plasmon loss and the same in three dimensions is called bulk plasmon loss. The energy loss to bulk plasmon is[74],

$$\hbar\omega_b = n(ne^2/\mathcal{E}_o m)^{1/2},$$

where n is the density of electrons of mass m, and charge e, and $\mathcal{E}_o$ is the permitivity of the medium.

The loss due to surface plasmon,

$$\hbar\omega_s = \hbar\omega_b / 2^{1/2},$$

The primary electron may use energy to excite shallow core level electrons to some empty states in the valence band or in the conduction band. The plasmon losses given above is derived form the free electron model of the electron gas where n is the free electron density and thus can be used to estimate the electron density in the solid. In case of some transition metals, mostly refractory metals, the free electron model does not hold good strictly. So the surface plasmon and bulk plasmons do not show the regular relation given above. The most important feature in these materials is that they show double plasmon losses for both volume and surface plasmons. This is attributed to the bcc nature of these solids[74] where the "lower plasmons" are of special interest and attention.

The inelastic scattering in the ELS is best described by the 'dielectric theory'[75]. Here the solid is associated with a characteristic dielectric constant $\varepsilon(q,\omega) = \varepsilon_1(q,\omega) + i\varepsilon_2(q,\omega)$, a function of wave vector q and frequency ω. In this model the Coulomb field of the scattering electrons interacts with electron gas in solid via a dipole field. The polarization field due to this interaction damps the motion of the electrons. Thus with the bulk of the dielectric (which is the characteristic of the solid) the amplitude of the field of electron is screened by a factor

$1/\varepsilon$ and the intensity by a factor $1/|\varepsilon|^2$. Obviously when the electron is moving in the dielectic, the damping is proportional to ε_2.

$$\omega_b(q,\omega) = -\mathrm{Im}\ \{1/\varepsilon\}.$$

For reflection, which gives the surface information the field is screened by a factor $1/(1+\varepsilon)$by the polarization field. And the loss is proportional to,

$$\omega_s(q,\omega) = \mathrm{Im}\ \{1/(1+\varepsilon)\}.$$

2.4.3. X-ray photoelectron spectroscopy :

All x-ray bombardment of solid surfaces give rise to the photoelectron emission according to the energy conservation relation,

$$E_k = h\nu - E_b - \phi$$

where E_k is the measured kinetic energy, $h\nu$ is the exciting photon energy, E_b is the binding energy of the electrons in the solid and ϕ is the analyser work function. For a standard x-ray spectrometer Mg K_α or Al K $_\alpha$ lines are used as the x-ray sources with energies 1253.6 and 1486.6 eV and natural line width of 0.7 and 0.85 eV respectively.

Like AES, the most important use of x-ray is to get a qualitative and quantitave analysis of surface composition[64]. Because the binding energy is measured in XPS, the chemical bonding state can be determined. Different valence states in compounds can be recognised by the chemical shift values and peak width changes. The valence band structure can also be detected by XPS if the energy resolution is sufficient, as by using monochromatized X-rays.

The intensity is directly related to the quantity of the element present on the surface. The quantification by XPS is more reliable than

AES, because of the following reasons : a) photoionization cross sections are well known, b) the peak intensities are not influenced by the back scattered electrons as in AES, c) the background is lower and easier to substract.

The lineshape deals with a lot of factors that happens in the process of photoelectric effect. It is influenced by the surface effects, the satellites and the ghosts of X-ray, multiplet splitting effect or the shake-up or shake-off satellite effects. The peak width is also one of the important parameters in the characterization of the X-ray induced peaks. It is directly proportionlal to the width of the level from which the photoelectrons are coming. However the width of the x-ray line and the resolution of the spectrometer matter in the width of the peak. The full width at half maxima is given by ,

$$\Delta E = (\Delta E_n{}^2 + \Delta E_p{}^2 + \Delta E_a{}^2)^{1/2}$$

where ΔE_n is the natural width of core level, ΔE_p is the width of photon source and ΔE_a is the analyser resolution. So to monitor the peak width for the understanding of the material characteristics a monochromatized x-ray beam is prefered[62].

The chemical shift in XPS, which is the most immediate quantity measured for chemical interaction, comes from initial state effects[61] and final state relaxation effects[62]. The initial state effect contributes mostly in the chemical shift phenomenon, which happens due to change in the electronic environment of the atom after chemical interaction. However the chemical shift and peak width change contribution arise due to effect of the core hole in the surrounding electrons, both intra-atomic and extra-atomic level is relaxation effects.

2.4.4. Autoionization process :

Electronic states of atoms or molecules are classified as belonging to various configurations. The effect of configuration interaction are particularly conspicious at energy levels above the lowest ionization threshold where states of different configurations coincide in energy exactly, since at least some of them belong to the continuous spectrum. The mixing of a configuration belonging to continuous spectrum configurations gives rise to the phenomenon of autoionization. The exact coincidence of energy of different configurations makes the ordinary perturbation theory inadequate, so that special procedures are required for the treatment of autoionization[76]. Thus autoionization can be defined as the de-excitation of an excited atom by the emission of an Auger like electron and is therefore associated with the atomic spectra studies. The radiation-less transiton because of the autoionization , particularly shown by the unfilled d electrons is a special probe to understand the above Fermi level electronic states before or after the chemical interaction.

Principally, (FIG.2.7) when a primary electron impacts with an atom, it can loose energy by exciting a core electron of the target of unfilled d transition metals. The process of excitation leaves two cases[77]. In the first case, the core electron is knocked out and the consequent de-excitation process gives the Super Coster Kronig (SCK) transition (from the same electronic level),

$$Np^6Nd^n \text{ ------------- } Np^5Nd^n + \xi_r$$

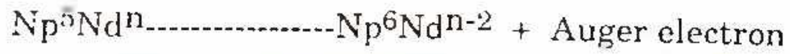

$$Np^5Nd^n \text{-----------------} Np^6Nd^{n-2} + \text{Auger electron}$$

when ξ_f denotes the electron emitted into the continuum. So in this relaxation process the atom is in the doubly ionised final state. In the other way of excitation, the p electrons are excited to some empty states above the Fermi level depending on the availability of the empty states in the d band. In this process,

$$Np^6Nd^n \text{-----------------------} Np^5Nd^{n+1}$$

$$Np^5Nd^{n+1} \text{--------------------} Np^6Nd^{n-1} + \xi_f$$

This ξ_f emitted electron is called the autoinization electron. Thus in the process of autoionization, the atom is singly ionised.

The process of autoionization is also understood by the model proposed by Penn in his work[78] for the resonant photoemission on Ni. He proposed a shake up process which involves the excitation of two-hole virtual bound states involving correlated d holes which resonantly interact with 3p--empty d-state transition at the threshold. However the importance of the core level photoexcitation in producing a resonance in the satellite was pointed out by Guillot et al[79]. In both absorption of synchrotron radiation and inelastic scattering electrons the transition from 3p to empty 3d levels , Dietz et al.[80] suggested that the interference lineshape is due to the 3p-3d excitation and the process where by a 3d electron is excited to the continuum. Thus several atomic models are available to explain the resonance photoemission in the synchrotron photoemission or the electron absorption.

According to Hirst[81], for 3d transition metals the Coulomb correlation energy U_{eff} between 3d electrons is responsible for the localization. For such a localized state the energy eigen values depends on

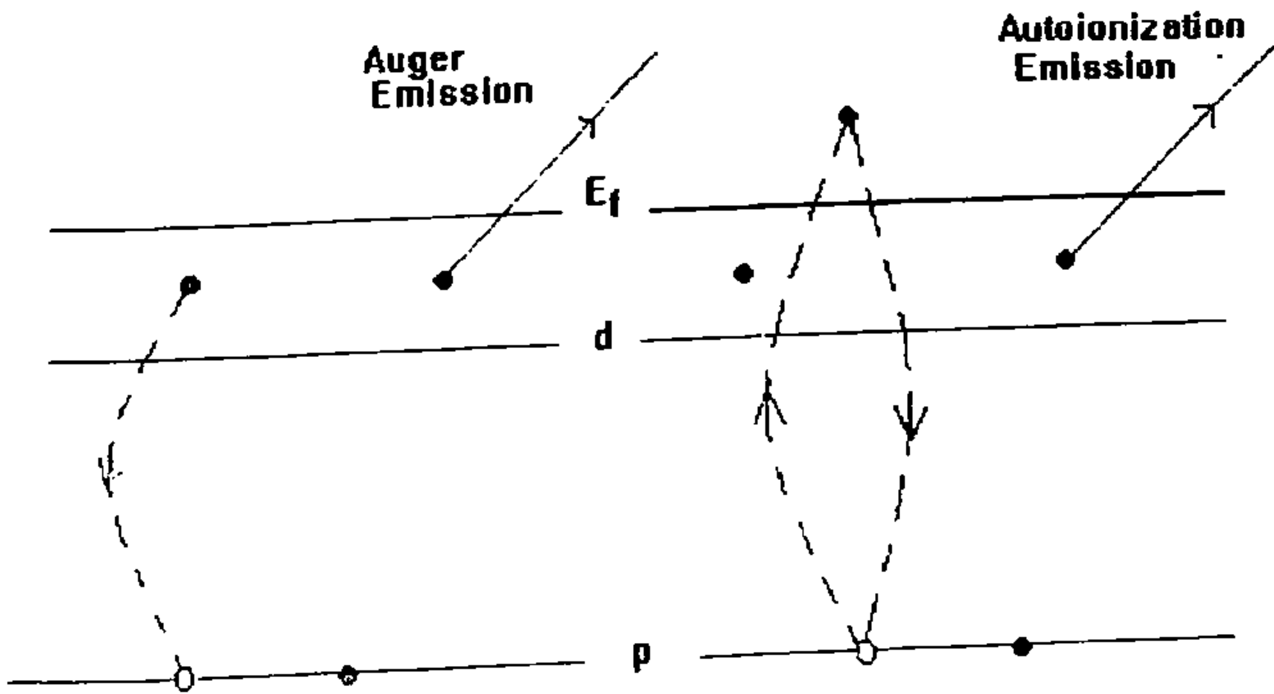

Fig.2.7 : Schematic of Auger and autoionization emissions.

the occupancy of the 3d band. Since p-d transition is a very fast process, all the possible final states of the d^{n+1} state under the influence of 3p core hole appear in the spectrum. According to Fano[76] the detailed shape of such excitation spectrum is determined by resonant interaction between different d^{n+1} discrete configurations and the continuum levels. In the model calculations dealing particularly with 3d transition metals series, Davis and Feldkamp[82] have ascribed the success of the atomic treatment in reproducing the solid state results to the strong perturbation of the open and narrow 3d band width. Autoionization emission associated with recombination of the resonant p--d transition have been examined by Zajac et al[77]. for the 3d transiton metal series. They showed that the intensity of the emission decreases with increase in the Z and the separation of the emission peak from the 3p threshold is large towards the beginning of the series (Sc---Cu) and abruptly drops towards the middle of the series. An explanation of this trend is available in the work of Davis and Feldkamp[82] as mentioned earlier. For low z elements low spin coupling was invoked which gave a very broad distribution of multiplet term of Cr. For higher z values high spin coupling was invoked. The resonant photoemission work of the 3d transition metals gives the same conclusions as obtained from the electrom impact autoionization process. The resonant photoemission for Ni is studied extensively and for Ni and Cu two hole satellites quiet clearly play an important role in the photoemission spectra as well. Resonant photoemission for Mn has been shown by Brhun et al[83] and it is shown that at 40 to 56 eV it shows the resonance. The resonance is interpreted in terms of the strong coupling of between 3p and 3d excitation levels. The electron impact autoionization

process for V, Zr, Nb, Mo and Ta is shown by Cornaz et. al[84] along with the SCK transiton and the process is explained in terms of different principal quantum numbers. The studies on compounds of transition metals have generated interest in finding the autoionization feature or resonant electron emission process in oxides and silicide of different transition metals like Ti. In Mo, Ta, Cr along with their oxides and silicides.

2.5. Conclusions :

Surface spectroscopic response of materials is different for different techniques and the complementary nature of these responses helps in modeling systems. Photoelectrons of materials gives the chemical information and valence band features at the different stages of reaction. Plasmon loss structure in Energy Loss study, or multiplet splitting in the Auger electron study of metals and Auger lineshapes are found to yield information on changes due to silicidation and oxidation. So our aim is to explore in these regions to obtain more information, or to establish earlier concepts. Another interesting property is autoionization. An unfilled transition metal undergoes such transitions as soon as it is bombarded with electron beam. So behaviour of autoionization transitions due to oxidation or silicidation of transition metals provides a good probe, both for scientific and technological applications. The above discussed techniques are found to be useful in our studies of silicidation and oxidation of Ti, Ta, Mo and Cu etc.

References :

1] S.P. Murarka, Silicides for VLSI Applications, Academic Press, Orlando, NY, 1983.

2] S. P. Murarka, J. Vac. Sci. Technol. 17, (1980)775.

3] W.B. Pearson, A Hand Book of Lattice Specings and Structure of Metals and Alloys. Vol.2 Pergamon, London, (1967).

4] G.V. Samsonov and I.M. Vinitskii, Hand Book of Refractory Compounds, IFI, Pienum NY, (1980).

5] C.N.R. Rao, D.D. Sarma, S. Vasudevan and M.S. Hegde, Proc. R. Soc. Lond. A 367 (1979) 239.

6] W.D. Buckley and S.C. Moss, Solid State Electron. 15 (1972) 15.

7] W.K. Chu, S.S. Lau, J.W. Mayer, H. Muller and K.N. Tu, Thin Solid Films, 25 (1975) 393.

8] A.H. Reader, A.H. van Ommen, P.J.W. Weijs, R.A.M. Wolters and D.J. Oostra, Rep. Prog. Phys. 56 (1992) 1397.

9] K.N. Tu, Appl. Phys. Lett. 27 (1975) 221.

10] K.R. Lawless, Rep. Prog. Phys. 37 (1974) 231.

11] L.H. Germer and J.W. May, Surf. Sci. 4 (1966) 452.

12] R.L. Park and H.E. Fransworth, 40 (1964) 2354.

13] L.B. Garmon and K.R. Lawless, J. Chem. Phys. (1969) Int. Cent. Nat. Res. Sci. No. 187 (1969) 61.

14] C.S. Fadley, Nucl. Instrum. and Methods (Netherlands) 177 (1980) 207.

15] M.A.H. Lanyon and B.M.W. Trapnell, Proc. R. Soc. A 227 (1955) 387.

16] J.W. May, Surf. Sci. 18 (1969) 431.

17] S. Inove, N. Toyokura, T. Nakamura, A. Ishikwa, Semiconductor--Si 1981", Electrochemical Soc. Princeton, New Jersey, 1981 , 596. J. Electrochem. Soc. 128 (1981) 128.

18] S. *Kritzinger and* K.N. *Tu*, J. Appl. Phys. 37 (1980) 205.

19] S.S. Lau, C.Canali, Z.L. Liau, K. Nakamura, M-A. Nicolet and J.W. Mayer, Appl. Phys. Lett. 28 (1970) 148.

20] H. Ishiwara, S.Saitosh and K.Hikosaka, Jap.J. Appl. Phys. 20 (1981) 843.

21] E.W. Maby, G.W. Geis, Y.L.. Lecoz, D.J. Silversmith, R.W. Mountain and Autoniadis, IEEE Electron. Dev. Lett. 2 (1981) 241.

22] G.V. Steene, M.Jardiner-Offergeldav and F. Bouillon, Surf. Interf. Anal. 11 (1988) 599.

23] A. Hiraki, J. Electrochemical Soc. 127 (1980) 2262.

24] I. Abbati, L. Braicovich, B. De Michelis, U del Pennino and S. Valeri, Solid State Comm. 43 (1982) 199.

25] R. Bultz, G.W. Rubloff, T.Y. Tan and P.S. Ho, Phys. Rev. B 30 (1984)5421.

26] E.J. Von Leonen, A.E. M.J. Fischer and J. F. Van der Veen, Surf. Sci. 155 (1985) 65.

27] R. N. Tromp, E.J. Van Leonen, M.Iwami, R.G. Smeenk, F.W. Saris, F. Nava and G. Ottaviani, Surf. Sci. 124 (1983)1.

28] G. Rossi, I.Abbati, L. Braicovich, I. Lindau and W.E. Spicer, Phys. Rev. B 25 (1982) 3627.

29] C. Pirri, J.C. Peruchetti, G.G. Ewinner and J. Derrien, Phys. Rev. B 29 (1984) 3391.

30] K.N. Tu, J.F. Jiegler, C.J. Kirchner, Appl. Phys. Lett. 23 (1973) 493.

31] A. Franciosi, D.J. Peterman and J.W. Weaver, J. Vac. Sci. Technol. 19 (1981) 657.

32] J. Stohr, R. Jaeger, G. Rossi, T. Kendelewicz and I. Lindau, Surf. Sci. 134 (1983) 813.

33] J. Derrien, G. Le Ley and I. Salvan, J. Physique 39 (1978) L287.

34] A. Hiraki, A. shimizu, M. Iwami, T. Narasawa and S. Kaniya, Appl. Phys. Letts. 36, (1980) 205.

35] A. Hiraki, Surf. Sci. Rep. (1984) 358.

36] L. Braicovich, C.M. Garner, P.R. Skeath, C.Y. Su, P.W. Chye, I.Lindau, and W.E. Spicer, J. Vac. Sci. Technol. 17 (1980)930.

37] I. Abbati, L. Braicovich, A. Franciosi, Solid State Comm.33 (1980) 881.

38] G. Rossi, L. Lindau, Phys. Rev.B 28 (1983) 3597.

39] T. Umezawa and H. Suzuki, Appl. Surf. Sci. 70/71 (1993) 419.

40] H.T. Anyele, S.A. Ding, L.W. Lu and J. Zhou, Appl. Surf. Sci. 70/71 (1993) 332.

41] G.Molnar, G.Peto, E.Zsoldos, Appl. Surf. Sci 70/71 (1993) 466.

42] J.-Y. Venillen, D.B.B. Lollman, T.A. Nguyen Tan and L. Magand, 65/66 (1993) 712.

43] J.A. Roth and C.R. Crowell, J. Vac. Sci. Technol. 15 (1978) 1317.

44] S.D. Bader, L. Richter, M. Brodsky, W.E. Brower and G.V. Smith, Solid State Comm. 37 (1981) 729.

45] D.E. Ramaker, Crit. Rev. in Solid State & Mat. Sci. 17 (1991) 211.

46] J.M. Gallego, J.M. Garcia, J.E. Orlega, A.L. Vazquez de Parga, J. de la Figuera, C. Ocal and R. Miranda, Surf. Sci. 269/270 (1992) 1016.

47] M. Iwami, S. Hashimoto and A. Hiraki, Solid State Com. 49 (1985) 459.

48] J. Vahakangas, Y.U. Idzerda, E.D. Williams and R.L. Park, Phys. Rev. B. 33 (1986) 8716.

49] S. Storp and R. Holm, Surf. Sci. 68 (1977) 10.

50] P. H. Holloway and J.B. Hudson, Surf. Sci. 43 (1974) 123.

51] P. H. Holloway and J.B. Hudson, Surf. Sci. 43 (1974) 141.

52] P. H. Holloway and J.B. Hudson, Surf. Sci. 33 (1972) 56.

53] J.L. Gland, B. Sexton and G.B. Fisher, Surf. Sci. 95 (1980) 587.

54] D. Schmeisser, K. Jacobi and D.M. Kolb, App. Surf. Sci. 11/12 (1982) 164.

55] R. Weißmann, Solid State Comm. 31 (1979) 347.

56] Graciela Brizuela, Norberto Castellani and Mirta Puentes, Surf. Interface. Anal. 18 (1992) 784.

57] T.A. Nguyen Tan, M. Azizan ans J. Derrien, J. Vac. Sci. Technol. A 5 (1987) 1412.

58] F. Ringeisen, M. Alaoui, D. Bolmont ans J.J. Koulmann, Appl. Surf. Sci. 62 (1992) 167.

59] C.S. Fadley, S. Kono, J.T. Lloyd and K.A. Thompson, Proc. ICSS -4 and ECOSS -3, Cannes (1980).

60] S.P. Murarka, J. Vac. Sci. Technol. 17 (1980) 775.

61] D.P. Woodruff and T.A. Delchar, Modern Techniques in Surface Science, Cambridge Solid State Science Series, Cambridge Univ. Press (1986).

62] Practical Surface Analysis, Ed. Brigs and Seah, John Wiely & Sons Ltd. (1987).

63] M.P. Seah, M.W. Holbourn, J. Elec. Spec. Rel. Phenon. 42 (1987) 255.

64] S. Hofmann, Surf. Interface Anal. 9 (1986) 3.

65] Hand Book on Auger Electron Spectroscopy (2nd Ed). Edited by, L.E. Davis, N.C. MacDonald, P.W. Palmberg, G.E. Riach and R.E. Weber. (Physical Electronics Industries)

66] P.M. Hall and J.M. Morabito, Surf. Sci. 83 (1979) 391.

67] Th. Writh, Surf. Interface Anal. 18 (1992) 3.

68] L. Fiermans, R. Hoogewijs and J. Vennik, Surf. Sci. 47 (1975) 1

69] D.R. Jennison, Phys. Rev. Letts. 40 (1978) 807.

70] F.L. Hutson, D.E. Ramaker, J. Chem. Phys. 87, (1987) 6824.

71] M. Cini, Solid State Comm. 20 (1976) 605.

72] G.A. Sawatzky, Phys. Rev. Letts. 39 (1977) 504.

73] G.A. Sawatzky and A. Lenselink, Phys. Rev. B, 21 (1980) 1790.

74] M. Prutton, Surface Physics (2nd. Edision) Oxford Physics Series, Oxford Univ. Press (1985).

75] H. Froitzheim, Topics in Current Physics, Springer- Verlag Series (4) (1977) 205.

76] U. Fano, Phys. Rev. 124, 6 (1961) 1866.

77] G. Zajac, S.D. Bader, A.J. Arko and J. Zak, Phys. Rev. B. 29 (1984) 5491.

78] D.R. Penn, Phys. Rev. Letts. 42 (1979) 921.

79] C. Guillot, Y. Ballu, J.Paigne, J. Lecante, K.P. Jain, P.Thiry, R. Pinchaux, Y. Petroff and L.M. Falicov, Phys. Rev. Letts. 39 (1977) 1632.

80] R.E. Dietz, E.G. McRae, Y. Yafet and C.W. Caldwell, Phys. Rev. Letts. 33 (1974) 1372.

81] L.L. Horst, Proc. of 20 th. Annual Conf. on Magnetic Mats. AIP Conf. Proc. No. 24, Ed. C.G. Graham, jr., G.H. Lander and J.J. Rhyne, NY (1975) 11.

82] L.C. David and L.A. Feldkamp, Solid state Comm. (1979) 413.

83] R. Bruhn, E. Schmidt, H. Schroder and B. Sonntag, Phys. Letts. 90A (1982) 41.

84] A. Cornaz, M.Erbudak, P.Aebi, F. Stucki and F. Vanini, Phys.Rev B 35 (1987) 3062.

Chapter III
Experimental

3. Introduction :

This chapter is aimed at providing the experimental details adopted in sample preparation and their analysis. The samples are prepared ex-situ in an UHV deposition system and are analysed by two different UHV set ups with different techniques. In the system with CMA (cylindrical mirror analyser) the analysis by AES and ELS are done. XPS experiments are performed by the system with a SCA (spherical capacitor analyser). Some details of the analysis chambers, analysers, and aspects of standardizing the systems are given here. The limitations of the techniques adopted and their probable solutions are mentioned at the end of the chapter.

3.1. Need for an UHV environment :

The special kind of defect in solid, the surface, needs some special arrangement for studying at an atomic level. As surface itself means few top atomic layers, so an ideal condition of free surface is required for probing the surface. Any surface in atmosphere is basically covered with atmospheric gas molecules, along with some other atmospheric contaminants. So to get an actual probe in the surface or clean deposition, one needs surface in an airless medium. From calculations the rate of gas molecules arriving per unit $cm.^2$ per s on a surface [1],

$$r =- 3.51X10^{22} P/(TM)^{1/2}$$

Auger Electron Spectroscopy System

X-ray Photoelectron Spectroscopy System

where P= pressure in torr and T the temperature in k and M is the atomic mass unit of gas molecules. For N_2, the arrival rate is calculated to be $3.88X10^{20}$ molecules/cm^2s. at 293K at 1 torr pressure. If a single atomic layer consists of 10^{15} to $2X10^{15}$ atoms/cm^2, assuming the molecules which are colliding the surface are sticking on the surface (Sticking coefficient =1). calculations give that for an experimental time of 1 hr requires a pressure of 10^{-10} torr or better for surface analysis without the atmospheric particles affecting the results. It is true, that many development in experimental surface science would not have been possible if UHV production were not available. The requirement of UHV for surface analysis thus makes a surface analytical equipment complicated, gigantic and expensive.

It is observed that simply UHV condition is not sufficient for getting a completely contamination free surface. So insitu surface cleaning is an integral part of surface analytical studies.

Several processes are developed for getting a contaminant free surface[1]. For intrinsically clean surface, cleaving in UHV is one of the best techniques. But this needs a cleavage face of the materials which limits its application. In-situ chemical processing is sometimes used to get a clean surface, but it needs thermal energy to vibrate out the chemically formed loosely bound compounds from the surface. Surface cleaning by heating or/and sputtering is the most widely used technique. In our analysis surface cleaning is done by Ar ion sputtering. Ar sputtering is an efficient technique. But it may cause structural damage[2] even at very low beam energies and sometimes induce chemical bonding[3] of the surface with the

contaminants. Details of the cleaning procedure followed for our experiments is given in Chapter 4, sectionA.

3.2. Sample preparation :

The samples for silicides and oxides were prepared in an UHV electron beam evaporation chamber. Thin films of the metal under study are deposited on a clean Si surface, and then annealed in inert or oxygen atmosphere to get the respective silicide or oxide. A brief description of the preparation of these two types of materials is given below :

3.2.1. Silicide preparation

All the thin film samples used in the present study were prepared in an oil free Varian 118A thin film deposition system. The preparation chamber 18" in diameter is of stainless steel (FIG.3.1) with Meander type water cooling arrangement. Rough pumping of the chamber is done by three sorption pumping units and the final base pressure of 10^{-9} torr is obtained by seven triode ion pumps of 110 l/s each. The chamber has a Ferrofluid rotating feedthrough to accomodate a planatery substrate holder of stainless steel in which 12 wafers of 2" dia can be loaded at one time (FIG.3.1). There are two electron guns of 10 KW each with a water cooled hearth of 40 cc crucible. The thickness of the film is measured in-situ by a quartz crystal thickness monitor fitted with an Inficon XTC process controller. The pressure in the chamber is measured by 890 AR Varian ionization gauge of Bayard-Alpert type.

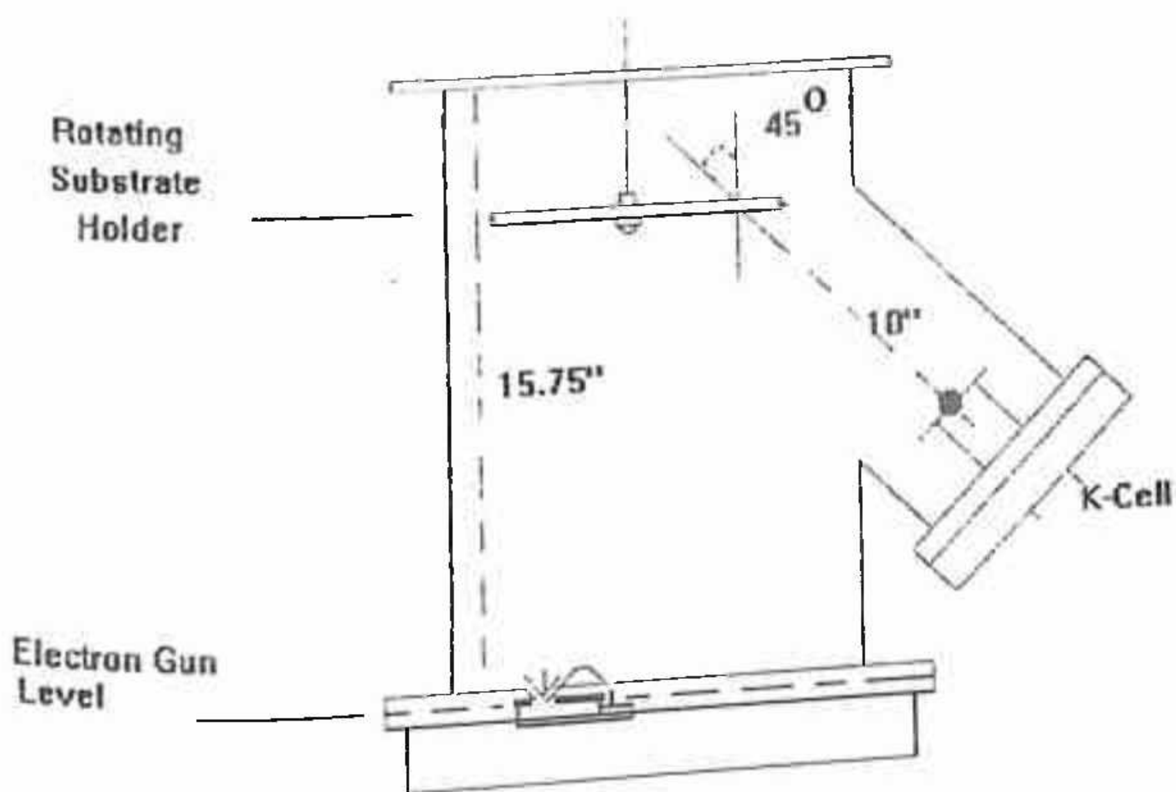

Fig. 3.1 : Schematic diagram of the preparation chamber including electron beam evaporation and effusion cell (Varian 118A).

The substrates used in the experiments were 50 mm dia p type boron doped 3-5 Ω-Cm Si (111) wafer. These were cleaned throughly by RCA cleaning process with a final buffered HF dip for 10s and then rinsed with deionised water (18 MΩ) . The essential steps used in the RCA cleaning process are given below :

i) boil wafer in trichloroethelene (TCE)

ii) clean ultrasonically in TCE

iii) rinse in acetone

iv) boil wafer in acetone

v) clean ultrasonically in acetone

vi) rinse in deionised water

vii) boil in deionised water

viii) boil in $NH_4OH : H_2O_2 : H_2O :: 1 : 1 : 5$ for 10 min.

ix) rinse in hot deionised water

x) boli in $HCl : H_2O_2 : H_2O :: 1 : 1 : 5$ for 10 min.

xi) rinse in hot deionised water

xii) dip 10 sec in buffer HF

xiii) rinse in deionised water

xiv) blow in dry N_2.

xv) load immediately in vacuum system.

The Ti layer was deposited by electron beam evaporation process at the rate of 5 Å /s to a thickness of 400Å at an ambient temperature (30°c). The base pressure was $4x10^{-9}$ torr, and $5X10^{-8}$ torr during deposition. A thin cap layer of Si (100Å) was deposited on the predeposited Ti, to prevent the oxidation of Ti layer when exposed to atmosphere. Mo was deposited similarly by electron beam evaporation process at a rate of 3Å/s

upto a thickness of 1000Å . Cu was evaporated from a Knudsen cell at a cell temperature of 1360°C, with an accuracy of ±0.1°C. In the present case the samples were subjected to silicidation in a diffusion furnace (Tempress model : Omega Junior --I). The quartz wafer boat carrying the samples was pushed into the hot central zone of the furnace at 800°C for 30 min for $TiSi_2$, 850°C for 30 min for $MoSi_2$ and 500°C for 30 min for $CuSi_2$ formation. For Ti and Cu silicidation, the ambient in the furnace was pure Ar gas and in case of Mo silicidation pure N_2 was used. The $TaSi_2$ sample was prepared by co-deposition of Ta and Si on Si (111) substrate and then the sample was annealed upto 900°C for 30 min and was supplied by Von Crigern and Co. of Germany. By Auger analysis, the stoichiometry and the sample cleanliness were examined. Some of the details are discussed in Chapter 4.

3.2.2. Oxide preparation

Oxides are prepared by annealing the metal films, or directly the respective metal sheets, in an oxygen atmosphere. TiO_2 was prepared by annealing the 1000Å metal film at 750°C for 5min, MoO_3 was prepared by annealing a Mo sheet at 450°C for 30 min and CuO was prepared by annealing a 1000Å Cu film at 700°C for 30 min. Ta_2O_5 was prepared by annealing the Ta sheet at 650°C for 10 min. The quality of the sample and the chemical state of the compound formed is checked by Auger and XPS studies.

3.3. Analysis :

For AES and ELS the electrons are collected with a suitable arrangement of Cylindrical Mirror Analyser (CMA). In case of X-ray, excitation of the surface, the photoelectrons are collected by a Spherical Capacitor Analyser (SCA).

Thus a surface analytical equipment typically contains a particle source, to bombard the sample surface, a manipulator to provide proper positioning for the sample of interest and a secondary electron analyser in UHV, with some cleaning arrangement. Here we distinguish two different techniques according to the analyser used in this work.

3.3.1. Apparatus for AES, ELS and autoionization study

The model 981-2001 of Varian, consists of an UHV chamber (VT-112) made of 304 non-magnetic stainless steel. It provides a ultrahigh purity environment ($1x10^{-10}$ torr) and a high degree of versatility for surface analyses like Auger electron spectroscopy (AES), low energy electron diffraction (LEED) and electron energy loss spectroscopy (EELS) (see FIG.3.2).

The rough pumping of the system is done by a pair of sorption pumps which can pump out the major constituents of air (O_2 and N_2) by physically trapping them in the molecular-seives at liquid nitrogen temperature to a pressure of 10^{-3} torr. The rough pressure is measured by a thermocouple gauge. Fast and efficient pumping for the active and the noble gases is provided by six 60 l/s triode ion pumps. With a backing pressure of 10^{-3} torr, the ion pumps are activated, which takes the

pressure to below 10^{-8} torr. Once very high vacuum of 10^{-8} torr is achieved, then the whole system is baked at about $150^{O}C$ for 24 hours. The aim of baking the system is to desorb the gas molecules from the chamber walls by providing them thermal energy. Dry nitrogen gas, cooled in liquid nitrogen to condense water vapour, is used for venting the system to minimize H_2O introduction into the chamber from atmosphere. Baking the system for 24 hours can give a final pressure of low 10^{-9} torr pressure. titanium sublimation pumping (TSP) and degassing of all filaments in the chamber provides lower 10^{-10} torr pressure which is suitable for surface analysis. The ultra high vacuum range is measured by an Bayard-Alpert type of nude ionization gauge of model 890-AR C.U. (Varian).

The electron gun in the chamber is mounted concentrically inside the CMA. *A schematic of the overall assembly is shown in FIG.3.2.* A resistance heated tungsten ribbon filament produces maximum beam current irrespective of beam size. The gun is designed to operate at energies from 100 eV to 10 keV, suitable for Auger and energy loss spectroscopic studies. It produces a beam diameter ≤ 5μ at an energy of 3 to 5 keV and with a beam current ≤ 2μA for energies above 5 KeV. Electrostatic deflection gun plates allow the electron beam to be scanned and is used with the scanning sample positioner, allowing sample positioning with a precision of better than 5 μm.

The high precision sample manipulator enables an accurate placement of samples in UHV. It enables 5 degrees of freedom-motion to the sample. It gives a direct rotary motion with a micrometer drive translator mechanism and unlimited rotation. The rotary mechanism has a position resolution of 0.1^{o} with a repeatability of ± 0.1^{o}. The

manipulator is UHV compatible, bakable and mounted from the top of the chamber through edge welded bellows. The manipulator is equipped with a carrousel that is a multiple sample tray and consists of a beam probe to measure beam current. It can accomodate simultaneously 15 samples and provides a 30^{0} angle between the sample normal and the cylindrical mirror analyser axis for efficient secondary electron collection by the CMA. The beam probe is a Faraday cup and can measure the primary electron beam current or the ion beam current, which can be correlated to obtain the sputter rates.

The electron energy analyzer is single pass CMA. Fundamentally, it consists of two co-axial cylinders of different radii. The inner cylinder is generally earthed and the outer cylinder is provided with a negative potential. Thus electrons emitted form the sample surface on the axis of the CMA at an angle a (generally 42^{0}) pass through an aperture in the inner cylinder and those of particular energy, within a band of $E + \Delta E$, are deflected by the outer cylinder potential through another aperture to a focus on the axis , where a channeltron detector is placed. Thus CMA behaves like a second order focussing instrument[4]. The resolution of CMA depends on the slit width and the angular aperture. Relatively wide angular aperture can limit the resolution. The resolution is observed to be ≈0.22% of the collected electron energy i.e. it is able to separate two peaks as close as 2.2 eV at an energy 1000 eV.

The system is provided with an ion gun for dual purpose, in-situ sample cleaning and depth profiling. The accelerating voltage for ion is variable ranging from 0 to 3 kev, and emission current is variable from 0 to 40 mA. The beam can be focused and can be deflected for adjustment in

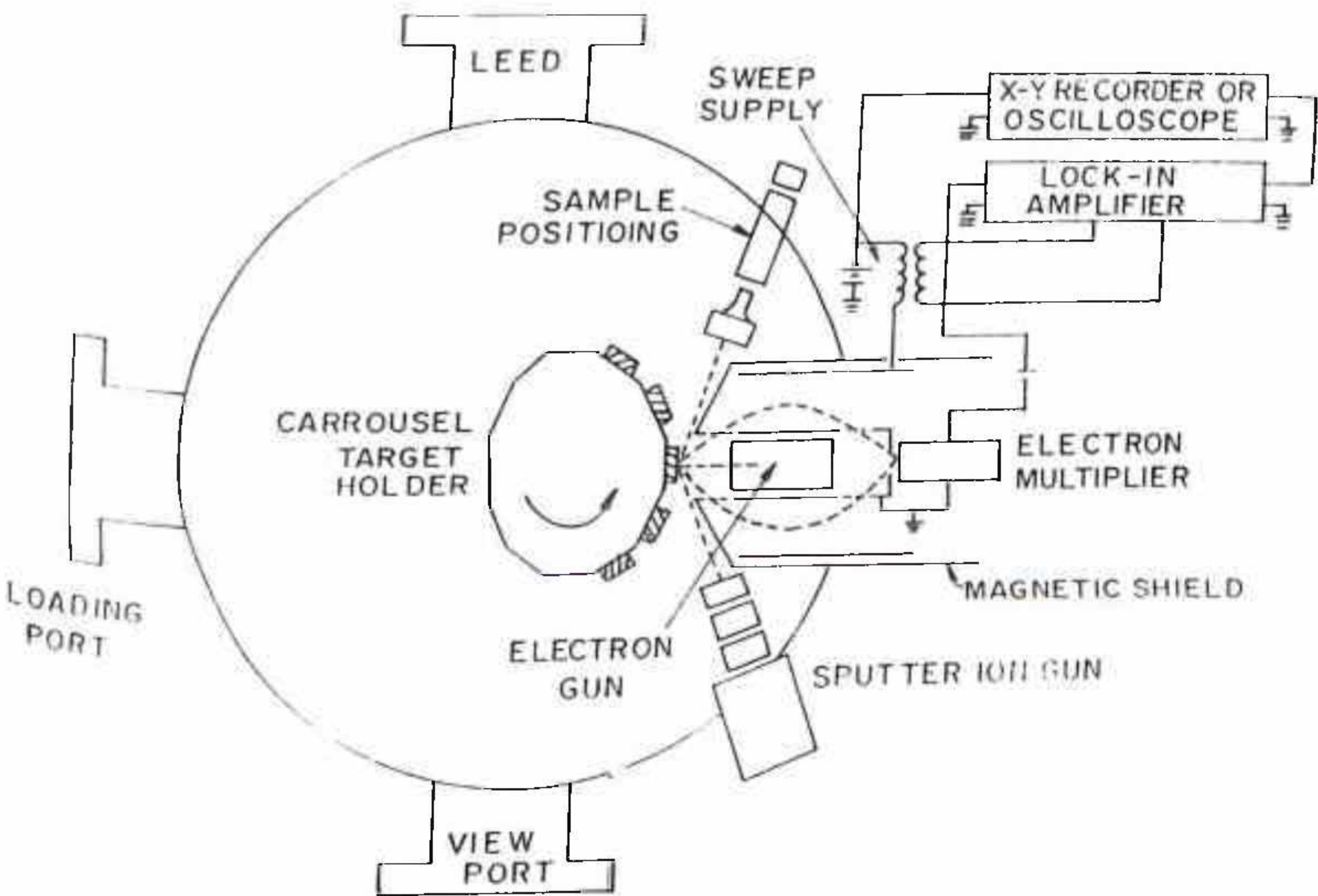

Fig. 3.2 : Schematic of UHV system with CMA used to perform AES EELS and autoionization.

X and Y direction over a range of ± 5mm. Sputter cleaning is done by Ar ion, due to, a) chemical inertness, b) large enough mass to impart momentum transfer and c) low enough ionization potential. The ion gun with optimised current and energy can be used to sputter layers of materials and profile the elemental composition in the depth of the sample. The electrons collected by the detector placed on the axis of the CMA (FIG.3.2) creates a pulse of signal which is preamplified before further modulation. The detection is further made by lock-in-amplifier model 128A of EG & G. The differential mode of signal controller uses 17 kHz reference signal from the phase sensitive detector (lock-in-amplifier) and scale it approximately for input to summing of a Kepco high voltage operational power supply.

The system discussed above is used to collect Auger signal in the differential mode or double derivative mode. In normal mode the intensity of Auger signal is very small in the huge background. So data is collected in the derivative mode which basically plots the gradient of intensity with respect to energy, hence enhances the signal and reduces the background. At this summing point the controller also provides an appropriate ramp voltage, for amplification by the unit, to provide the high voltage potential for the mirror electrode of the cylindrical mirror spectrometer. The electron selected by the spectrometer are detected by the channel electron multiplier (channeltron). A schematic diagram of the signal generation to collection is shown in FIG.3.2.

3.3.1.a System standardization :

The standardization of the instrument is done with a Cu sample. Cu shows two major Auger transitions, at 60 eV and at 920 eV. According to the ASTM (American Society for Testing and Materials)[5] study of standarizing the Auger system, it is observed that the ratio of the these two peaks vary tremendously from instrument to instrument depending on choice of phase or channeltron multiplier voltage or the proper peak to peak modulation voltage for data collection. The ranges of the ratio of the two peaks of Cu, is observed[5] to vary from 0.08 to 5.5 for different instruments, and was obtained with median of 0.8. In FIG.3.3 Auger spectrum obtained for Cu is shown at 10 V peak to peak modulation, from the instrument. The 60eV/920eV peak intensity ratio is ~ 0.77, which tallies well with the standard value. So by Cu AES survey scan, the energy value and the intensity of the spectrum is calibrated.

The resolution of the instrument at 5 V peak to peak modulation condition is shown in FIG.3.4., where the 2 keV elastic peak is shown. The seperation between the positive and negative excursion is 8.8 along the X-axis. The resolution is given by(FIG.3.4),

$$\text{Res.} = \Delta E/E \text{ (Where } \Delta E \text{ is peak to peak separation)}$$

$$= (4.4 /2000).\ 100$$

$$= 0.22\%$$

Usually phase shift occurs between the reference signal and the detected signal due to the setting of the tuned components and various capacitances in the circuit[6], which causes the variation in the intensities in the spectrum. Generally, the phase shift control of the phase sensitive

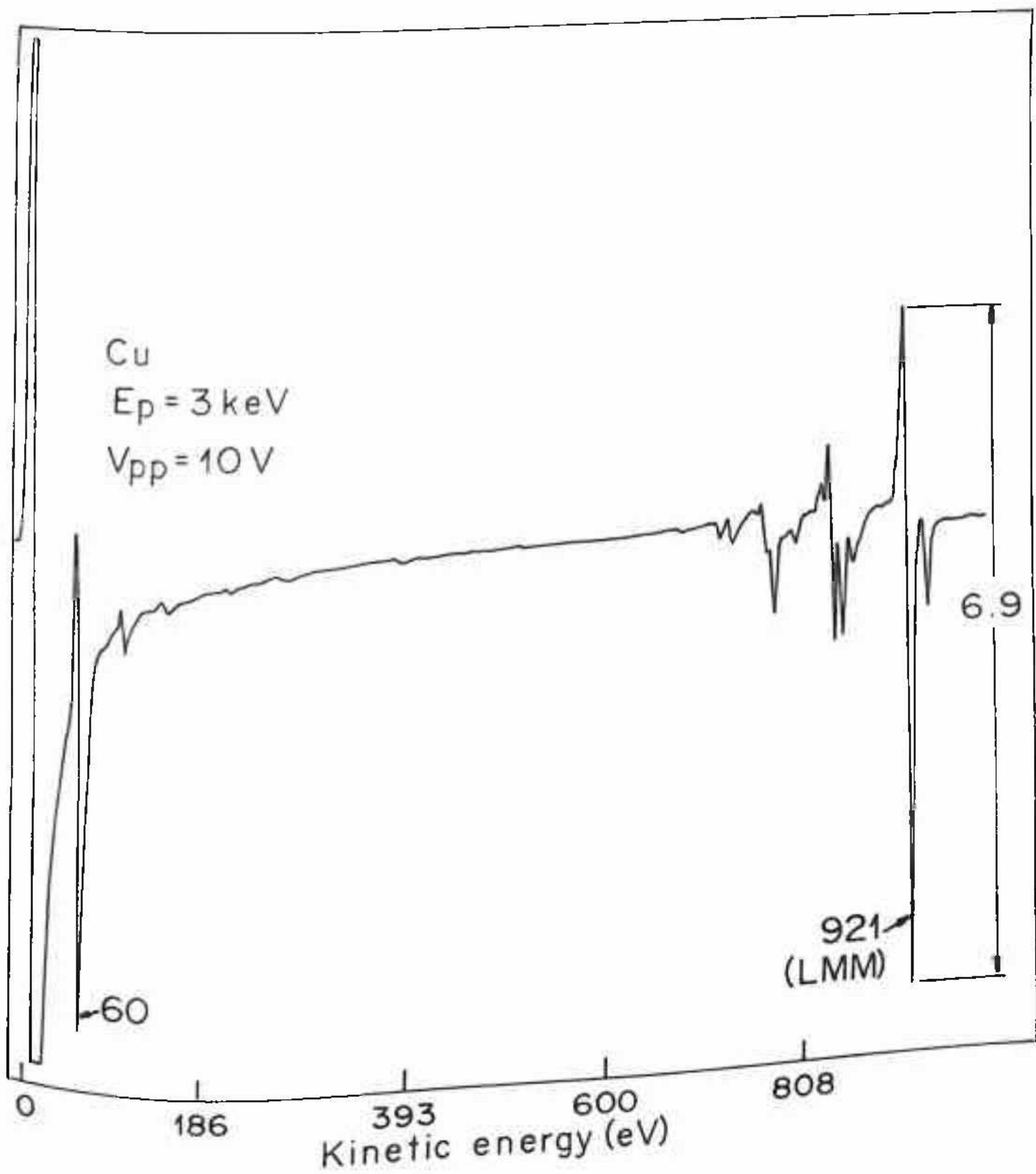

Fig.3.3 : Auger spectrum of Cu after standardization where the peak ratio of 60 and 921 eV peak is ≈ 0.77.

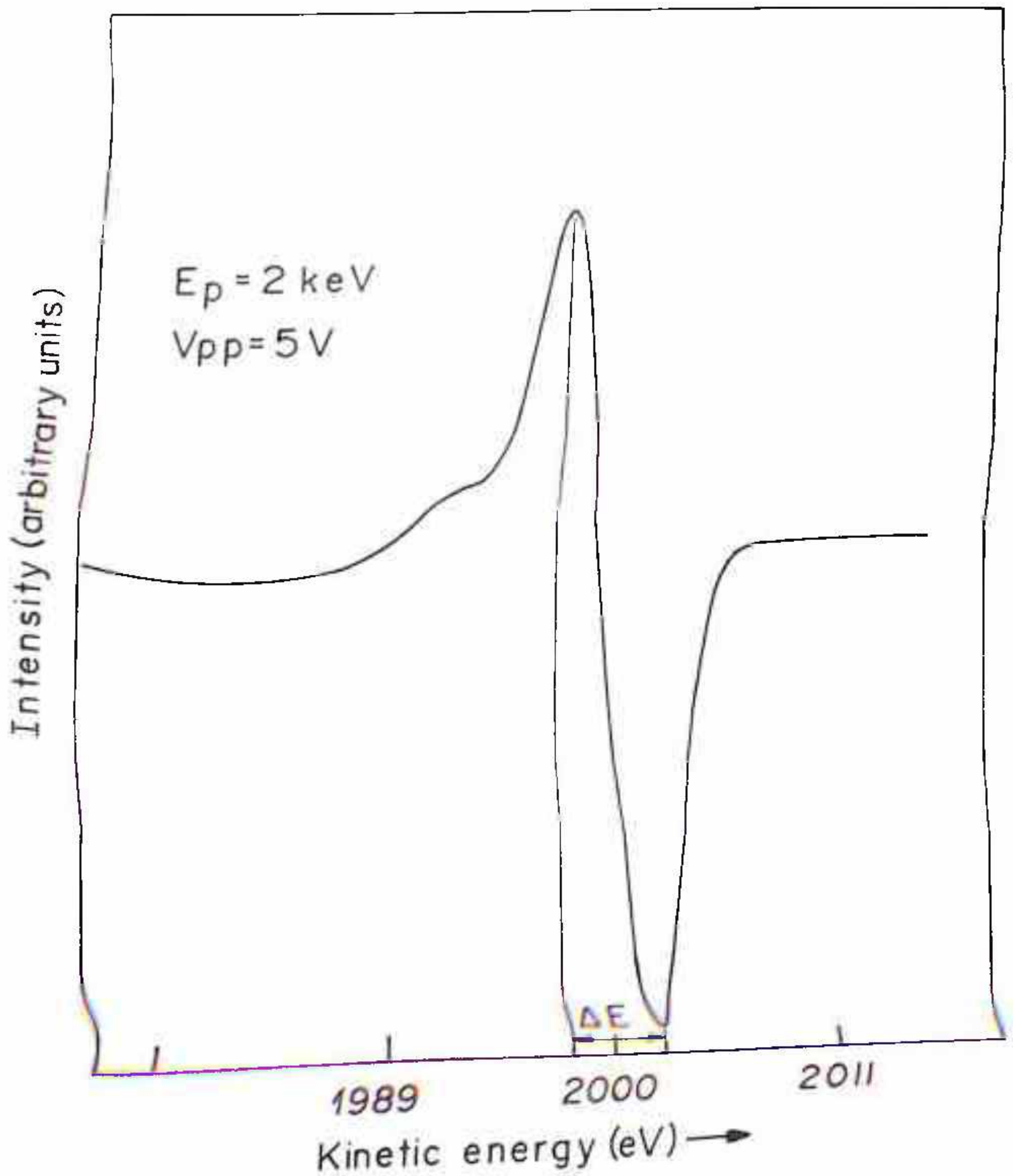

Fig.3.4 : Elastic peak used to determine the energy of resolution of the instrument (VT-112), $\Delta E = 4.4$ eV

detector is optimised by maximizing the signal. But if one peak is optimised then the other peak at different energy is still not correct, i.e. some phase shift occurs between the signals. The cause of the phase shift is assumed to be due to the different times of flight of different energy Auger electrons contributing to the signal. The signal in our case is optimised at 2000 eV. In FIG.3.5 the change in phase as a function of energy is shown. It is known that the detected signal intensity at any other energy is directly reduced by the cosine of the difference between the shifts indicated at 2000 eV and the energy concerned. So the reduction trend may be calculated as a function of Auger peak energy. The reduction nature is shown in FIG.3.6. It is observed from the curve that the high energy peaks do not change much, but the low energy peaks , below 200 eV is reduced ~ 9% of the original intensity. Of course the energy dependence of the phase shift (0-2000 eV) may be reduced by reducing the frequency of oscillation (17 kHz at this moment) , using a 100 pf feed-back capacitor, and a less than $\pm$ 2° phase shift is reported for 1.7 kHz oscillation. But due to this the intensity will be reduced which is not desired for our study. So the 17 kHz signal is selected as optimal.

The channeltron is an electron multiplier having its active surface coated with an oxide material with low work function. The secondary electron yield is dependent on the energy of the beam incident on it, and so does its efficiency. Generally, the lower energy electrons are collected with less efficiency than the higher energy electrons[7]. For differentiated mode, it is known[7] that biasing the front of the channeletron multiplier the variation of the detector sensitivity may be reduced. The field penetration is removed by a wire mesh, which is a part of the instrument.

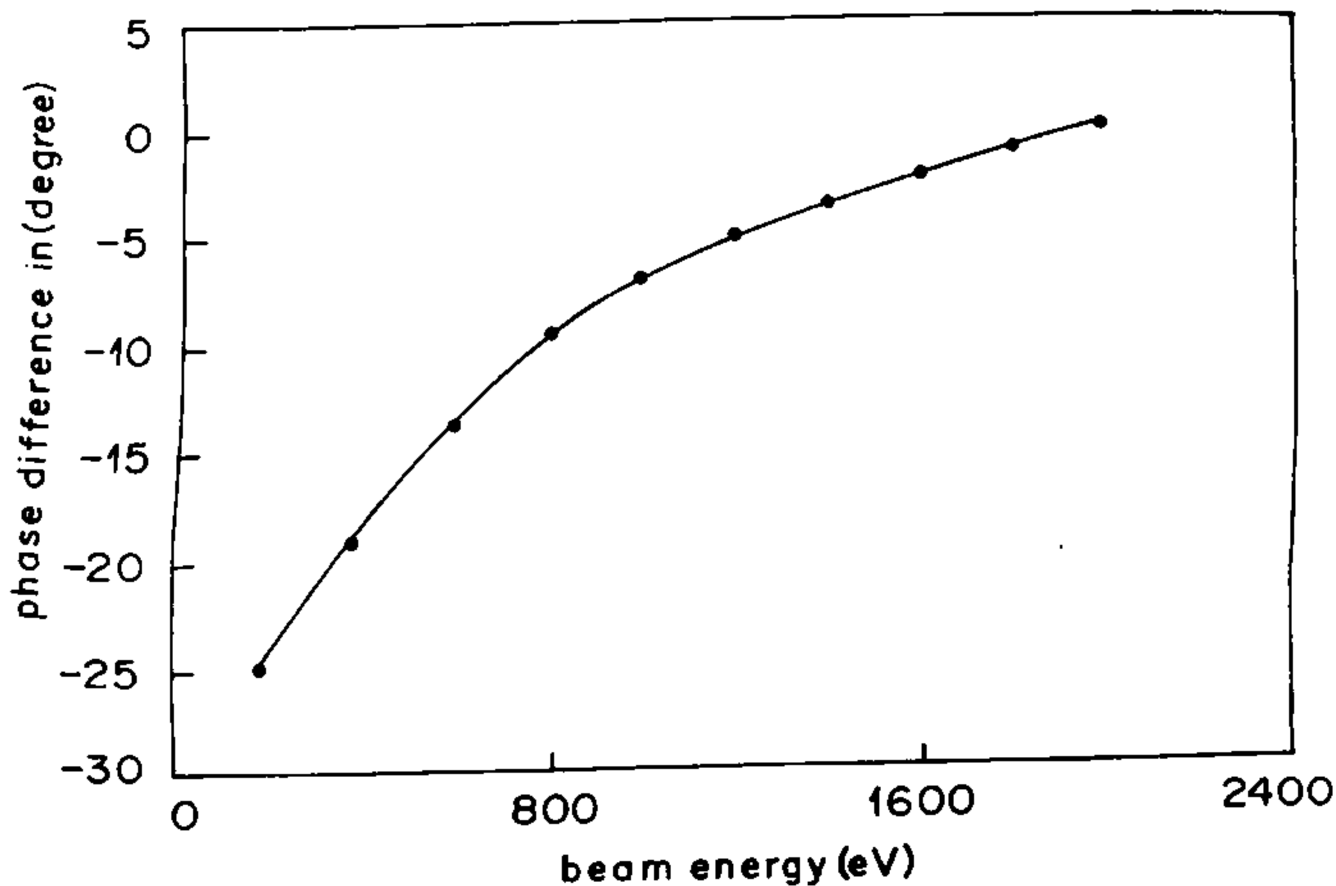

Fig.3.5 : A plot of the change in phase of the elastic peak as a function of the energy of electrons. The phase difference is made zero at 2 keV.

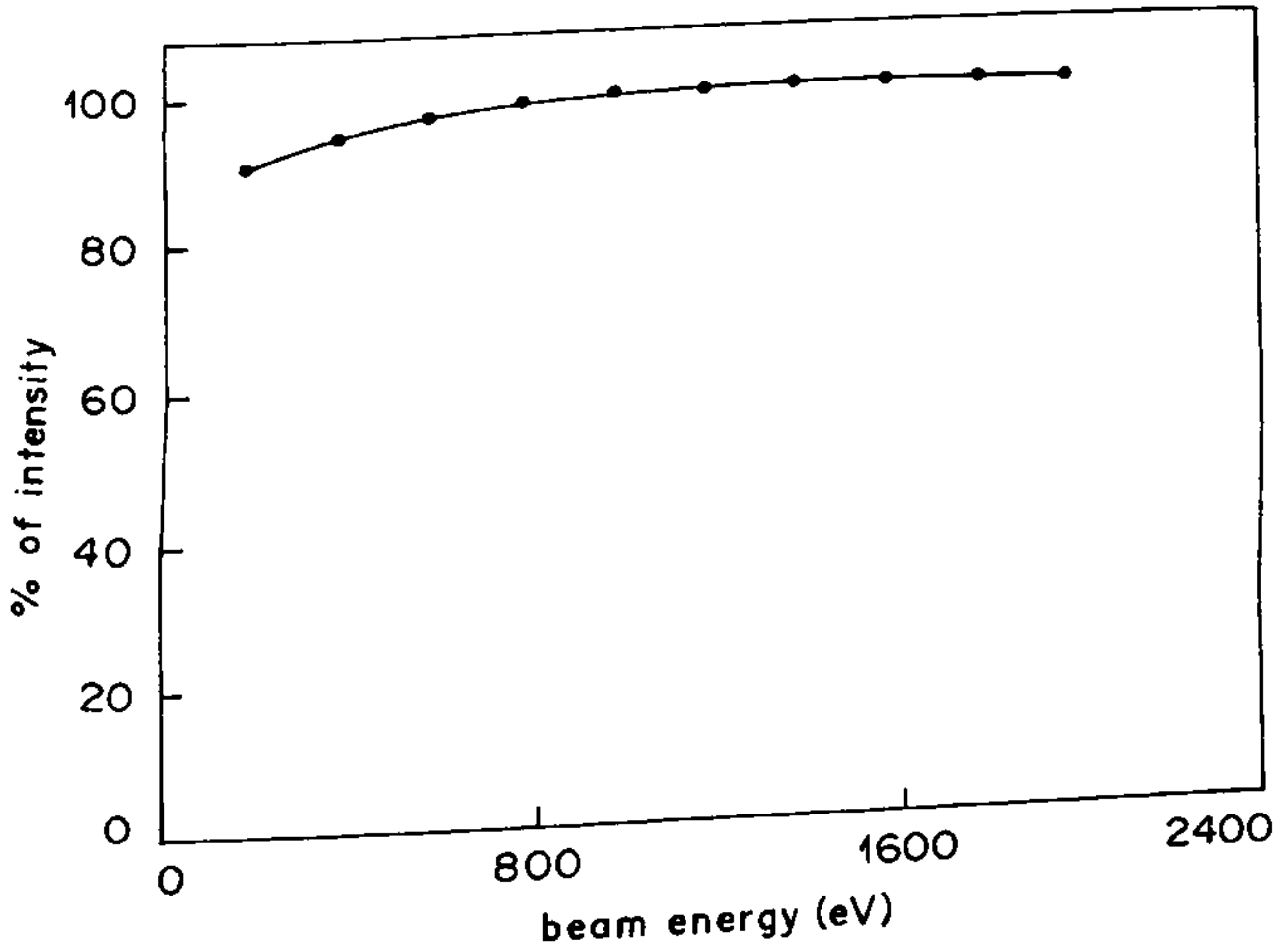

Fig.3.6 : Plot of percentage of intensity versus the beam energy.

In FIG.3.7 the variation of the intensity of the Cu 60 eV signal with the channeltron multiplier voltage is shown. A saturated signal can be achieved at around 2500 V.

3.3.1.b Parameters for AES :

Typically, most elements have Auger peaks occur in the 0-1000eV scan of the secondary electron specrum. A primary beam energy of 3 keV has been used in this study and the respective Auger peak sensitivity values for standard samples have been taken from the Auger Hand Book[8], and a 10 V peak to peak modulation is used during data collection. For lineshape analysis, two regions are selected, i) valence band related higher energy Auger transitions and ii) the low energy SCK (Super-Coster-Kronig) transition along with the autoinization transitions. For higher energies the primary beam energy is kept three times the highest binding energy of the levels taking part in the particular Auger transitions because according to Gryzinsky[9], ionization crosssection is maximum of any level is achieved by giving the incident beam energy three to four times the binding energy of that level. For low energy Auger, the beam energy selected is in the range 200--300 eV. For the later two spectra, 5 V peak to peak modulation is used for better resolution.

3.3.1.c Parameters for loss studies :

The loss spectroscopy was studied with an incident beam energy of 170--500 eV, in the double derivative mode to get the distinct position of the peaks. An optimum value for intensity and resolution of 5 V peak to peak modulation was used to observe the loss features. Rest of the acquisition techniques are similar to the AES studies.

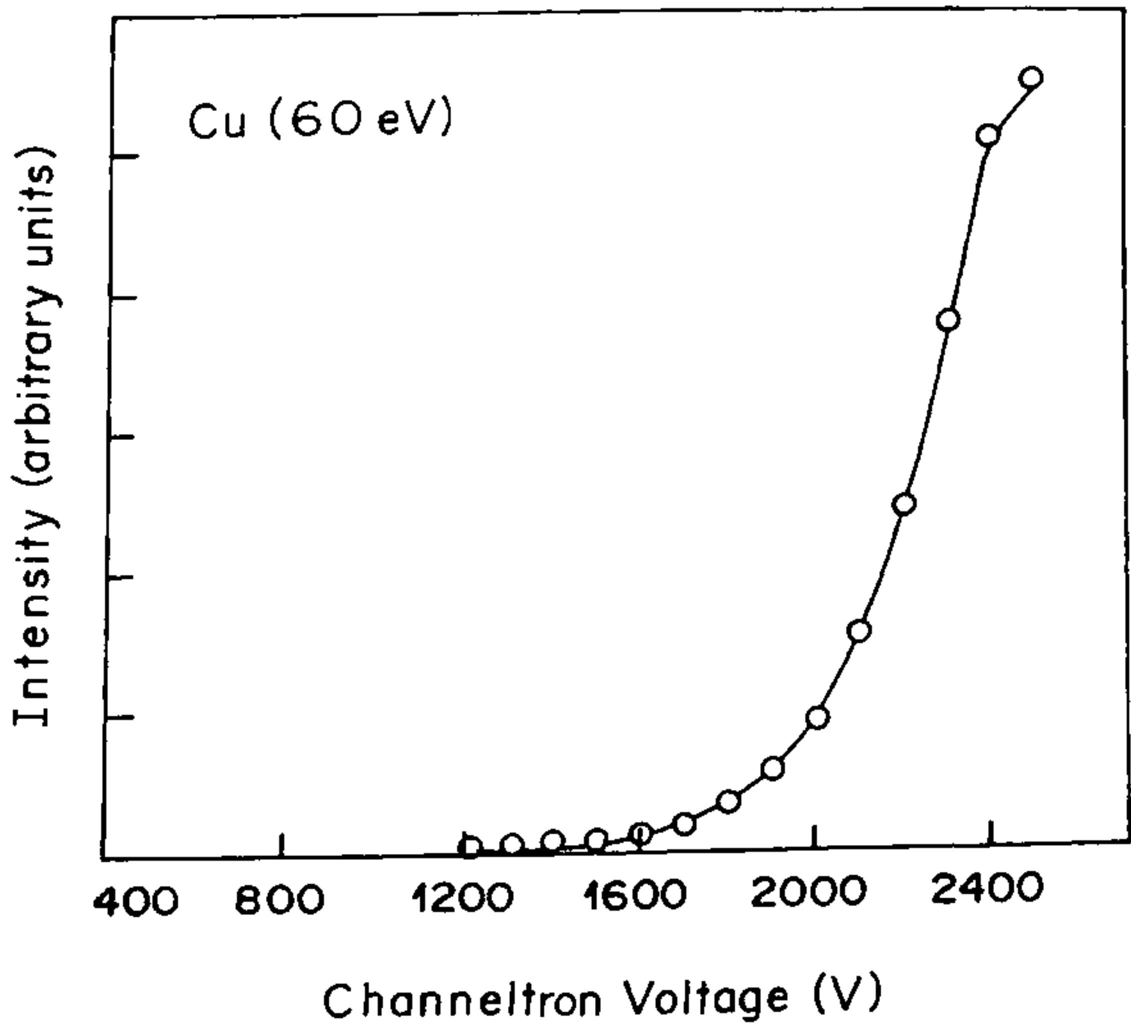

fig.3.7: Mode of variation of Cu (60 eV) peak intensity with the channeltron voltage.

3.3. 2. XPS study :

XPS has been used here to complement the observations obtained by AES and ELS. XPS not being one of the main techniques used for this study , only a brief description of the apparatus is given below :

The system is a multitechnique surface analytical instrument (M/S Perkin Elmer : model 1257), capable of giving a pressure of 10^{-11} torr by a combination of turbo molecular, ion and sublimation pumping units. The PHI Models 04-500/04-548 x-ray source is comprised of water cooled dual anode to which a high positive voltage is applied, and also houses two thoriated tungsten filaments in a water cooled shroud. The anode combination is Al and Mg, capable of giving X-rays of Mg and Al, K_{α} lines with energy of 1253.6 and 1486.6 eV respectively. A thin window at the front x-ray source prevents anode contamination by sputtered materials and also avoids sample heating by radiation. The system is equipped with a precision manipulator on which the sample is mounted and has X, Y, Z and θ degrees of freedom. For signal collection and conditioning, the PHI model 10-360 precision energy analyser is a spherical capacitor analyser (SCA) type. A schematic is shown in FIG.3.8. Its a combination of two hemispherical surfaces of different radii positioned concentrically. A potential difference is applied between the surfaces so that the outer sphere is negative and the inner is positive. The data is acquired by a PC interface capable of setting acquisition parameters and also allowing some data manipulation.

The system is standarized with respect to the contaminant free Ag 3d line as shown in the FIG.3.9 using Mg K_{α} line as the incident photon

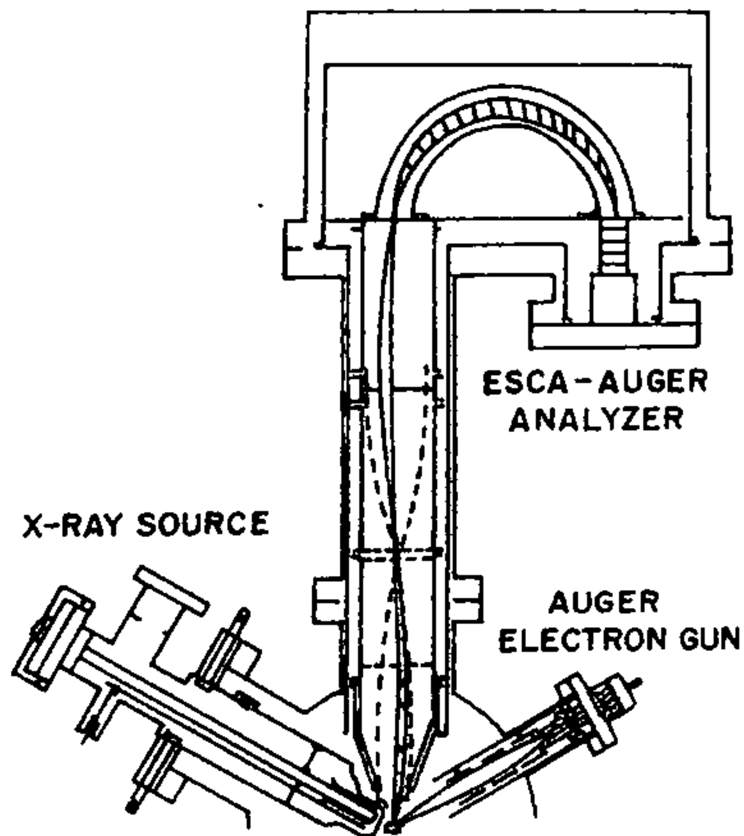

Fig.3.8 : Schematic arrangement of X-ray source, electron gun and analyser (SCA) in the multi-technique system

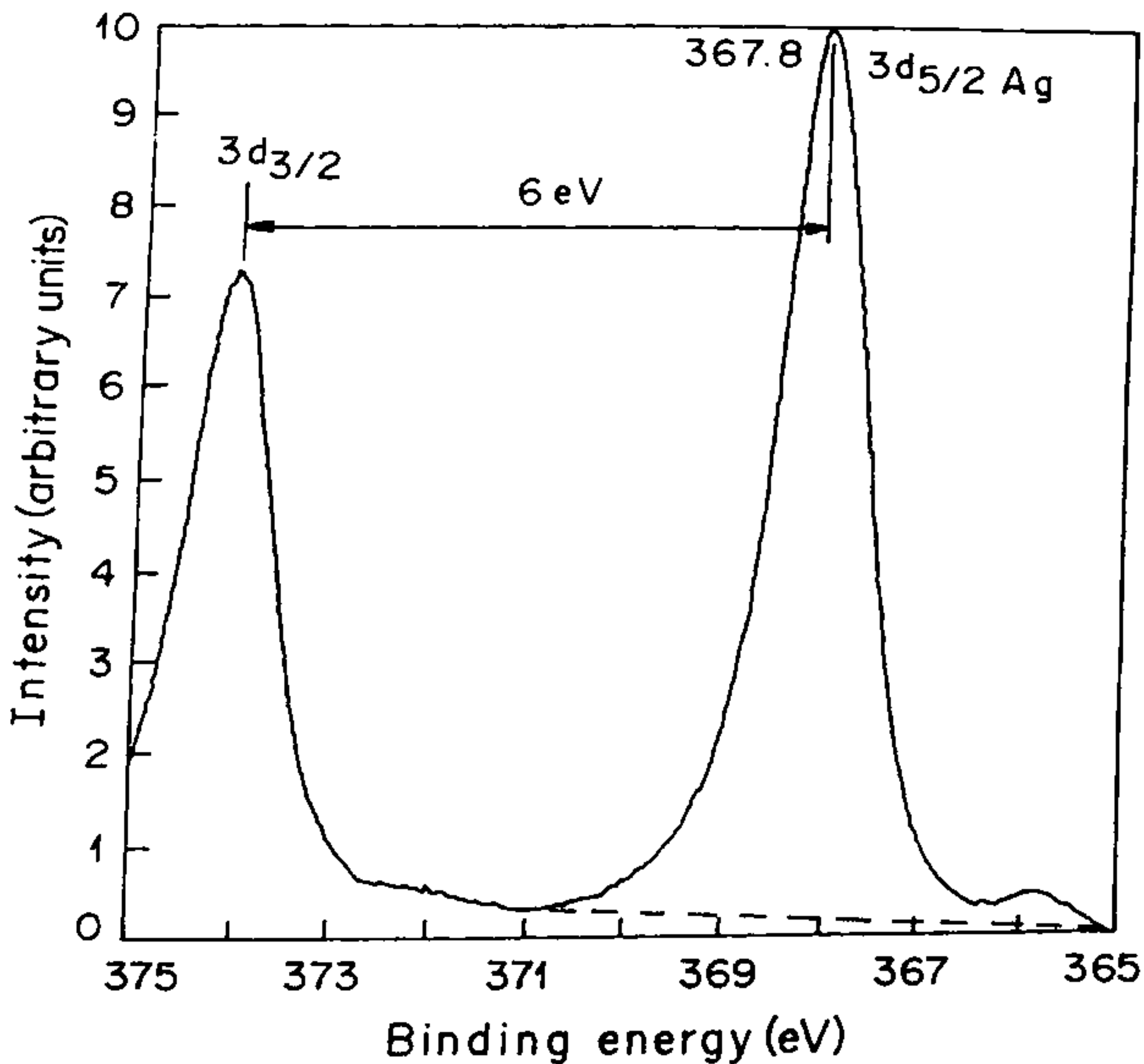

Fig.3.9 : XPS $3d_{5/2}$ and $3d_{3/2}$ peaks of Ag obtained on standard sample after calibration of instrument. The data compares well with that of Ref.10.

and photoelectrons are collected in the computer controlled SCA. The best resolution possible is 25 meV in CRR (constant resolution ratio). The ion gun is used for in-situ sample cleaning by Ar ion sputtering at different angles with an energy upto 5 keV over a rastered area.

References :

1] D.P. Woodruff, and T.A. Delchar, Modern Techniques of Surface Science, Cambridge Solid State Science Series, Cambridge Univ. Press (1986) 4.

2] J.K.N. Sharma, Santanu Bera, N. Sen and S.M. Shivaprasad, Communicated to J. Appl. Phys. (1994).

3] J.K.N. Sharma, Santanu Bera and B.R. Chakraborty, Appl. Phys. Letts. 59 (1991) 3247.

4] H.E. Bishop, J.P. Coad & J.C. Riviére, J. Elec. Spec. 1, 389 (1972-73).

5] C.J. Powell, N.E. Ericson and T.E. Madey, J.Elec. Spec. Rel. Phenon. 25 (1982) 87.

6] M.P. Seah and M.W. Holbourn, J. Elec. Spec. Rel. Phenon. 42 (1987) 255.

7] K. Kanaya and S. Ono, Electron Beam Interaction with Solids, Proc. 1st Pfefferkorn Conf. Asilomar, (1982), SEM INC., AFM O'Hare, Chicago, 1L, (1984) p69.

8] Hand Book of Auger Electron Spectroscopy (2nd. edition) Ed. L.E. davis, N.C. MacDonald, P.W. Palmberg, G.E. Riach and R.E. Weber(1978).

9] M. Gryzinsky, Phys. Rev. A138 (1965) 336.

10] Hand Book of X-ray Photoelectron Spectroscopy, Ed. C.D. Wagner, W.M. Riggs, L.E. Davis, J.F. Monlder, G.E. Muilemberg (1979) (Perkin Elmer).

Chapter IV
Results & Discussions

Chapter IV
Section A
Ion beam effect

4a. Sample cleaning and ion beam effect :

Due to the shallow information depth in surface science techniques, the cleanliness of the surface under investigation becomes a very crucial aspects in all experiments. We have performed many experiments to understand the contaminations of our samples and aspects of cleaning them. Some of the results thus obtained are described below.

The contaminants observed commonly on the surface are oxygen and carbon. Hydrogen may be present, but AES or XPS techniques cannot identify it. The contaminations may arise due to several processes like,
i) adsorption of layers of residual atmospheric gases,
ii) sample preparation background and their preservation and
iii) the sample handling methods.

So insitu surface cleaning is an integral part of surface science. Generally five processes are adopted for this, i) insitu cleaving or fracture, ii) scrapping of surface , iii) Ar^+ ion sputtering, iv) sample heating upto the 80 % of its melting point and v) by sputtering and annealing cycles. Though the first two techniques are used in special cases, we have adopted the later methods due to their suitability to our samples.

The Ar ion beam, that is employed to sputter away loosely held contaminants by momentum transfer, is itself found to induce some surface reactions[1]. We have observed that the ion beam used intending to remove carbon, induces the carburization of Ta[2], Si[3], Mo[4], but does not

seem to do so on Ti and Cu. The carbides formed which are harder material, limits the cleaning ability of Ar ion bombardment. The carbon fingerprinting in AES, XPS and ELS are employed for identifying and understanding the carburization.

4a.1. Modification of carbon by ion beam bombardment :

Even after taking maximum care during sample handling outside UHV, it is almost inevitable to find some carbon and oxygen on the sample surface. The contaminant carbon observed on the sample surface shows a lineshape that indicates that it is mostly in the graphitic form, i.e. sp^2 hybridized. Through Ar ion bombardment of 2 keV energy, this graphitic carbon loses its identity and assumes carbidic form. The ion beam seems to alter the valence band DOS of carbon and facilitate its phase transformation. These changes have been monitored by Auger fingerprinting and EELS studies. AES is very sensitive towards the different hybridization state of carbon[5].

The ground state of carbon is denoted as $1s^2 2s^1 2p^3$, Where 2s and 2p electrons are in the valence band. Particularly in graphite two types of bond are formed between the carbon atoms, σ and π bond for parallel and perpendicular mode of orbital overlapping respectively. Indeed the binding energies of 2s and 2p levels are at -13 and -5 eV below the valence level. In the layered graphite, the hybridization of s orbitals forms a covalently bound lattice of graphite planes with an angle of 120° between the segments connecting nearest neighbour atoms. These pile up on each other and are weakly bound by the residual forces that arise from the

hybridized (side on overlapping) p_z orbitals (denoted by π) perpendicular to the planes.

In FIG. 4a.1 the AES for single crystal graphite is shown with the characteristic excursion seperation of 23 eV. The effect of 3 keV Ar ion bombardment on it is shown , where a new peak appears at aroud 279 eV, 7 eV away from the main 272 eV peak. This indicates the modification of the surface by the ion beam, which may be in some parts of the few layers analyzed of the graphite surface. So the ion bombarded graphite shows the Auger transitions from the two different layers of surface, damaged and non damaged graphite which co-exist. The peak at 279 eV is assumed to be contributed from the altered component of graphite. It is conjuctered that due to the ion bombarment the valence band is affected maximum and this results in the loss of its sp^2 hybridization structure, and the σ bonds becomes loosely bound π bonds in the surface region.

The Auger transition for the two hole final state in the valence band is given by,

$$E_A = E_k - E_{v1} - E_{v2}$$

$$E_v = E_k - E_A$$

where $E_{k,v1,v2}$ are the binding energies of K, v1 and v2 energy levels and E_A is the Auger enery. V1, V2 levels are in the valence band and $E_v = E_{v1} + E_{v2}$. The ionization energy for 1s (E_k) electron is approximately given by, 284 eV.

Before ion bombardment, E_A=272 eV, which implies that E_V = 12 eV. But due to the ion bombardment, along with the 272 eV, peak the peak at 279 eV is observed i.e. E'_V = 5eV. So it is assumed that $E_V = (E_{v1}$

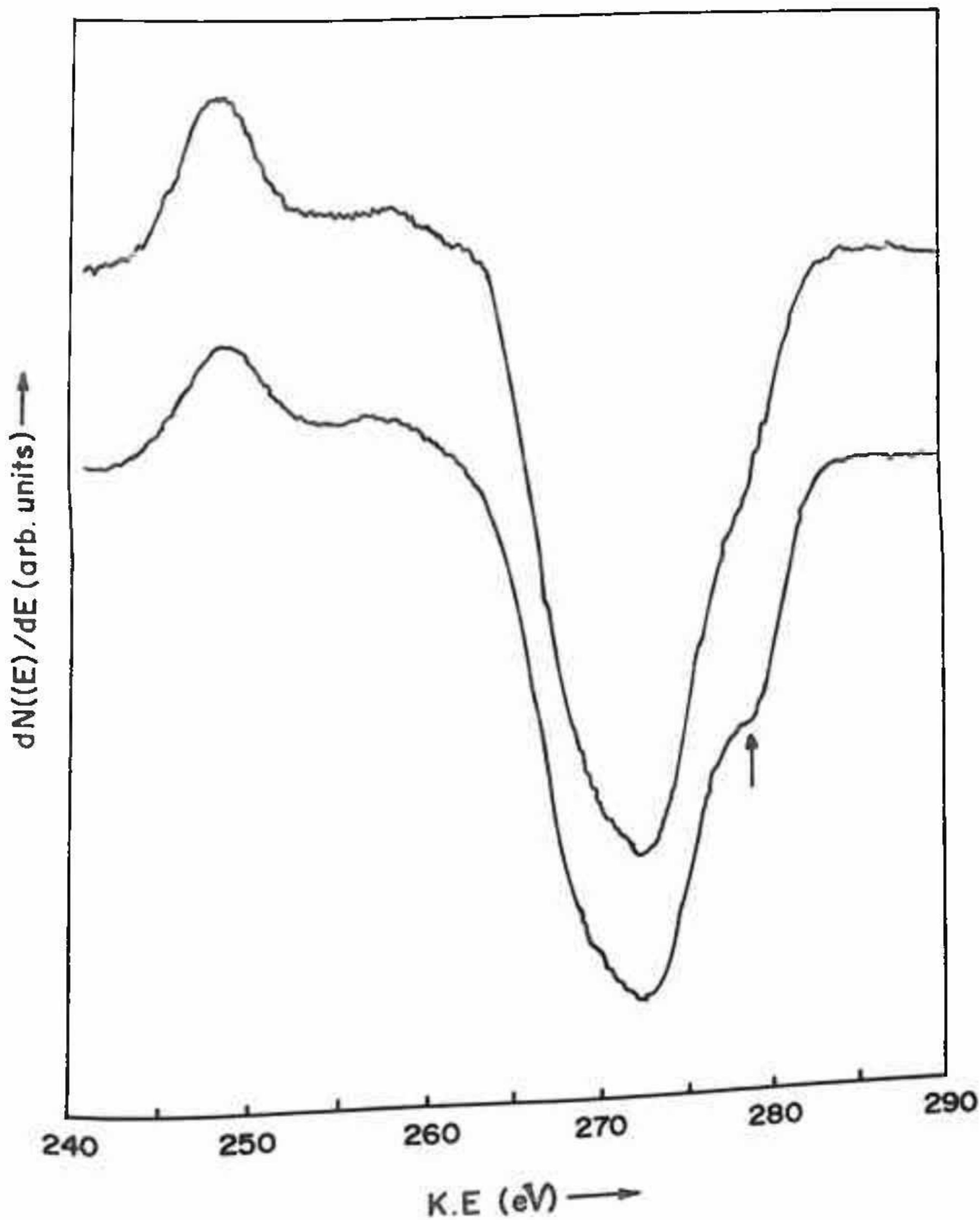

Fig.4a.1 : AES of single crystal graphite before and after ion bombardment. The arrow indicates the appearance of a new peak after ion bombardment.

+ E_{v2}) =12 eV is the transition involved in the σ and π bond but E_v = 5 eV corresponds to the transition involving the π bond only. Thus the peak at 279 eV indicates the creation of new π states due to ion bombardment. But there is not a resolvable change in the excursion separation which suggests that band width is not changed much due to ion bombardment.

The effect of ion bombardment is also observed in our EELS study of the single crystal graphite as shown in FIG.4a.2. The ELS spectrum shows two peaks at 6.5 and 26.5 eV which are due to π plasmon loss and σ plasmon loss[6]. The peak at 19 eV is the surface σ plasmon loss feature. The peak at around 21 eV is the loss due to 3p electron excitation. π plasmon loss process is the most probable loss as seen from its large intensity, and undergoes a change after ion bombardment. In case of ion bombardment the intensity of the 19 eV peak is decreased considerably indicating the surface transformation due to the ion bombardment. The multiple π plasmon loss peak at 12 eV is found to increase confirming the observations made in the AES experiments.Thus by ion bombardment an increase in the conduction p electrons occurs.

In FIG.4a.3(a) the k loss spectrum for C is shown . The 1s electrons can be excited to states in the valence band. The 1s--σ transition at 294 eV is observed to be stronger than the 1s -- π transition at 288 eV. A quantitative study of the transitions shows that the ratio of transition 1s--π to 1s--σ transition (measured by peak heights) is 0.47 whereas after ion bombardment the 1s - π transition increase with a new ratio of 0.684.

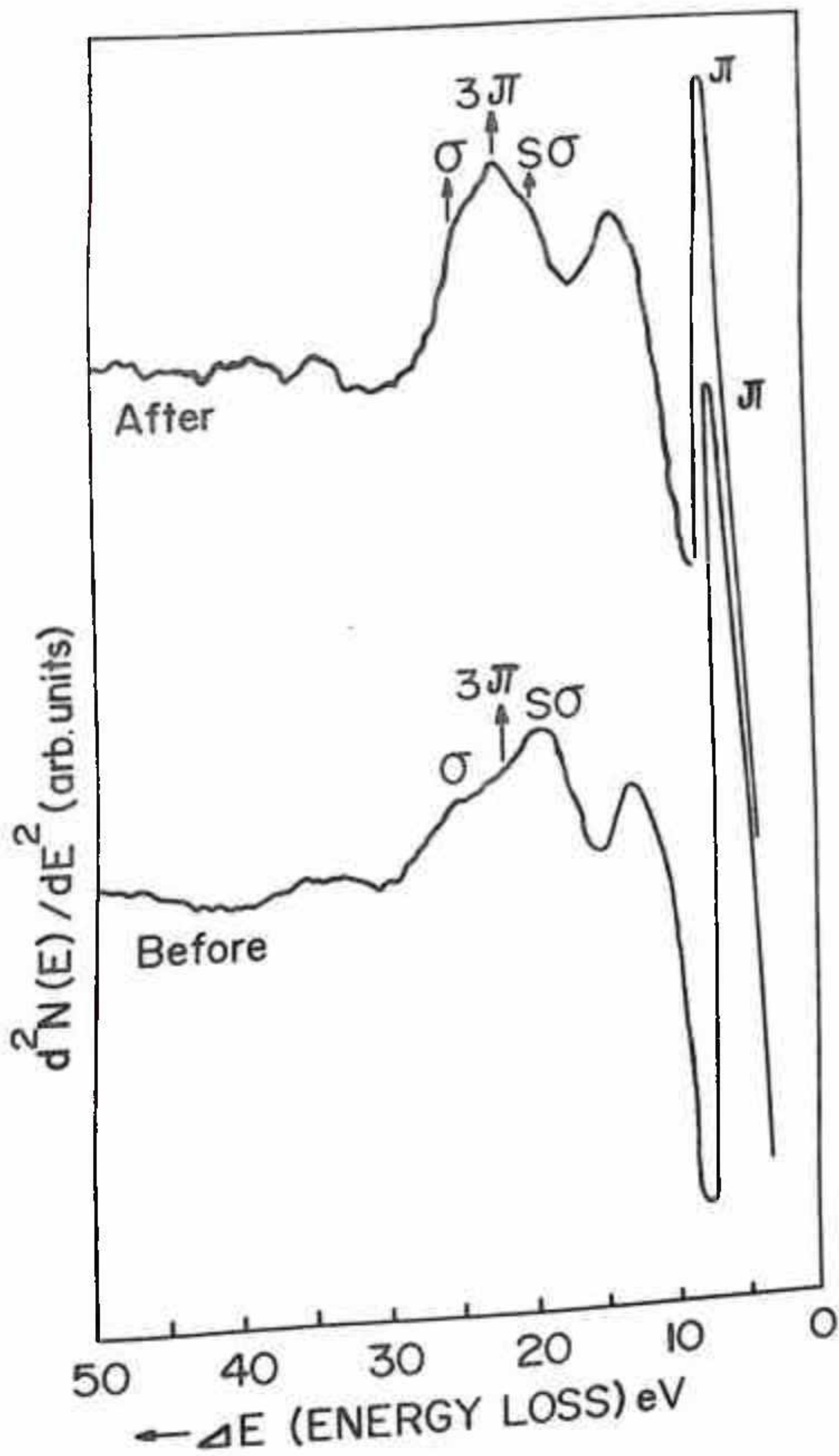

Fig.4a.2 : ELS of single crystal graphite before and after ion bombardment (3 keV).

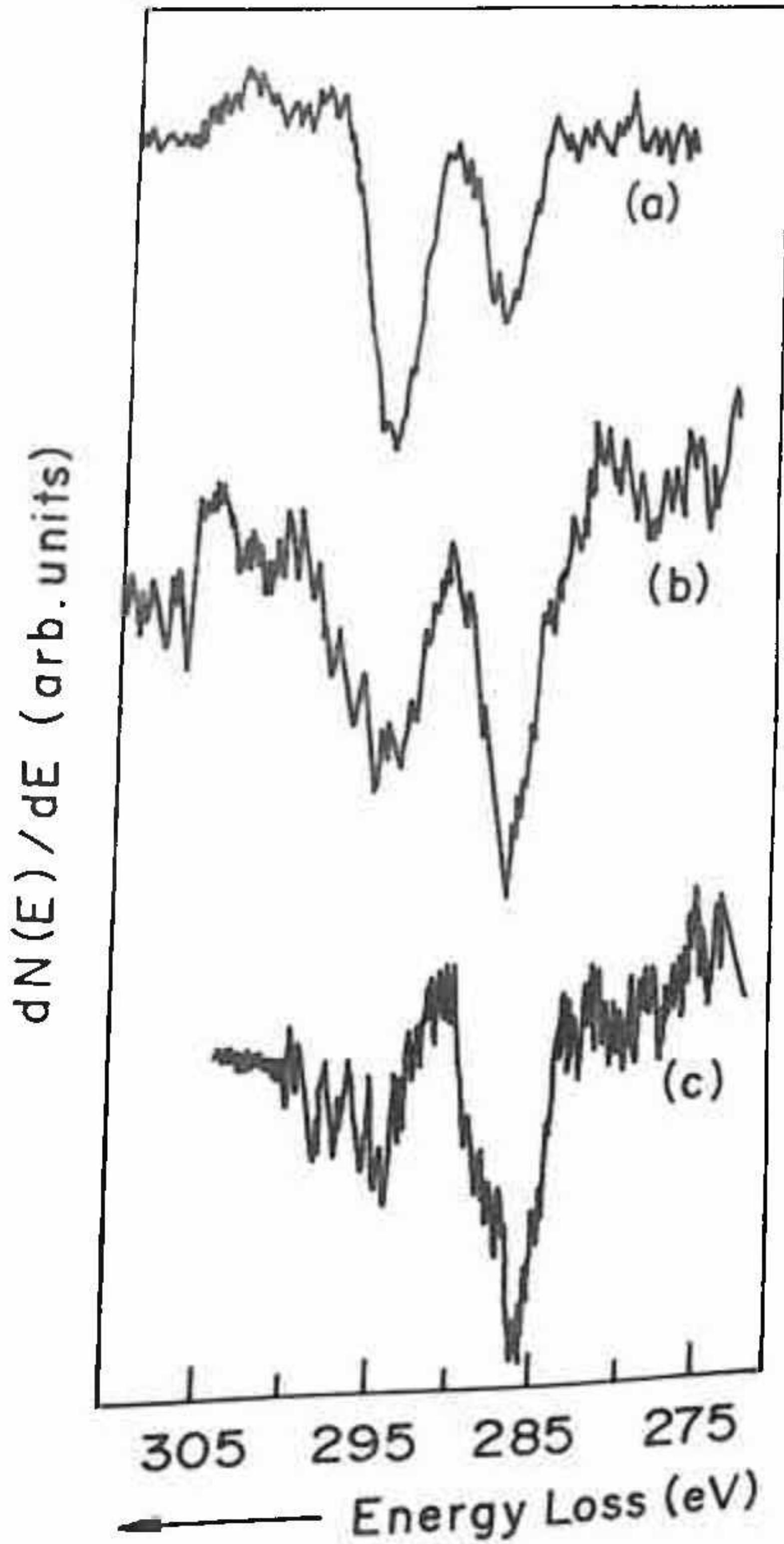

Fig.4a.3 : K- loss of C in a) single crystal graphite, b) partially carburized Mo and c) completely carburized Mo.

According to the work done by L. Papagno et. al[6]. the ion bombardment creates more states so that the 1s--π transition supresses the 1s--σ transition.

4a.2 Ion beam effects on contaminated Ta :

The aspects of carburization of Ta surfaces induced by Ar ion bombardment are discussed here. The graphitic carbon observed on the Ta surface does not match all the detailed properties of single crystal graphite. The results are explained based on the properties showed by the single crystal graphite. In FIG.4a.4 Ta NNN Auger transition along with the graphitic carbon (KLL) is shown in the first derivative mode.

The observation of the carburization is centered around two peaks and their changes i) the change in Auger KVV line shape and ii) the change in the ELS spectrum. FIG.4a.4(a) shows the Auger electron spectra of Ta (NNN) and graphitic carbon (KLL) peaks in the first derivative mode. The graphitic carbon peak has an energy separation between the major positive going and negative going excursion peak as 23 eV which is in good agreement with the work of Galuska et. al[7] The energy separation has also been observed by Lascovich et. al[5] in case of cent per cent carbon-carbon sp^2 type of bonding to be 22.5 eV.

FIG.4a.4(b) shows the AES of the sample after it was bombarded with 3 keV Ar ions for 30 sec. with an angle of incidence of 60° . It is clear from the fingerprint that a major change is observed in the graphitic peak lineshape. The energy seperation between positive and negative excursion separation is now reduced to 6 eV, which shows the C-C bonding is

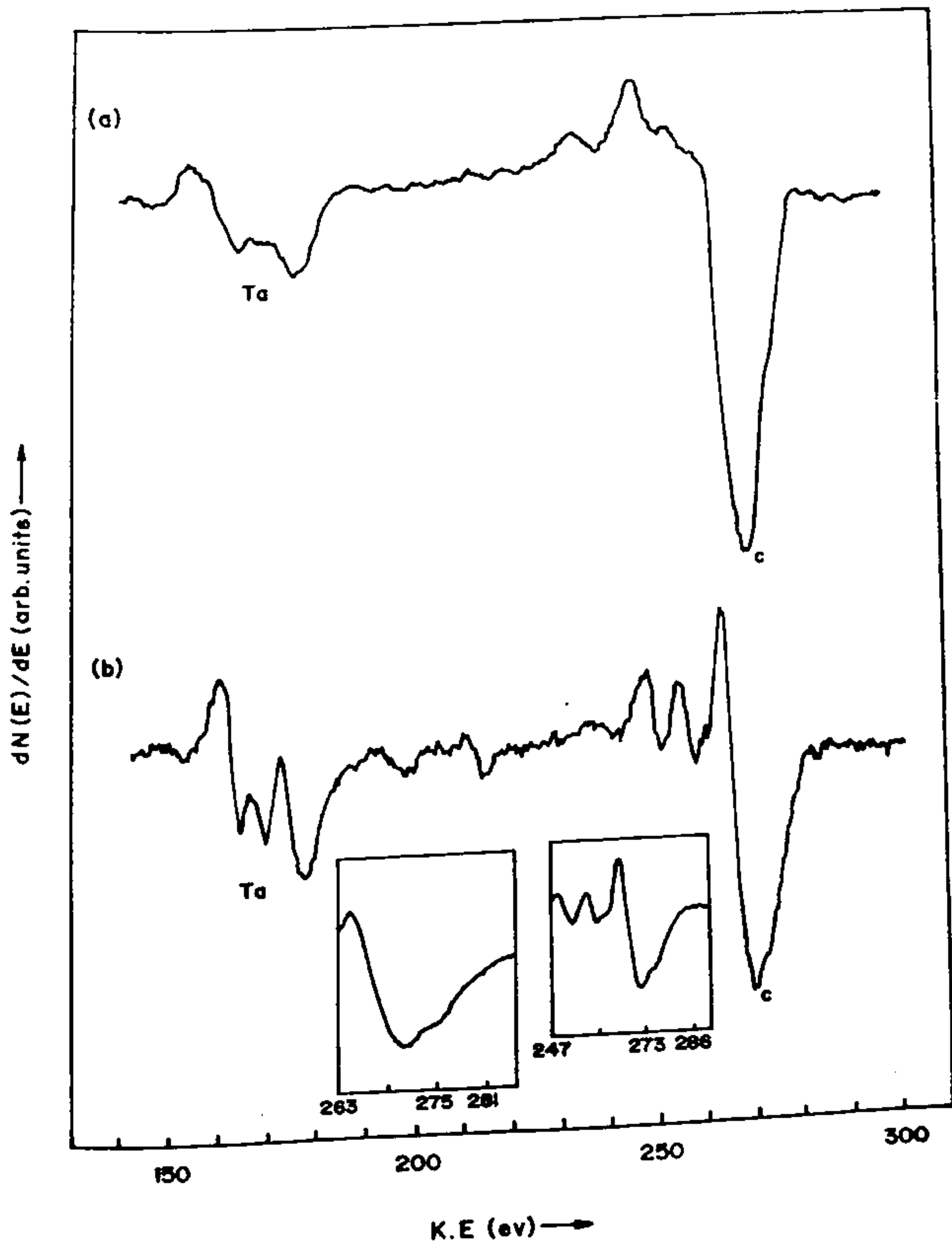

Fig.4a.4 : AES of Ta (NNN) and graphitic carbon (KLL) peaks a) before and b) after ion bombardment. The inset shows the apperance of a new peak at 276 eV.

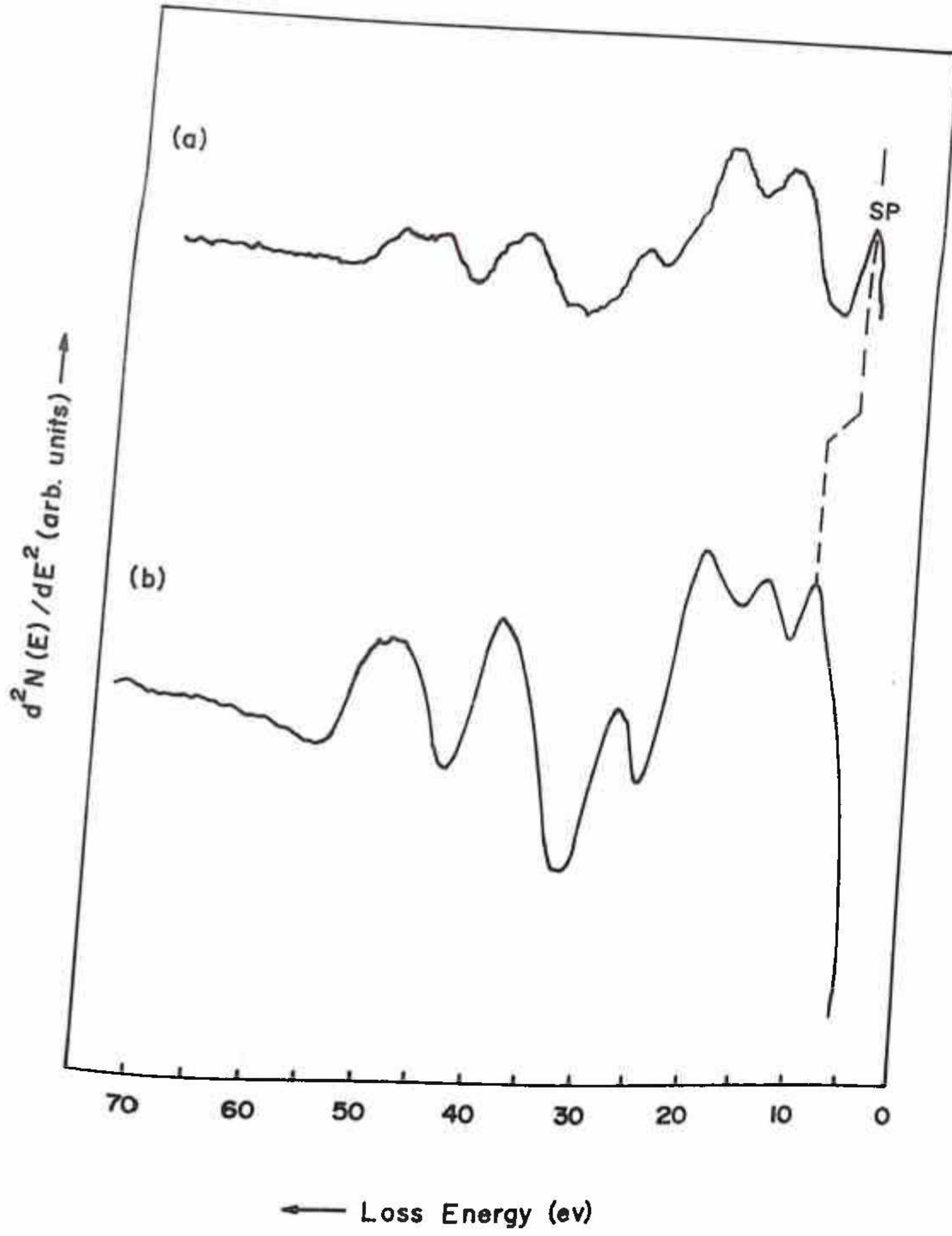

Fig.4a.5 : ELS of Ta surface with graphitic carbon as contaminant (a) and with bonded (ion induced) carbon (b).

neither sp^3 nor sp^2 type. The carbon is now chemically bonded with the metal Ta showing this characteristic as a 6 eV separation. A new peak appears as shown in the inset, approximately at 276 eV which confirms the carbide formation[8]. The Ta peaks at 164, 169 and 177 eV are found to become more prominant presumbly due to surface cleaning, showing thereby that the carbon which was the major contaminant has got bonded with Ta due to ion bombardment and Ta Auger signals are now coming from the Ta in the Ta_xC_y compound[2].

A comparison of the EELS of the Ta with graphitic carbon as contaminant on the surface (a) and with bonded carbon (b) is shown in FIG.4a.5. The low energy surface plasmon peak was found to change from 7 eV to 9 eV. However the bulk plasmon peak at 20 eV remains unchanged. The other peaks due to different interband transitions do not change in energy appreciably but definitely shows variation in intensity.

4a.3 Ion - beam effect on contaminated Mo :

FIG.4a.6 shows the surface of Mo film deposited on Si (111). The carbon present on the surface is not exactly graphitic in nature. It's shape is slightly distorted from the pure graphitic carbon peak shape. The pure graphitic form shows excursion separation of 23 eV, but here it is observed to be approximately 9 eV with the energy at 270 eV, and the incident electron beam energy used was 1000 eV. According to Laschovich et. al[5]. the excursion seperation for diamond is 14.2 eV and the mixture of graphite (sp^2) and diamond (sp^3) gives separations in between these two values depending on the percentage of diamond phase present in the

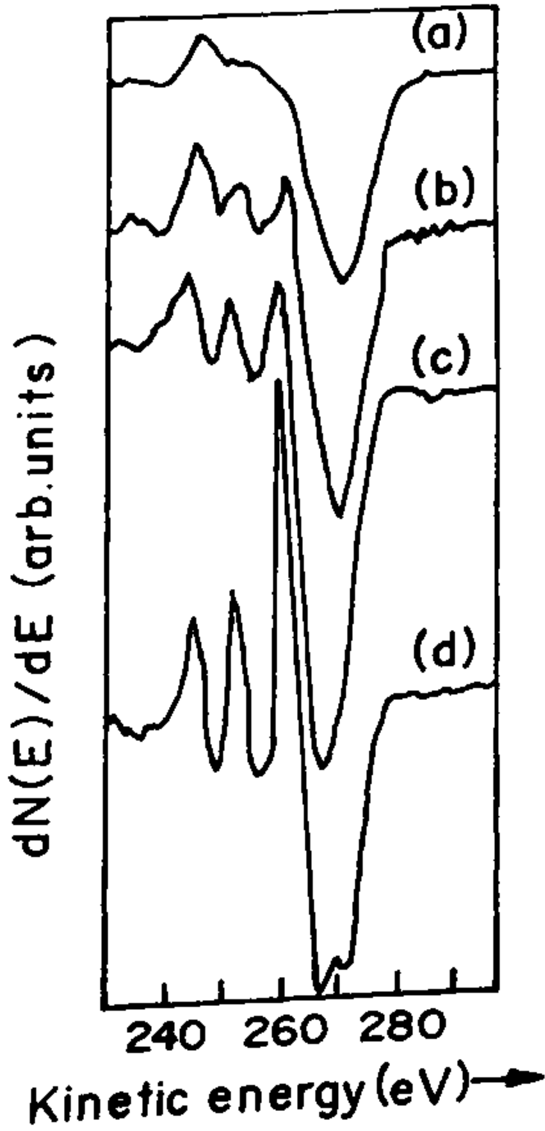

Fig.4a.6 : C- KVV Auger fingerprint in a) Single crystal graphite, b) C-on Mo film, c) 600 eV electron bombarded film or 700 eV ion bombarded metal sheet and d) 3 keV ion bombarded surface, which shows complete carburization.

analyzed region. It is observed that with the increase in the beam voltage, the peak separation changes from 9 eV to 7.5 eV and finally to 7 eV at around 6 keV of electron beam energy. With further increase in the beam voltage this value does not show any change. With 3 keV Ar ion bombardment this peakshape is changed further, such that, the excursion separation is not decreased but a new peak appears at 276 eV which is characteristic of carbidic carbon. It can be said here that, in case of Mo, the carbon peak observed on the surface was graphitic type and does not show any change due to electron bombardment. But it forms its carbide due to ion bombardment , showing the characteristic carbidic excursion seperation of 7 eV and with the new peak at 276 eV. The on set of carburization of Mo sheet as a function of Ar ion beam energy was observed by AES. It is observed that at around 700 eV of Ar ion energy the C KVV lineshape starts changing. At around 2 keV the peak shape completely changed to the carbidic form with the characteristic excursion separation.

In pure graphitic carbon, only C-C contributes to the whole C KVV Auger line. But when the metal is partially carburised as observed in case of electron beam effect in the Mo film and low energy ion beam effect in the Mo sheet, the signal comes from both C-C and C-M type carbon[9] and so this case may be attributed to the partial carburization of the metal. So a linear combination of the C-C and C-M contribution gives the particular peak shape indicated above, which is neither purely graphitic nor completely carbidic.

The Mo carburization and the affect of electron beam was confirmed by the K edge loss for the three cases as shown in FIG.4a.3. The K loss for

the pure graphite shows two transitions 1s--σ and 1s--π at around 294 eV and 288 eV, respectively. In case of pure graphitic carbon 1s --σ transition is more intense than 1s--π transition. But due to electron beam exposure on the Mo films, the C - K edge loss peak shape was observed to change. The relative peak intensity for 1s--π transition increases. So from this spectrum, it is found that the Mo is partially carburised in the analysed volume. Here K edge loss shows a linear combination of graphitic K-loss and the carbidic K-loss. After ion bombardment, the peak shape is further changed and the 1s--σ transition completely depletes. This suggests that the d electrons from Mo mostly occupy the carbon valence band states which decreases relatively 1s --σ transitions showing the characteristic K loss for the pure carbidic film[9].

4a.4. Ion beam effect on contaminated Si (111) surface :

Chemically cleaned Si (111) surface shows ion induced chemical bonding with contaminant C due to Ar ion bombardment. Initial ex-situ cleaning was done by dipping the acetone cleaned Si(111) in 2% HF solution in ethyl alcohol for 120sec which leaves carbon and a small amount of oxygen on the surface[10].

The effect of Ar ion bombardment was analysed by XPS. The effect of ion bombardment like the change in the geometry and the electronic structure was monitored by angle dependent -XPS technique. For angle dependent-XPS the angle of the substrate with respect to the X-ray source was varied from 12 to 120°. The carbon contaminant was found to be approximately 20 % before Ar ion bombardment. The peak shape of Si

and C and their detailed analysis was done by deconvoluting the observed spectra into their Gaussian components..

FIG.4a.7 shows the XPS peak position of the C(1s) peak as a *function of incident ion energy and demonstrates a change in the chemical* state of C. In case when two peaks can be resolved, the position of the peak with the higher amplitude is measured, to plot this graph. The dependence clearly shows a sharp shift at about 750 eV ion beam energy. This chemical shift is attributed to be due to the breaking of the C-C bonds (peak at 285.0) eV and formation of the Si-C bonds (peak at 283.2 eV).

The signature of the (C 1s) peak by XPS and the deconvoluted components are shown in FIG.4a.8 before and after carbide formation (750 eV ion energy). The peak at 285 is due to the C-C bond and that at 283.3 is related to the Si-C bond. The peak at about 286.2 eV has been attributed to C-O-H kind of bonds[11]. It has also been reported earlier[12] how the conventional techniques have been utilized to fingerprint the different forms of bonded carbon. Thus the fingerprinting clearly enables us to measure the unbonded and bonded carbon components. The inset in the figure shows the lineshape change in the Auger C-LVV spectra in the differentiated mode, demonstrating the change at 750 eV ion energy, similar to the observation made by XPS. This dependence does not alter by using different ion current densities, confirming the presencee of an energy threshold for the formation of the carbide. Both the AES and XPS spectra show that there is a co-existence of C bonded with Si and in the unbonded phases, and the chemical shift in XPS is not 2.5 eV that is observed in single phase SiC samples. The Auger fingerprint of the 750 eV bombarded sample is in the incomplete carbidic form[9], as clear from

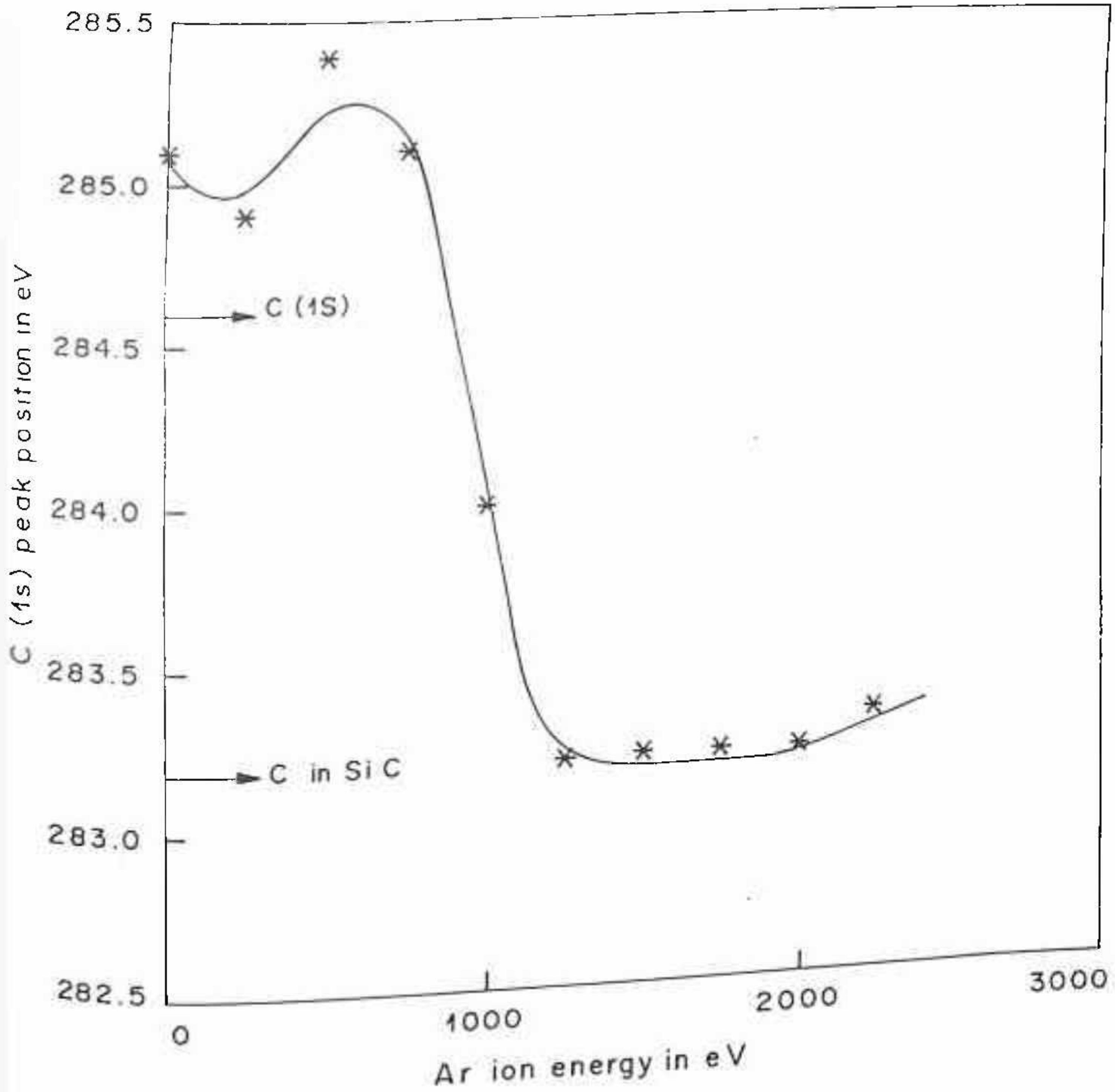

Fig.4a.7: C(1s) XPS peak position at different Ar^{+} ion energies. The dominant peak is considered to plot this, since bonded and free C components co-exist.

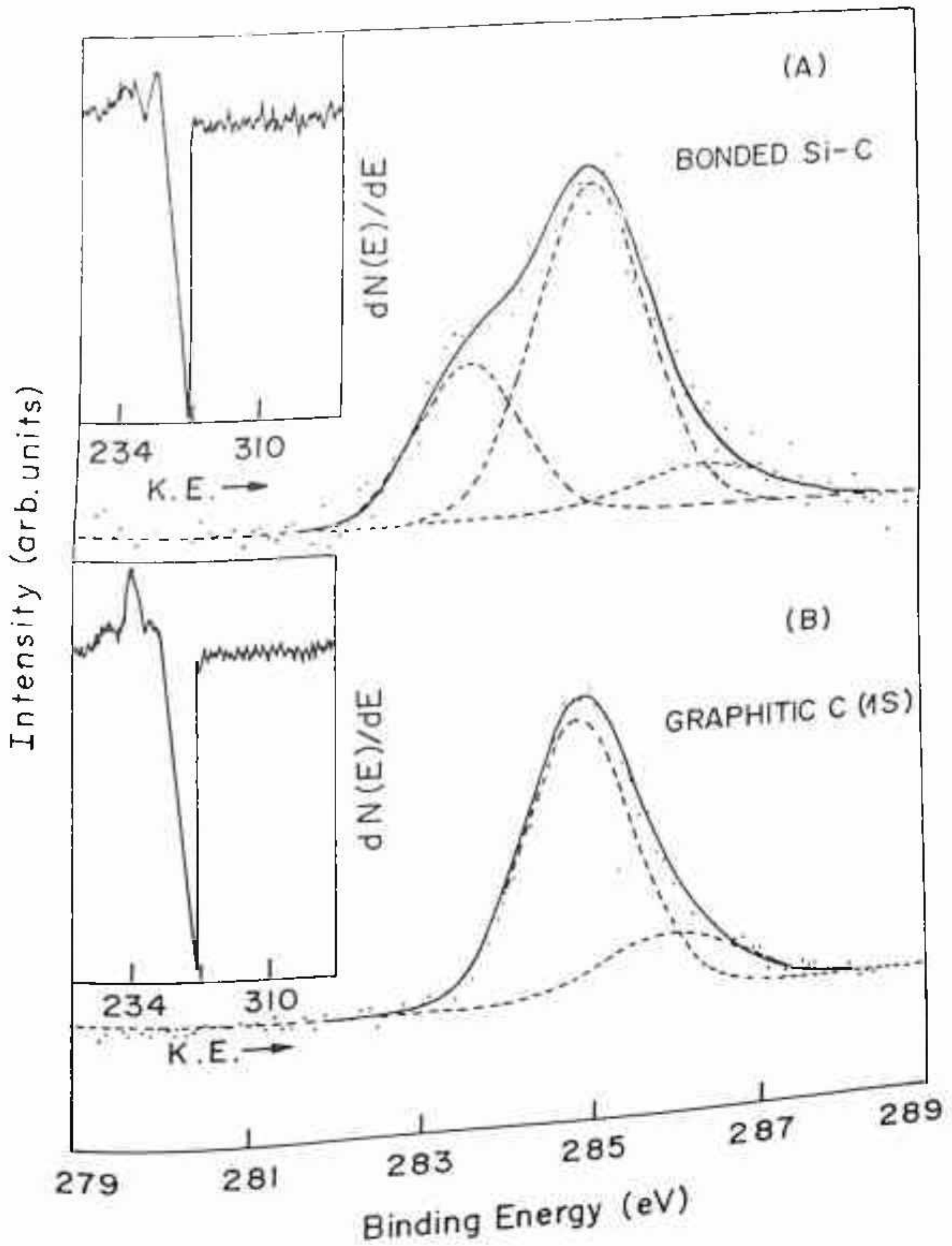

Fig.4a.8: C(1s) XPS peak shapes with deconvolution into their guassian components: a) C bonded with Si and b) as contaminated surface. The insets show the respective Auger lineshapes.

the shoulder at about 240 eV carbidic form, however it is amply clear from this figure that 750 eV ion-bombardment has induced the formation of Si -C bonds.

FIG.4a.9 shows the abundance of the bonded carbon (C_b) (at 283.3 eV) and the free carbon (C_f) (285 ev) as a function of ion beam energy. The plot contains two data sets, one for analyzer normal to the surface and other for glancing angles that is surface sensitive. The XPS peaks obtained have been deconvoluted into the C_b and C_f components by fitting Guassian peaks, using the FWHM of 1.6 eV and 1.5 eV respectively[13]. It must be noted that the data has been obtained by substracting a linear background. (However it has been verified that in this case using Shirley background substraction does not significantly change the results). The data with the analyzer aligned along the surface normal clearly shows the threshold for Si-C bonding to be about 750 eV ion energy in FIG.4a.9. After that, the amount of bonded carbon increases sharply to a maximum at about 1500 eV ion energy. Then on, the C_b/C_f ratio drops sharply. In comparison, the data point for glancing angles shows that most of the bonded carbon is around the interface. That is to say that the ion beam induces a reaction at the interface, while the surface carbon is less affected and so the lower curve remains fairly flat at all energies.

A relative percentage composition of Si, C and O as a function of ion-beam energy is shown in FIG.4a.10. Here the amount of C is the sum of both bonded and free components. The relative abundance has been calculated simplistically by using the expression and XPS sensitivity factors given in Ref.14. This curve demonstrates that carbon is sputtered away at lower energies, exposing more Si. However, C reduces only to

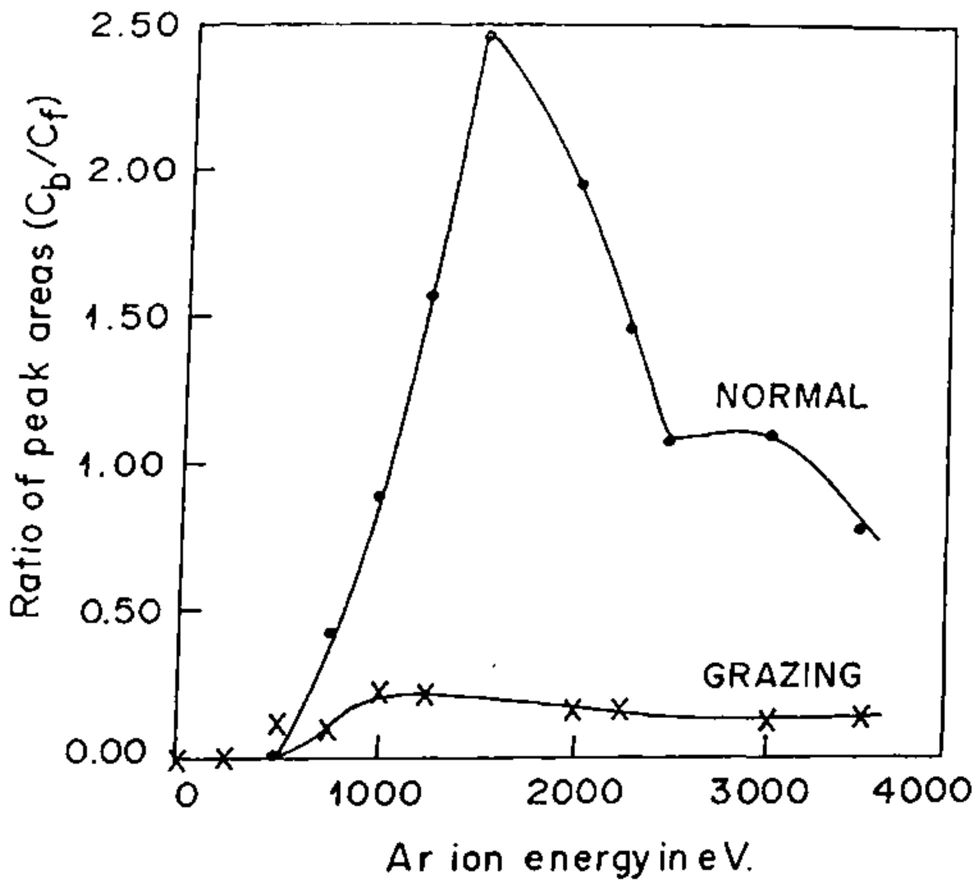

Fig.4a.9. : The ratio of the C(1s) XPS areas of bonded (C_b) and free (C_f) components as a function of ion beam energy. The top curve is when the analyzer is positioned normal to the sample surface and the bottom for grazing exit angles.

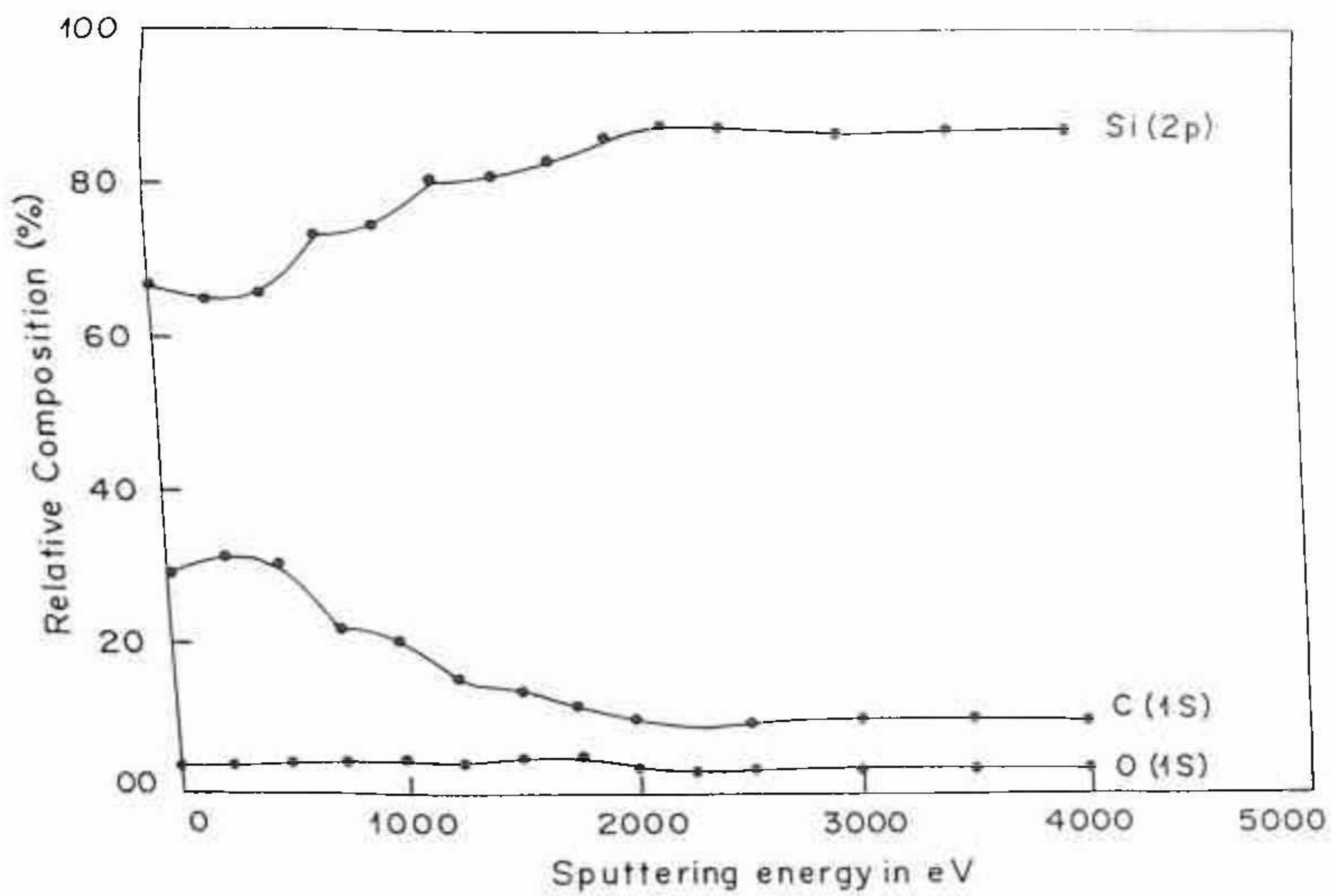

Fig.4a.10: Relative % composition of Si, C and O at different Ar^{+} ion bombardment energies.

about 10 % and then remains unalterd with higher energy ion bombardment. This is attributed to the formation of SiC or related phases that are harder materials with lower sputtering yield in the ion energy range studied. FIG.4a.9 had showed the reduction of bonded C also at ion energies greater than 1500 eV, but this FIG.4a.10, shows the total amount of carbon reducing in the ion energy range from 1500 to 2250 eV. So FIG.4a.10 indicates the effect on total carbon, including both bonded and unbonded, while FIG.4a.9 gives us information of the bonded to unbonded ratio. Also note that there is not much change in the oxygen stoichiometry, in the entire range of ion beam energies studied.

FIG.4a.11. Shows the signature and the deconvoluted components of the C (1s) peak as seen by XPS at different angles of analysis. This figure demonstrates the difference in surface sensitivity and thus confirms that the carburization occurs at the interface. Spectra after the sample was bombarded by a typical energy of 1500 eV has been chosen for this purpose. The grazing exit angle spectra (a) shows a larger free carbon (284.5 eV) component, while that observed at normal to the surface shows more of bonded carbon (283 eV). The third component at 286.3 eV is due to C-O-H[15], which has been avoided in our discussion due to its complexity and relative less abundance.

FIG.4a.12 shows the valence band features as observed by XPS, for some representative energies of ion bombardment, for normal exit angles. The 250 eV curve, is the spectrum of the contaminated sample, with peaks at about 4.0 eV, 8.0 eV and 11.0 eV. The binding energies of the Si(3p) and (3s) electrons are approximately 4 eV and 8 eV respectively. C in the graphitic form shows shallow core level peaks at 13.0 eV and 7.0 eV. With

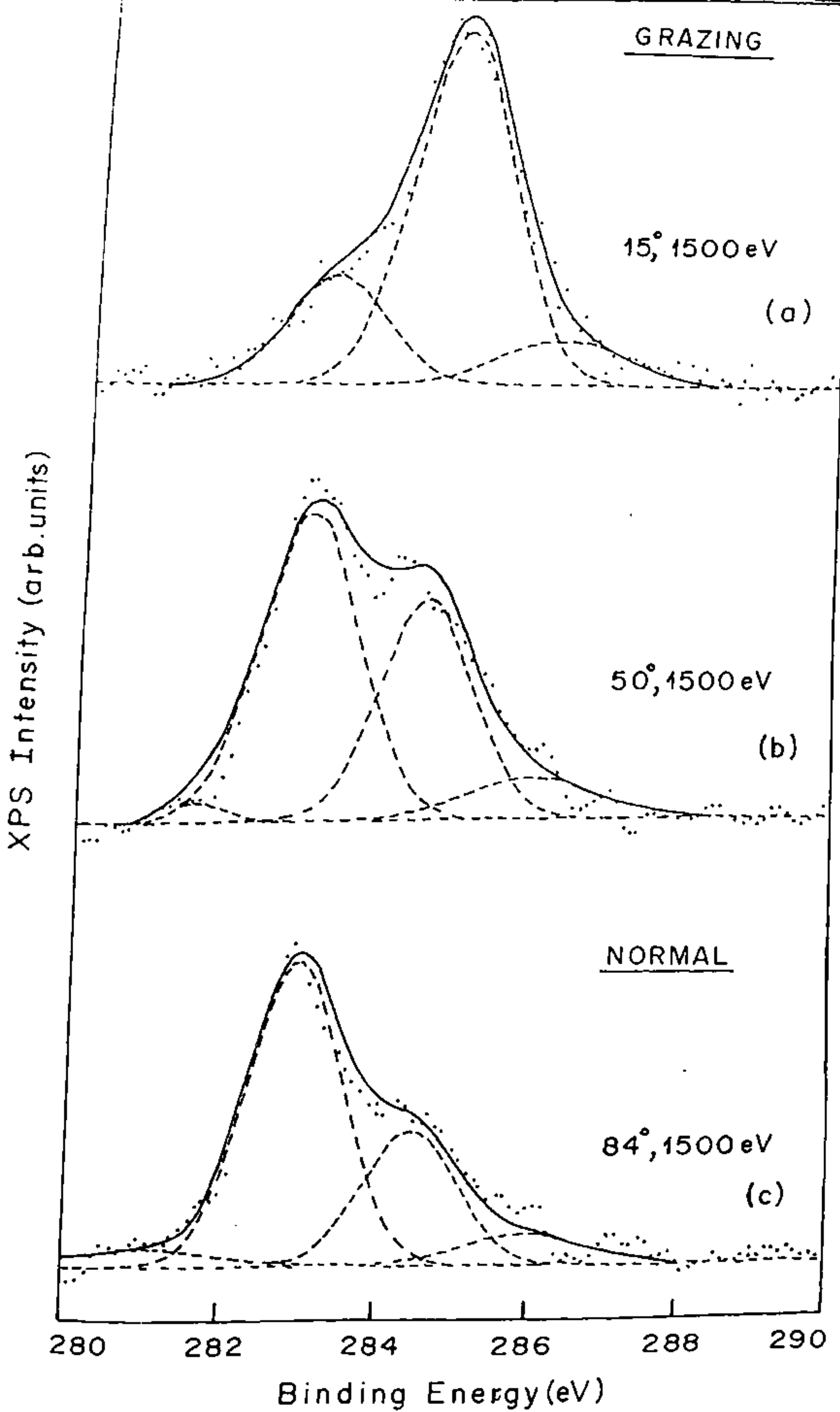

Fig. 4a.11: The C(1s) XPS peak shapes observed at different secondary electron exit angles. 84^{0} denotes sample normal to analyzer and 15^{0} is at grazing angle.

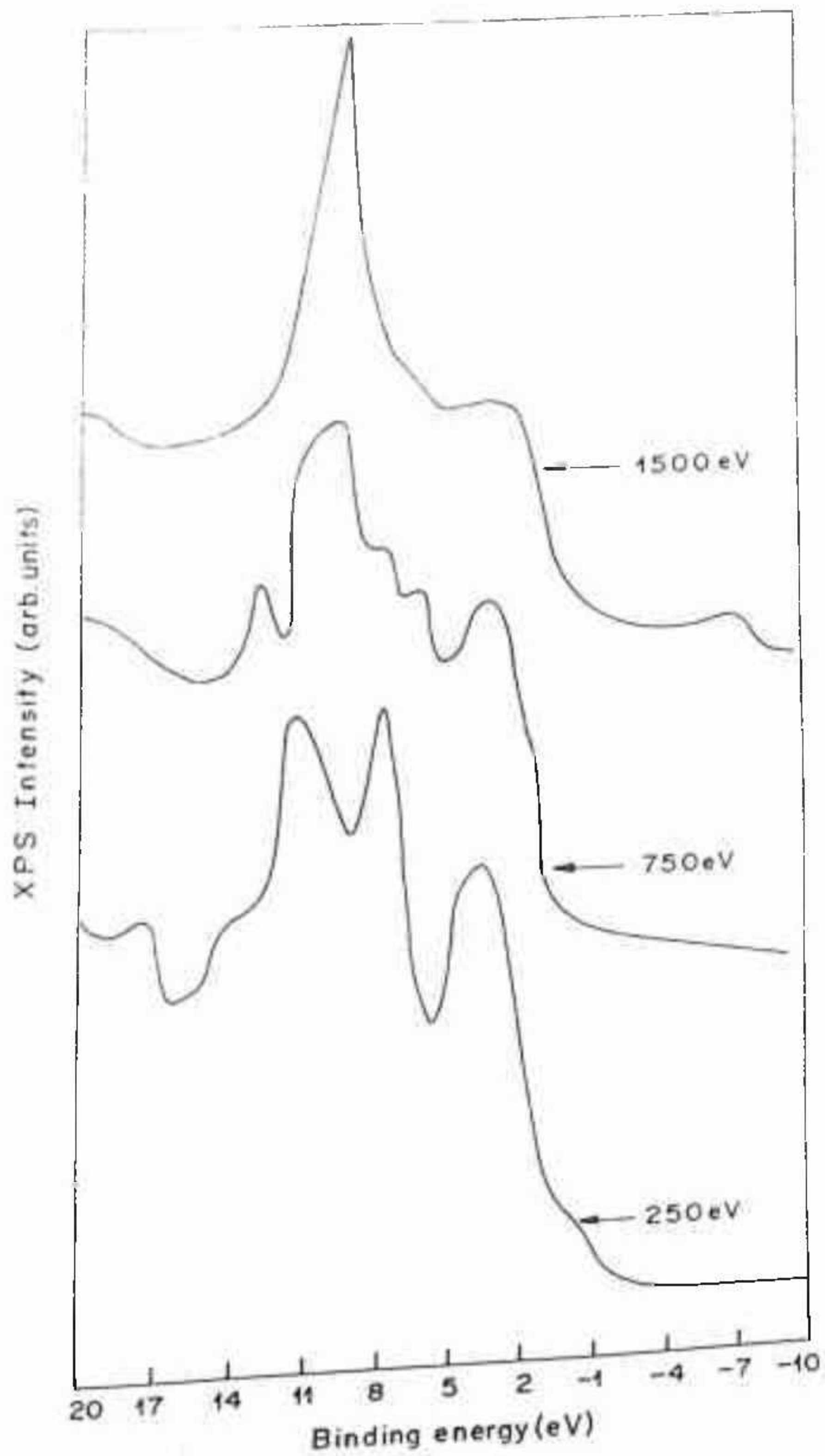

Fig. 4a.12: XPS valence band features of the C/Si system at different incident ion beam energies.

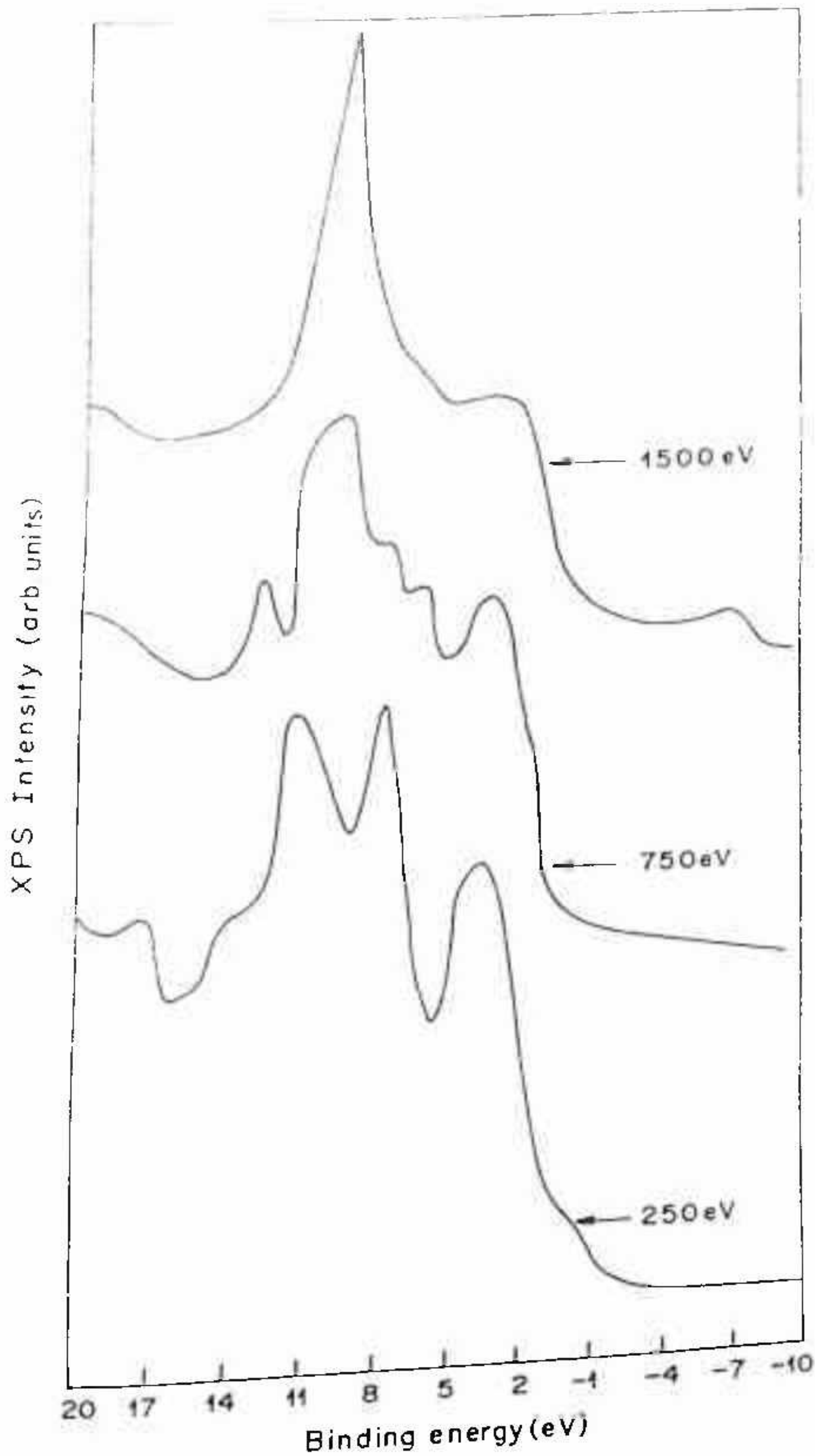

Fig. 4a.12: XPS valence band features of the C/Si system at different incident ion beam energies.

the beginning of the carbide formation by incidence of 750 ev Ar^+ ion, there is a significant reduction of the peak at 7.5 eV. With further higher energy ion interaction at 1500 eV, where the carbide formation is maximum (FIG.4a.9) , we can observe that the 3.5 eV peak has diminished and a sharp peak at 9 eV remain. The reduction in the carbon concentration (as seen in FIG.4a.10) and the charge transfer in the formation of carbide phases may have caused the changes in the valence band features. The 9.0 eV peak may be the result of the chemical shifts of *Si(3s)* and *C(2s)* peaks. The incompletion of the formation into a single phase SiC is also evident.

FIG.4a.13 demonstrates the changes in the anisotropy of secondary electron (Si 2p) emission as a function of ion beam bombardment of different energies. On the as-loaded sample, three peaks are clearly visible at 95°,55° and 30°. These peaks have been attributed[16] to the forward scattering of Si (2p) electrons due to nuclei of Si atoms occuring in their paths to the detector. Basically, without going into the details of the forward scattering aspects, the peaks demonstrate the presence of a crystal structrure, that is consistent with the Si (111) surface[16], however modified by the presence of impurities (C & O) on the surface. As the surface is bombarded with energetic ions, along with the induced carburization described earlier, the forward scattering features are sucessively seen to diminish. The Ar^+ ion sputtering induces a collision cascade and destroys the symmetric structure[15] of surface atoms, which is manifested in the almost isotropic secondary electrons emission. The fall

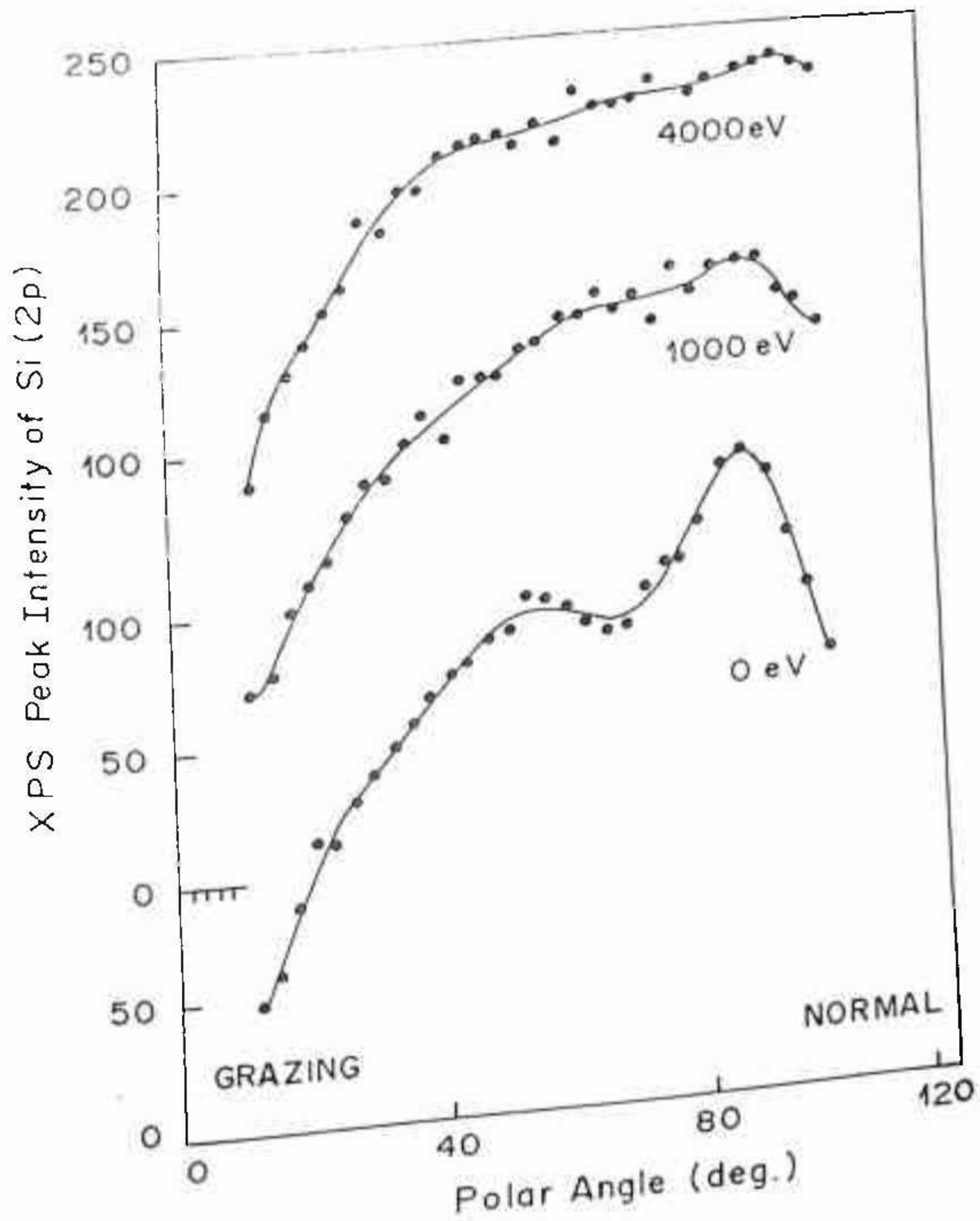

Fig. 4a.13: Polar angle dependent XPS data of Si(2p) as a function of Ar^{+} ion beam energy, showing the reduction of forward scattering effects along the direction parallel to the $(1\bar{1}0)$ plane.

in the intensity at grazing exit angles is due to the presence of impurities like C and O on the surface, that reduce the amount of Si observed within the probed region.

Thus this study of the interaction of energetic ion beam with a contaminated Si surface, by using angle dependent XPS gives a wealth of information regarding bonding, sputtering and surface structure. It is clear from the observations that the ion-beam with energy greater than or equal to 750 eV, induce Si-C bonding. Observing the line shapes at grazing exit angles indicate clearly that the Si-C bonding takes place at the interface region, thus ruling out any major diffusion of C into Si or vice versa. *The loss of structrure of the forward scattering effects* demonstrates the destruction of surface structure with sputtering due to energetic ions. There seems to be significanit changes in the valence band electronic structure that indicates the charge transfer that may have taken place.

4a. 5 Conclusion :

Contaminated Ta, Mo and Si undergo carburization in the Ar ion sputter cleaning process, at a threshold ion energy. However in case of Ti, the carbon observed on the surface was very small which was sputtered out easily. Cu does not show any carbide formation at all.

Glancing angle sputtering may be better due to the increase in sputtering rate of carbon on top of the surface and avoids its contact with the substrate with which it may react. Some ex-situ chemical cleaning is preferred before introducing which leaves only a small amount of carbon

on the surface. Using a low ion beam energy this carbon can easily be removed, since higher energies cause reactions and implantation. The metals like Ta, Mo were cleaned ultrasonically dipping the successievely in C_2H_5OH and CH_3OH, which leaves a small amount of carbon on the surface. Ion beam rastered at 2 kev beam energy is used to clean the samples. Si was cleaned ultrasonically by dipping the Si wafer in 2% HF in methyl alcohol for 2 mins. So to get a clean Si surface suitable for surface analysis was obtained by simultaneous sputtering and heating the sample in a cyclic order. The sputtering was done at glancing angle with beam energy 500eV and heating was done upto 1200K temperature for 30 s per cycle.

References :

1] E. Kny, J. Vac. Sci. Technol. 17 (1980) 685.

2] J.K.N. Sharma, Santanu Bera and B.R. Chakraborty, Appl. Phys. Letts. 59 (1991) 3247.

3] S.M. Shivaprasad, Santanu Bera, N. Sen and J.K.N. Sharma, J. Appl. Phys. Communicated.

4] J.K.N. Sharma and Santanu Bera, Proc. Solid State Phys. Symposium, Sri Venkateswar Univ. Tirupati, Dec. 28 (1992) 393.

5] J.C. Lascovich, R. Giorgi & S.S. Scaglione, Appl. Surf. Sci, 47 (1991) 17.

6] L.Papagno and L.S. Caputi, Surf. Sci. 125 (1983) 530.

7] A.A. Galuska, H.H. Madden & R.E. Allred, Appl. Surf. Sci. 32 (1986) 253.

8] G.R. Gruzalski and D.M. Zehner, Phys. Rev. B 34 (1986) 3841.

9] F.L. Hutson, D.E. Ramaker and B.E. Koel, Surf. Sci. 248 (1991) 104.

10] C. Anandan, Ph.D. Thesis, Univ. of Wales College of Cardiff, (1990)

11] F.G. Bell and L. Ley, Phys. Rev. B 37 (1988) 8383.

12] Y. Mizokawa, T. Miyasatre, S. Nakamura, K.M. Geib and C.W. Wilmsen, J. Vac. Sci. Technol. A5, (1987) 2809.

13] T.N. Taylor, J. Mat. Res.4 (1989) 189.

14] C.D. Wagner, W.M. Riggs, L.E. Davis and J.F. Moulder, Handbook of X-Ray Photoelectron Spectroscopy, Perkin Elmer Corp. USA, (1979).

15] Hartnell et al. J. Vac. Sci. Technol. 8 (1990) 2133.

16] S.M. Shivaprasad and Santanu Bera, to be published.

Chapter IV
Section B
VB related electron spectroscopies

Valence Band related Electron Spectroscopies

4b.Introduction :

In this second section of the results and discussions chapter, the loss peaks and Auger lineshapes along with the autoionization features are studied. The results and their brief discussions are given here technique-wise to understand the subtle changes in the materials studied. In this part the peak position, the origin of the peaks and the the variation of the peakshapes due to oxidation and silicidation are presented and discussed in brief. The results from ELS and autoionization transitions determines the above Fermi level behaviour and AES gives information of the DOS below Fermi level of oxidation and silicidation process.

4b.1. Electron Energy Loss Spectroscopy :

Chemical reactions like silicidation or oxidation of metals creates a redistribution of the valence band of the reactants. So ELS is expected to show some signature of the chemical interaction and the bonding nature of the product. In this section the changes in the different features in ELS due to oxidation and silcidation of Mo, Ti, Ta and Cu is measured. The changes are obvious and distinct, mostly in two regions, e.g. plasmon losses and the interband transition losses. Interband transition associated with p-d quasiatomic transition is found to increase in the oxidation and

decrease in the silicidation. The p-d transition intensity directly depends on the available d-holes in the d band. So the decrease or increase in the intensity is explained in terms of d band change after silicidation or oxidation. Plasmon loss changes are quiet abrupt due to oxidation and silicidation for a particular metal, but has a systematically changing value among the silicides. A qualitative and semi-quantitative measurement of these changes are given in this chapter.

4b.1.1 ELS in Ta, Ta_2O_5 and $TaSi_2$:

The loss characteristics of materials is a direct function of the dielectric properties of the material, which is further defined in terms of optical properties like absorbance and reflectivity of the material. In literature optical experiments with Ta have been done in the ultraviolet and visible regions of the spectrum. Data for the pure clean Ta, for reflectivity and absorbance is available[1]. The electronic structure of Ta was considered by Mattheiss[2] with the relativistic effects. A considerable similarity was observed between Fermi surface and the band structure near the Fermi level. The APW (augmented plane wave) non-relativistic band structure calculations of crystalline Ta is available in the work of Petroff and Viswanathan[3].

Different loss features for Ta along with its oxide and silicide are shown in FIG.4b.1. The features listed in Table I for Ta are in good agreement with the optical data published by Weaver et al[1]. and the ELS results by Martinez Duart et. al[4]. From the optical properties and the band structure calculations it is found that Ta shows two types of volume

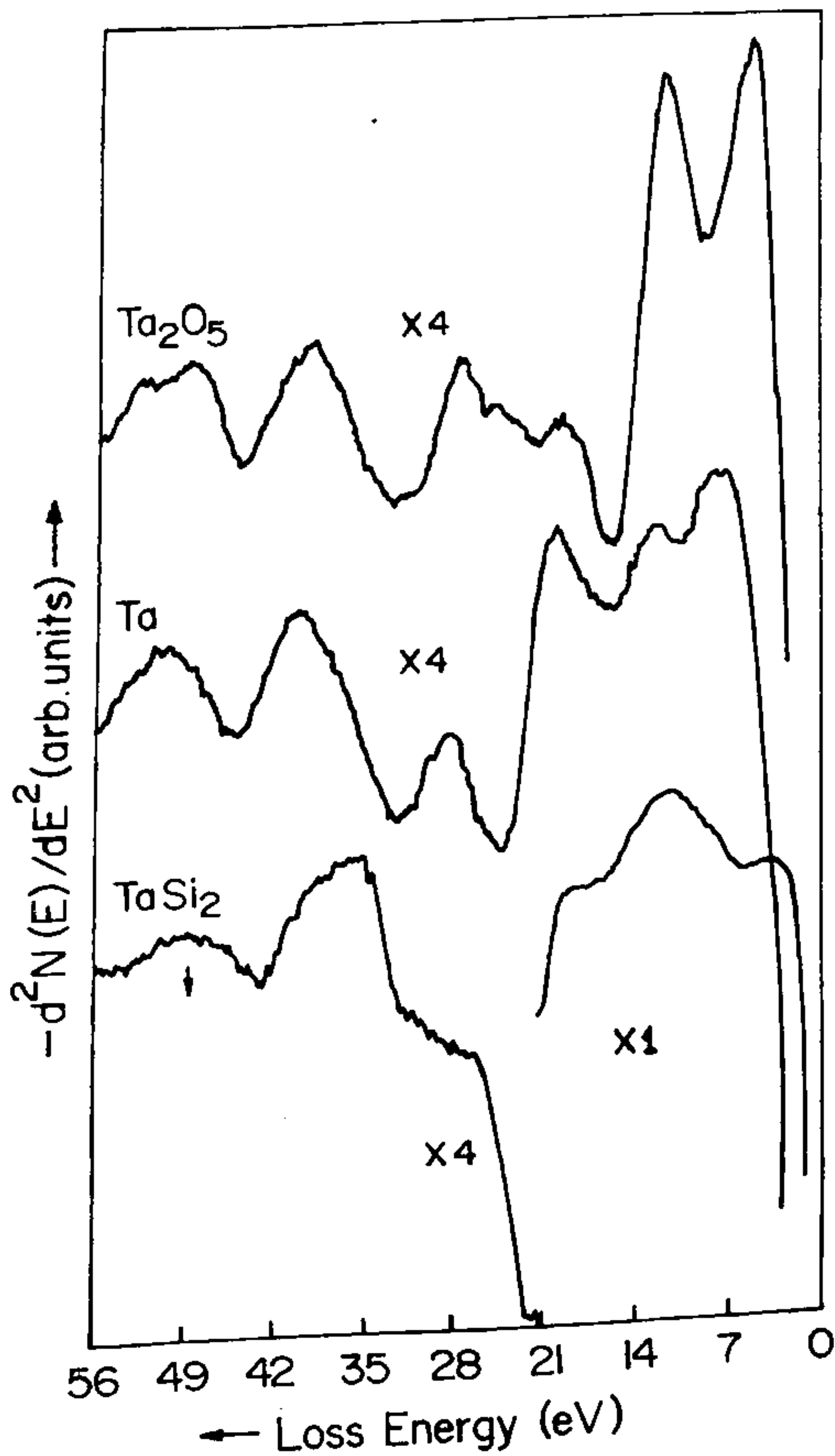

Fig.4b.1 : ELS in Ta, Ta_2O_5 and $TaSi_2$ in the double derivative mode. The arrow indicates the probable position of the $5p_{1/2}$ --$E_f+\Delta E$ transition.

and surface plasmon losses, the low energy and high energy plasmon losses. In our study low energy and high energy volume plasmon losses are observed at 8.5 and 20.5 eV respectively which agrees with the results given by Weaver et al[1]. High energy surface plasmon is seen around 17 eV. According to Weaver et al[1] the low energy volume plasmon and surface plasmon losses are expected at 8.9 and 8.6 eV respectively. So due to the limitation of our experimental energy resolution, the broad peak at 8.5 eV may be including both these two losses.

The volume plasmon loss at higher energy is close to the free electron gas plasmon value, but the higher energy surface plasmon related peak is not. The observed volume plasmon loss peak can be interpreted in terms of collective oscillation of s and d electron in the bulk of the material. But the associated surface plasmon loss peak is shifted from the $h\omega_p/\sqrt{2}$ value. The shift can be seen as due to the screening of the coulomb force by the valence electron as suggested by Weaver et al[1]. The volume plasmon at lower energy (8.5 eV) probably involves only a group of electrons, perhaps the core charge density of the d like electrons does not participate. Clearly the situation is not like a free electron case. Although a part of the oscillations (20.5 eV) obey the free electron model. In shallow core level range the prominent features are associated with the transition from the 4f levels to the states above the Fermi level. Due to spin orbit interaction Ta 4f line it shows a splitting of ≈2 eV which is shown in XPS. For $4f_{5/2}$ the binding energy is 23.53 and $4f_{7/2}$ it is 21.61 eV. According to the work by Penchina[5] the theoretical density of states for crystalline bcc Ta, shows some empty states at about 5 eV above the E_f. So the loss features at 28.9 or 26.5 eV are associated with the

transition of 23.53 and 21.61 eV 4f electrons to the states above the Fermi level. Same thing happens to the 5p electrons, where a spin orbit splliting of $5p_{1/2}$ and $5p_{3/2}$ levels of energy values 32.7 and 42.4 eV give the transitions losses at 39 and 49 eV respectively.

In case of oxide some more loss features are added due to the transitions related to the oxygen. In the lower energy loss feature the characteristic bulk plasmon loss is observed at around 19.6 eV which is in good agreement with the result given by Martinez Duart and Palacio[4]. The surface plasmon is found at 15.4 eV and the peak at around 11 eV is assumed to be associated with interband transition. In Ta_2O_5 the O 2p feature is found around 6.5 eV below the Fermi level. So the transition from O 2p to the level 5 eV above the Fermi level may be attributed to the peak at 11 eV. The peak at 28.5 eV is attributed to the transition from the 4f levels to the states above the Fermi level. The 5p electrons also show the transition to the empty states above the Fermi level by showing the loss features at around 50 and 40 eV.

In the $TaSi_2$ the nature of the loss peak is completely changed. In the lower region the 19.5 eV gives the bulk plasmon loss and the surface plasmon loss feature at 13.5 eV. Si 3s--conduction band transition is observed at 6.5 eV[6]. However the transition related to the 5p levels to the states above the Fermi level are existing but with less domination than the other two cases of pure and oxidised Ta[7]. The details of the loss transitions observed are given in the Table I.

In FIG.4b.2 the normal mode of the spectrum is used to show the sharp changes for these three samples. It is observed that the transitions related to the 4f levels are not distinct in the oxide because of other

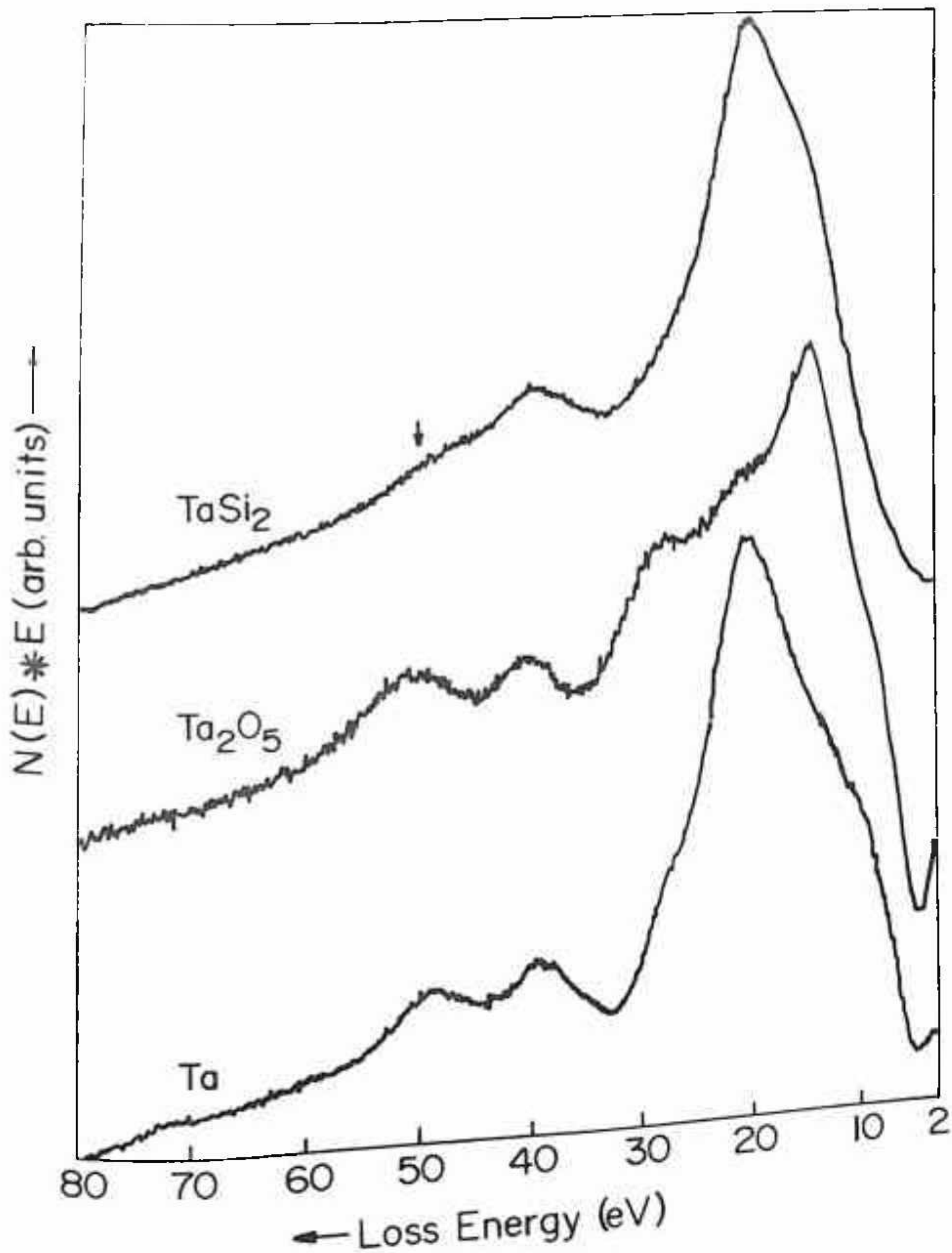

Fig.4b.2 : ELS of Ta, Ta_2O_5 and $TaSi_2$ in the normal mode. The arrow indicates the probable position of the $5p_{1/2}$ --$E_f + \Delta E$ transition.

Table I : EELS in Ta, Ta_2O_5 and $TaSi_2$

Transitions involved	Ta (eV)	Ta_2O_5 (eV)	$TaSi_2$ (eV)
$5p_{1/2}$--E_F+ ΔE	49.0	50	48.0
$5p_{1/2}$ -- Threshold	not resolved		
$5p_{3/2}$--E_F+ ΔE	39.0	40.0	38.5
$5p_{3/2}$ -- threshold	33.5	34	
2X Vol. Plasmon (VP)--		--	36--39
$4f_{5/2}$--E_F+ ΔE	28.9	28.5	--
$4f_{7/2}$--E_F+ ΔE	26.5	--	--
Vol. plasmon (higher energy)	20.5	19.6	19.5
Surface Plasmon (SP) (higher energy)	17.0	15.4	--
Low VP+Low SP	10.3	--	--
Low Vp and /or Low SP	8.5	--	--
Surface plasmon	--	---	13.5
O 2p	--	6.5	--
Si 3s --CB	--	---	6.5

transitions around the same values. In oxide 5p related loss features are found to increase where as in the silicide these are decreased . These loss features distincly show the change in the valence band after the oxidation and silicidation of Ta. The loss feature at 38.5 eV in silicide is not decreased, though the feature at 48.0 eV is decreased.

4b.1.2. ELS in Mo, MoO_3 and $MoSi_2$:

The refractory metal Mo interacts strongly with both Si and O. The data of room temperature oxidation of Mo and their study by ELS for understanding the different oxidation states is available[8] where the qualitative and semiquantitative investigation of the local density of states is investigated. The main characteristic loss spectra are due to excitation of collective oscillations (bulk and surface plasmon) and interband transitions. Due to the bcc nature of Mo it also shows two bulk and surface plasmons[1].

In pure Mo films, the low energy peaks are mostly associated with the plasmon loss peaks (FIG.4b. 3). According to Weaver et al[1] the optical calculations on Mo should show two bulk and two surface plasmon loss peaks. The peak at 11 and 24 eV are asociated with surface and bulk plasmon losses respectively[9,10]. In this loss structure the double volume and surface loss structures are not observed. According to the optical calculations[1], both low energy surface and bulk plasmon losses are expected at 10.4 and 9.5 eV respectively. So 11 eV may be a superposition of these two transitions also. The high energy surface plasmon loss peak is expected at around 14.8 eV, which is not observed here, may be due to

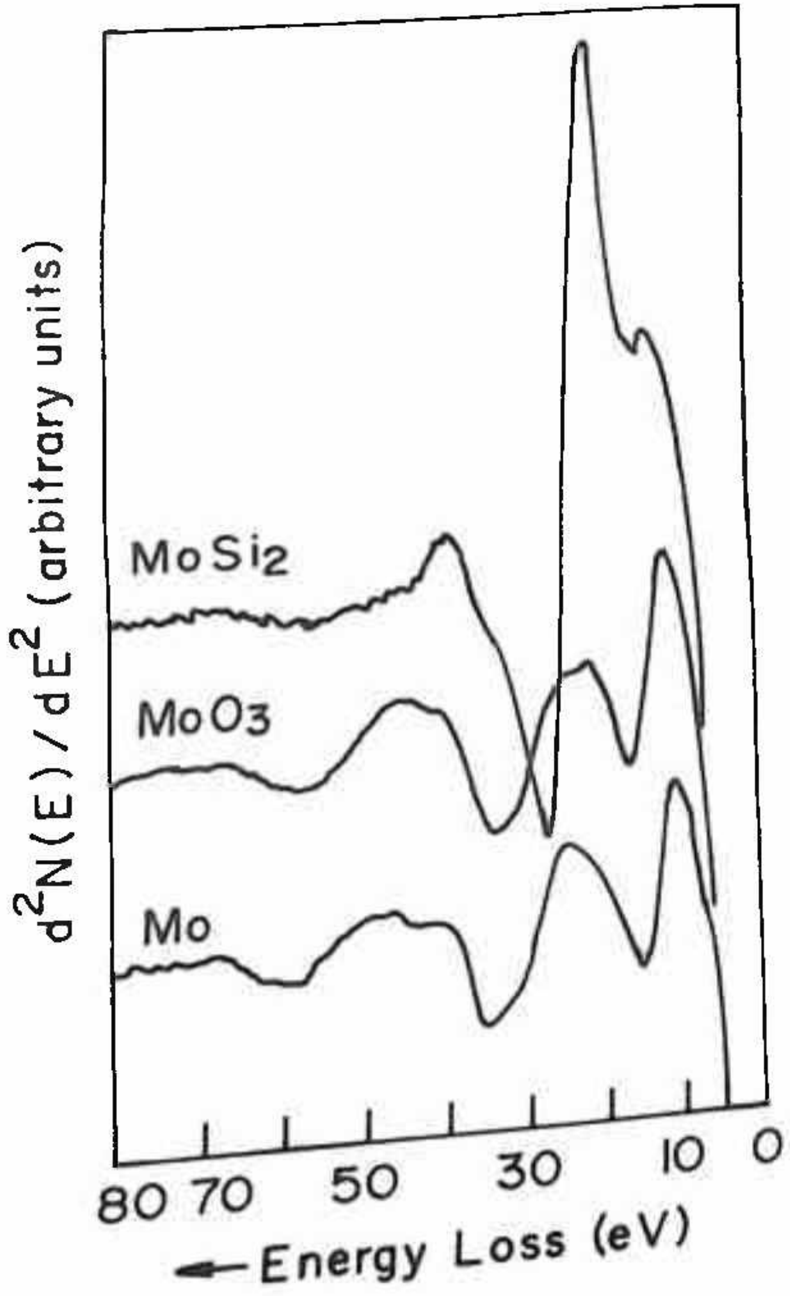

Fig.4b.3 : ELS spectra in the double derivative mode in Mo, MoO_3 and $MoSi_2$.

the volume plasmon loss peak at 24 eV with its large background. From free electron model, calculations indicate that bulk plasmon peak should have an energy loss at 17 eV. But no such peak is observed, which may be due to the inapplicability of free electron model to Mo. The loss peak at 38 eV is associated with the interband transition as shown in the Table II.

The peak at 47 eV is neither a plasmon loss peak nor an interband transition, according to the X-ray absorption data given by Beardeen and Burr[11]. This structure is not new, since it has been observed in Mo in previous ELS work and in the X-ray work by Sonntang et al and Haeasel et al[12,13]. This type of structure, seen in V was explained by Missel and Atkins[14] as the splitting of the excited state through an exchange interaction between the unfilled d shell and 3p hole. Zashkvara et. al[15] proposed yet another mechanism for similar structure in the second and the third transition metal series. This explanation says that " ionization plasma " process which involve the ionization of 4p level to a transition of 4d state accompanied by the excitation of a lower plasmon. It is suggested that the 47 eV feature is a result of 3p hole interaction with unfilled d shell, and that splits the excited level causing this special feature relating to the p--d quasiatomic transition. In the MoO_3 the surface plasmon was found around 12 eV. The bulk plasmon was observed at 22 eV with a shoulder at 27 eV, as observed by Minni and Werfel[8] also. The higher energy peaks are mostly associated with the interband transitions. The loss peak at 39 eV is due to the excitation of 4p electrons which persists with the same intensity, suggesting the availability of the empty states after oxidation.

Table II : EELS in Mo, MoO_3 and $MoSi_2$

Loss characters	Mo (eV)	MoO_3 (eV)	$MoSi_2$ (eV)
Low VP/low SP	11	12	15
Higher VP	24	22	20.5
Mo 4p --E_f+ΔE	38	39	--
2 X VP	--	--	38--40
p--d quasiatomic related transition	47	47	--
Mo 4s -- E_f+ΔE	65	66	64 (↓)

In the oxidised case the peak at 47 eV is more prominent than the pure Mo case. In the silicide the surface and bulk plasmon losses are found at around 15 eV and 20.5 eV respectively[16]. The broad peak at around 40 eV may be the second multiple of the volume plasmon loss peak. The 4p--d transition peak expected at around 38 eV is not distinct due to the presence of the intense plasmon loss feature at 40 eV. The 47 eV peak is also observed to be quite small[17].

4b.1.3. ELS in Ti, TiO_2 and $TiSi_2$:

The energy loss for low energy electron incident on the clean Ti, $TiSi_2$ and TiO_2 thin films resulting from the plasmon oscillation and shallow core level losses are utilised to find the behaviour of d electrons in the formation of the two compounds. The study of the oxidation for Ti and Stoichiometric TiO_2 is available from different publications[18,19]. $TiSi_2$ is a well characterised material and different surface analytical techniques like XPS, IXPS[20] (internal X-ray photoelectron spectroscopy) and UPS[21,22] etc. are used to understand the chemistry of both the oxidation and silicidation. To get a more complete picture of silicidation and oxidation of Ti the results of AES and ELS is useful.

EELS of Ti provides different plasmon loss and shallow core level excitation. In FIG.4b.4 The surface and volume plasmon losses are observed at 11 and 19 eV[23]. However like Ta and Mo, Ti does not show double surface and bulk plasmon losses. The peak at 5 eV is associated with the transition of $M_{4,5}$ electrons to the empty states above the Fermi level. From the x-ray spectroscopic data (Appendix) the peak at 34.5 eV

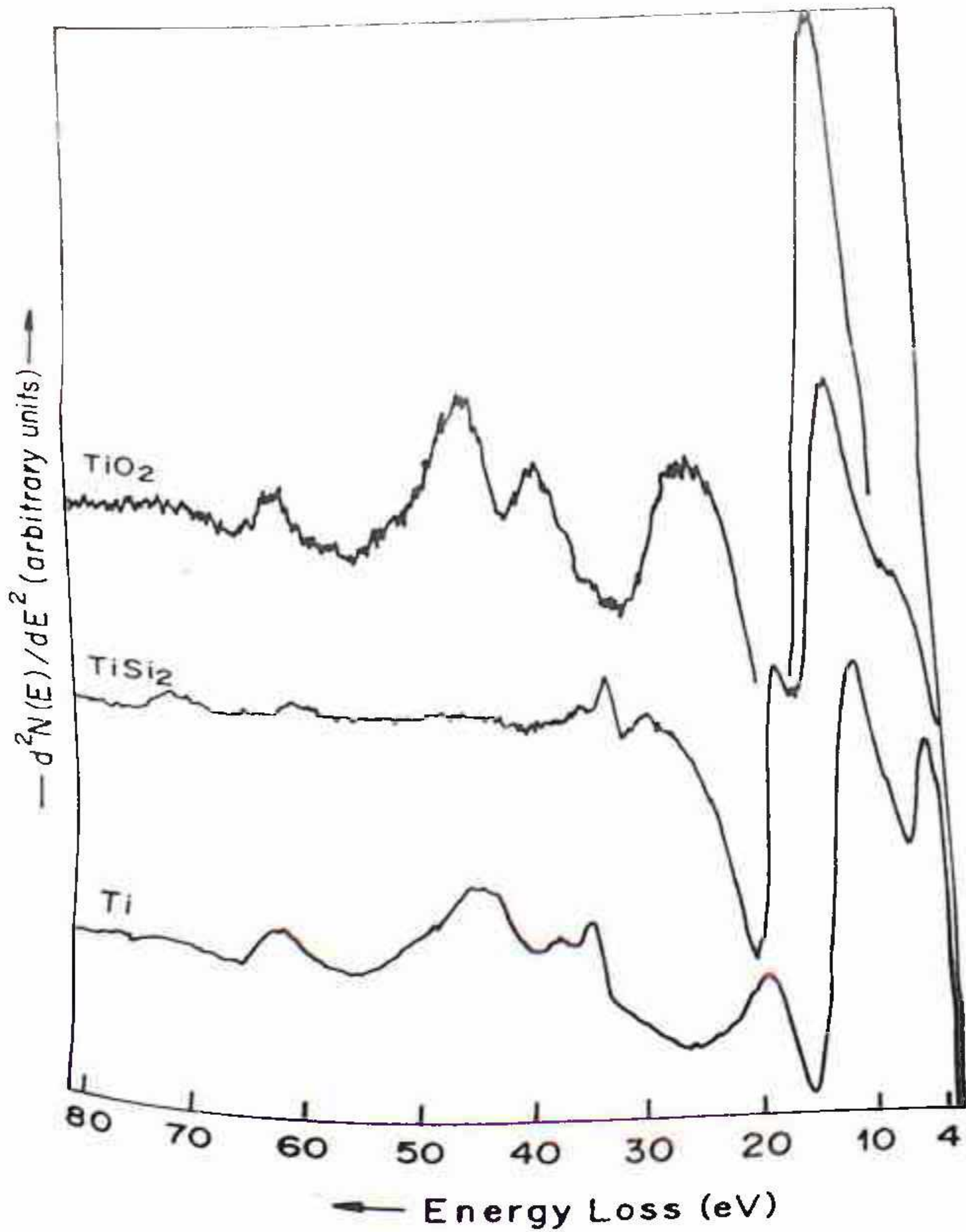

Fig.4b.4 : ELS of Ti, TiO_2 and $TiSi_2$ in the double derivative mode.

may be taken as the threshold of the $M_{2,3}$ level and the peak at 37.5 eV is the transition of $M_{2,3}$ electrons approximately 2 eV above the Fermi level. Similar transition found at 61 eV is the transition of 4s electrons to the states above the Fermi level in the d band. Like in Mo an unexpected peak is observed at 45 eV (47 eV for Bertels[18] work) This is explained in terms of strong exchange interaction which splits the excited state at approximately 14 eV above the threshold[18].

The sharp change in the ELS of TiO_2 is found both in lower and higher energy losses. Transitions related to oxygen 2p is found at around 7.0 eV, is the O 2p threshold[23]. The O 2p to Ti 3d band transition is found at around 10 eV which suggests the availablity of empty states above the Fermi level even after oxidation. The intense and broad (23-24 eV) is associated with bulk plasmon loss as well as the O 2s transition. Due to the intense nature of this peak the surface plasmon loss peak expected at around 16.5 eV is probably buried in it. Same thing happens to the $M_{2,3}$ related transition. The broad peak is associated with the M_{23} threshold at 34.5 eV and the transition to empty states above the Fermi level is at around 36.5 eV, which causes the broadness of the peak. The peak at 43 eV in the oxide, which is around 45 eV in Ti is associated with 3p--3d transition. The peak is more intense than in the case of Ti suggesting that localization of the $3d^*$ state is still available after oxidation. The transition at around 60.5 eV is associated with the Ti M_1 (3s) excitation to empty states above Fermi level.

$TiSi_2$ resembles the result given by Iwami et al[24]. The peak at 7.5 eV is associated with the Si 3s transition probably the threshold of Si 3s. The plasmon losses observed at 12.5 eV and 18.5 eV are surface and

Table III : EELS in Ti, TiO_2 and $TiSi_2$

Loss character	Ti (eV)	TiO_2 (eV)	$TiSi_2$ (eV)
M_{45} related	5.0	--	--
O 2p threshold		7.0	
Si 3s threshold			7.5
Surface Plasmon	11 .0		12.5
O 2p --3d transition		10	
Bulk plasmon	19.0	(23-24)	18.5
Si related transition	--	--	29.5
M_{23} threshold	34.5	not resolved	34.0
M_{23} --E_F+ΔE	37.5	36.5	--
p-d quasiatomic related transition	45. 0	43.0	45.0 (↓)
M_1 --E_F + ΔE	61.0	60.5	61.0

volume plasmon losses. However the broad peak at around 29.5 eV is
probably associated with the combined volume and surface plasmon
losses. The peak at around 34 eV is distinctly observed, which is
associated with the $M_{2,3}$ related transition. The peak expected at around
37.5 (for interband transition) is not found to be prominant. Similar thing
happens to the peak around 61 eV which is associated with the Ti 3s
transiton. The p-d quasiatomic transition at 45 eV in Ti, is almost
vanishing in the silicide.

4b.1.4. ELS in Cu, CuO and $CuSi_2$:

The ELS of Cu in the lower region is mostly associated with
plasmon losses, as the shallow core level for copper is at 74 eV ($M_{2,3}$).
The interaction of Cu with Si or O is strongly reflected in the plasmon loss
and their changes in this material (shown in FIG.4b.5). The loss spectrum
of Cu studied by Jenkins et al[25] gives some fundamental information
about the plasmon losses. The understanding of Cu oxidation by ELS and
AES, was done by Bendrof et al[26] But the silicidation by ELS or the
bonding nature of oxide and silicide are yet to be studied.

In ELS of Cu the loss structures are mostly associated with
plasmon losses. The loss features at 8 eV and 20.5 eV give the surface and
bulk plasmon losses respectively. But the surface plasmon loss peak is not
observed at $\hbar\omega_p/2^{1/2}$ energy value which states the limitation of the
applicability of the free electron model to plasmon loss of Cu. The peaks
at 4.5 eV and 10.5 eV are due to the interband transition of Cu d electrons.
The loss peak at 28.5 eV is associated with some combination scattering

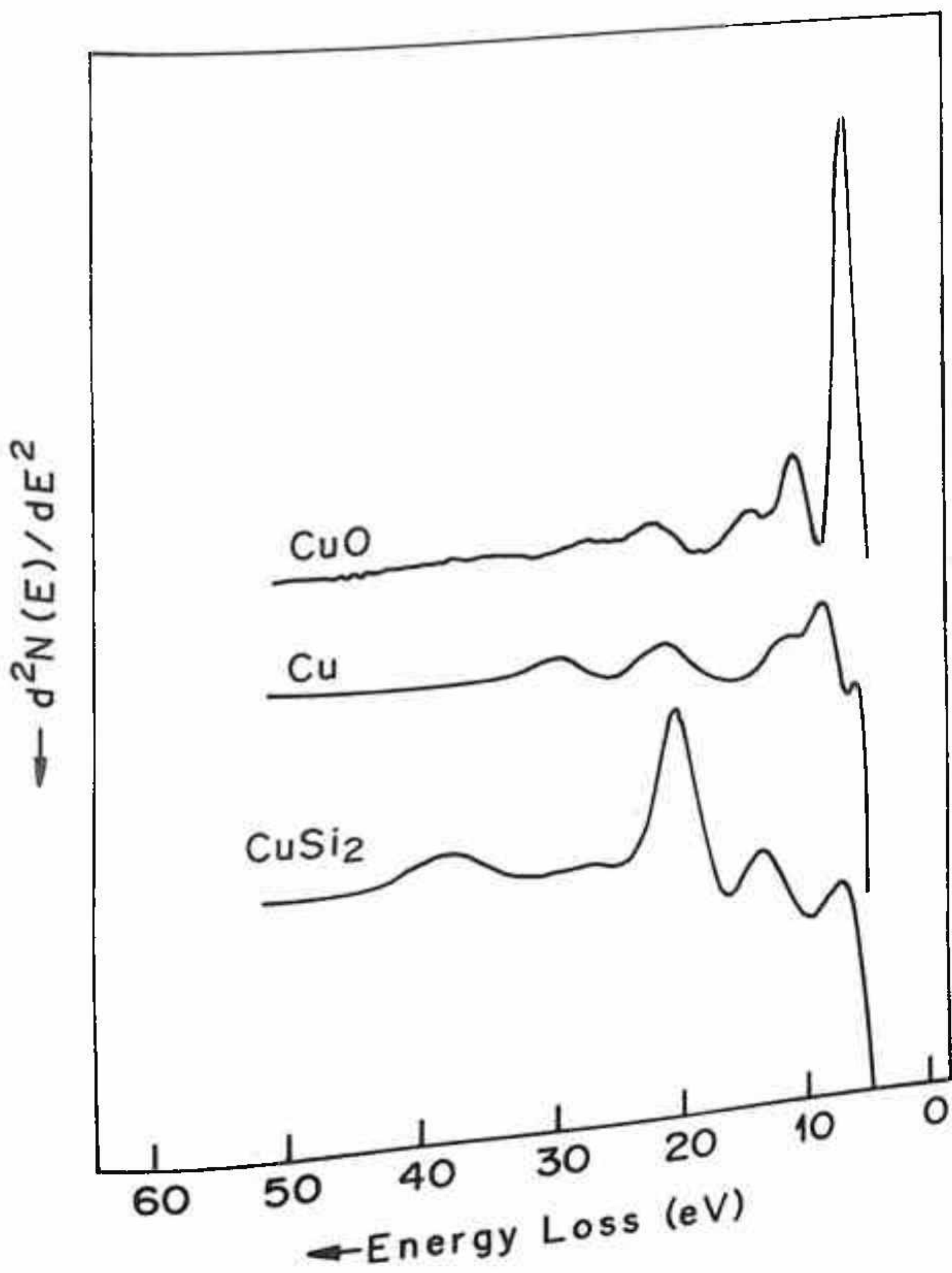

Fig.4b.5 : ELS of Cu, CuO and $CuSi_2$ in the double derivative mode.

Table IV : EELS of Cu , CuO and $CuSi_2$

Loss characteristics	Cu (eV)	CuO (eV)	$CuSi_2$ (eV)
Interband transition	4. 5		
O 2s or Si 3s transition	--	6.5	7
Surface plasmon	8	11.5	12
interband transition	10.5 (?)	14 (O 2s--2p)	
bulk plasmon	20.5	23.5*	19
SP+ VP	28.5	--	
2X vol. plasmon	--	--	37

*interband transition of O also. '?' indicates possible transition.

like bulk and surface plasmon losses. But there is no p--d quasiatomic transition related loss in the polycrystalline Cu.

In the oxide a peak is observed at 6.5 eV which may be associated with O 2s threshold which is the characteristic of the oxide. The peak at 23.5 eV is associated with bulk plasmon loss or interband transition of O. The surface plasmon loss peak is found at 11.5 eV. The new peak at 14 eV is associated with O 2s -- 2p transition. The interband transition at 4.5 eV in Cu is assumed to exist even after oxidation or may be lost in the intense O 2s loss peak at 6.5 eV. It is clear that the loss peak at 28.5 eV is not associated with any interband transition. In the silicide the peak at 7 eV is associated with the Si 3s transition. The peaks at 12 eV and 19 eV are respectively surface and bulk plasmon losses. We could not find any interband transition from Cu matrix after the silicidation indicating the covalent interaction which depletes some of the empty states available for interband transition in Cu. The peak at 37 eV is associated with double volume plasmon loss.

4b.2. Auger Electron Spectroscopy :

Detailed analysis of Si LVV Auger transition is available only in case of Ni, Pd and Ca[27-29] interaction with Si. And in the oxides different Auger transition ratios of O KVV Auger for fingerprint analysis is available[30,31]. In this section the lineshape change of the metal valence band related Auger transitions due to oxidation and silicidation is explained. Si LVV lineshape changes due to silicidation and O-KVV peak changes for oxidation of metals of Ti, Ta, Mo and Cu is explained in the

light of existing models. The fingerprint analysis is done in the first derivative mode. XPS results are also given here to complement the AES results and conclusions.

4b.2.1. AES of Ta, Ta_2O_5 and $TaSi_2$:

Different bonding and antibonding states formed in the Ta and Si interaction is available by UPS work[32]. In the work by Azizan et al[33] the bonding state is observed far below the Fermi level. The non bonding state is also observed near the Fermi level in the silicide. The increase in the DOS above the Fermi level in concordance with the metallic character and the high electrical conductivity helped in predicting the antibonding state in the silicide. LEED study shows a change in the 7x7 structure to 1x1 pattern at 850°C annealing of the 4 ML of Ta on Si. The onset of the rapid silicidation was observed at 500°C and a stable phase was obtained at 850°C[34].

In FIG.4b.6 the Ta NOO and NNN , two valence band related Auger transitions in d(N)/dE mode for pure Ta and its two compounds, are shown. The spectrum of pure Ta shows a doublet at 167 and 172 eV and is associated with multiplet splitting of the $N_4O_3O_3$ transition. The transition at 180 eV can be attributed to the NNN transition which shows an Auger chemical shift of 2 eV in case of oxidation but almost no shift in case of silicidation. The 172 eV (170.5 eV in oxide) decreases in intensity with respect to the peak at 167 eV (165.5 in oxide) following oxidation and

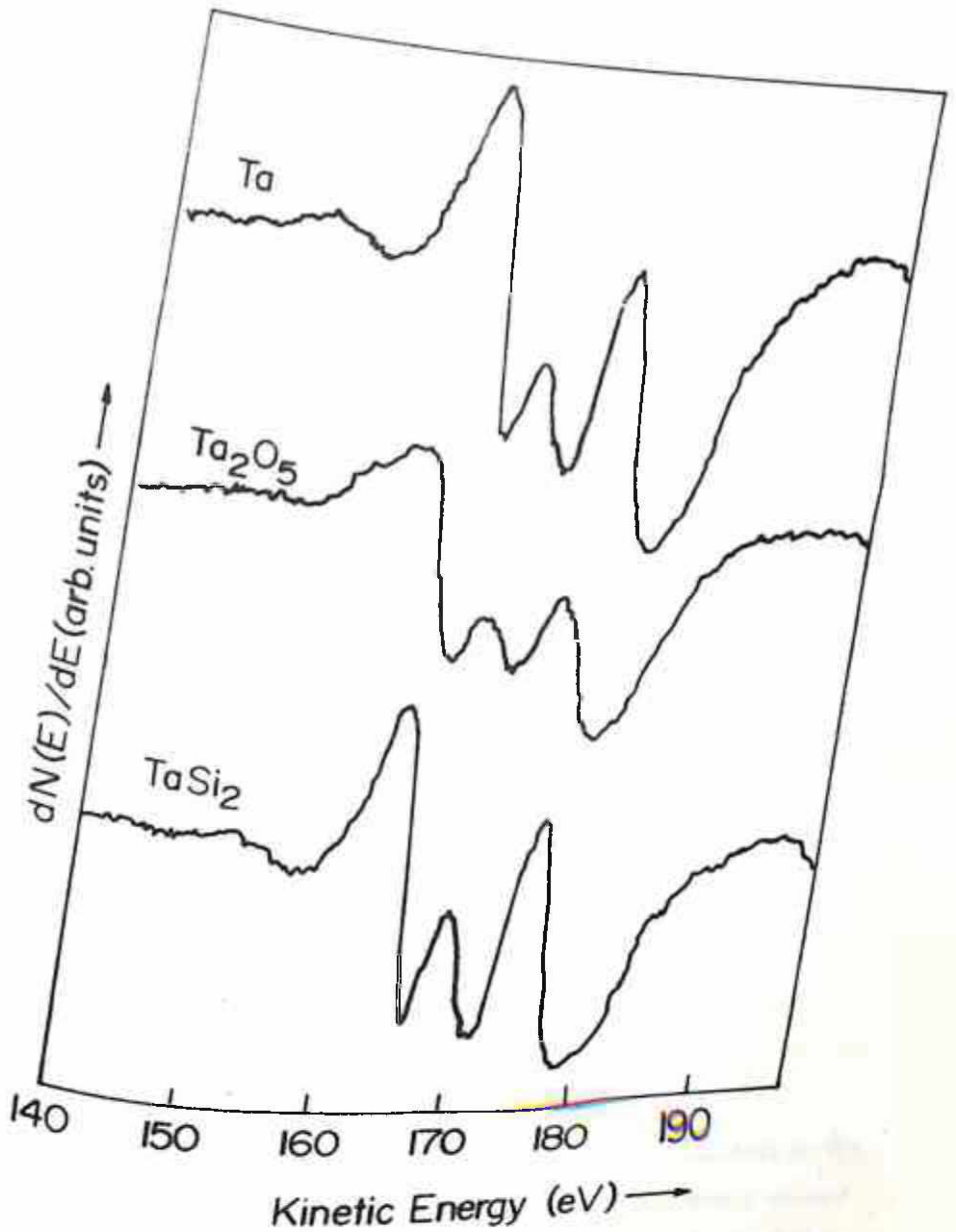

Fig.4b.6 : Auger NOO and NNN transitions in pure, Ta in Ta_2O_5 and $TaSi_2$ compounds.

increases with silicidation. TableV shows peak energies and relative peak intensities for the three samples, and serves to demonstrate the differences for the two bonding states of Ta[7].

Table V : Variation in multiplet splitting due to oxidation and silicidation of Ta.

Materials	$N_4O_3O_3$ p_1(eV)	$N_4O_3O_3$ p_2(eV)	NNN (eV)	Peak to peak height ratio of p_2/p_1
Ta	167.0	172.0	180.0	.32
Ta_2O_5	165.5	170.5	178.0	.27
$TaSi_2$	166.0	171.5	179.0	.39

The change in the Auger fingerprinting in the oxide and silicide is also explained in terms of participation of d electrons differently for oxidation and silcidation.

Complementary XPS results, give an account of the chemical shift and the below Fermi level picture of the materials are shown in the FIG.4b.7&8. As these two effects are explained in Auer electron spectroscopy, so XPS results are also obtained to confirm the observations. In FIG.4b.7 the chemical shift of Ta 4f line is shown. It shows a splitting of $4f_{5/2}$ and $4f_{7/2}$ at the peak binding energy values 23.5 and 21.6 eV respectively. In the silicide the chemical shift is 0.7 eV whereas in the oxide the shift is approximately 5.7 eV which shows the different amount of charge transfer in the two processes. But the chemical shift obtained in case of the Auger transition is 2 eV, because of the formation of two hole final state in the Auger process .

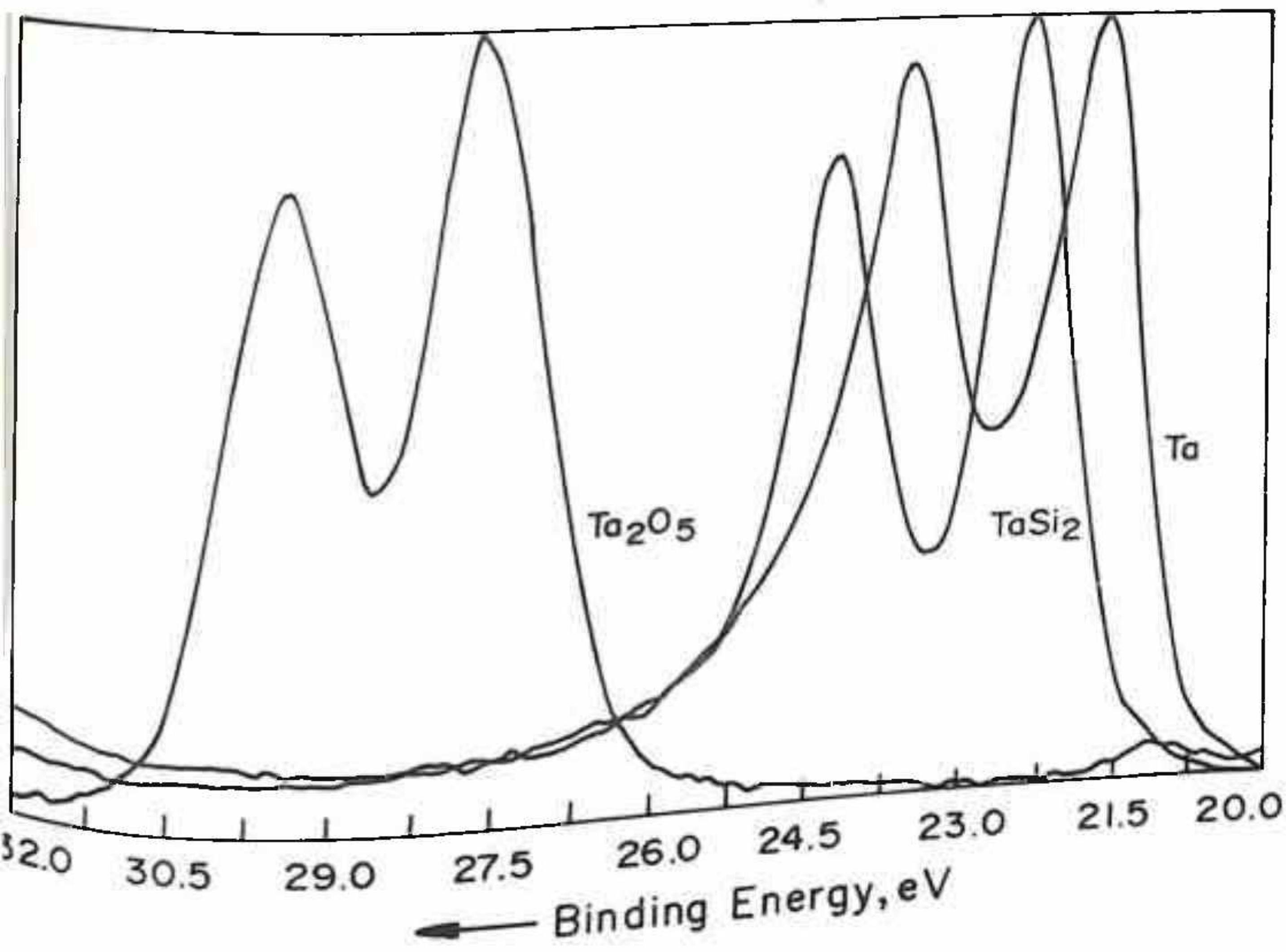

Fig.4b.7 : Ta 4f XPS line after oxidation and silicidation.

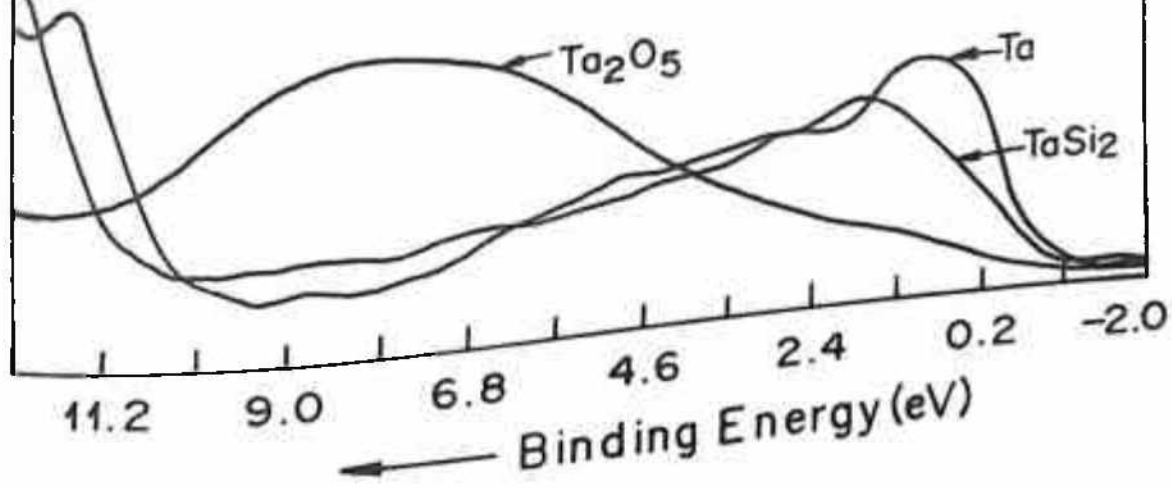

Fig.4b.8 : Valence band features of Ta, Ta_2O_5 and $TaSi_2$ compounds obtained from XPS.

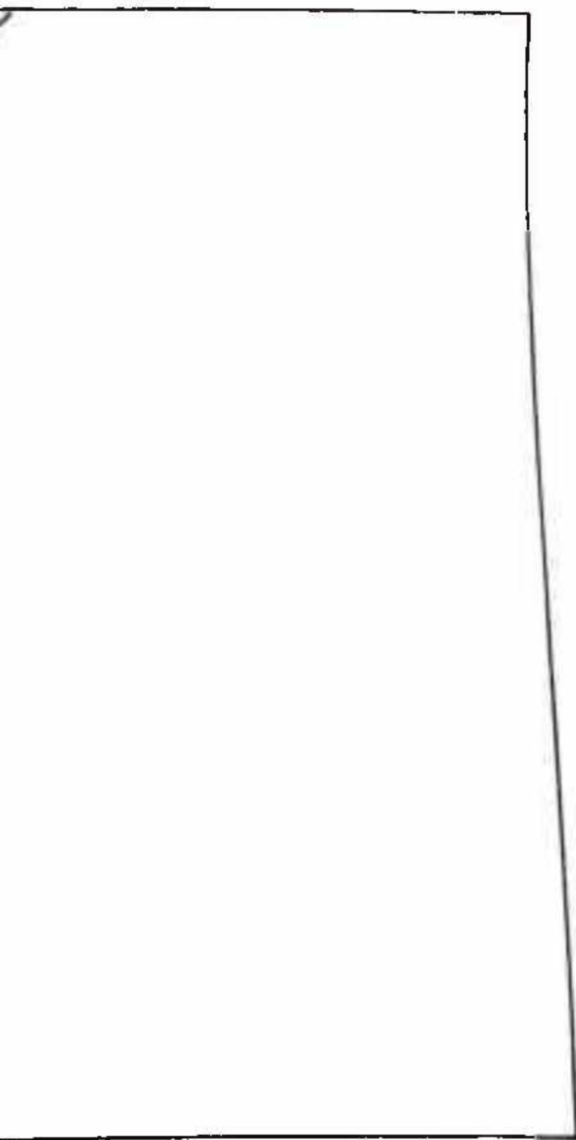
sity (arb. units)

The variation in splitting structure in the oxide and silicide, and their cause explained in the Auger NNN transitions, can be confirmed in the valence band related XPS results. In FIG.4b.8 the valence band picture is shown. In the oxide the depletion of the d band near the Fermi level is observed along with an appearance of a new oxide peak at around 6 eV below the Fermi level. In the silicide the Si p and metal d bonding states are observed very near to the Fermi level. The broadness of the peak may be due to the presence on some non-bonding metal d state in the silicide.

4b.2.2. AES of Mo, MoO_3 and $MoSi_2$:

Mo and and its silicide is an extensively studied material both theoretically and experimentally. The band structure of $MoSi_2$ is calculated by Bhattacharya et al[35] using a self consistent semi-relativistic and relativistic pseudo-potential method. The $MoSi_2$ resembles the total DOS and main projected partial DOS. Azizan et al[32,33] showed the IPE (Inverse photoemission) spectra to show the upper part of the valence band. Different bonding and antibonding states of Si 3p and metal d are available. Localised Si 3s state was observed in the XPS work. XPS and BIS study by Speier et al[36] shows the different features in the XPS for the Mo d states at 3 eV below E_f and 2 eV above E_f (from BIS data) and are interpreted as the bonding and antibonding states. These effects are also reflected in the Auger spectra.

In the oxide, typical changes at different exposures of oxygen was found by Minni et al[8]. The influence of chemisorption on the surface core

levels has been established by Floodstrom et al[37] and explained by Johnsson and Martensson[38]. The localised effect of small charge transfer of Mo 4d electron towards oxygen was observed by the XPS work. However the magnitude of broadening and shift of XPS peak is such that there is not a complete transfer of Mo electrons to oxygen atoms as observed in MoO_2 by F.Werfel and E. Minni[8] To get the idea of charge transfer in oxidation and silicidation , the valence band related Auger transition MNN fingerprint is analysed.

The MNN Auger line shapes for Mo in pure and in compound states are shown in FIG.4b.9. The peak at 188 and 220 eV are due to $M_{45}N_{23}N_{45}$ and $M_{45}N_{45}N_{45}$ transitions respectively (FIG.4b.9.). The changes due to chemical bonding are more evident in the $M_{45}N_{45}N_{45}$ Auger transition. In molybdenum silicide the peak intensity at 220 eV is apparently found to decrease, resembling the result by Atzrodt et al[39] . However the area under the positive excursion of the Auger peak increases. The change in intensity was calculated by finding the area under that peak of oxide and silicide[17]. In the table, the ratios are shown.

XPS core level binding energy for Mo-3d line is shown in the FIG.4b.10. In the oxide the chemical shift is observed to be 4.74 eV where as in the silicide it is approximately 0.5 eV. The valence band of pure Mo (FIG.4b.12) is constituted of very sharp d band at approximately

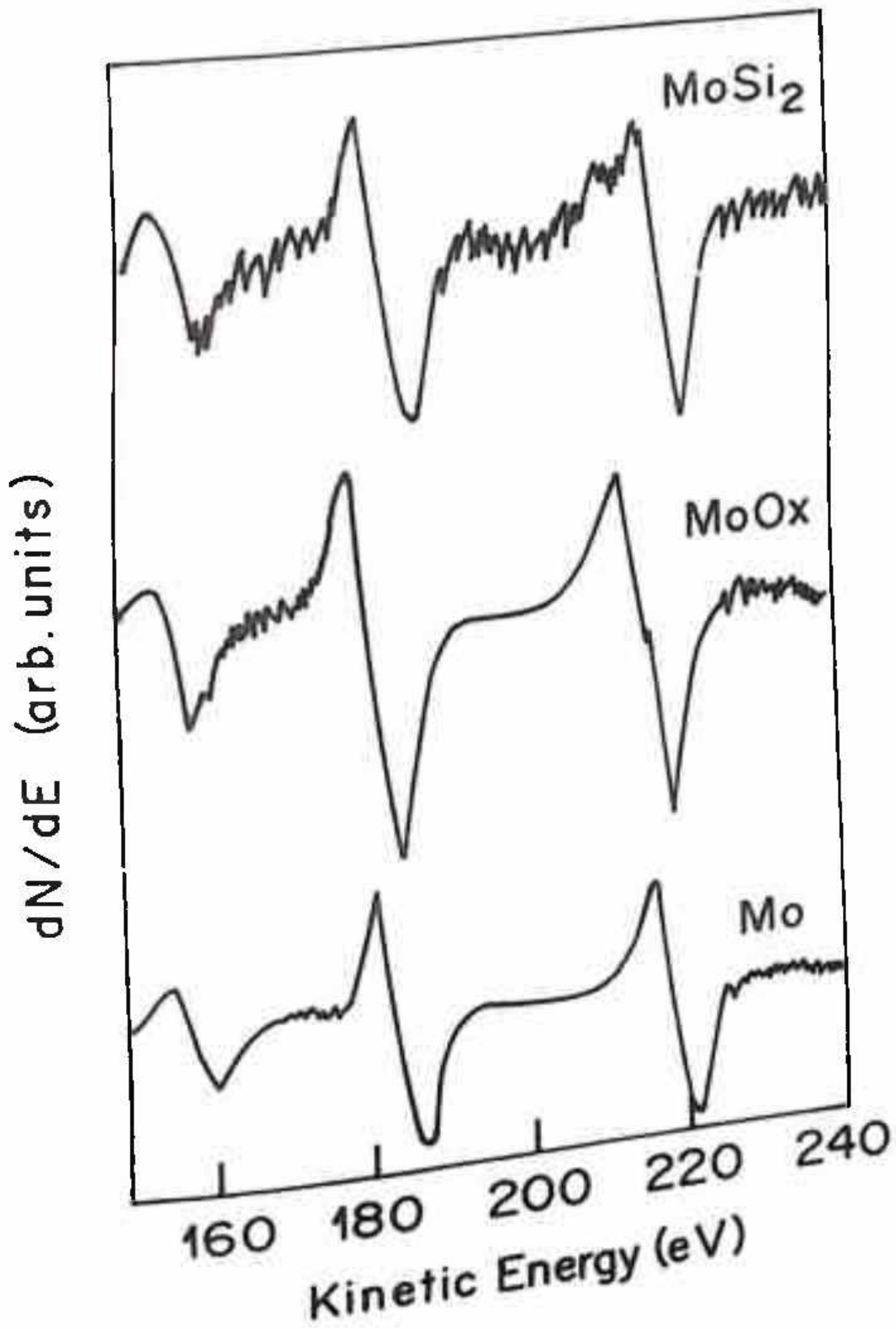

Fig.4b.9 : NNN Auger transition in the derivative mode of Mo and its compounds.

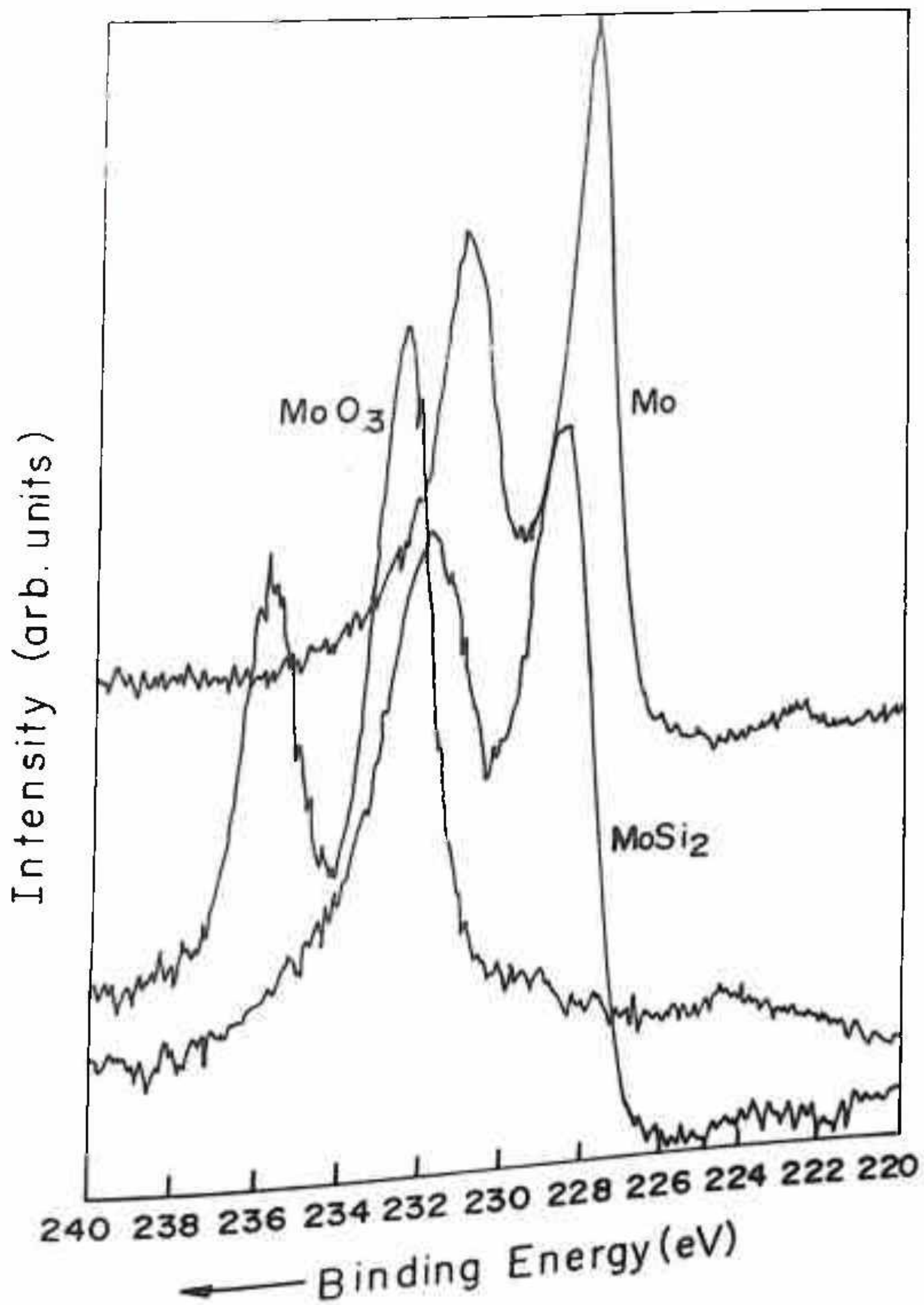

Fig.4b.10 : Mo 3d line after oxidation and silicidation.

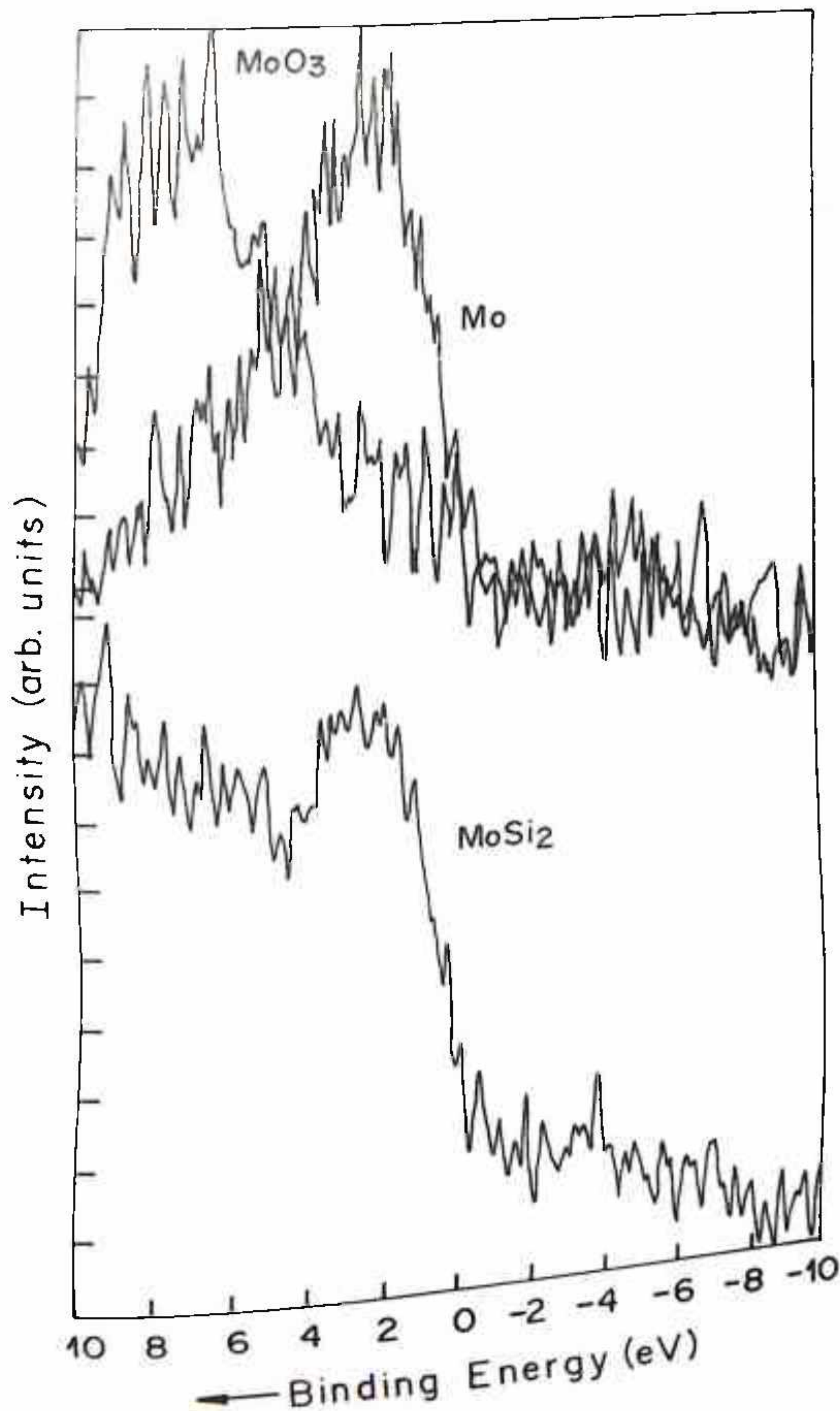

Fig.4b.11 : Valence band spectra of Mo, MoO_3 and $MoSi_2$ obtained from XPS.

Table VI : Variation in VB related Auger transitions in Mo due to oxidation and silicidation.

Samples	$M_{45}N_{23}N_{45}/M_{45}N_{45}N_{45}$
Mo	1.12
$MoSi_2$	1.02
MoO_3	1.14

2 eV below the Fermi level. Due to the silicidation the bonding and non bonding states are observed near the Fermi level. The main metal d and Si p bonding states are found at ≈ 3 eV. In the oxide the depletion of the d band near the Fermi level and the oxide valence band appears at ≈ 5eV below the Fermi level.

4b.2.3. AES of Ti, TiO_2 and $TiSi_2$:

Different chemical properties of Ti/Si and Ti/O as studied by surface analytical technique is of interest. The composition , electronic structure and reactivity of Ti/Si surface is studied as a function of temperature and deposition (ML). According to Butz et al[21] the reaction starts at considerably lower temperature below 300°c, and the reaction can extend over a distance of 100Å from the Si interface. The low temperature intermixing leads the different structural properties from

that of the high temperature silicides. At sufficiently high temperature (≥ 600°C) *the growth of TiSi and* $TiSi_2$ was observed.

To study the oxidation and silicidation the $L_3M_{23}M_{23}$ Auger transition at 383 eV and $L_{23}M_{23}M_{45}$ transition at 418 eV is shown in FIG.4b.12. The peak at 383 eV shows the splitting with a peak at 387 eV. This splitting was eluded by adequate explanation. This doublet is explained as being due to the interaction of the two hole final state in the 3p (M_{23}) level with the unpaired d electrons. In the oxide the $L_3M_{23}M_{23}$ and $L_{23}M_{23}M_{45}$ transitions are found with deformed peak intensities[23]. The splitting of $L_{23}M_{23}M_{23}$ and its variation with respect to $L_{23}M_{23}M_{45}$ is shown in the table. Although it is very tough to quantify the data due to the background of the splitted peak .

Table VII : Variation in multiplet splitting in Ti AES due to oxidation and silicidation.

Materials	387/$L_3M_{23}M_{45}$	$L_3M_{45}M_{45}$(449) /$L_3M_{23}M_{23}$ (direct mode)
Ti	0.75	0.1
TiO_2	0.62	0.05
$TiSi_2$	1.12	0.2

The change in the Ti LMM fingerprint due to silicidation and oxidation is monitored by measuring the different LMM ratio in direct and derivative modes. From the Table it is observed that the multiplet splitting intensity increases in $TiSi_2$ but decreases in TiO_2. Similarly the

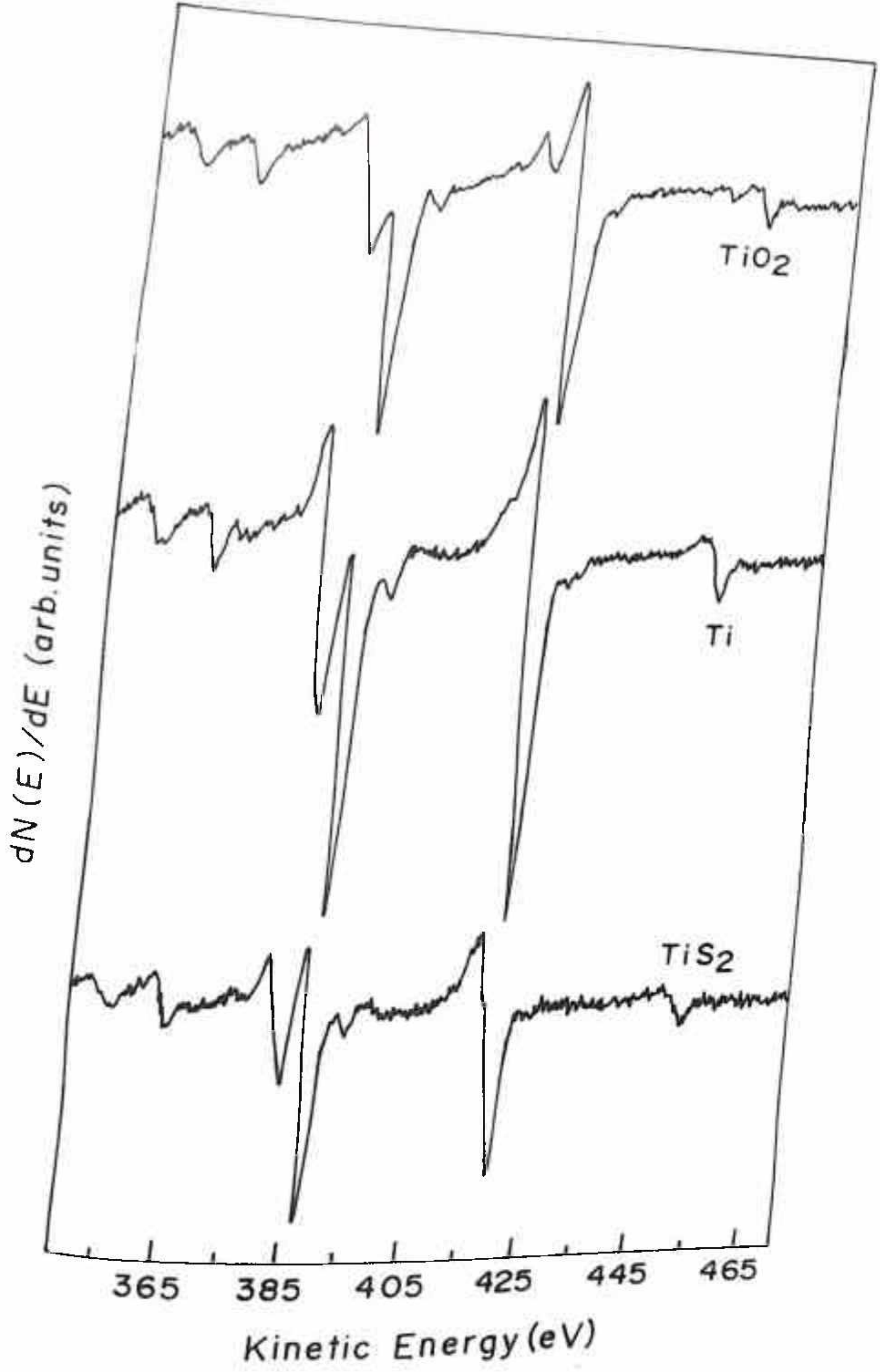

Fig.4b.12: *Ti LMM Auger transition in derivative mode showing the multiplet splitting in Ti, TiO_2 and $TiSi_2$.*

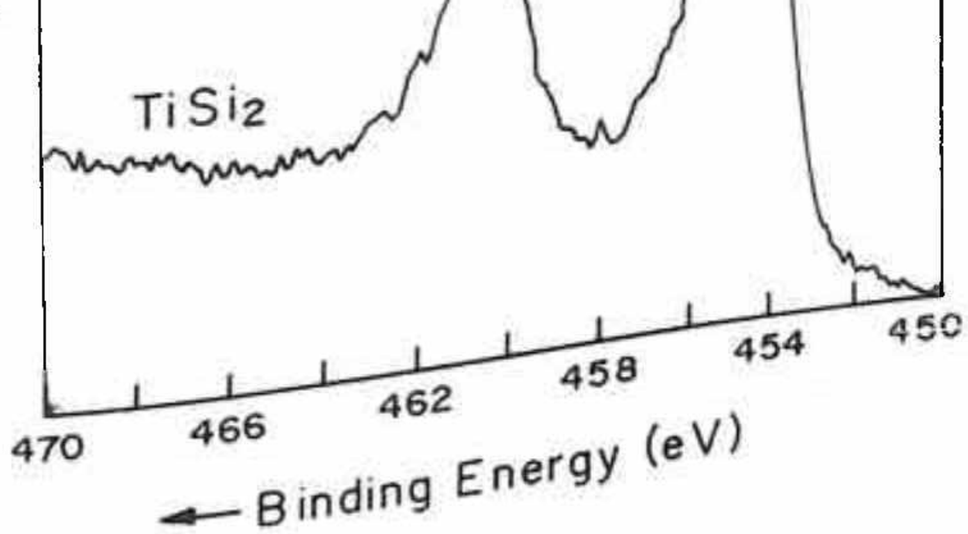

Fig.4b.13 : Ti 2p line after oxidation and silicidation.

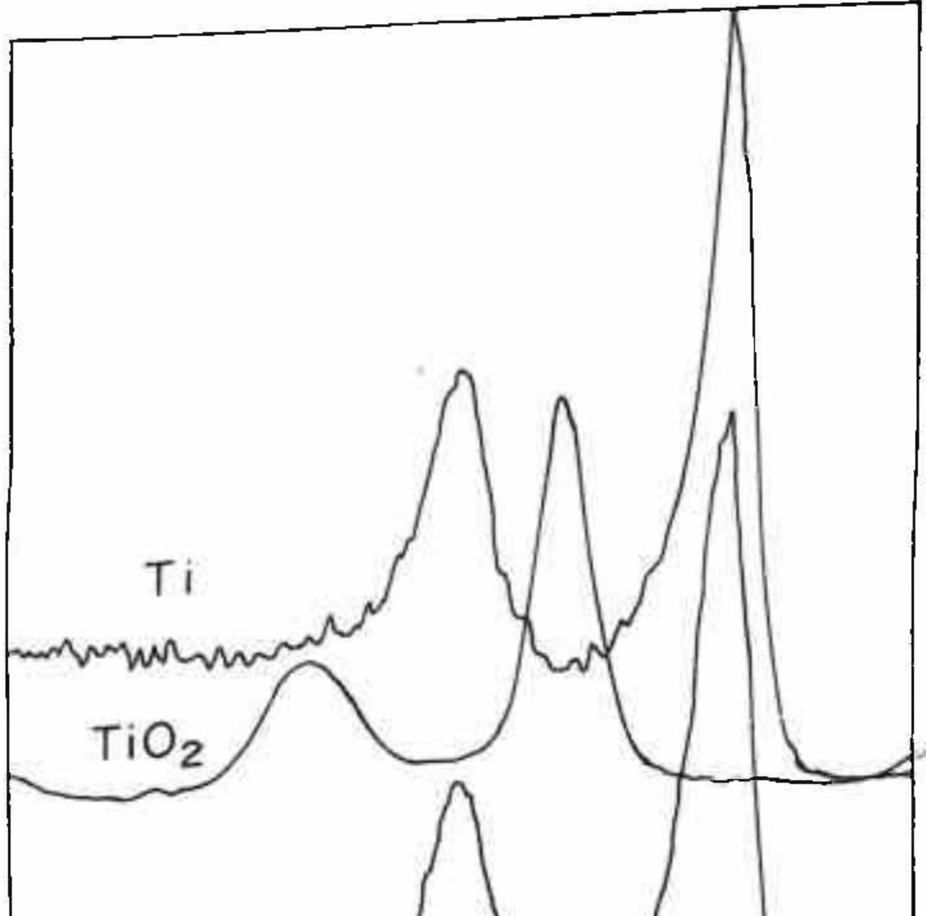
ntensity (arb units)
Ti
TiO_2

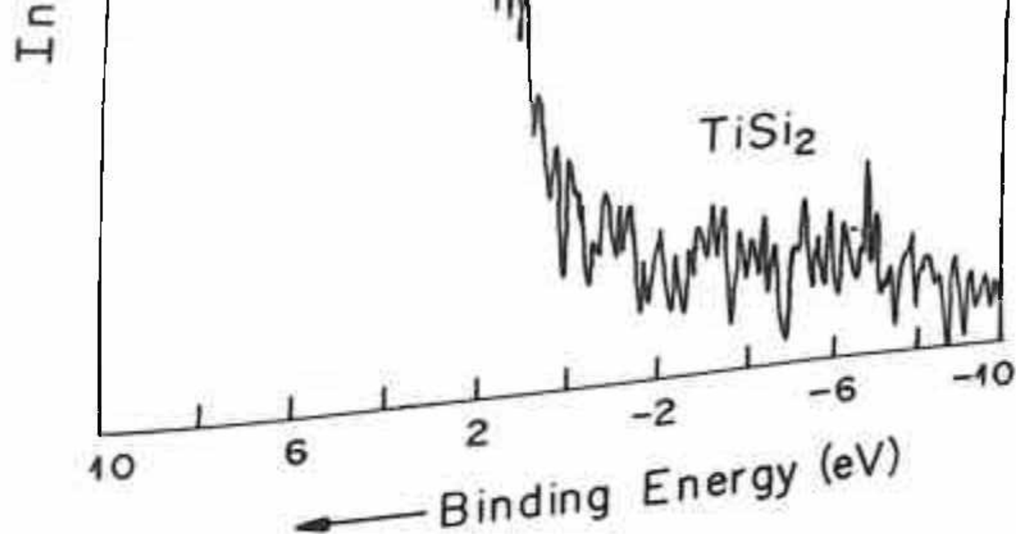

Fig.4b.14 : Valence band spectra of Ti and $TiSi_2$ obtained from XPS.

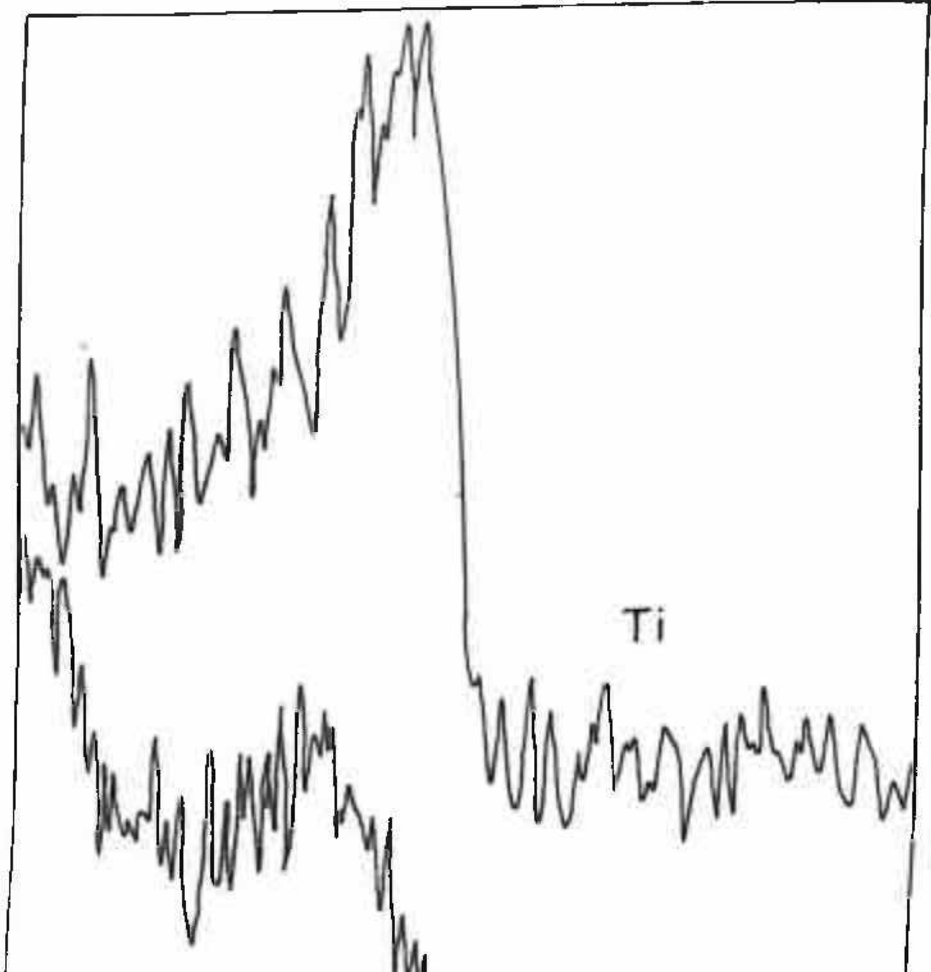
tensity (arb.units)
Ti

variation of $L_3M_{45}M_{45}$ /$L_{23}M_{23}M_{23}$ is found to increase in the silicide and decrease in the oxide. The conclusions in the Auger electron spectroscopy results is supported by the XPS results for chemical shifts and the valence band pictures. In the oxide a large chemical shift of 5 eV is observed which shows a strong chemical interaction by the process of d electron transfer from metal to oxygen (FIG.4b.13). In the silicide a very small chemical shift is observed, which is beyond the resolution of our instrument. However the valence band picture (FIG.4b.14) , the sharp d band observed in Ti at 1.5 eV below E_f is observed to be suppressed by a strong feature at 2.4 eV below the Fermi level indicating the metal d and Si p hybridization states. Thus a rising feature starting from 8 eV is due to the Si 3s band, which shows the non--participation of the 3s electrons in the metal Si interaction.

4b.2.4. AES in Cu, CuO and $CUSi_2$:

In FIG.4b.15, the LMM transition for Cu and its two compounds is shown. The LMM of Cu is interesting theoretically because of its splitting transitions. Here we concentrate on the $L_3M_{23}M_{45}$, $L_3M_{23}M_{23}$ and $L_3M_{45}M_{45}$ transitions at 841, 768 and 921 eV respectively. However in the present observation the $L_3M_{23}M_{23}$ transition is important. The other two transitions are strongly influenced by localization of 3d holes[40]. In general, the spliting of $L_3M_{23}M_{23}$ (768 eV) is directly connected with the interaction of M_{23} (3p) holes with the unpaired d electrons. In case of Cu though the d orbitals are completely filled, the splitting is observed. To account for the origin of the splitting the transition may be represenred in

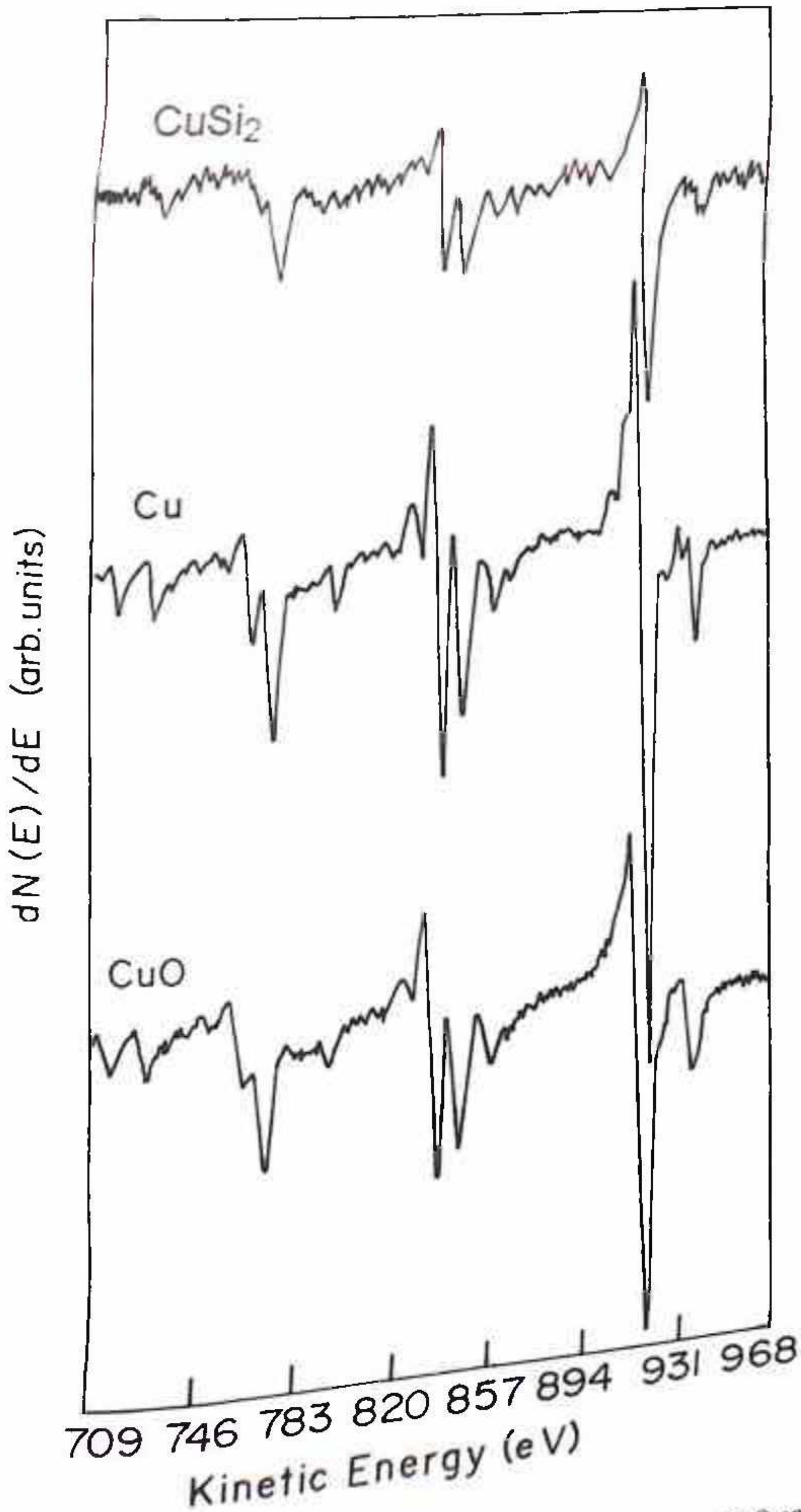

Fig.4b.15 : Multiplet splitting of Cu LMM Auger transition in Cu, CuO and $CuSi_2$

terms of the entire two hole outer electronic cinfiguration i.e. $3p^4 3d^{10}$. The observed seperation may be related to the exchange interaction between the unpaired electrons in the two hole state.

In the oxide 777 eV peak (splitted $L_3M_{23}M_{23}$) peak is found to be very sensitive. The intensity of the positive excursion changes. The nature of variation is shown in table , where in the oxide the ratio is observed to decrease and in the silicide it increases.

Table VIII : Variation in multiplet splitting in Cu due to oxidation and silicidation.

Materials	$777/L_3M_{23}M_{23}$
Cu	1.375
CuO	1.036
$CuSi_2$	1.83

In case of Cu, the Cu-Si interface is very small and the chemical shift of Cu 2p line towards the lower binding energy is very small. But the change in the Cu 2p lineshape indicates interaction. In CuO the chemical shift was observed to be 1.2 eV (FIG.4b.16). In the valence band picture the Cu 3d signal is very strongly localised with a peak at 3.5 eV below the

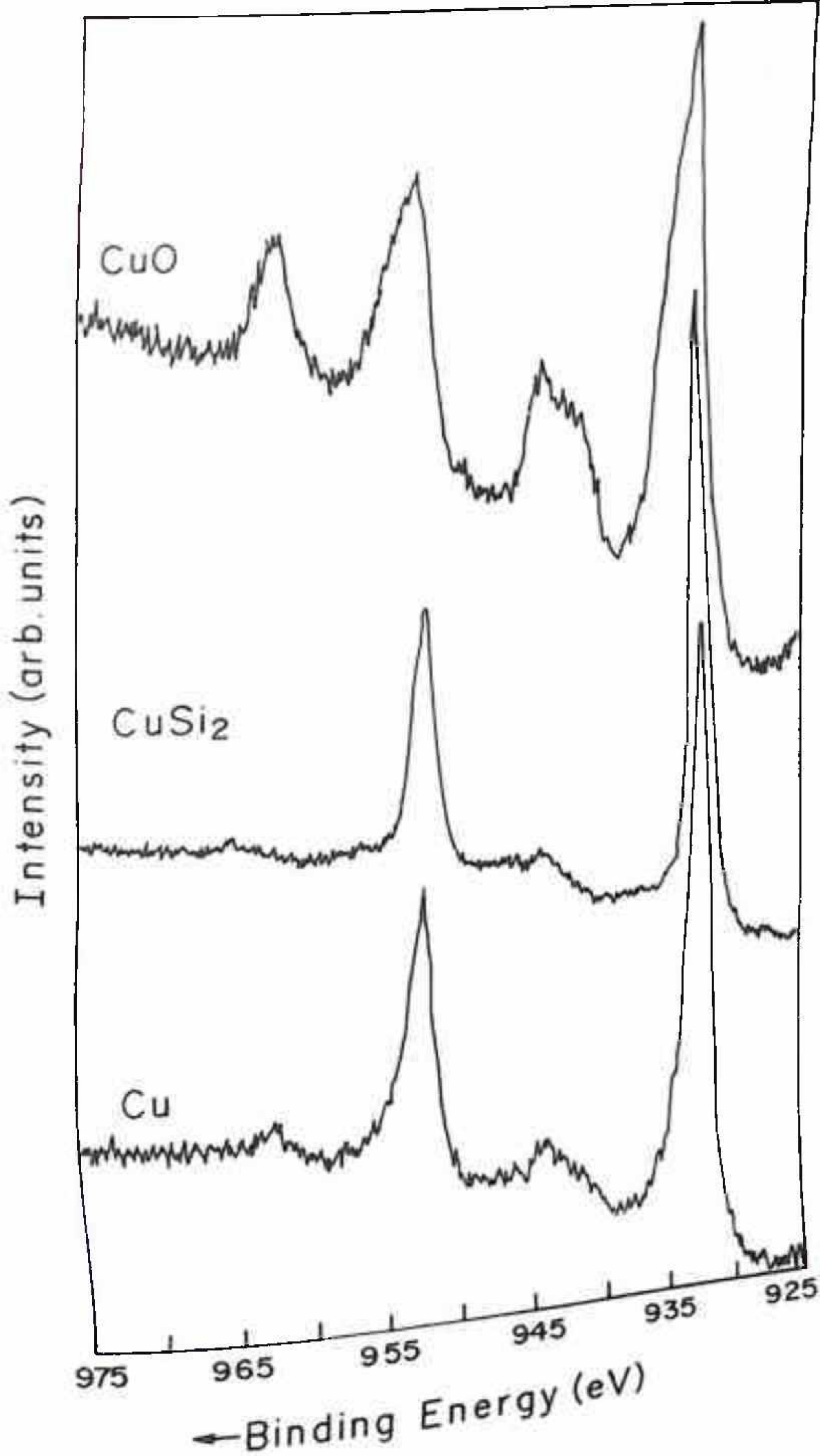

Fig.4b.16 : Cu 2p XPS line after oxidation and silicidation.

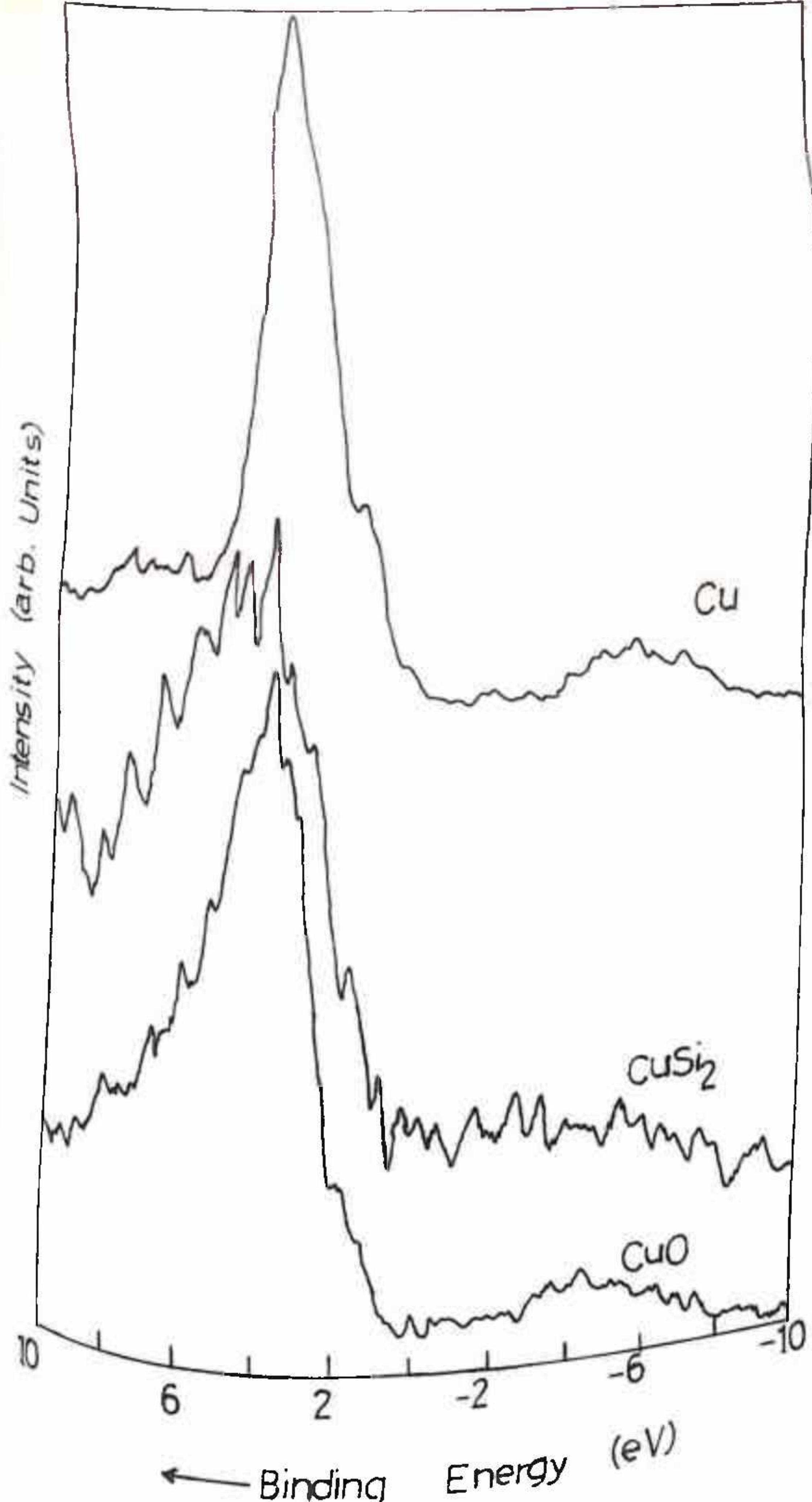

Fig.4b.17 : Valence band features in Cu, CuO and $CuSi_2$ obtained from XPS.

Fermi level. In the silicide the 3d feature gets broadened because this includes the metal d and Si p bonding states. In the oxide the d band is shifted towards the higher binding energy and is observed to be broadend (FIG.4b.17).

4b.2.5. Si LVV Auger analysis :

Si LVV Auger fingerprint has derived a lot of interest both in theoretical and experimental investigation to understand the interface characteistics and electronic structure of the silicide materials. Theoretical electronic structure calculations indicate qualitatively the behaviour of metal silicides and experimentally for $PdSi_4$ or $CaSi_2$. The changes in the Si fingerprinting for different silicides has been observed by Roth and Crowell[27], . Feibelmann[41]. showed that the shape of Si LVV peak can be predicted from an independent electron treatment of Auger transitions . Si LVV Llineshape is associated with three types of final state valence band Auger transition : two p holes, one s hole and one p hole, or two s holes known as as the pp, sp and ss types, respectively. These three contributions are not equal owing to the surface effects or delocalization of 3s orbitals in the presence of core holes[42]. So an irregular Si line shape convoluted with these three contributions is observed in general. The intensity ratio s for ss, sp and pp obtained from the actual experimantal data and the fit of the equation (given in the background equ.no.) is found[42] to be pp/ss is 100/1 and pp/sp is 10 .

In silicide, the Si LVV lineshape changes noticebly from its Si origin (FIG. 4b.18). To appreciate the small change, we define a parameter[43]

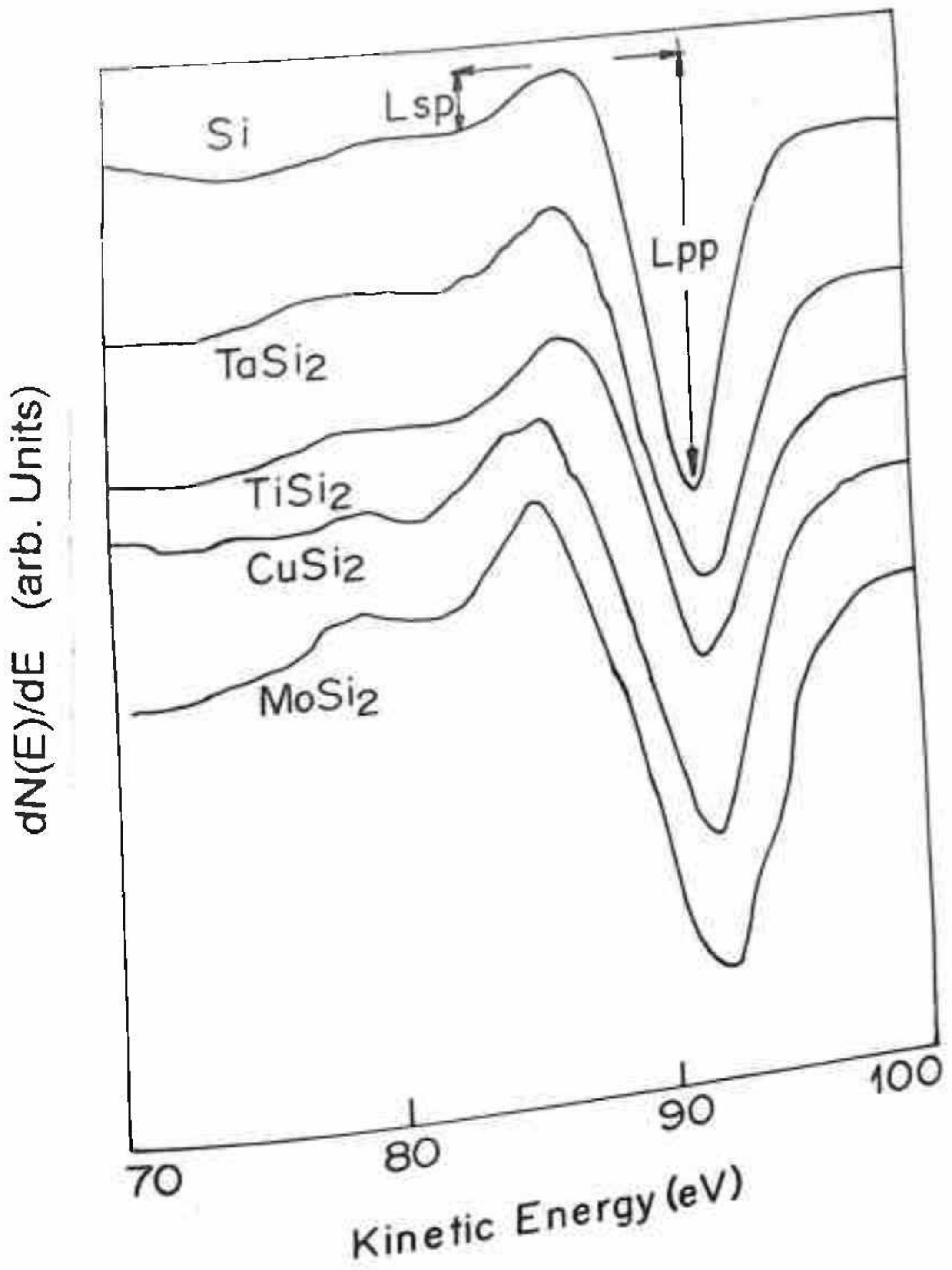

Fig.4b.18 : Si LVV Auger transition in pure element and in different silicides.

Table IX : The ratio of the excursion heights $R_{pp/sp}$ in Si LVV lineshape analysis.

Materials	d electron conf.	L_{pp}/L_{sp}	ΔH_f/TM atom4
Si		8.5	
$TaSi_2$	3	4.62	1.21
$MoSi_2$	5	4.38	1.36
$TiSi_2$	2	4.79	1.4
$CuSi_2$	10	5.13	

* ΔH_f/TM atom is a measure of relative covalency of metal-Si bonds.

$R_{pp/sp} = L_{pp}/L_{sp}$ where L_{pp} and L_{sp} are excursion heights as shown in FIG.4b.18. The $R_{pp/sp}$ data for silicides ad Si are shown in the Table IX, which indicates a decrease in the value for silicides as compared to Si. The table IX shows the variation of the $R_{pp/sp}$ with silicidation, and a decrease in the value is observed. Among the silicides there is variation but the variation is too small to comment. The probable reasons for the variation of the Si lineshape in silicides is explained later.

4b.2.6. O KVV Auger Lineshape :

The ground state of oxygen is $1s^2 2s^2 2p^3$. So in an atomic model K, L_1 and L_{23} level contains two, one and three electrons respectively. In solid state compound the KLL Auger spectra of oxygen have generally four structures, $KL_{23}L_{23}$, KL_1L_{23} (^3p) and KL_1L_{23} (^1p) and KL_1L_1(^1s) transitions. The symbols in the brackets indicate the spectral term of the final two hole configuration. The local atomic charge depends on the chemical bonding of the oxygen to the other element. If we assume that L_{23} shell participating in the bonding we get[31],

$$q(L_{23}) = 4e + \Delta qe$$

$$\text{and} \qquad q(L_1) = 2e,$$

4e and 2e are the electron charges associated with the L_{23} and L_1 shells of the isolated neutral atom. Δqe is the additional charge which will be added by the chemical reaction.

Weißmann[31] showed that the intensity ratio of $KL_1L_1/KL_{23}L_{23}$ depends on the amount of charge transfer (due to the above discussed argument) in the process of oxidation. In the present observation we have

studied transition metal oxides of Cu, Ti, Ta, Mo with their oxidation states +2, +4, +5 and +6 respectively, to understand the behaviour of the oxygen KLL fingerprint in these materials. The data for Fe(+3) is taken from literature to get the trend.

In the chemical process of oxidation the valence band redistribution takes place which depends on the amount of charge transfer that causes a change in the O KLL transitions. So the ratio of different KLL transitions is taken to characterize the oxidation process in these materials.

In FIG.4b.19 oxygen $KL_1L_{23}/KL_{23}L_{23}$ intensity ratio in the derivative mode for different oxides are shown . It is observed that,

i) form Ti to Mo the ratio increases with the increase in the oxidation state and decreases from Mo to Cu and

ii) the ratio seems to be dependent on the no of d electrons.

In the ionically bonded oxide the oxygen Auger signal originates from the oxygen ions from the matrix of the metal ions and hence it is a complicated system than that arising from room temperature chemisorbed oxygen (which is mostly covalent in nature). In the oxidation process of metal due to metal d and and oxygen 2p interaction , the 2p band effectively become more populated. So L_{23} related transitions should increase with more charge transfered to oxygen. But the chemical shift values do not show any consistency with the change in the ratio. So chemical shift may not be a good parameter to explain the variation (in Fe_2O_3, FeO , the chemical shift in Fe_2O_3 is more than that in FeO, but the atomic charge transfer in FeO is more than that in Fe_2O_3). As the Auger transition probablity depends on the DOS of the final state, so the localization behaviour of 2p electrons is thought to be an important factor

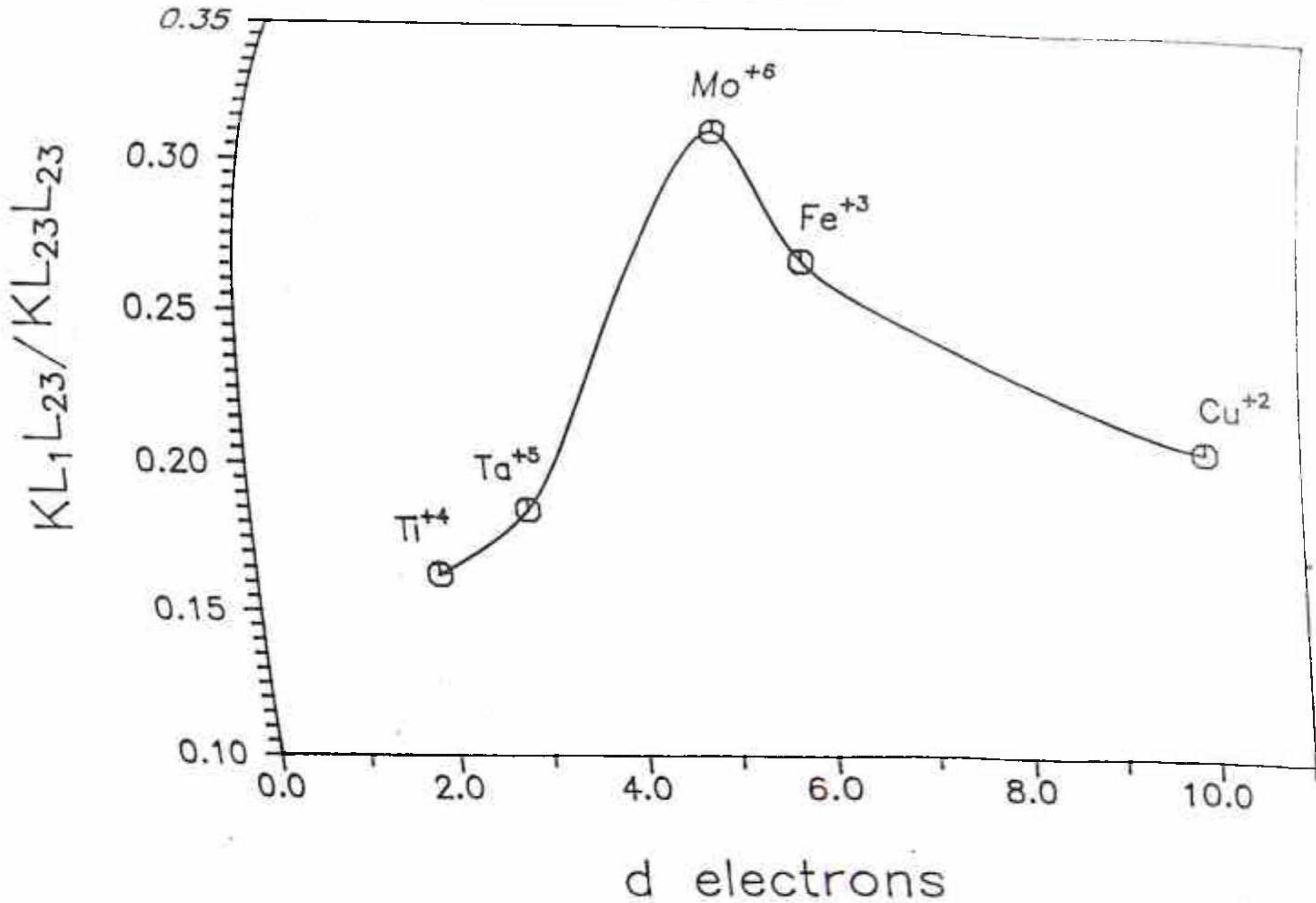

Fig.4b.19. : Dependence of O $KL_1L_{23}/ KL_{23}L_{23}$ peak intensity ratio on d electrons.

in determining the intensity ratio. In the metal -O system the localization or delocalization behaviour is influenced by the metal d band, which is involved in the chemical bonding. With the increase of the number of unpaired d electrons , the 2p electrons become less localised and so the $KL_{23}L_{23}$ transition decrease more than KL_1L_{23} hence increasing the ratio. On the other hand the electrons are getting paired in case of Fe and Cu, the oxygen 2p electrons become more localised than in MoO_3. So the $KL_{23}L_{23}$ transitions increase more than KL_1L_{23} hence the ratio decreases.

However the ratio $KL_1L_{23}/KL_{23}L_{23}$ in Cu and Fe is more than the value for Ti or Ta though O 2p electrons in Cu or Fe are more localised that in Ti and Ta. So the extra charge added to the oxygen neutral as well as the localization of O 2p electrons[44,45] (which is strongly influenced by metal d band) are the two important factors in the O $KL_1L_{23}/KL_{23}L_{23}$ ratio. We can make only qualitative remarks and we do not have relevant and sufficient data to come to any quantitative conclusion.

4b.3. Electron Impact Autoionization Process :

As discussed earlier, the valence band DOS information can be obtained from the Auger spectra involving the valence band electrons as the Auger lineshape is the valence band density of states convoluted with itself. Similarly, the autioionization transition which is also a radiationless transiton particularly shown by the unfilled d electron transiton metals is directly associated with valence band and of the

unfilled d states. So the feature is of special interest in studying the chemical interaction in transiton metals.

The electronic configuration of transition metals (of course the interest is more on 3d transition metals) show very special and intense spectral features in the loss or AES study which is related to the atomic multiplet. These peaks have been explained in terms of the resonant configuration that follows from the excitation to the quasi-discrete d levels and to the continuum in the synchrotron photoemission study. It has been established that the existence of autoionization levels should influence both absorption and emission spectra. As autoionization levels show strong autoexcitation it should show strong emission, either in photoimpact or electron impact process of electron (or atomic) excitation. In general the spectral features are interpreted in a single particle scheme associated with the Fano type interference[46].

4b.3.1.Autoionization in Ta, Ta_2O_5 and $TaSi_2$:

FIG.4b.20 displays the autoionization in Ta and its two compounds along with the SCK transition. From the clean Ta surface the peaks are observed at 6, 16.5, 23.5, 27, 34.5 and 44.5 eV. The transitions at 34.5 and 44.5 eV are related to the autoionization process due to the excitation of 5p electrons above the Fermi level and their subsequent relaxation. Due to strong spin-orbit interaction, p levels are split with a separation of 10 eV. Thus the peak at 44.5 and 34.5 eV arise due to recombination of d-p transitions involving $O_2(p_{1/2})$ and $O_3(p_{3/2})$ respectively. The peak at 23.5 eV is associated with the autoionization via $4f_{5/2}$-d recombination.

According to the binding energy level given by Nyholm et al[47]. the calculated O_3VV Auger transition is expected at around 24 eV. A peak *observed at around 23.5 eV may be attributed to this Auger transition. This is in good agreement with the results by Palacio et al[4]. It is conceivable that the 5d electrons of Ta show some atom-like character in* the excited state and interact with the potential of 5p holes, which is clear from the interference of the two resonances produced in the autoionization features. The strong feature at 16.5 eV corresponds to the $N_7O_{45}O_{45}$ Auger transition. However the feature at 10 eV can be associated with Auger transition from the binding energy calculation given by Nyholm et al[47].

The valence band related either Auger transition or autoionization feature can be helpful to get the information of near Fermi-level d band states at reasonably low energy of the secondary electron. The ground state of Ta i.e. $5p^65d^36s^2$ has unfilled d orbitals. As discussed earlier, the electron atom interaciton will cause 5p--5d quasiatomic transition. The p-d excitation and consequent relaxation are reflected in the ELS and Auger spectra and thus it manifests the occupancy of the d state. The energy of autoionization electrons can be given as,

$$E_{auto} = E_{exe} - E_{5d} - \phi$$

where E_{exe} is the excitation from the 5p levels obtained from the ELS results, E_{5d} is the binding energy of the 5d electrons and $\phi = 4.5$ eV is the work function. Using this, calculated autoinozation peaks are expected at 43.5 eV and 33.5 eV for $p_{1/2}$ and $p_{3/2}$ levels respectively, which agrees well with the low energy AES peak positions shown in the FIG.4b.20.

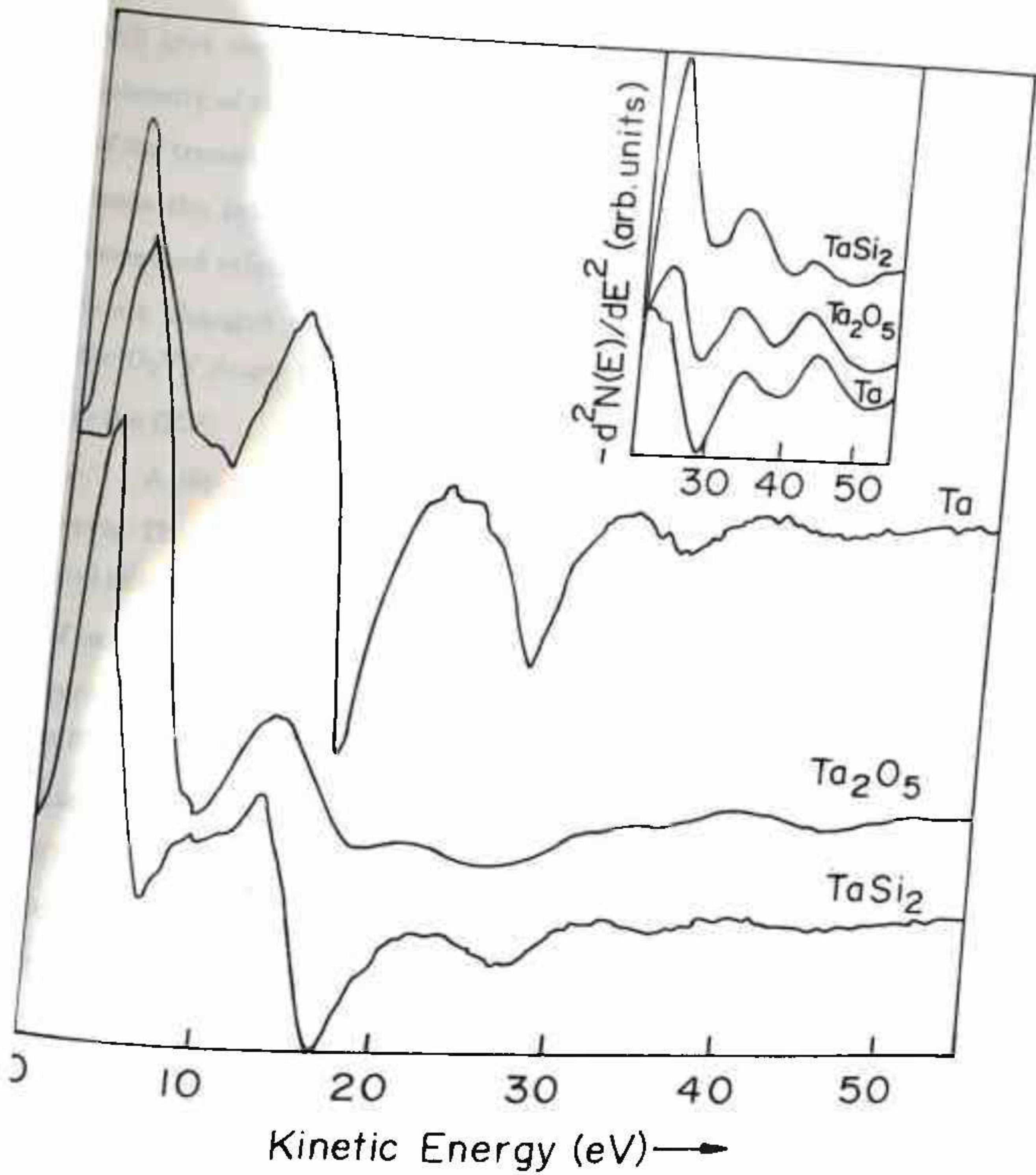

..4b.20: Low energy AES of Ta, Ta_2O_5 and $TaSi_2$ in the first derivative mode showing autoionization features. The inset shows the same in the double derivative mode.

In oxide and silicide of Ta the nature of the autoionization feature will give the d band redistribution after the compound formation. The intensity of the auoitoinzation feature is directly related to the probablity of the transition, which in turn gives the empty DOS in d band. In case of oxide the intensity at 44.5 eV is increased and in silicide the peak is decreased relative to the feature in pure Ta. However the peak at 34.5 eV is not changed much. It is observed that this peak is also associated with the O_2VV Auger transition which is not much affected due to the change in the DOS.

A dip in the DOS is observed in silicide and is increased in the oxide. This indicates about the charge transfer in the process of oxidation and silicidation. The $O_2O_{45}O_{45}$ Auger transition at around 34.5 eV in case of oxide is found to decrease relative to the peak at 44.5 eV, though in pure Ta the 44.5 eV peak is more intense than the 34.5 eV peak. The peak at 27 eV, associated with the $O_3O_{45}O_{45}$ SCK transition is found to vary in intensity in the oxide and silicide as shown in the double derivative mode (FIG.4b.20). It is obvious that in oxide , this transition is decreased to a definite extent than that in Ta and also indicates that the charge is transferred from the metal to the oxygen. In the normal mode we have shown the broadening of the autoionization feature due to the compound formation.

4b.3.2. Autoionization in Mo, MoO_3, $MoSi_2$:

Autoionization features in Mo occurs due to 4p -- 4d quasiatomic transition. The autoionization mechanism from the empty excited state of

the 4p electrons and the effect of oxygen exposure on autoionization is studied by Colavita et al[48]. The electron emission spectra for Zr, Nb, Mo is observed by Cornaz et al where along with the $M_{23}VV$ Auger transition the autoinozation features are observed and the atomic behaviour of the 4p-4d excitations are manifested from the observed structures and their energy spread.

The ground state of Mo is $4p^64d^55s^1$ which undergoes different electronic excitation due to electron impact. In an atomic model where p electron is knocked out completely from the atom and the successive relaxation process gives rise to the $N_{23}VV$ Auger SCK process. In the other excitation, when the p electrons are excited to d levels to some empty state to give a configuration d^{5+1}, then the relaxation process gives rise to the autoionization phenomenon. So the energy of the autoionization feature calculated from the equation given earlier is expected at around 32 eV, taking 4p excitation to be 38 eV from ELS[17]. In the FIG.4b.21 a broad feature centering at about 34 eV is observed and is attributed to the autoionization process. The $N_{23}O_{45}O_{45}$ Auger transition is observed at 29 eV. In case of MoO_3 the autoionization showed mostly two changes firstly the energy and secondly the width of the autoionization feature. These two observations can be explained by a change in the distribution of empty final states above the Fermi level. The number of d holes are expected to increase due to the charge transfer to the oxygen and more over a higher number of sp like states should be available for the direct transitions from 4p core levels, as it is oxidised . The broadness can be explained as due to the delocalization of the p and d electrons after the oxidation.

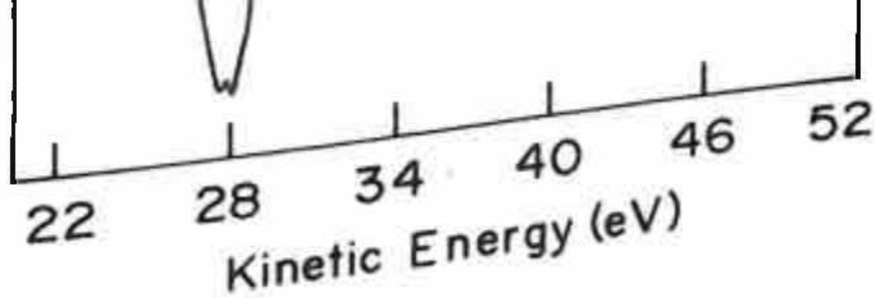

Fig.4b.21 : Low energy AES spectra in Mo, MoO_3 and $MoSi_2$ showing the autoionization transition.

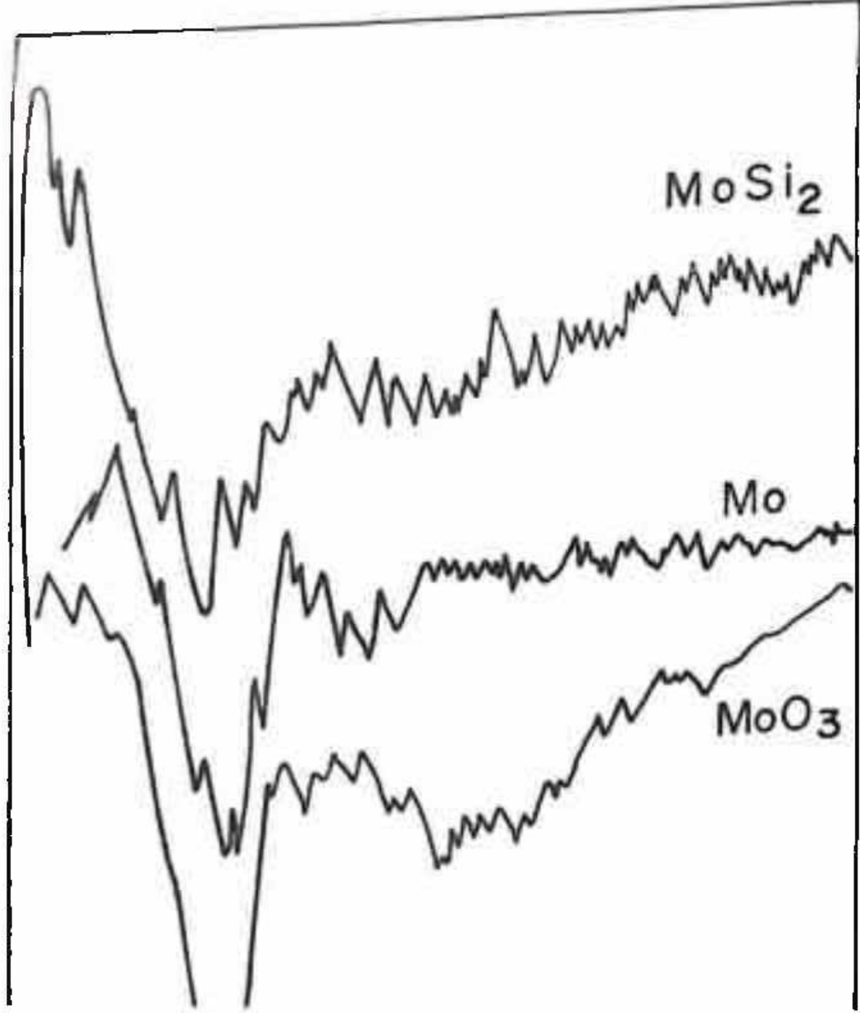

dN (E) / dE (arb. units)
MoSi2
Mo
MoO3

4b.3.3. Autoionization in Ti, TiO_2 and $TiSi_2$:

In the oxidation process of 3d transition metals studied by Zajac et al[49], it is shown that the Auger process shifts dramatically to lower energy but the autoionization emission is left as a seperate peak pinned above the 3p threshold. In the resonant photoemission in Ti, the resonance was observed at a photon energy 14 eV above the threshold. However it was found simultaneously that in TiO_2 the oxide valence band emission is enhanced at the 3p resonance energy. In FIG.4b.22 the low energy peaks are found at 28 and 47 eV. The peak at 28 eV is $M_{23}M_{45}M_{45}$ SCK peak. As evident from the ELS and soft x-ray absorption spectroscopy the the 3p electrons can be resonantly excited to a final state 47 eV above the ground state i.e 14 eV above the the threshold. So the kinetic energy of the emitted electron is calculated from the equation,

$$E_{auto} = E_{exe} - E_{3d} - \phi$$

to be at around 38 eV, taking E_{exe} =45.5 eV from ELS data and binding energy for 3d electrons (E_{3d}) to be 3 eV. But the broad autoionization feature at around 41 eV is observed in the pure Ti.

In the oxide two new peak appears at 15 and 23 eV along with the above mentioned transitions. These two peaks are associated with the Auger transitions as it is not shifted with the change in the primary beam energy. The peak at 23 eV is mostly associated with the crossed Auger transitions involving levels M_{23} of Ti and L_{23} of oxygen. Due to the change in the valence band structure the autoionization feature at ~41 eV is enhanced in the oxide over the pure Ti.

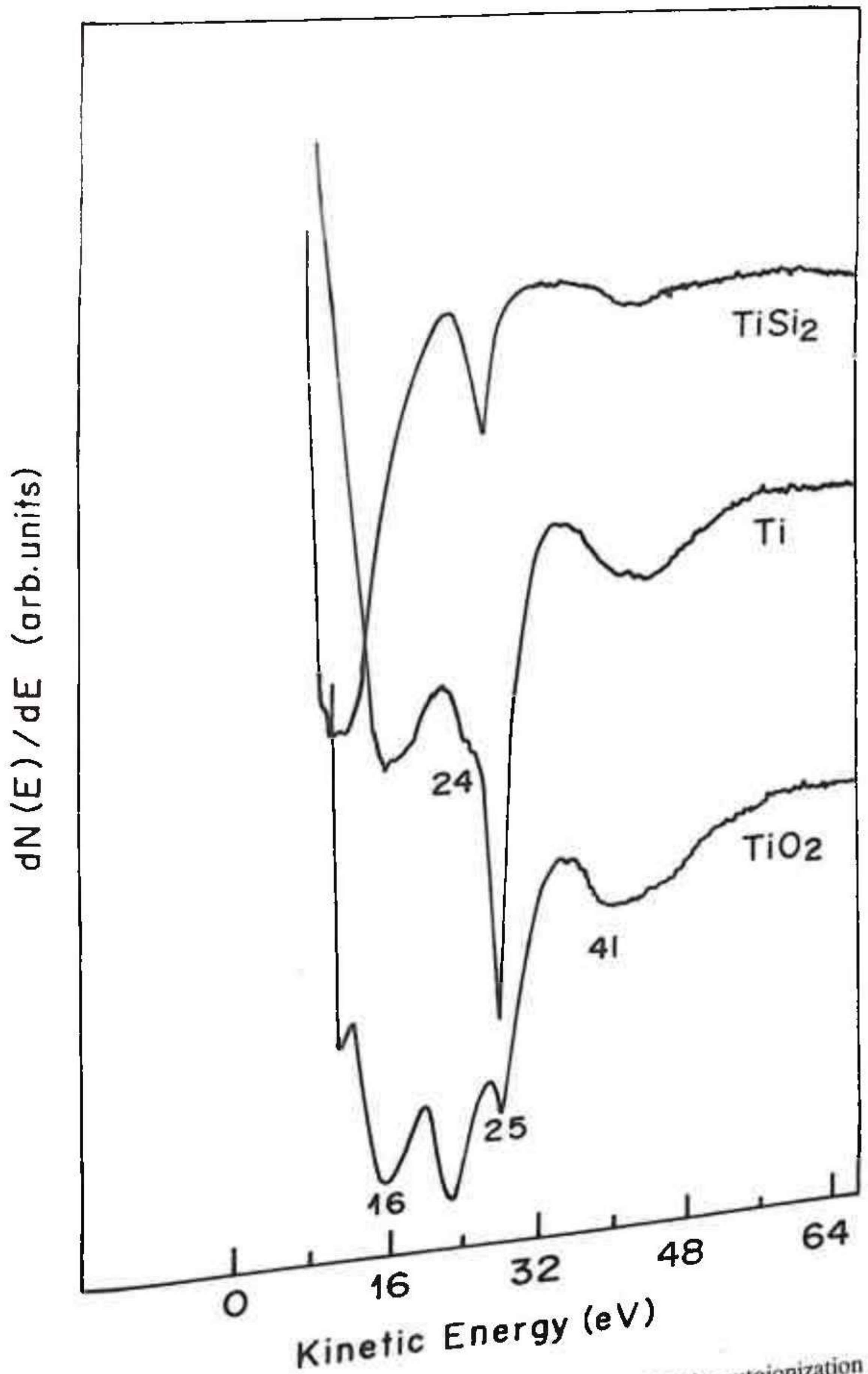

Fig.4b.22 : Low energy AES in Ti, TiO_2 and $TiSi_2$ showing the autoionization peak at 41.5 eV.

4b.3.4. Autoionization in Cu, CuO and $CuSi_2$:

In the ELS of Cu, we found no p-d quasiatomic transition loss, which is in good agreement with the work by Zajac et al[49]. where no discrenible gain satellite was observed in Cu. At 60 and 58 eV $M_{23}VV$ Auger transition is observed with a sharp spin orbit splitting of 2 eV of M_2 and M_3 levels[50,51] (FIG.4b.23), which is observed to be very sensitive towards oxidation. The splitting vanishes, indicating the oxidation of Cu. This indicates the migration of d electrons from metal to oxygen, which decreases the splitting giving Ni like configuration. In the silicide the splitting is maintained. It shows that the d band population remains unchanged even after silicidation.

From the above model it is clear that autoionization feature may be a good probe to get information above the Fermi level, in a chemical interaction. In Si/metal interaction the cause of conductivity of the silicides is due to the p-d antibonding states. But it is suggested that the antibonding states are empty for refractory metal disilicides. But by BIS [illegible] studies it is established that

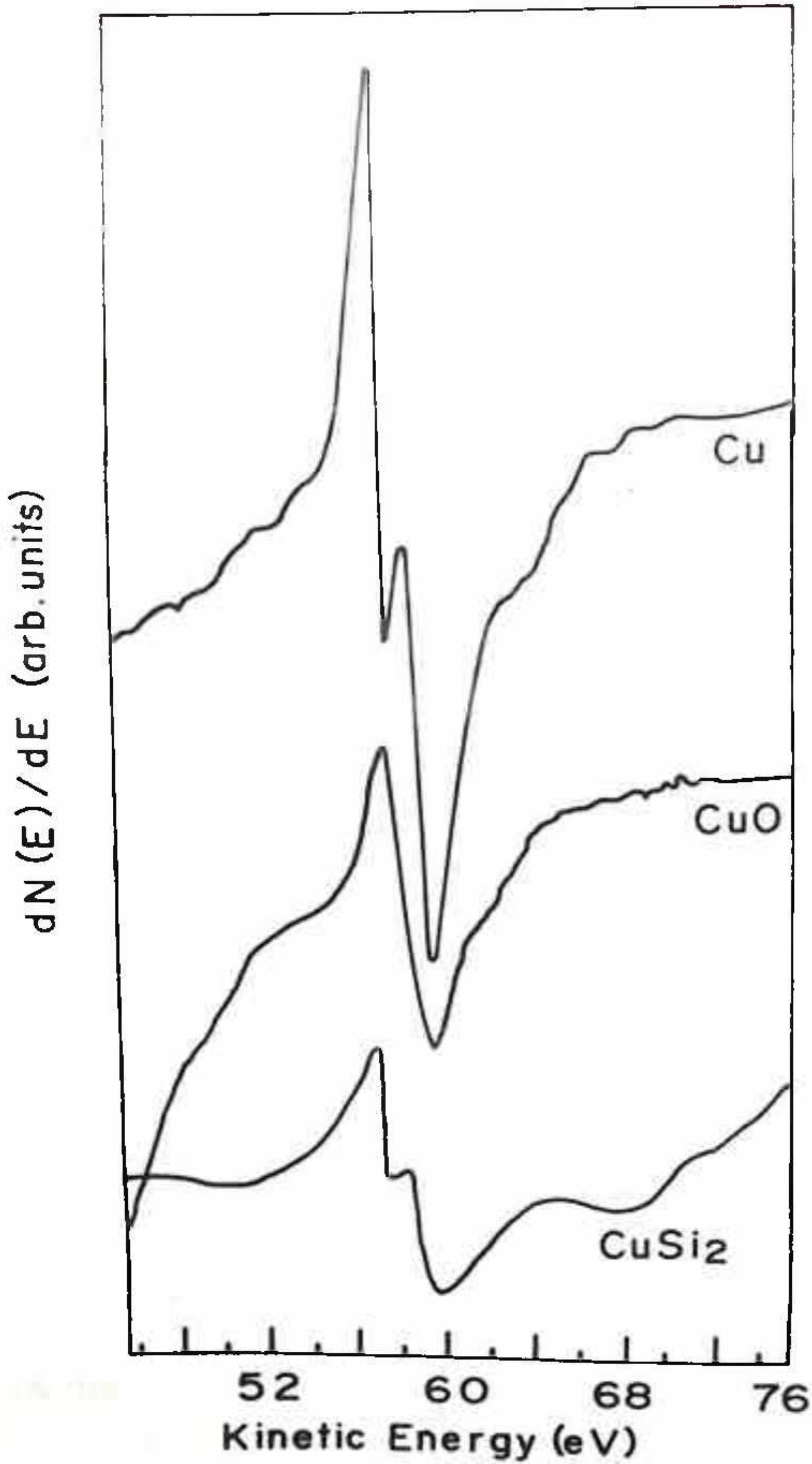

Fig.4b.23 : Low energy AES in Cu, CuO and $CuSi_2$. No autoionization peak is observed.

4b.3.4. Autoionization in Cu, CuO and $CuSi_2$:

In the ELS of Cu, we found no p-d quasiatomic transition loss, which is in good agreement with the work by Zajac et al[49], where no discrenible gain satellite was observed in Cu. At 60 and 58 eV $M_{23}VV$ Auger transition is observed with a sharp spin orbit splitting of 2 eV of M_2 and M_3 levels[50,51] (FIG.4b.23), which is observed to be very sensitive towards oxidation. The splitting vanishes, indicating the oxidation of Cu. This indicates the migration of d electrons from metal to oxygen, which decreases the splitting giving Ni like configuration. In the silicide the splitting is maintained. It shows that the d band population remains unchanged even after silicidation.

From the above model it is clear that autoionization feature may be a good probe to get information above the Fermi level, in a chemical interaction. In Si/metal interaction the cause of conductivity of the silicides is due to the p-d antibonding states. But it is suggested that the antibonding states are empty for refractory metal disilicides. But by BIS (Bremstrahlung Isochromat Spectroscopy) studies it is established that the antibonding states are mostly found in the 2-4 eV above the Fermi level . So autoionization feature is a measure of the formation of states above the Fermi level. In Cu the p-d quasiatomic transition is not observed which indicates that the d band is filled, so there is no d* autoionization level for the autoionization transition to occur.

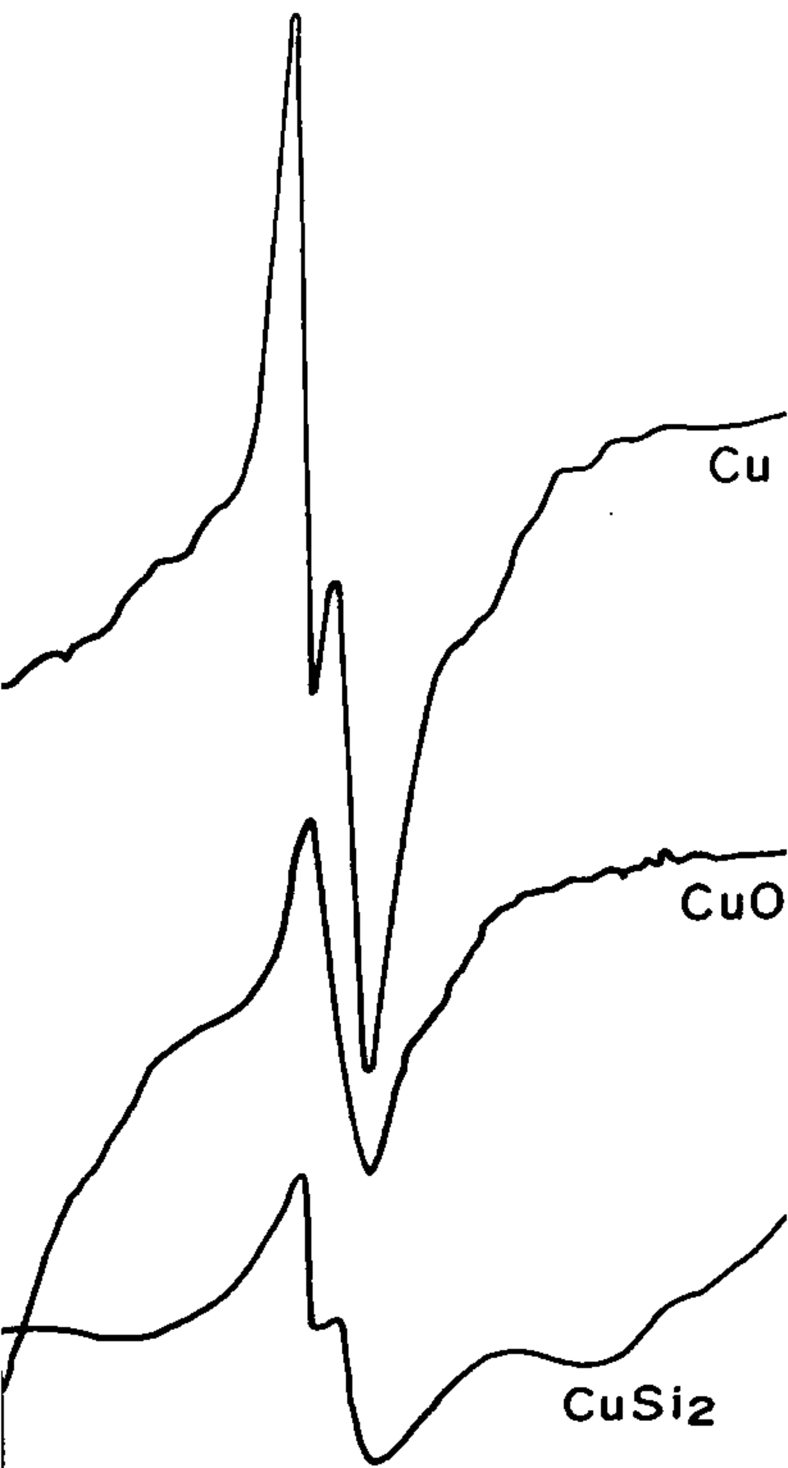

Cu
CuO
CuSi2

References :

1] J.H. Weaver, D.W. Lynch and C.G. Olson, Phys. Rev. B 10 (1974) 501.

2] L.F. Mattheiss, Phys. Rev. 139 (1965) 1893.

3] I. Petroff and C.R. Viswanathan, Phys. Rev. B 4 (1971) 799.

4] C. Palacio, J.M. Martinez-Duart, Surf. Interface Anal.15 (1990)675.

5] C.M. Penchino, Phys. Rev. B 14 (1976) 4407.

6] J.K.N. Sharma, B.R. Chakraborty, S.M. Shivaprasad and J. Cazaux, Surf. Sci. 193 (1988) L58.

7] J.K.N. Sharma, B.R. Chakraborty and Santanu Bera , Surf. Sci. 285 (1993) 237.

8] E. Minni and F. Werfel, Surf. Interface Anal. 12 (1988) 385.

9] Y. Ballu, J. Lecante and R. Rousseau, Phys. Rev. B 14 (1976) 3201.

10] W.L. Schubert and E.L. Wolf, Phys. Rev. B 20 (1979) 1855.

11] J.A. Bearden and A.F. Burr, Rev. Mod. Physics.39 (1967)125.

12] B. Sonntag, R. Haensel and C. Kunz, Solid State Comm. 7 (1969) 597.

13] R. Haensel, K. Radler, B. Snntag and C. Kunz, Solid State Comm. 7 (1969) 495.

14] D.L. Misell and A.J. Atkins , Phil. Mag. 27 (1973) 95.

15] V.V. Zashkvara, M.I. Korsunkii, V.S. Redkin and K. Sh. Chokin, Sov. Phys. Solid, State 140 (1973) 1891.

16] R.S. Rastogi, V.D. Vankar and K.L. Chopra, J.Vac. Sci.Technol. A 10 (1992) 2823.

17] Santanu Bera, S.M. Shivaprasad and J.K. N. Sharma, Appl. Surf. Sci. 74 (1994)13.

18] E.Bertel, R. Stockbauer and T.E. Madey, Surf. Sci.141 (1984) 355.

19] M.H. Mohamed, H.R. Sadeghi and V.E. Henrich, Phys. Rev. B,37 (1988)8417.

20]J.K.N. Sharma, B.R. Chakraborty and S.M. Shivaprasad, J.Vac. Sci. Technol.6 (1988) 3120.

21] R. Butz, G.N. Rubloff, T.Y. Tan, P.S. Ho, Phys. Rev. B 30 (1984) 5421.

22] S.A,. Chamber, D.M. Hill, F. Xu and J.H. Weaver, Phys. Rev. B 35 (1987) 634.

23] J.K.N. Sharma, B.R. Chakraborty and S.M. Shivaprasad, J. Elec. Spec. Rel. Phenon. 50 (1990) 185.

24] M. Iwan, F.J. Himpsel and D.E. Eastman, Phys. Rev. Letts. 43 (1979) 1829.

25] L.H. Jenkins, M.F. Chung, Surf. Sci. 26 (1971) 151.

26] C.Benddrof, B.Egert, G. Keller, H.Seidel and F. Thieme, Surf. Sci.80 (1979) 287.

27] J.A. Roth and C.R. Crowell, J. Vac. Sci. Technol.15 (1978) 1317.

28] S.D. Bader, L. Richter and M. B. Brodsky, Solid State Comm. 37(1981) 729.

29] L. Calliari, F. Marchetti, M. Sancrotti, O. Bisi, A. Indelli, G.L. Olcese and A. Palenzona, Phys. Rev. B 41 (1990) 7569.

30] Gracieler Brizueler, Norberto Castellani, Mirter Puentes, Surf. Interface Anal. 18(1992) 784.

31] R. Weiβmann, Solid State Comm. 31 (1979) 347.

32] T.A. Nguyen Tan, M. Azizan and J. Derrien, Surf. Sci. 189/190 (1987) 339.

33] M. Azizan, R. Baptist, T.A. Nguyen Tan, J.Y. Vellillen, Appl. Surf. Sci.38 (1989) 117.

34] M. Azizan, T.A. Nguyen Tan, J. Derrien, R. Baptist, A. Brenac, G. Chauvet, Proc. Workshop on Refractory Metals and Silicides, Aussois, March, 1987, LeVide, Les Couches Minces, 42 (1987) 9.

35] B.K. Bhattacharya, D.M. Bylander and L. Kleinman, Phys. Rev. B32 (1985) 7973.

36] W. Speier, E.V. Lenken, J.C. Fuggle, D.D. Sarma, L.Kumar, B. Dauth, K.H.J. Buschow, Phys. Rev. B39 (1989) 6008.

37] S.A. FloodstrOm, W.B. Martinsson, G. Kalkoffen and C. Kunz, Mat. Sci. Engineer, 42, (1980) 31.

38] B. Johansson and N. Martensson, Helvatica Physical Acta, 56 (1983) 405.

39] V. Atzort, W. Tifa, Th. Wirth and H. Lange, Phys. Status Solidi(a) 75, (1983) K15.

40] L.I. Yin, T. Tsang and I. Adler, Phys. Rev. B15 (1977) 2974.

41] P.J. Feibelman and E.J. McGuire, Phys. Rev. B 17 (1978) 690.

42] D.E. Ramaker, Crit. Rev. of Solid State and Mat. Sci, 17 (1991) 211.

43] J.K.N. Sharma, B.R. Chakraborty and Santanu Bera, Surf. Interf. Anal.20 (1993) 841.

44] P.Humbert and J.P. Deville, J.Phys. C, Solid State Physics 20 (1987) 4679.

45] J.K.N. Sharma, Santanu Bera and S.M. Shivaprasad, National Symposium on Vacuum Science and Technology (6-8 Oct.) (1993) p-cp34.

46] U. Fano. Phys. Rev. 124 (1961) 1866.

47] R. Nyholm, A. Berndtsson and N. Mar'tensson, J. Phys. C 13 (1980) L1091.

48] E. Colavita, A. Amoddeo, R. Agostino, A. Bonanno, G. Chiarello, V. Formoso and L.S. Caputi, Surf. Sci 211/221 (1989) 481.

49] G. Zajac, S.D. Bader, A.J. Arko and J. Zac, Phys. Rev. B 29 (1984) 5491.

50]M.Salmer'on, M. Baro', J.M. Rajo, Phys. Rev. B 13 (1976) 4348.

51] A.M. Baro', M. Salmer'on and J.M. Rojo, J. Phys. F Metal Phys. 5 (1975) 826.

Chapter IV
Section C
Discussions and Trends

Chapter IV : Section C

Discussions and Trends

4c.1 Consolidation for each metal :

We have discussed in section IV B, the results of all four metals as studied by each of the four different techniques employed. In this section we consolidate the results of different techniques for each of the metals. This material approach provides an integral picture of DOS of individual metals as it binds chemically with oxygen or Si. Though this section re-views the results already presented, a complete picture of each metal is found necessary for clarity of understanding.

Ta, Ta_2O_5, $TaSi_2$: In the loss transition of Ta, and its compounds, particularly the features at 49 and 39 eV are found to be interesting. In pure Ta, these sharp peaks show the availability of the empty DOS ≈ 5 eV above the Fermi level. Due to oxidation and silicidation these peaks show marked changes. In case of the oxide the peaks are enhanced, which shows the increase in the empty DOS after oxidation. But after silicidation, the peak at 49 eV is decreased remarkably as distinctly shown in the normal mode of the spectra (FIG. 4b.2, chapter IVB). In the covalently bonded silicidation due to p-d antibonding state formation, empty DOS decreases effectively, thus decreasing the peak intensity. This indicates the formation of the p-d hybridization state after silicidation which causes a dip in the empty DOS. However the peak at 39 eV does not

show the decrease in intensity as it is expected (because of the dip in DOS) as it can be associated with the double volume plasmon loss also.

In case of Auger electron fingerprint the multiplet splitting of NNN transition manifests the state of the valence band after silicidation or oxidation. The multiplet splitting of transition at 167.0 and 172 eV arises due to the interaction of the two hole final state in the p level with the unpaired 5d electrons[1]. Following Ta oxidation there is a decrease in the number of d electrons in the valence band that reduces the electron hole interaction and hence we see a reduction in the splitting of the shoulder peak at 170.5 eV. For silicides, however this splitting still exists and there is some increase in the shoulder peak intensity (TableV) thus indicating an effective increase in the d electron population due to the overlapping of Si p orbitals with metal d orbitals. The Ta NNN transition in the oxide, at 180 eV shows a shift of 2 eV due to the fact that following oxidation, the 5d electrons of Ta are donated to oxygen. This situation does not occur in the silicide where mutual sharing of electrons takes place in the form of p-d hybridization states. Ta NOO transition in the oxide decreases (decrease on the positive excursion), and can be interpreted in terms of the depopulation of the d band. This is further complemented by the XPS results which show the formation of some bonding states near the Fermi level.

So the depeltion of d electron in the oxide and the p-d hybridization in the silicide leaves all the signatures in autoionization spectroscopy[1]. In autoionization, the peak at 44.5 eV is informative. The related transition shows the availability of empty DOS in E_f (5 eV above the Fermi level) in case of oxide. The d electrons in the oxide are donated to the oxygen 2p

orbital to form predominantly ionic bonding that cause an increase in the probablity of the p-d transition. Again, Si has incompletely filled 3p valence states, so there is a mutual sharing of electrons from the Si p and Ta d band levels to form antibonding states. This sharing effectively decreases the empty DOS near the Fermi level in Ta, which supresses the quasiatomic transition in accordance with the model given by Penn[2] to explain the resonant photoemossion.

Mo, MoO_3, $MoSi_2$: In Mo the loss peaks at 38 and 47 eV are related to the excitation of the shallow core level electrons above the Fermi level. These interband transitions in the silicides are diminished or vanished because of dip in the DOS above the Fermi level after silicidation. In the oxidised case these peaks are observed to be more prominent. This is due to the ionic nature of MoO_3 , where d electrons are transferred to the oxygen atom causing more vacant states and consequently more p-d quasiatomic transition. It is observed that the autoionization peak intensity centred at 34 eV is almost vanished in silicide. So the formation of p-d antibonding states is the cause of the decrease in the p-d quasiatomic transiton obeying the Penn model[2]. However the formation of the bonding state is confirmed by AES. The trend of the change of the $M_{45}N_{23}N_{45}/M_{45}N_{45}N_{45}$ with change in the 4d band occupancy is measured from the standard Auger spectrum shown in the FIG.4c.1. From the nature of the curve we can qualititavely infer that with the increase in d electrons in the valence band, $M_{45}N_{45}N_{45}$ transition probablity increases consequently decreasing the $M_{45}N_{23}N_{45}/M_{45}N_{45}N_{45}$ ratio in the

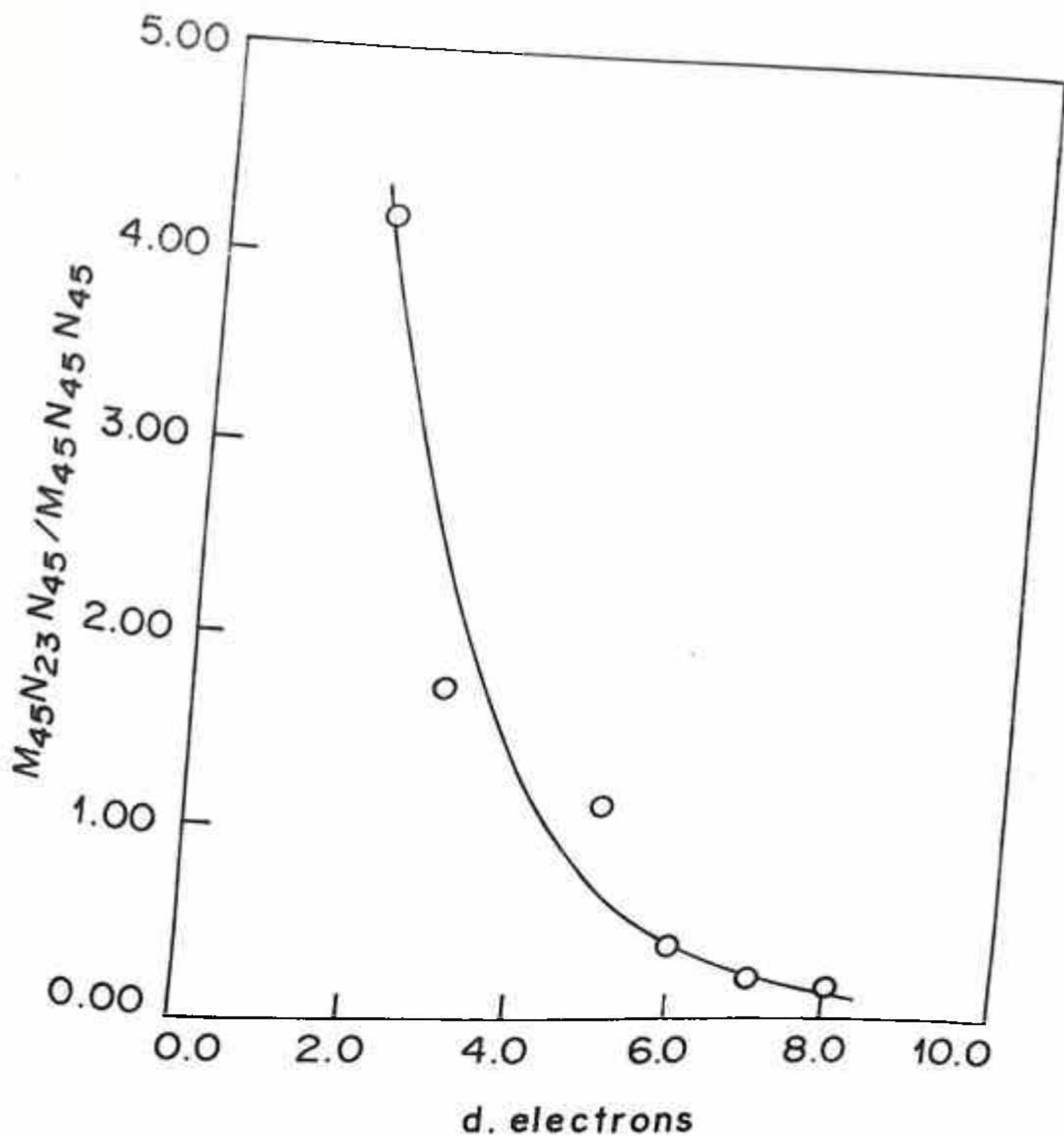

Fig.4c.1 : A plot of $M_{45}N_{23}N_{45}$ /$M_{45}N_{45}N_{45}$ peak to peak intensity ratio versus number of 4d-electrons in transition metals obtained from standard spectra (Auger Hand Book).

graph. Thus in molybdenum oxide the number of d electrons in the Mo valence band is decreased effectively and consequently shifting the $M_{45}N_{23}N_{45}/M_{45}N_{45}N_{45}$ intensity ratio towards the lower d electron region in case of the silicide[3]. Thus the increse is explained in terms of p-d hybridization state, which effectively increases the d band population in the local DOS. Thus a strong interaction in the oxide due to electronic charge transfer and a weak interaction arising due to p-d hybridization influences the change in the Auger fingerprint as discussed.

Ti, TiO_2, $TiSi_2$: In loss feature of Ti, the interband transition peak at 37.5 and p-d quasiatomic transition loss peak at 45 eV indicate the status of the DOS above Fermi level. The peak at 37.5 eV particularly indicates the p-d interband transition ≈14 eV above the Fermi level. In the silicide the p-d loss transition decreases, which suggests that the p-d transition is not dominant in the silicide. Similarly, the p-d transition ralated autoionization peak at 41 eV is observed to decrease in silicide, but increases in the oxide. Since z (atomic number) dependence of the emission intensity is presumbly related to the d band, oxidation depopulates the d band, which should act to enhance the ξ_f (autoionization) emission. By the same argument it is explained that the valence band related Auger transition $M_{23}VV$, is decreased significantly because of the lack of availability of all the d electrons than the pure Ti case. In the silicide the $M_{23}M_{45}M_{45}$ Auger transition becomes broad in width and its peak intensity increases. But due to high background, it is not possible to estimate the change. But the autoionization peak at 41 eV

is almost vanished in the silicide. This clearly shows a decrease in the p--d quasiatomic transition due to the depletion of the Ti- empty d states after silicidation.

Allen[4], in analysing the valence band related Auger lineshape, had shown the dependence of the $L_2M_{45}M_{45}/L_{23}M_{23}M_{23}$ ratio with respect to the d electrons, and is observed that with the increase of d electrons in the 1st transition metal series, the ratio increases. So, in our analyses the increase in the ratio in the silicide suggests the effective increase in the d electrons due to the p-d hybridization of the metal with Si, thus the bonding state is observed in the Auger fingerprint. In the oxide as the d electrons are given to oxygen, the M_{45} related Auger transitions decrease which is noticed in the second column of the TableVII (chapter IVB) In the multiplet splitting the positive excursion of the peak at 387 eV is very much sensitive and it increases with the increase in the d electrons. This is explained from the interaction of the unpaired d electrons with the 2p holes created in the same atom in the Auger process[5]. In silicide, the population of unpaired d electrons is effectively increased which increases the splitting intensity but the reverse is in case of the oxide. Thus the Auger fingerprint shows the formation of the bonding states near the Fermi level in the silicide and depletion of the d electrons in case of the oxide. However the valence band picture in XPS , the sharp d band observed in Ti at 1.5 eV below E_f is observed to be suppressed by a strong feature at 2.4 eV below the Fermi level indicating the metal d and Si p hybridization state.

Cu, CuO, $CuSi_2$: In Ti, Ta and Mo the main interest of ELS is the change in d band due to silicidation or oxidation of these materials. The transition of 49 or 39 eV in Ta, 38 or 65 eV in Mo and 37.4 ev or 62 eV in Ti are related to the excitation of the shallow core level electrons to the states above the Fermi level. All these materials have d band empty states so that they show these type of transitions. But in case of Cu where d band is filled we did not find any such transiton (as is evident from FIG.4b.23, chapter IVB). The interband transition in the ELS may be related to the transition to the 4s level. In the silicide of these materials these transitions are decreased or vanished which shows metal d and Si p hybridization , the effective density of states above the Fermi level is decreased.

The variation of LMM lines of Cu due to oxidation or silicidation is explained by an energy parameter, defined later, and a localization parameter. From the work by Yin et al[6,7] the energy parameter $\nabla\varepsilon$ defined by,

$$\nabla\varepsilon = [\, B(j) - B(k) - B(l)\,] - K(jkl).$$

B(i)'s be the experimental binding energy of the ith shell obtained from XPS and K(jkl) is the experimental jkl Auger kinetic energy in a metal relative to its Fermi level. The first term [B(j)--B(k)--B(l)] is the single hole (hypothetical) final state kinetic energy of jkl Auger transition where as K(jkl) is the observed double hole final state kinetic energy . This measures the difference between the kinetic energy obtained from the same sample and is independent of the reference level or other systematic uncertainities. $\nabla\varepsilon$ gives a rising trend as d orbitals are getting filled that physically implies high degree of localization of electrons at its higher

values. Thus the splitting in this case is mostly supported by these parameters depending on the localization of the electrons particularly in case of Cu the $L_3M_{45}M_{45}$ creates two holes in the valence band so that the two hole state interacts with the out going electrons, resulting in some splitting shown in FIG.4b.15 (chapter IVB). The localization of holes is important in the multiplicity and the intensity of splitting. In the oxide these splitting kinks are almost vanished showing the delocalization of the holes in the oxide relative to the the pure case. In case of silicide there is still some kink, which is more prominant than the case of pure Cu. So in the silicide the d holes are more localised than the oxide and pure Cu.

Si LVV line : The cause of Si LVV line shape have been explained by the reports in the literature regarding its change due to silicidation. At the Si surface the dangling bonds are being mostly p electrons result in the dominant feature in the LVV lineshape. In case of silicides owing to the chemical interaction of Si with metals , interface states are formed that can accomodate the surface charge. This situation implies that the surface states are removed from the gap region and are replace by some chemisorption states. So that a decrease in the pp contribution is observed in the silicides compared to the pure Si (Table IX). The localization behaviour of Si 3s orbital can be explained from this, according to the explanation given by Ramaker et al[8]. Si 3s orbitals are much more localised in silicides compared to the Si, where they are involved in the bonding. This localization effect increases the intensity of the s related contributions in silicides.

4c.2 Trends :

The central role of d electrons in determining the compound properties emerges from the stability of the structures. Calendra et al[9] showed the various crystal structures with the number of d electrons and relating them with the electronegativity differences between the Si and the corresponding metal. In fact, valence electrons which include the d electrons, determine bonding and the stability of the silicide. The dependence of electron transition features observed, on the number of d electrons in the respective metal are listed below:

i) From the plasmon loss, assuming the free electron model is valid, the effective free electron density (n) can be calculated by using the equation for the plasmon loss as $\hbar\omega_p \alpha (n)^{1/2}$ where n is the free electron density. In FIG.4c.2 it is shown that n increases (proportionately with $\hbar\omega$) with number of d electrons, among the refractory metals. But in case of Cu though it has ten d electrons per atom it shows a reduction in the loss. This indicates a weak interaction between Cu and Si. Among the refractory metal silicides the free electron density increases directly with the number of electrons in the d shell. n cannot be calculated for all the systems since they hardly are free electron metals.

ii) In the loss study the peaks at 39 eV in Ta , 47 eV for Mo and 45 eV in Ti have similar energies and are 5, 12 and 14 eV respectively above their XPS binding energy values. The states available at these energy values cause the p-d quasiatomic transition which vanishes after silicidation and enhances in oxidation. This is also explained from the change in the d band due to oxidation and silicidation as explained earlier. In Cu, due to the d^{10} nature of the d band, this type of peak is not observed. In 5d

transition metal Ta, this interference loss transition is not observed. So, in Ti (3d) the p--d+14 (eV), in Mo(4d) p--d+9 (eV) and in Ta (5d) p--d+5 (eV) transitions are useful in understanding the nature of the bonding formed. The vanishing of these transitions in the silicides indicates the depletion of the p--d transition, which is due to the M-d and Si-p hybridization causing the depletion of the empty DOS in the silicide. In oxides the localised states for p--d transitions are still available. In Cu no p--d transitions are observed because of the filled d orbital.

ii) In the metal Auger lineshape analysis, three aspects are interesting as discussed seperately for the four metals. The $L_3M_{23}M_{23}$ Auger transition for Cu and Ti does not involve the valence band directly. Therefore one expects their behaviour to be essentially atomic. Similarly, in case of the $N_4O_3O_3$ transition in Ta . All these transitions result in two holes in the p level nearest to the valence band. But in Mo the $M_4N_{23}N_{23}$ gives the two hole final state in the p level and does not show any such observable splitting, within the resolution of our instrument.

The splitting involves two parameters, i) energy and ii) the intensity. The observed $L_3M_{23}M_{23}$ splitting of the first transition metal series shows a gradual increase across the transition metal series from ≈5 eV in Ti to ≈9 eV in Cu. The cause of the splitting is the creation of the two holes in the Auger process. These holes for which s=1/2, l=1, can couple to give S=0 or 1, L=0 or 2 (for atom). There will be a spin splitting between the singlet (S=0 spin non-aligned) and triplet (spin aligned) states. Thus that the splitting of the LMM that can be due to spin correlation, seems to provide the explanation. In our observation the change in splitting due to oxidation or silicidation is not observed, may be

because the change is too small to be resolved. But the change in intensity is obvious and distinct. The relative variation of the intensity of the two components of the split peak as a function of d electrons for the first transition metal series is shown in FIG.4c.3. It can be observed that with the increase of the d electrons the intensity ratio increases.

The variation of the multiplet splitting in Ti, Ta, Cu are the same for oxidation and silicidation. For oxidation the splitting decreases due to decrease in the d electrons in the ionic bond and increases for increase in effective d electrons in silicidation. Due to oxidation of Cu, the number of unpaired electrons increases but still a decrease in the splitting intensity is observed. In case of Cu the interaction with O and Si is very weak. So other factors e.g. localization of 3d holes is the influencing factor. The 3p holes are completely localized because of the high binding energy of the 3p electrons. So the small deviation is due to the delocalization of 3d holes.

In Mo, peak around 160 eV is due to the MNN transition with p holes in the final state. The peak 148 and 160 eV may be the splitted peak of the MNN Auger transition (FIG.4c.4). It is observed that even in this case the higher energy peak i.e. 160 eV peak is sensitive towards oxidation and silicidation. Like the case of Ta, Ti, and Cu the splitiing is decreased with oxidation and increases with silicidation.

iv) In all these silicides it is observed that the $R_{pp/sp}$ ratio of the Si LVV lineshape (discussed in chapter IVB) decreases relative to that in Si. In FIG.4c.5 the mode of variation of the ratio with d electrons is shown. However in all these cases the changes are due to the removal of the surface p states by the metal-Si chemisorption state. However, the

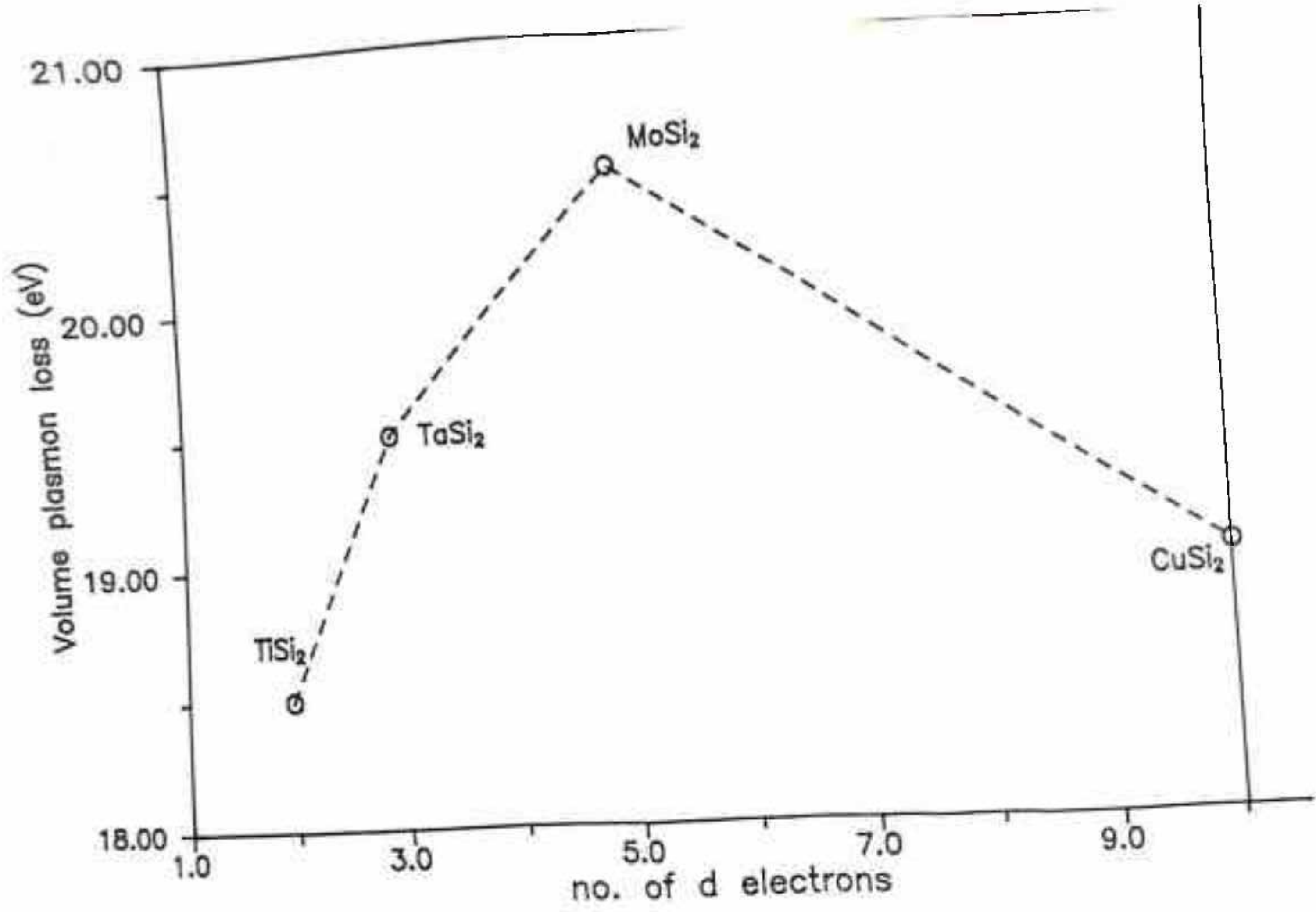

Fig.4c.2 : Change in volume plasmon loss energy in different silicides under study.

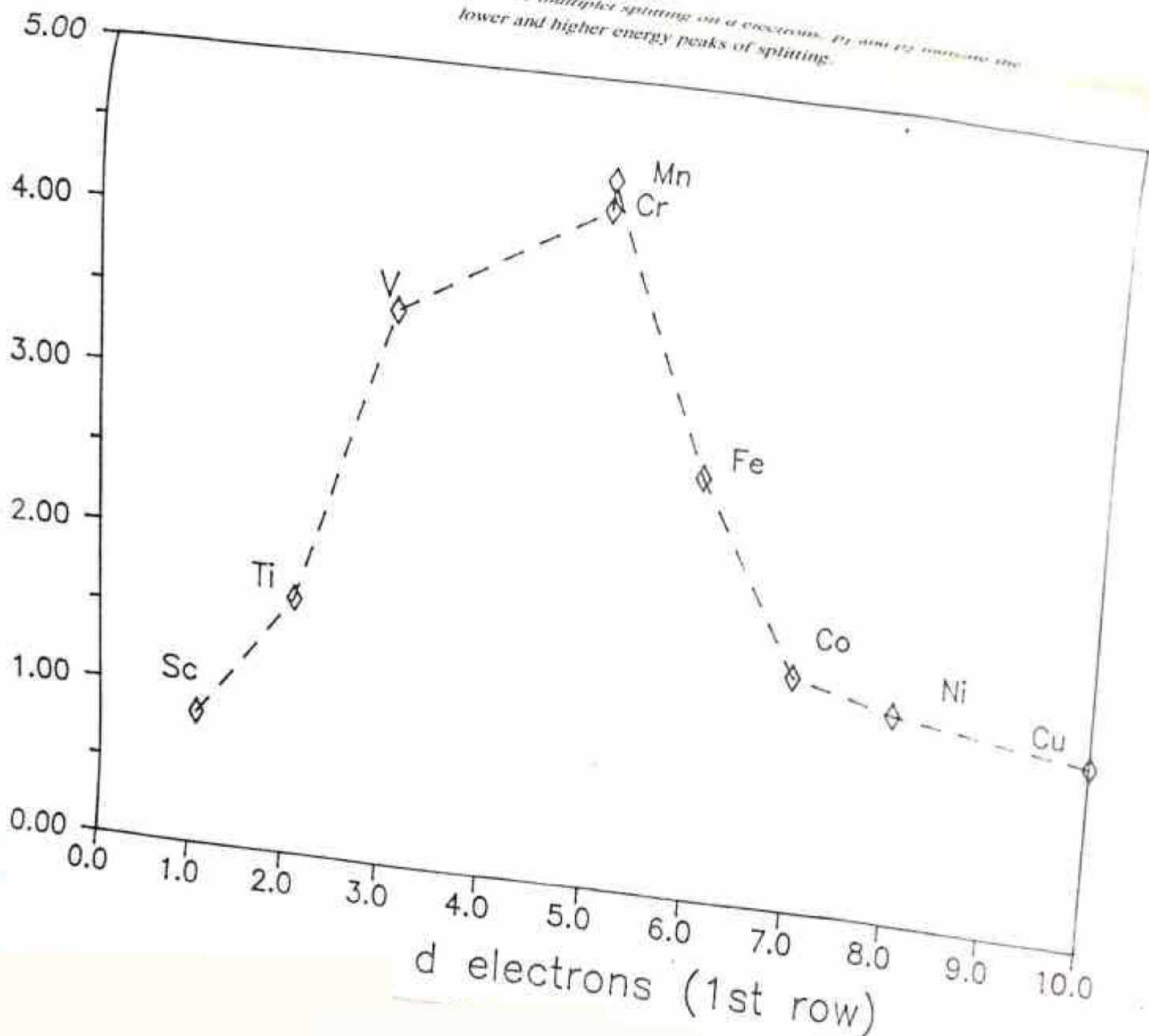

Fig-4c.3 : Dependence of multiplet splitting on d electrons. P_1 and P_2 indicate the lower and higher energy peaks of splitting.

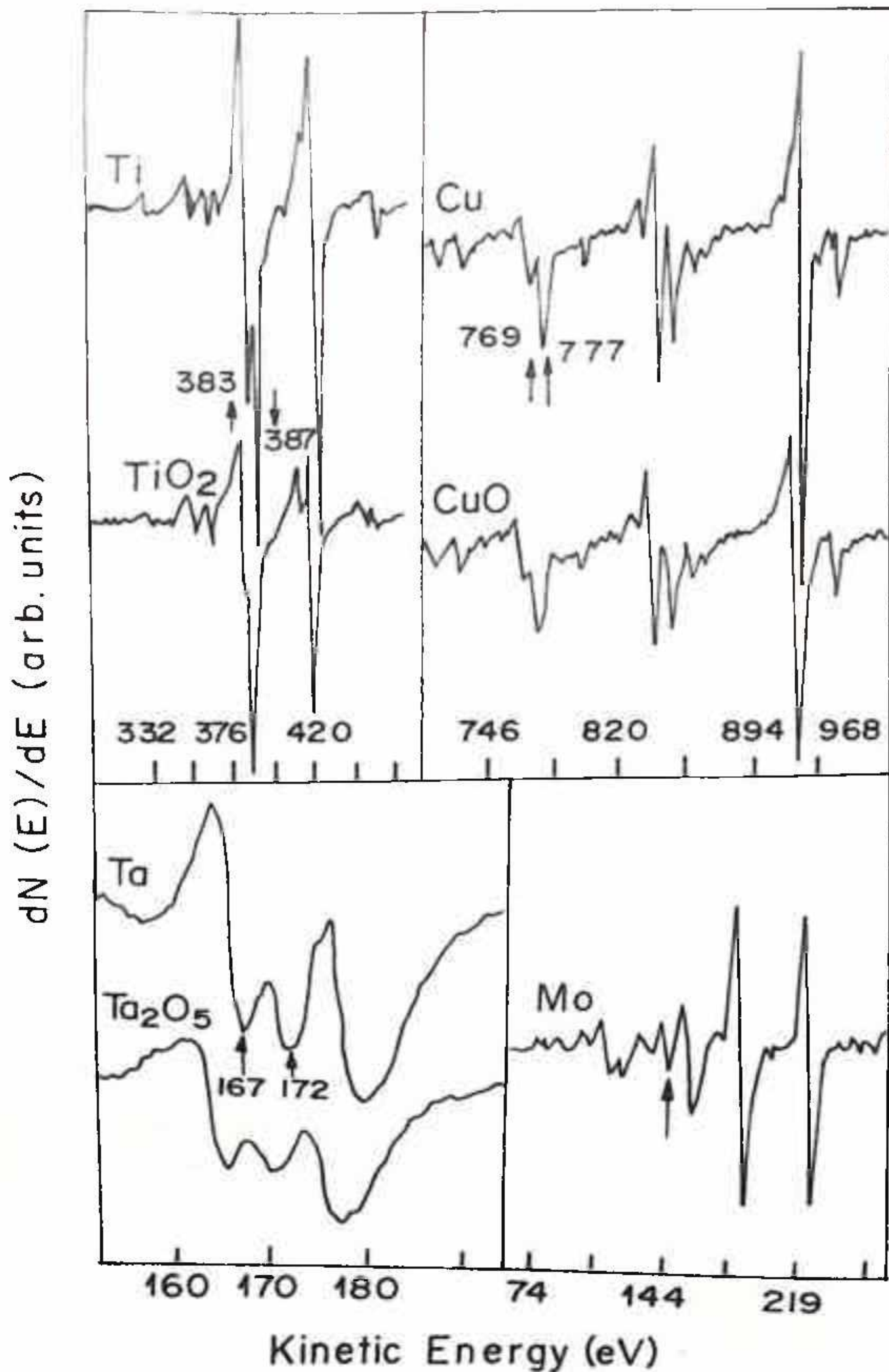

Fig.4c.4 : Multiplet splitting in Ti, Cu and Ta. Arrows indicate the components (split) . In Mo, arrow indicates the probable position of splitting.

variation does mean that it is not only the p dangling states which cause the disimilar contribution of the p and s related Auger transitions in LVV lineshape. With Cu, Si interacts weakly. And as the d orbital is filled in Cu, the s electrons may partially contribute to the interaction. Thus the change in the ratio of the $R_{pp/sp}$ in the silicide may contribute to the order of localization of Si 3s orbitals in the different silicides. It is observed that from d^1 to d^5 the 3s orbital shows an increasing trend of the localization, but it is less localised in the Cu-Si interaction compared to the other silicides which may be due to its involvement in the Cu-Si interaction.

iv) The resonance effects, in studies by synchrotron radiation, are strongly dependent on the number of d electrons (particularly observed in 3d transition metal series). In electron impact process, the feature associated with p-d transition, autoionization feature is dependent on the number of d holes available. In case of Ti, Ta, Mo autoionization, the availability of some localised empty d state above the Fermi level are observed. Due to compound formation two parameters are expected to change, the intensity and the energy value of the peak.

The intensity of the autoionization peak is dependent on the d electrons (reversely d holes) for pure metal as shown qualitatively by G. Zajac et al[10]. It is observed that with the increase of d electrons the intensity decreases or vice versa. So in the oxidation process the increase in the autoionization feature may be accounted for by the depopulation of d band and hence the migration of d electrons to oxygen. Similarly the decrease in the autoionization feature in silicides is due to an effective

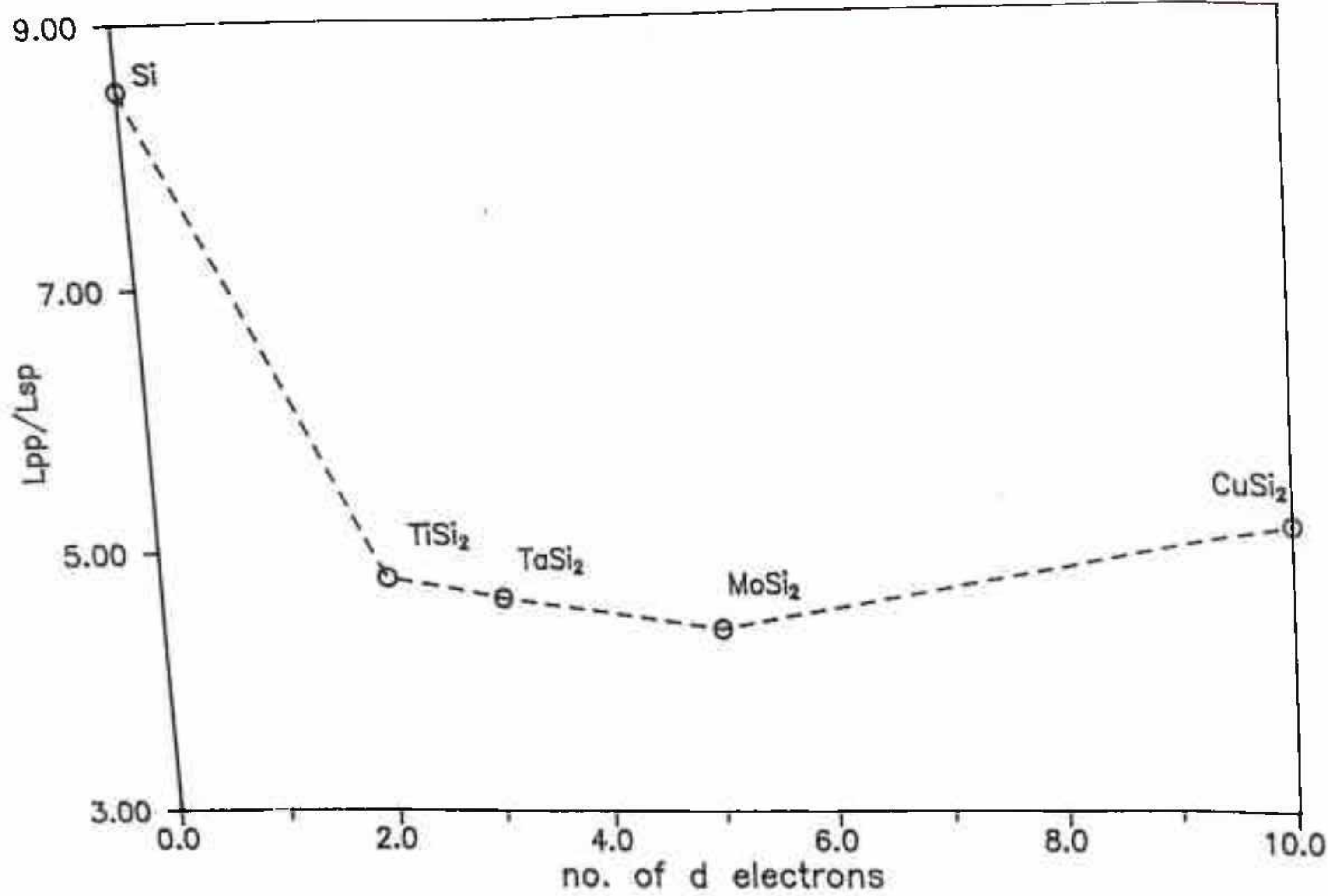

Fig.4c.5 : Si LVV Auger finger-print analysis. The parameter L_{pp}/L_{sp} decreases in all the silicides.

increase in d electrons because of Si p and metal d covalent hybridization states. Cu or its silicide do not show any autoionization feature and can be explained in the same light. But in CuO, though some autoionization transition is expected due to depopulation of d band, it is not observed. This is attributed to the weak interaction between the components as discussed earlier. Even CuO , whose d band picture can be compared to the d band of Ni (because of migration of Cu d electrons to O), also shows very weak autoionization transition that is probably lost in the intense Auger transition.

Another parameter defined below may be interesting. The seperation of autoionization feature and the nearest Auger feature (that creates two holes in the d band) gives the separation between the d and d* levels (δ) in the metal atom which is characteristic of the metals.

$$\delta = E_{auto} - E_{Auger} = \{(E_p + \Delta E) - E_d - \phi\} - (E_p - 2E_d - \phi)$$
$$= \Delta E + E_d$$

where (E +ΔE) is the E_{exe} , excitation of the p electrons ΔE above the Fermi level. So finally we get, $\delta = E_{auto} - E_{Auger}$ = seperation between d and d*, which indirectly gives the location of the localised state above the Fermi level.

In FIG.4c.6, the variation of the δ with the d electrons for the 3d and 4d transition metal series is shown. The data is collected from references[10-12]. Further data is not yet available to the best of our knowledge. It is seen that in TiO_2 the δ value is decreased indicating the migration of d electrons and in MoO_3 the value is increased to show the migration of d electrons to oxygen[13]. The 5d transition metal is not

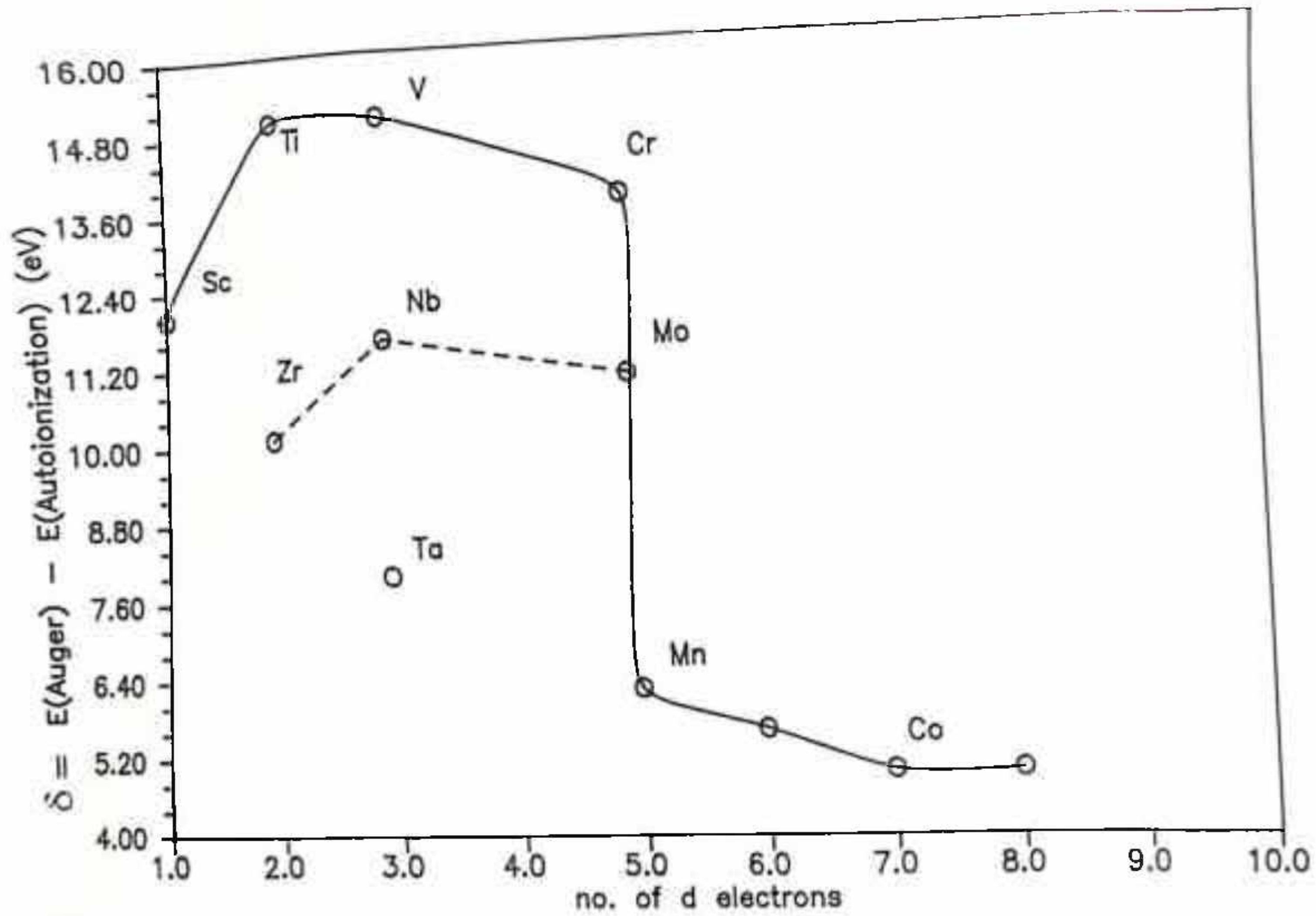

Fig.4c.6 : A plot of the difference δ between low energy Auger peak position and the energy position of the autoionization peak of respective d metals, as a function of d electrons in the metal.

plotted due to lack of data and in the case of Ta the the variation of δ is too small to be resolved in our studies.

v) O KVV lineshape shows changes in different oxides and the change is monitored to understand the oxidation. In O KVV line, $KL_{23}L_{23}$ and KL_1L_{23} transitions and their ratios, it is important to monitor the differences. As the Auger transition probablity depends on the density of states of the final state, the localization behaviour of 2p electrons is thought to be an important factor in determining the intensity ratio. In the metal -O system the localization or delocalization behaviour is influenced by the metal d band which is involved in the chemical bonding. With the increase in the number of unpaired d electrons , the 2p electrons become less localised and so the $KL_{23}L_{23}$ transition decreases more than KL_1L_{23} hence, increasing the ratio. On the other hand, the d electrons are getting paired (number d electrons is > 5) in case of Fe and Cu, the oxygen 2p electrons are more localised than in MoO_3. So the $KL_{23}L_{23}$ transitions increase more than KL_1L_{23} hence the ratio decreases.

References :

1] J.K.N. Sharma, B.R. Chakraborty and Santanu Bera, Surf. Sci. 285 (1993) 237.

2] D.R. Penn, Phys. Rev. Letts. 42 (1979) 921.

3] Santanu Bera, S.M. Shivaprasad and J.K.N. Sharma, Appl. Surf. Sci. 74 (1994) 13.

4] G.C. Allen, P.M. Tucker and R.K. Wild, Surf. Sci. 68 (1977) 469.

5] W. Palmer, Surf. Interf. Anal. 13 (1988) 55.

6] L.I. Yin, T.Tsang and I. Adler, Phys. Rev. B 15 (1977) 2974.

7] L.I. Yin, T.Tsang and I. Adler,Phys. LettsA57 (1976) 193.

8] D.E. Ramaker, Crit. Rev. of Solid State and Mat. Sci 17 (3) (1991) 211.

9]1] C. Calandra, O. Bisi and G. Ottaviani, Surf. Sci. Reps. 4 (1985) 271.

10] G. Zajac, S.D. Bader , A.J. Arko and J. Zak, Phys. Rev. B 29 (1984) .

11] A. Cornaz, M. Erbudak, P. Aebi, F. Stucki and F. Vanini, Phys. Rev. B 35 (1978) 3062.

12] C. Palacio, and J.M. Martinez-Duart, Surf. Interface Anal. 15 (1990) 675.

13] Santanu Bera, S.M. Shivaprasad and J.K.N. Sharma, Communicated for publication.

Chapter V
Conclusions

The preceeding chapters have described the studies undertaken on some technologically important transition metal silicides and oxides. The oxides and silicides were formed by evaporation in UHV the respective metals, and annealed in oxygen and inert gas ambients. The metals were chosen such that the d electron dependence can be investigated, like Ti(d^2), *Ta(d^3), Mo(d^5) and Cu(d^{10}). The analyses were done by electron* spectroscopic techniques in UHV like AES, EELS, Autoionization and XPS. The sample surface cleanliness, effect of ion beam sputtering on surface cleaning and the stoichiometry are probed by these techniques. In all the techniques, the transitions that involve the d band are probed to understand the d electron population of the metal and other features of the DOS. Crucial information on charge transfer and the concequences on DOS in the chemical bond formation have been carefully probed by fingerprinting the spectra obtained in the above four techniques. The subtle changes have been interpreted and the changes of various features as a function d electrons have been obtained to provide different trends.

In the loss transitions of Ta and its compounds, particularly the interband transition loss features at 49 and 39 eV are found to be interesting. In pure Ta, the sharp peaks at 39 and 49 eV show the availability of the empty DOS ≈5 eV above the Fermi level. In case of oxide the peaks are enhanced which show the increase in the empty DOS after oxidation. But after silicidation, the peak at 49 eV is decreased remarkably due to the formation of p-d hybridization states, which decreases the empty DOS effectively, thus decreasing the peak intensity.

In case of Auger electron fingerprint the multiplet splitting of NNN transition informs about the valence band after silicidation or oxidation. The multiplet splitting transition at 167.0 and 172 eV arises due to the interaction of the two hole final state in the p level with the unpaired 5d electrons. Following Ta oxidation there is a decrease in the number of d electrons in the valence band that reduces the electron hole interaction and hence we see a reduction in the splitting of the shoulder peak at 170.5 eV. For silicides, however this splitting still exists and there is some increase in the shoulder peak intensity thus indicating an effective increase in the d electron population due to the overlapping with Si p orbitals. The autoionization features in low energy AES are associated with p-d quasiatomic transition. In Ta these features are found at 34.5 and 44.5 eV. In case of silicide the autoionization peak at 44.5 eV decreases, and increases in case of the oxide. This also reflects the increase or decrease in the empty DOS after silicidation or oxidation, respectively.

In Mo the loss peaks at 38 and 47 eV are related to the excitation of the shallow core level electrons above the Fermi level. These interband transitions in the silicides are diminished or vanished because of dip in the DOS above the Fermi level after silicidation. In the oxidised case these peaks are observed to be more prominent. This is due to the ionic nature of MoO_3 , where d electrons are transferred to the oxygen atom causing more vacant states and consequently more probablity of p-d quasiatomic transition. It is observed that the autoionization peak intensity centred at 34 eV almost vanishes in the silicide. So the formation of p-d antibonding states is the cause of the decrease in the p-d quasiatomic transition. The

formation of the bonding state is further analytically confirmed by measuring the change of the $M_{45}N_{23}N_{45}/M_{45}N_{45}N_{45}$ Auger transition ratio. Thus a strong interaction in the oxide due to electronic charge transfer and a weak interaction arising due to p-d hybridization influences the change in the Auger fingerprint.

In loss features of Ti, the interband transition peaks at 37.5 and 45 eV indicate the status of the *DOS* above Fermi level. The peak at 45 eV particularly indicates the p-d interband transition ≈14 eV above the Fermi level. In the silicide the p-d loss transition decreases, which suggests that the p-d transition is not dominant in the silicide. Similarly the p-d transition ralated autoionization peak at 41 eV is observed to decrease in silicide, but increases in the oxide. The oxidation process depopulates the d band, which should enhance the autoionization emission. The autoionization peak at 41 eV almost vanishes in the silicide. This clearly shows a decrease in the p--d quasiatomic transition due to the depletion of the Ti-d band after silicidation. In the multiplet splitting the positive excursion of the peak at 387 eV is very much sensitive and it increases with the increase in the d electrons. This splitting originates from the interaction of the unpaired d electrons with the 2p holes created in the same atom in the Auger process. In silicide, effectively the population of unpaired d electrons is increased which increases the splitting intensity but the reverse is in case of the oxide. Thus the Auger fingerprint shows the formation of the bonding states near the Fermi level in the silicide and depletion of the d electrons in case of the oxide.

In case of Cu where the d band is filled, we did not find any such transition. The interband transition in ELS are related to the transition to

the 4s level. The variation of LMM lines of Cu due to oxidation or silicidation is explained by the localization of holes which is important in the multiplicity and intensity of splitting. In the oxide these splitting kinks almost vanish, manifesting the delocalization of the holes. In case of silicide there is still some kink, which is more prominent than in the case of pure Cu. So in the silicide the d holes are more localised than in the oxide and pure Cu.

In all these silicides it is observed that the $R_{pp/sp}$ (a parameter described to analyse the Si fingerprint) ratio decrease relative to that in Si. The change in the ratio of the $R_{pp/sp}$ among the silicides may contribute to the formation of Si p and metal d interface state or the amount of localization of Si 3s orbitals in the different silicides. It is observed that from d^1 to d^5 the 3s orbital shows an increasing trend of the localization, but it is less localised in the Cu-Si interaction compared to the other silicides which may be due to its involvement in the Cu-Si interaction.

Thus all these transition metals show common qualitative behaviour upon oxidation and silicidation as observed by the AES, ELS, XPS and Autoionization processes. Like in the covalently bonded silicides, the existence of bonding states and antibonding states are monitored for the oxides. Here the charge transfer is observed for this ionic bond by these spectral changes. So different trends of volume plasmon losses, multiplet splitting and the localization of the empty states above the Fermi level by autoionization as a function d electrons in the metal are drawn to picturize the behaviour of the silicides and oxides. The shapes of

Si LVV and O KVV transitions are also observed as being complementary to the conclusions drawn from the metal line shape analysis.

The information of all the techniques employed for this work is within few layers of surface (20-30A). So some surface contaminations were encountered and removed during these experiments. The chemical bonding of carbon contaminant on surface of Ta, Si and Mo during sputter cleaning was observed. The chemical interaction, type of compound formation and the development mode of hard carbide films were studied by all these surface analytical techniques. Low beam energy of sputtering can avoid this effect to some extent. Proper chemical ex-situ processing leaves small amount of carbon, and then in-situ sputtering with suitable ion energies help in getting contaminant free surfaces.

5.2. Limitations of study :

The experiments and analysis presented here encountered some limitations that are listed below. The list also indicates the direction of future work.

i) The study is for four transition metals. However, to get a better and detailed understanding of the trends, more d metals have to be probed. Similar work on the complete 3d and 4d series of transition metals will help in better understanding.

ii) The thin films of oxides and silicides have been prepared ex-situ. In situ preparation of ultra thin films is better for this kind of study. The in-situ preparation of monolayer films may lead to the understanding of the initial stages of nucleation and growth by these techniques, at different

conditions of temperature and thickness. Effort are being made in our laboratory to perform such studies.

iii) The data is collected by lock-in techniques in the derivative mode and are interpreted accordingly. The problem in the normal mode is the huge background and very small Auger signal. However, in the derivative mode the background is less but some subtle information (peak shapes etc.) may be lost due to electronic derivation of the data. A quantitative study can enhance the utility of the studies.

iv) Complementary results by using Synchrotron radiation or UPS can shed more light on the detailed valence band picture.

v) Radiation damage or beam damage in surface analysis refers to any changes in the physical structure or chemical make up of the sample that happens as result of the electron or photon beam. Ion sputtering used for sample cleaning can induce structural damage and chemical interactions as discussed in chapter IV A.

vi) Geometrical structural information along with the electronic structural results can be very useful. Our films were mostly polycrystalline in nature and the analysis is limited to electronic structural studies. So studies on epitaxial films may be more revealing.

The direction of our future research is motivated by the limitations observed in this study. We conclude that such studies done by complementary techniques, even using conventional surface analytical techniques, can throw light on final-geometry of silicides and oxides and the trends can indicate the ways to search and tailor make new materials for use in devices that perform better, faster and cheaper.

A] Ta [Ref. R. Nyholm et al, J.Phys. C 13 (1980)L1091]

Levels	Binding Energy (eV)
$4d_{3/2}$ (N_4)	237.9
$4d_{5/2}$ (N_5)	226.4
$4f_{5/2}$ (N_6)	23.53
$4f_{7/2}$ (N_7)	21.61
$5s_{1/2}$ (O_1)	69.7
$5p_{1/2}$ (O_2)	42.4
$5p_{3/2}$ (O_3)	32.7
$5d_{3/2}$ (O_{45})	2.0

B] Mo [Ref. Burr et al, Rev. Mod. Phys. 39 (1967) 125.]

Levels	Binding Energy (eV)
$3d_{3/2}$ (M_4)	230
$3d_{5/2}$ (M_5)	227
$4s_{1/2}$ (N_1)	62
4p (N_{23})	35
4d (N_{45})	1.3

C] Ti [Ref. Feldman and Mayer, Fundamentals of Surface and Thin Film Analysis, ESP Co. Ltd.(1986)]

Levels	Binding Energy (eV)
$2p_{1/2}$ (L_2)	461
$2p_{3/2}$ (L_3)	455
$2s_{1/2}$ (M_1)	59
$3p$ (M_{23})	34
$3d$ (M_{45})	3

D] Cu [Same as Ti]

Levels	Binding Energy (eV)
$2p_{1/2}$ (L_2)	951
$2p_{3/2}$ (L_3)	931
$2s_{1/2}$ (M_1)	120
$3p$ (M_{23})	74
$3d$ (M_{45})	2

LIST OF PUBLICATIONS

1] J.K.N. Sharma, **Santanu Bera** and B.R. Chakraborty, " Ion induced chemical bonding of C with Ta as studied by AES and SEELS" Appl. Phys. Letts.59 /25 (1991) 3247.

2] J.K.N. Sharma, B.R. Chakraborty and **Santanu Bera**, " Study of oxidation and silicidation of Ta by electron impact autoionization process", Surf. Sci. 285 (1993) 237.

3] J.K.N. Sharma, B.R.Chakraborty and **Santanu Bera**, " Si LVV Auger lineshape analysis to study the oxygen chemisorption om $TaSi_2$ thin film",Surf. Interf. Anal.20 (1993) 841.

4] **Santanu Bera**, S.M. Shivaprasad and J.K.N. Sharma, " Observation of electron transfer in the silicidation and oxidation of Mo by AES and EELS", Appl. Surf. Sci 74 (1994)13.

5] S.M.Shivaprasad, **Santanu Bera**, N.Sen and J.K. N. Sharma, " Angle dependent XPS study of ion induced bonding of C contaminant on Si (111) surface" Communicated to J. Appl. Phys.(1994).

6] **Santanu Bera**, S.M. Shivaprasad and J.K. N. Sharma, " Studies on oxidation and silicidation of some transition metals by AES and EELS" on preparation.

National Symposium attained :

1] " Ion induced chemical bonding of C in Ta and Ta_2O_5 films as studied by AES and EELS" Second AGM, MRSI, NPL Feb. 9-10 (1991).

2] "Electron and ion beam effect on single crystal graphite" Proc. of Solid State Physics Symposium, BHU Dec. 21-24 (1991) 34C p339.

3] "Electron impact autoionization process in Ta, Ta_2O_5 and $TaSi_2$ " Proc. of Solid State Physics Symposium, BHU Dec. 21-24 (1991) 34C p398.

4] "O KVV Auger lineshape analysis for studying transition metal oxides" National Symposium on Vac. Sci. and Technology. NPL, Oct 6-8 (1993).